

**Functional and regional selectivity of the  
cardiac preganglionic sympathetic  
neurones**

Thesis submitted for the degree of

Doctor of Philosophy

at the University of Leicester

by

**Reshma A Chauhan, BSc**

Department of Cardiovascular Sciences

University of Leicester

April 2018

## Abstract

Upregulation of sympathetic activity is known to be a significant factor in the development of life threatening arrhythmias that can lead to sudden cardiac death. Sympathetic pathways therefore pose as a target for treatment, however a better understanding of the anatomy and physiology of cardiac sympathetic nerves is necessary. Right and left spinal sympathetic neurones differentially innervate specific regions of the heart but whether they exhibit functional selectivity and distinct effects on cardiac electrophysiology has yet to be demonstrated.

A novel refinement of the original isolated innervated rabbit heart preparation, that allows controlled segmental stimulation, was used to study the effects of left and right-sided sympathetic chain stimulation on effective refractory period, action potential duration restitution and ventricular fibrillation threshold. A right-left difference in the functional effects was observed, with the left sympathetics displaying a preferential effect on ventricular electrophysiology with shorter effective refractory periods, steeper restitution slopes and smaller ventricular fibrillation thresholds than the right. The results also reveal previously unidentified characteristics of the lower thoracic spinal outflow on the left side having a dominant effect on cardiac electrophysiology and high potential to cause ventricular arrhythmias. Optical mapping was used to investigate the heterogeneous regional selectivity of the left and right sympathetics. The base of the ventricle elicited the shortest action potential durations and steepest restitution curves with sympathetic stimulation, which was reversed by removal of the left sympathetics.

This knowledge improves our understanding of sympathetic nerve control and highlights the potential for more focused clinical treatments for a variety of chronic cardiac arrhythmias, by selectively removing caudal sympathetic outflows on the left side. Our findings also suggest that the left sympathetics primarily innervate at the base of the ventricle and for the first time reveal the mechanisms that give rise to the antiarrhythmic results of left cardiac sympathetic denervation.

## Acknowledgements

I would firstly like to thank my primary supervisor Prof André Ng for the opportunity to undertake this PhD and for his continued advice and expertise. Secondly, thank you to my second supervisor Dr John Mitcheson for his guidance and feedback. Many thanks to my former second supervisor Dr Kieran Brack for teaching me the whole heart techniques and supporting me with analysis, presentation of data and feedback.

The completion of this work would not have been possible without the help and expertise of Prof John Coote, who played an essential role in shaping my project. I am very grateful for getting the opportunity to learn nerve isolation and dissection techniques from Prof Coote and to learn from his vast experience and knowledge. I would also like to extend my gratitude to Emily Wake and Pott Pongpaopattanakul for their assistance with the surgical procedures and general advice and support throughout this experience. Special thanks go to Emily for training me to perform the surgical techniques. My thanks also extend to Dr Xin Lee for developing, and adapting several times, the MATLAB program for the optical mapping analysis, teaching me how to use it and answering all my questions.

I would also like to thank Dr Gabriella Kocsis-Fodor for all the help with learning analysis and experimental techniques when I first started. I am also grateful to Dr Glenn Rodrigo and Hayley Crumbie for teaching me the calcium imaging techniques and analysis, assisting with cell isolations and allowing me to use their rigs in my first year. Also, thanks to Glenn for his guidance as member of my probation and second year panel.

I would also like to thank Dr Karl Herbert for his advice and support. My thanks also go to everyone in the office, especially Emily, Pott and Meetal, for making the stressful periods much more bearable.

And finally, thank you to my family and friends for their love, support and encouragement throughout the three years.

## Contents

Abstract	i
Acknowledgements	ii
List of figures	viii
List of abbreviations	xiii
Publications	xix
<b>Chapter 1. Introduction</b>	<b>1</b>
<b>1.1 Electrophysiology of the heart</b>	<b>2</b>
1.1.1 Pacemaker activity	2
1.1.2 The cardiac action potential	4
1.1.3 Excitation-Contraction coupling	7
<b>1.2 The autonomic nervous system</b>	<b>10</b>
1.2.1 Sympathetic and parasympathetic activity in the heart	13
<b>1.3 The sympathetic neurones</b>	<b>16</b>
1.3.1 Interneurones	16
1.3.2 Preganglionic neurones	16
1.3.3 Cardiac postganglionic nerves	18
1.3.4 Right and left sympathetic chains	20
<b>1.4 Cardiac disease and arrhythmia</b>	<b>22</b>
1.4.1 Mechanisms of arrhythmia	22
1.4.2 APD restitution	25
1.4.3 Clinical implications	27
1.4.4 Neural remodelling	29
<b>1.5 Clinical interventions</b>	<b>30</b>
1.5.1 Sympathectomy	30
1.5.2 Spinal cord stimulation	34
1.5.3 Thoracic epidural anaesthesia	35
1.5.4 Other methods	35
<b>1.6 Summary</b>	<b>36</b>
<b>Chapter 2. Aims</b>	<b>36</b>
<b>Chapter 3. Methods</b>	<b>38</b>

<b>3.1</b>	<b>Animal model .....</b>	<b>40</b>
<b>3.2</b>	<b>The dual innervated isolated heart preparation .....</b>	<b>40</b>
3.2.1	Langendorff perfusion .....	42
3.2.2	Haemodynamics .....	43
<b>3.3</b>	<b>Cardiac electrophysiology and pacing .....</b>	<b>44</b>
3.3.1	Ventricular pacing .....	44
3.3.2	Monophasic action potentials .....	45
3.3.3	Restitution protocol .....	46
3.3.4	Ventricular fibrillation threshold protocol.....	47
3.3.5	Data recording and statistical analysis .....	48
<b>3.4</b>	<b>Optical mapping technique .....</b>	<b>48</b>
3.4.1	Principles of optical mapping.....	48
3.4.2	Voltage sensitive dyes.....	49
3.4.3	Optical mapping apparatus.....	53
3.4.4	Motion artefacts .....	56
<b>3.5</b>	<b>Sympathetic chain denervation .....</b>	<b>59</b>
<b>Chapter 4. Differential effects of right and left sympathetic nerve</b>		
<b>stimulation on ventricular electrophysiology and arrhythmia inducibility 59</b>		
<b>4.1</b>	<b>Introduction .....</b>	<b>61</b>
<b>4.2</b>	<b>Methods .....</b>	<b>64</b>
4.2.1	Right and left sympathetic nerve stimulation .....	64
4.2.2	Method Development .....	65
<b>4.3</b>	<b>Results .....</b>	<b>67</b>
4.3.1	Changes in heart rate and left ventricular pressure with right and left sympathetic stimulation .....	67
4.3.2	Effect of right and left sympathetic stimulation on monophasic action potential duration .....	70
4.3.3	Effect of right and left sympathetic stimulation on effective refractory period	74
4.3.4	Action potential duration restitution and the effects of right and left sympathetic stimulation .....	75

4.3.5	Effect of right and left sympathetic stimulation on ventricular fibrillation threshold .....	77
4.3.6	Correlation between sympathetic modulation of ERP and VF threshold	79
4.3.7	Correlation between sympathetic modulation of effective refractory period and VF threshold maximum slope of restitution and VF threshold .....	80
<b>4.4</b>	<b>Discussion.....</b>	<b>81</b>
4.4.1	Clinical implications .....	84
4.4.2	Limitations .....	85
4.4.3	Conclusions .....	86
<b>Chapter 5. Functional selectivity of right and left spinal segmental preganglionic neurons .....</b>		
		<b>86</b>
<b>5.1</b>	<b>Introduction .....</b>	<b>88</b>
<b>5.2</b>	<b>Methods .....</b>	<b>91</b>
5.2.1	Sympathetic nerve stimulation.....	91
5.2.2	Method Development .....	93
<b>5.3</b>	<b>Results .....</b>	<b>96</b>
5.3.1	Effect of left or right sympathetic chain stimulation on Heart Rate (HR) and Left Ventricular Pressure (LVP).....	96
5.3.2	Effect on atrioventricular (AV) conduction.....	101
5.3.3	Monophasic action potential (MAP) duration changes.....	103
5.3.4	Changes in effective refractory period with right and left sympathetic stimulation at different spinal segments .....	106
5.3.5	Electrical restitution MAP duration and the effects of right and left sympathetic stimulation at different spinal segments.....	109
5.3.6	Effect of right and left sympathetic stimulation at different spinal segments of ventricular fibrillation threshold.....	113
<b>5.4</b>	<b>Discussion.....</b>	<b>115</b>
5.4.1	Clinical implications .....	119
5.4.2	Limitations .....	119
5.4.3	Conclusion.....	120

<b>Chapter 6. Regional heterogeneities of the cardiac sympathetic</b>	
<b>neurons</b> .....	<b>121</b>
<b>6.1 Introduction</b> .....	<b>123</b>
<b>6.2 Methods</b> .....	<b>129</b>
6.2.1 Mounting Isolated innervated rabbit heart preparation.....	129
6.2.2 Preparation of sympathetic chains.....	129
6.2.3 Positioning and stabilising the preparation.....	130
6.2.4 Loading the dye.....	131
6.2.5 Optical Mapping.....	131
Optical action potentials were recorded from the anterior left ventricular surface. An LED light source (535nm) was projected on to the heart using a dichroic mirror (570nm). Emitted light was filtered through a 630 nm long-pass filter and collected using a Hamamatsu 16 × 16 element photodiode array (Cairn Research, Faversham, UK).....	131
6.2.6 Sympathetic nerve stimulation.....	131
6.2.7 Removing the sympathetic chains.....	133
6.2.8 Data analysis.....	133
<b>6.3 Results</b> .....	<b>134</b>
6.3.1 Effect of Blebbistatin.....	134
6.3.2 Heart rate.....	134
6.3.3 Action Potential Duration.....	135
6.3.4 Effective Refractory Period.....	140
6.3.5 Action Potential Duration Restitution.....	142
<b>6.4 Discussion</b> .....	<b>148</b>
6.4.1 Clinical implications.....	151
6.4.2 Limitations.....	153
6.4.3 Conclusion.....	154
<b>Chapter 7. Conclusion</b> .....	<b>154</b>
<b>Chapter 8. Appendix</b> .....	<b>161</b>
<b>8.1 Abstract</b> .....	<b>162</b>
<b>8.2 Introduction</b> .....	<b>164</b>

8.2.1	Introduction to the Epac protein .....	164
8.2.2	Epac activators.....	166
8.2.3	Epac and ion channel function.....	167
8.2.4	Epac and cardiac calcium signalling.....	173
8.2.5	Epac and arrhythmia.....	179
8.2.6	Epac and hypertrophy.....	182
8.2.7	Summary.....	185
<b>8.3</b>	<b>Aims and hypothesis.....</b>	<b>186</b>
8.3.1	Aims .....	186
8.3.2	Hypothesis .....	186
<b>8.4</b>	<b>Methods .....</b>	<b>187</b>
8.4.1	Animal model.....	187
8.4.2	Langendorff whole heart perfusion.....	187
8.4.3	Haemodynamics .....	188
8.4.4	Cardiac electrophysiology and pacing .....	188
8.4.5	Effects of 8-CPT on cardiac function.....	192
8.4.6	Effects of positive control isoproterenol on cardiac function.....	193
8.4.7	Data recording and statistical analysis .....	193
8.4.8	Calcium Imaging.....	193
<b>8.5</b>	<b>Results.....</b>	<b>197</b>
8.5.1	The effect of Epac on whole heart physiology .....	197
8.5.2	The effect of positive control isoproterenol on whole heart physiology 208	
8.5.3	The effect of Epac activator 8-CPT on cardiomyocyte Ca <sup>2+</sup> handling .....	213
<b>8.6</b>	<b>Discussion.....</b>	<b>221</b>
8.6.1	The effect of Epac activator 8-CPT on whole heart guinea pig physiology 221	
8.6.2	The effect of positive control isoproterenol on whole heart guinea pig physiology.....	223
8.6.3	Epac's effect on Ca <sup>2+</sup> handling in rat and guinea pig cardiomyocytes ...	225
8.6.4	Limitations .....	226

<b>8.7 Conclusions .....</b>	<b>227</b>
<b>References.....</b>	<b>228</b>

## List of figures

Figure 1.1. Pacemaker action potential.....	4
Figure 1.2. Cardiac action potential.....	6
Figure 1.3. $\beta$ -AR signalling pathway.....	9
Figure 1.4. Sympathetic and parasympathetic outflows to target organs. ....	11
Figure 1.5. Regional distribution of the principle cardiac nerves. ....	13
Figure 1.6. Schematic of the upper thoracic (T1–T6).....	16
Figure 1.7. Illustration of sympathetic preganglionic and postganglionic neurone projections.....	19
Figure 1.8. Mechanisms of arrhythmia. ....	23
Figure 3.1. The dual innervated isolated rabbit heart preparation. ....	44
Figure 3.2. Diagram illustrating the generation of MAP recordings by contact electrodes.....	45
Figure 3.3. Pacing protocols.....	47
Figure 3.4. Voltage-dependent changes in emission spectra of a typical electrochromic dye. ....	50
Figure 3.5. Major components of optical mapping apparatus.....	51
Figure 3.6. Ultrastructural changes in the Di-4-ANEPPS molecule. ....	52
Figure 3.7. Mechanism of Di-4-ANNEPS. ....	53
Figure 3.8. Image of the optical mapping apparatus. ....	56
Figure 4.1. Diagram showing the placement of electrodes on right and left sympathetic chains parallel to the spinal column at levels between T2-T3. ....	64
Figure 4.2. Image of isolated innervated heart preparation with bipolar electrodes used for right and left sympathetic stimulation.....	66
Figure 4.3. The effect of right and left sympathetic stimulation heart rate and left ventricular pressure.....	69
Figure 4.4. Raw data traces of basal and apical action potentials during constant pacing at 240ms.. ....	70
Figure 4.5. The effects of right and left sympathetic stimulation on monophasic action potential (MAP) duration. ....	71
Figure 4.6. Effects of left and right sympathetic stimulation on APD restitution.	72

Figure 4.7. Restitution loops during left and right sympathetic stimulation at (a) the base and (b) the apex. ....	73
Figure 4.8. Changes in effective refractory period (ERP) with right and left sympathetic stimulation. ....	74
Figure 4.9. The effects of right and left sympathetic stimulation on action potential duration restitution. ....	76
Figure 4.10. Changes in maximum slope of restitution with right and left sympathetic stimulation. ....	77
Figure 4.11. The effects of right and left sympathetic stimulation of ventricular fibrillation (VF) threshold. ....	78
Figure 4.12. Relationship between ventricular fibrillation threshold (VFT) and effective refractory period (ERP).. ....	79
Figure 4.13. Relationship between maximum slope of restitution and VF threshold with linear regression analysis. ....	80
Figure 5.1. Diagram to illustrate the methods used to stimulate the cardiac sympathetic preganglionic neurones projecting to the stellate ganglion from that upper thoracic spinal cord. ....	92
Figure 5.2. Custom made electrodes used for stimulation of the left and right sympathetic chains. ....	94
Figure 5.3. Final set up of preparation with isolated sympathetic chains and fixed electrodes. ....	95
Figure 5.4. Raw data heart rate and left ventricular pressure traces recorded during right and left sympathetic chain stimulation, a spinal segmental levels between T1-T6. ....	97
Figure 5.5. The effect on heart rate (HR) with right and left sympathetic stimulation at different spinal segments. ....	98
Figure 5.6. The effect on left ventricular pressure (LVP) with right and left sympathetic stimulation at different spinal segments. ....	100
Figure 5.7. Dromotropic effects upon right and left sympathetic stimulation between T1-T6. ....	102
Figure 5.8. Effects of right and left chain stimulation on monophasic action potential (MAP) duration. ....	104

Figure 5.9. Percentage change in MAP duration for RSS and LSS at spinal segments T1-T6 .....	105
Figure 5.10. Changes in effective refractory period with right and left sympathetic stimulation at levels stimulated between T1-T6.. .....	107
Figure 5.11. Relationship between heart rate and effective refractory period.	108
Figure 5.12. Electrical restitution of monophasic action potential (MAP) duration and the effects of right and left sympathetic stimulation at the levels stimulated between T1-T6. ....	110
Figure 5.13. Effect of right and left sympathetic stimulation on maximum slope of restitution.....	111
Figure 5.14. (a) Percentage change in the maximum slope of restitution at the base for RSS and LSS at spinal segments T1-T6.....	112
Figure 5.15. Effect of right and left sympathetic stimulation on ventricular fibrillation threshold (VFT). ....	114
Figure 6.1. Distributions of the left and right sympathetic chains (trunks) as described by Kralios et al., 1975. ....	126
Figure 6.2. Image showing right sympathetic chain with suture thread underneath.....	130
Figure 6.3. Image showing final set up of preparation.....	132
Figure 6.4. Effect of 5uM Blebbistatin. ....	134
Figure 6.5. Chronotropic effects of differential sympathetic stimulation. ....	135
Figure 6.6. Effects of sympathetic stimulation and denervation on action potential duration (APD).....	137
Figure 6.7. Regional action potential duration (APD) changes during differential sympathetic stimulation.....	138
Figure 6.8. Percentage change in action potential duration (APD).....	139
Figure 6.9. Effects on effective refractory period (ERP).....	141
Figure 6.10. Action potential duration restitution curves.....	143
Figure 6.11. Derivative of fitted restitution curves.. .....	144
Figure 6.12. Action potential duration restitution curves at multiple sites over left ventricle.....	145
Figure 6.13. 2D plots of regional differences in maximum slope of restitution across left ventricle. ....	146

Figure 6.14. Percentage change in maximum slope of restitution.....	147
Figure 8.1. Structure of Epac. . . . .	165
Figure 8.2. Effects of Epac on $I_{Ca}$ window current. ....	168
Figure 8.3. Epac's effect on $K_{ATP}$ channels.....	169
Figure 8.4. Mechanisms of the downregulation of IKs by sustained $\beta$ -AR stimulation.....	171
Figure 8.5. Effect of Epac on action potential duration. ....	172
Figure 8.6. Acute Epac activation increases $Ca^{2+}$ transients in a PLC dependent manner.....	174
Figure 8.7. Epac increases $Ca^{2+}$ spark frequency.....	174
Figure 8.8. Proposed Epac pathway in cardiac myocytes.....	177
Figure 8.9. Chronic Epac activation causes triggered activity. ....	180
Figure 8.10. Epac application results in ventricular tachycardia.....	181
Figure 8.11. Acute and Chronic Effects of Epac activation. Both acute and chronic effects of Epac activation displayed in a myocyte.....	184
Figure 8.12. Langendorff whole heart perfusion preparation for guinea pig heart. Tyrode solution is perfused via the cannula at 20ml/min.....	189
Figure 8.13. Diagram illustrating the generation of MAP recordings by contact electrodes.....	190
Figure 8.14. Pacing protocols.....	192
Figure 8.15. Protocol for recording $Ca^{2+}$ transients.....	196
Figure 8.16. The effect 8-CPT on LVP, PP, MAPs and HR.....	197
Figure 8.17. Effect of $1\mu M$ 8-CPT on monophasic action potential duration (MAPD). ....	199
Figure 8.18. Effect of $10\mu M$ 8-CPT on action potential duration (APD). ....	200
Figure 8.19. Effect of 8-CPT on effective refractory period. ....	201
Figure 8.20 Effect of $1\mu M$ 8-CPT on standard restitution curves.....	202
Figure 8.21. Effect of $10\mu M$ 8-CPT on standard restitution curves.....	203
Figure 8.22. VF induced by dynamic pacing protocol.....	205
Figure 8.23. Dynamic restitution data with $1\mu M$ 8-CPT.....	206
Figure 8.24 . Dynamic restitution data with $10\mu M$ 8-CPT.....	207
Figure 8.25. The effect of 1nM ISO on LVP, PP, MAPs and HR. ....	209

Figure 8.26. Effect of 1nM ISO on monophasic action potential duration (MAPD). .....	211
Figure 8.27. Effect of 1nM Isoproterenol on standard restitution curves. ....	212
Figure 8.28. Dynamic restitution data with 1nM isoproterenol (ISO).. .....	213
Figure 8.29. Electrically evoked Ca <sup>2+</sup> transient traces and the effect of Epac in rat cardiomyocytes. ....	214
Figure 8.30. The effect of Epac on electrically evoked Ca <sup>2+</sup> transients in rat cardiomyocytes. ....	215
Figure 8.31. The effect of Epac on caffeine evoked Ca <sup>2+</sup> transients in rat cardiomyocytes. ....	217
Figure 8.32. Electrically evoked Ca <sup>2+</sup> transient traces and the effect of Epac in guinea pig cardiomyocytes.....	218
Figure 8.33. The effect of Epac on electrically evoked Ca <sup>2+</sup> transients in guinea pig cardiomyocytes. ....	219
Figure 8.34. The effect of Epac on caffeine evoked Ca <sup>2+</sup> transients in guinea pig cardiomyocytes. ....	220

## List of abbreviations

8-CPT: 8-pCPT-2'-O-Me-cAMP

AC: Adenylate cyclase

Ach: Acetylcholine

ANOVA: Analysis of variance

AP: Action potential

APD: Action potential duration

ARI: Activation recovery interval

AV: Atrioventricular

AVN: Atrioventricular node

$\beta$ -AR:  $\beta$ -adrenergic receptor

BL: Baseline

Bpm: Beats per minute

Ca<sup>+</sup>: Calcium ion

[Ca<sup>2+</sup>]<sub>i</sub>: Intracellular calcium concentration

CaCl<sub>2</sub>: Calcium chloride

CaMKII: Calmodulin kinase II

cAMP: Cyclic adenosine monophosphate

cGMP: Cyclic guanosine monophosphate

CICR: Calcium induced calcium release

CL: Cycle length

Cn: Calcineurin

CPVT: Catecholaminergic polymorphic ventricular tachycardia

CSD: Cardiac sympathetic denervation

DAD: Delayed afterdepolarisation

DAG: Diacylglycerol

DI: Diastolic interval

DMSO: Dimethyl sulfoxide

EAD: Early afterdepolarisation

ECG: Electrocardiograph

EDHF: Endothelium-Derived Hyperpolarizing Factor

Epac: Exchange protein activated by cAMP

ERP: Effective refractory period

GEF: guanine nucleotide exchange factor

G<sub>i</sub>: Inhibitory G protein

GPCR: G-protein coupled receptor

G<sub>s</sub>: Stimulatory G protein

HCN: Hyperpolarisation-activated cyclic nucleotide-gated channels

HDAC: Histone de-acetylase

hERG: Human ether-a-go-go-related gene

HF: Heart failure

HR: Heart rate

$I_{Ca}$ : Calcium current

$I_{Ca, L}$ : L-type calcium current

ICD: Implantable cardioverter-defibrillator

$I_{K1}$ : Inward rectifier potassium current

$I_{Kr}$ : Delayed outward rectifier  $K^+$  current, rapid

$I_{Ks}$ : Delayed outward rectifier  $K^+$  current, slow

$I_{Kur}$ : Delayed outward rectifier  $K^+$  current, ultra-rapid

$I_{Na}$ : Inward sodium current

$I_{Na/Ca}$ : Sodium calcium exchanger current

$IP_3$ : Inositol trisphosphate

ISO: Isoproterenol

$I_{TO}$ : Transient outward currents

$K^+$ : Potassium ion

KCl: Potassium chloride

LCSD: Left cardiac sympathetic denervation

LD: Left sympathetic denervation

L&RD: Left and right sympathetic denervation

LSS: Left sympathetic stimulation

LTCC: L-Type calcium channels

LV: Left ventricle

LVP: Left ventricular pressure

LQTS: Long QT Syndrome

MAP: Monophasic action potential

MAPD: Monophasic action potential duration

MAPD<sub>90</sub>: Monophasic action potential at 90% repolarisation

MAPD<sub>50</sub>: Monophasic action potential at 50% repolarisation

MgCl<sub>2</sub>: Magnesium chloride

MI: Myocardial infarction

Na<sup>+</sup>: Sodium ion

NaCl: Sodium chloride

NaHCO<sub>3</sub>: Sodium hydrogen carbonate

NaH<sub>2</sub>PO<sub>4</sub>: Sodium dihydrogen phosphate

NCX: Sodium-calcium exchanger

NFAT: Nuclear factor of activated T cells

NGF: Nerve growth factor

NO: Nitric oxide

PDE: Phosphodiesterase

PIP<sub>2</sub>: Phosphatidylinositol biphosphate

PKA: Protein kinase A

PKA: Protein kinase C

PLB: Phospholamban

PLC: Phospholipase C

PP: Perfusion pressure

Rap1: Ras-related protein 1

RSS: Right sympathetic stimulation

RyR: Ryanodine receptor

RT: Restitution

RT<sub>max</sub>Slope: Maximum restitution slope

RV: Right ventricle

RyR: Ryanodine receptor

SAN: Sinoatrial node

SCD: Sudden cardiac death

SERCA: Sarcoplasmic reticulum calcium ATPase

SR: Sarcoplasmic reticulum

SS: Sympathetic stimulation

VA: Ventriculo-atrial

VGCC: Voltage gated calcium channels

VF: Ventricular fibrillation

VFT: Ventricular fibrillation threshold

VT: Ventricular tachycardia

## **Publications**

**Chauhan RA**, Coote JH, Wake E., Pongpaopattanakul P, Brack KE, Ng GA. Functional selectivity of cardiac preganglionic sympathetic neurones. International Journal of Cardiology 2018, in press.

**Chauhan RA**, Coote JH, Wake E, Brack KE, Ng GA. Differential effects from left and right sympathetic nerve stimulation on ventricular electrophysiology and arrhythmia inducibility. Physiology 2016; Poster communication.

Coote JH, **Chauhan RA**, The sympathetic innervation of the heart: Important new insights, Auton. Neurosci 2016. <http://dx.doi.org/10.1016/j.autneu.2016.08.014>

Lim Z, **Chauhan RA**, Kocsis-Fodor G, Brack KE, Ng GA. Electrophysiological effects of  $\beta$ -adrenergic stimulation on pharmacologically induced LQTS 1 & 2. Physiology 2016; Poster communication.

# **Chapter 1**

## **Introduction**

# 1. Introduction

Approximately 50% of deaths attributed to coronary heart disease occur within an hour of the onset of symptoms (Zipes and Wellens, 1998), referred to as sudden cardiac death (SCD), claiming 90,000 lives per year in the UK. Ventricular arrhythmias can occur in the presence or absence of cardiac disorders however they account for the majority of SCD (Bayes de Luna et al., 1989). Current therapy includes implantable cardioverter defibrillators (ICD) and antiarrhythmic drugs; however these are not without problems and do not provide a preventative solution. A better understanding of the mechanisms underlying arrhythmias is therefore necessary.

The autonomic nervous system has a significant influence over the development and maintenance of arrhythmias (Shen and Zipes, 2014), especially in cardiac diseases such as heart failure and in patients with previous myocardial infarction and in arrhythmia storms. Sympathetic activity is often upregulated in these conditions and beta blockade of sympathetic activity reduces the risk of SCD (Hjalmarson, 1997). In order for clinical interventions to advance, a clearer understanding of the organization and innervations of the cardiac sympathetic nerves is essential.

## 1.1 Electrophysiology of the heart

Electrical impulses in the heart are responsible for the coordination of contraction through excitation-contraction coupling. These impulses originate in the sinoatrial node (SAN) and spread throughout the heart via gap junctions and conduction fibres. In cardiac myocytes, the electrical impulses give rise to the cardiac action potential.

### 1.1.1 Pacemaker activity

Spontaneous action potentials at the SAN spread through the left and right atria, reaching the atrioventricular node (AVN). AVN conduction is slow and thus provides a delay. This allows time for the atria to contract and for the ventricles to fill with blood before they too contract. The impulse from the AVN travels down

the bundle of His which divides into left and right bundle branches each side of the ventricular septum, from the base of the ventricle to the apex. The branches divide further into Purkinje fibres which disperse throughout the ventricular endocardium. This allows for coordinated contraction, essential for the maintenance of normal sinus rhythm. Geis et al (1973) electrically stimulated individual mediastinal cardiac nerves in canines to identify the course and distribution of autonomic nerves to the SAN and AVN. Both sympathetic and parasympathetic fibres were identified in the majority of nerves stimulated. Right sided sympathetic stimulation preferentially activated the SAN whereas left sided sympathetic activation was associated more with AVN activation (Geis et al., 1973, Van Stee, 1978).

Several inward currents underlie the depolarisation of the pacemaker action potential; time dependent currents ( $I_f$ ,  $I_{Ca,T}$ ), background currents ( $I_b$ ,  $I_{st}$ ) and the sodium calcium exchanger current ( $I_{Na/Ca}$ ) (Fig 1.1). The funny current ( $I_f$ ) is central to setting the rate of depolarisation of the pacemaker (Wainger et al., 2001). Unusually, it activates upon hyperpolarisation and flows through hyperpolarization activated cyclic nucleotide gated channels (HCN), which are non-selective cation channels modulated by cyclic adenosine monophosphate (cAMP). Binding of cAMP to the cyclic nucleotide binding domain (CNBD) of the HCN channel leads to channel opening. Therefore during sympathetic stimulation, downstream of beta adrenergic receptor ( $\beta$ -AR) activation, there is an increase in cAMP which causes increased HCN opening and  $I_f$  current (Wainger et al., 2001). Thus, sympathetic stimulation increases the rate of depolarisation of the pacemaker action potential and so the heart rate will increase.  $I_{K_r}$  also plays an important role in pacemaker depolarisation by decreasing and reducing the repolarising current, thus potentiating depolarisation (Ito and Ono, 1995). Unlike in the cardiac action potential, the L-type  $Ca^{2+}$  current ( $I_{Ca,L}$ ) is responsible for the pacemaker action potential upstroke and there is no plateau phase.

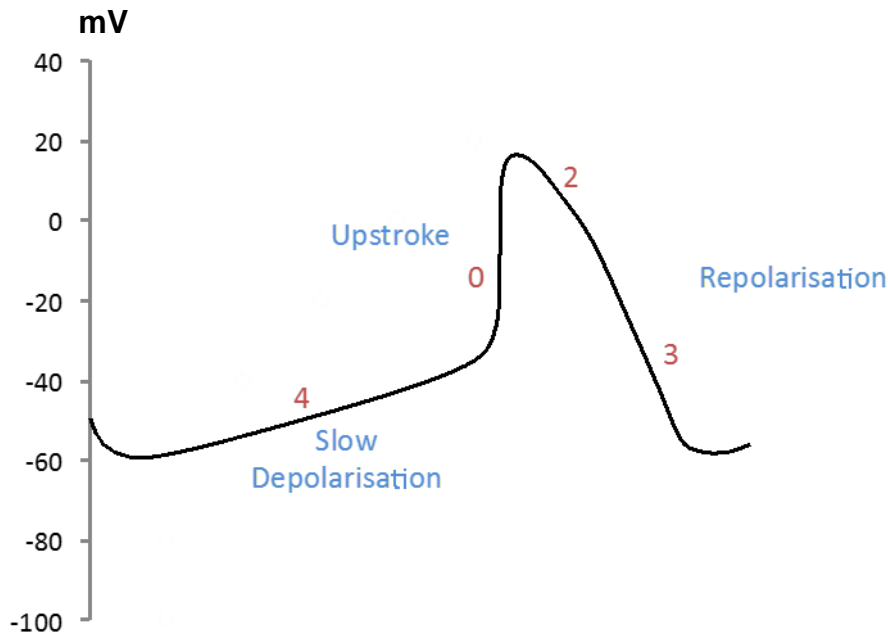


**Figure 1.1. Pacemaker action potential**

### 1.1.2 The cardiac ventricular action potential

The cardiac ventricular action potential is divided into 5 phases; phase 0 the action potential upstroke, phase 1 the notch phase, phase 2 the plateau, phase 3 the repolarisation and phase 4 the resting potential as shown in fig 1.2. The action potential upstroke in phase 0 is due to the rapid activation of  $\text{Na}^+$  current in which membrane potential rises from  $-90\text{mV}$  to  $+10\text{mV}$  (Fozzard, 1992, Nerbonne and Kass, 2005). The  $\text{Na}^+$  channels activate at negative potentials and produce a large but brief current before inactivating. The inactivation prevents re-excitation and thus reflects the effective refractory period (ERP) and relative refractory period (RRP). During the ERP,  $\text{Na}^+$  channels are inactivated and an action potential cannot be generated. The RRP refers to the period in which the  $\text{Na}^+$  channels begin to recover from inactivation and only a strong stimulus will elicit an action potential. Delay in the activation of the  $\text{Na}^+$  channels can lead to prolonged action potentials and gene mutations of this channel have been associated with arrhythmias (Nerbonne and Kass, 2005). Phase 1 is attributed to the transient outward current ( $I_{\text{TO}}$ ), a large  $\text{K}^+$  current which activates a positive potentials ( $+10\text{mV}$ ) and quickly inactivates, causing partial, early repolarisation.

$I_{TO}$  is known to have a transmural gradient with higher densities of expression in the epicardium than the endocardium (Antzelevitch, 2001, Antzelevitch, 2005, Antzelevitch and Belardinelli, 2006, Li et al., 2002, Szabo et al., 2005) and hence is the cause of the shorter action potentials observed in the epicardium. During the plateau in phase 2, there is a balance of inward depolarising currents and outward repolarising currents. The  $I_{Ca,L}$  is responsible for the large depolarising current and plays an important role in slowing repolarisation as well as in excitation-contraction coupling. Whole cell patch clamp studies in guinea pig ventricular myocytes studies (Hadley and Hume, 1987, Hadley and Hume, 1988) removed  $Ca^{2+}$  as the charge carrier and reported that  $I_{Ca,L}$  has a slow inactivation that is  $Ca^{2+}$  dependent and voltage sensitive. The repolarising currents during the plateau phase are attributed to the delayed rectifier  $K^{+}$  currents  $I_{Kr}$ ,  $I_{Kur}$  and  $I_{Ks}$ , each with different gating properties.  $I_{Kur}$  (ultra-rapidly activating  $K^{+}$  current), mainly important in the early stages of the plateau, has a rapid activation and does not inactivate (Nattel, 2008, Chen et al., 2016, Tamargo et al., 2004). It is highly expressed in atrial cells as opposed to ventricular cells. The subunit hERG of  $I_{Kr}$  (rapidly activating  $K^{+}$  current) is unusual in that it passes small currents at positive potentials due to rapid inactivation and has a large tail current due to fast recovery from inactivation (Nattel, 2008, Chen et al., 2016, Thomas et al., 2006, Tamargo et al., 2004). Thus, this current increases with repolarisation.  $I_{Ks}$  (slowly activating  $K^{+}$  current) is a large current that plays an important role in repolarisation and determining the action potential duration (Jost et al., 2007, Tamargo et al., 2004). Studies have shown higher densities of  $I_{Ks}$  at the base of the ventricle and hence shorter action potential durations in this region (Ng et al., 2009). In addition to these  $K^{+}$  currents, in phase 3, the inward rectifying current  $I_{K1}$  is activated. During the action potential  $I_{K1}$  passes a short outward current to rapidly repolarise the membrane potential.  $I_{K1}$  is responsible for maintaining the resting membrane potential close to the equilibrium potential for  $K^{+}$  and hence is the current responsible for phase 4 (Tamargo et al., 2004, Snyders, 1999). It does not pass current at positive potentials as it elicits strong inward rectification due to block by polyamines or  $Mg^{2+}$  (Snyders, 1999).

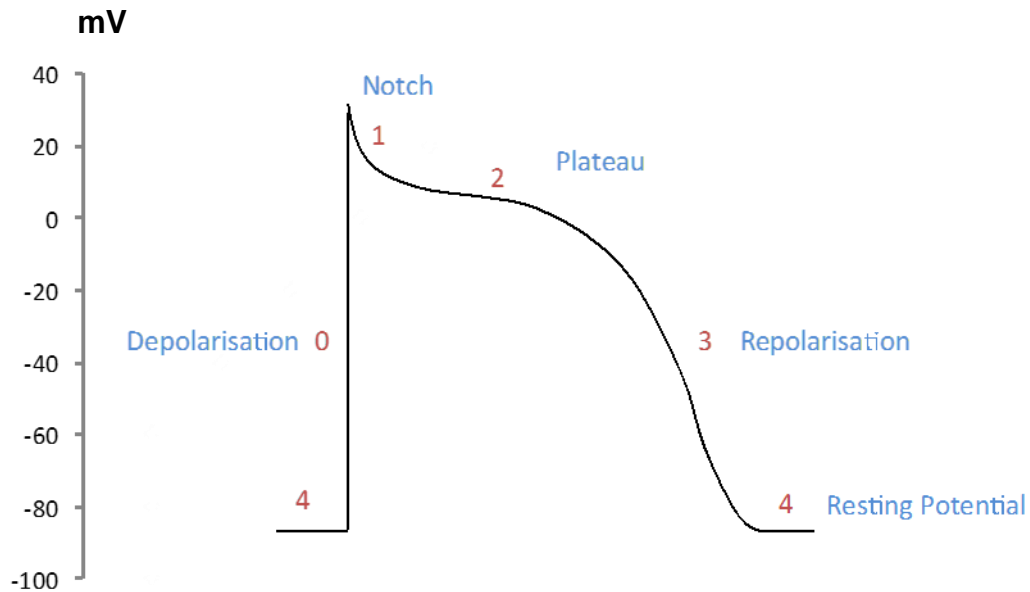


**Figure 1.2. Cardiac action potential**

Ion channel distribution is heterogeneous from epicardium to endocardium and base to apex (Antzelevitch, 2001, Antzelevitch, 2005, Antzelevitch and Belardinelli, 2006, Ng et al., 2009, Brahmajothi et al., 1997a, Cheng et al., 1999). The differential gradients of expression result in non-uniformity of APD and dispersion of repolarisation across the myocardium. In diseased states, APD is prolonged due to slower or delayed repolarisation (Janse, 2004, Li et al., 2002). This increases the likelihood of early afterdepolarisations (EADs) and thus promotes arrhythmia initiation (Rose et al., 2005, Li et al., 2004a, Li et al., 2002, Janse, 2004). Prolonged APDs can be attributed to decreased  $K^+$  currents, slowing repolarisation (Furukawa et al., 1992). In heart failure patients and animal models, both  $IK_1$  and  $I_{TO}$  currents are reportedly decreased (Beuckelmann et al., 1993, Qin et al., 1996, Rozanski et al., 1997).

The action potential in one myocardial cell can depolarise a neighbouring electrically coupled cell to threshold, thus spreading the impulse throughout the cardiac muscle. The myocardial cells are arranged in series and are connected via intercalated disks consisting of a high density of gap junctions. Gap junctions allow metabolic and second messenger signals between cells and assist with coordinating contraction (Bernstein and Morley, 2006). The regional variations in

APD can be modulated by electrotonic interactions between cells (Laurita et al., 1996, Walton et al., 2013), which can influence APD gradients depending on the activation sequence (Myles et al., 2010). Cells are influenced by electronic load from neighboring cells and this cell to cell electrotonic coupling is important for synchronization between myocytes and plays a critical role in propagation, repolarization, and arrhythmias. Studies in the rabbit ventricular myocardium have suggested that electrotonic influences have an important role determining the transmural repolarization sequence (Myles et al., 2010). Electrotonic potentials decay passively as a function of time and distance and the distance at which electrotonic potentials decay from their point of origin is known as the space constant (Suszkiw, 2012). In the dog myocardium the space constant was found to be between 0.712 and 1.202 mm (Spear et al., 1983). Cells that are poorly-coupled exert limited electrotonic influence over neighbouring cells and thus have a lower space constant (Rio et al., 2016). This can result in increased heterogeneity and dispersion of repolarisation which can lead to arrhythmias.

During sympathetic stimulation,  $I_{Ca,L}$  is increased due to increased phosphorylation by protein kinase A (PKA) downstream of  $\beta$ -AR. The increase in  $I_{Ca,L}$  would on its own increase the action potential duration (APD) but this is counterbalanced by  $K^+$  currents (mostly  $I_{K_s}$ ).  $I_{K_s}$  is also increased during sympathetic stimulation resulting in more rapid repolarisation. The overall effect is APD shortening which is necessary during sympathetic stimulation in order to accommodate the faster heart rates. Canine studies have shown that isoproterenol increased and accelerated  $I_{K_s}$ , shortening of APD, but limited  $I_{K_s}$  contribution to APD was observed at baseline (Volders et al., 2003). Hence,  $I_{K_s}$  is more prominent during sympathetic stimulation.

### **1.1.3 Excitation-Contraction coupling**

Adrenaline or noradrenaline are released from postganglionic sympathetic nerve terminals which activates adrenergic receptors.  $\beta$ -AR are the target receptors in heart muscle. Signalling of  $\beta$ -AR's activates a  $G_s$  protein signalling cascade in which cAMP is activated (fig 1.3). Downstream of cAMP, protein kinase A (PKA)

is activated and phosphorylates several targets. Phosphorylation of L-type  $\text{Ca}^{2+}$  channels (LTCC) and ryanodine receptors (RyR's) cause a positive inotropic effect (increase in contractility) by increasing  $I_{\text{Ca,L}}$  and increasing the open probability of RyR's (Wehrens *et al.*, 2005) inducing a larger  $\text{Ca}^{2+}$  release from the sarcoplasmic reticulum (SR) via  $\text{Ca}^{2+}$  induced  $\text{Ca}^{2+}$  release (CICR). This also induces a positive chronotropic effect (acceleration of heart rate) due to earlier activation of the pacemaker current as a result of changes in LTCC gating. Phospholamban (PLB) is another target of PKA and its phosphorylation relieves inhibition of SR  $\text{Ca}^{2+}$ -ATPase (SERCA). This has both a positive lusitropic effect (myocardial relaxation) by allowing sequestering of  $\text{Ca}^{2+}$  in to the SR and a positive inotropic effect by increasing the SR  $\text{Ca}^{2+}$  load (Bers, 2007, Bers, 2008). Once in the SR,  $\text{Ca}^{2+}$  becomes associated with the  $\text{Ca}^{2+}$  binding protein calsequestrin which holds  $\text{Ca}^{2+}$  in the SR where it is high in concentration.  $\text{Ca}^{2+}$  is also extruded via the  $\text{Na}^+/\text{Ca}^{2+}$  pump (NCX) in which 3  $\text{Na}^+$  are exchanged for 1  $\text{Ca}^{2+}$ , and the  $\text{Ca}^{2+}$ -ATPase pump (Eisner and Sipido, 2004). At the beginning of the action potential, NCX produces a net outward current as it acts in reverse mode;  $\text{Ca}^{2+}$  enters the cell and  $\text{Na}^+$  exits. The overall  $\text{Ca}^{2+}$  influx is minimal. Towards the end of the action potential, when intracellular  $\text{Ca}^{2+}$  concentration is high, NCX switches to forward mode;  $\text{Ca}^{2+}$  exits the cell and  $\text{Na}^+$  enters. In this way, the NCX provides the primary mechanism of  $\text{Ca}^{2+}$  extrusion (Eisner and Sipido, 2004).  $\text{Ca}^{2+}$  handling within the cell is also important for cross bridge cycling and contraction, in which  $\text{Ca}^{2+}$  binds to troponin and relieves the block by tropomyosin. This exposes the myosin binding sites allowing myosin to bind to actin filaments and cross bridge cycling to continue (Lehman *et al.*, 1994). A positive lusitropic effect is also seen when PKA phosphorylates myofilament proteins assisting relaxation (Ruiz-Hurtado *et al.*, 2013).

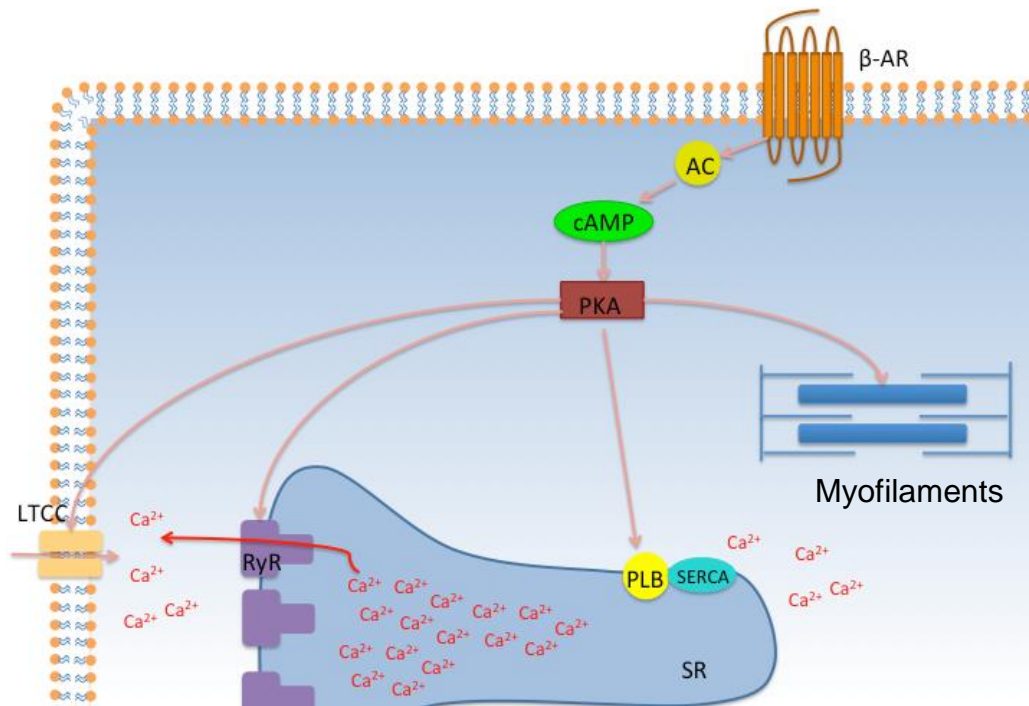


**Figure 1.3.  $\beta$ -AR signalling pathway.** The typical view of the  $\beta$ -adrenergic receptor ( $\beta$ -AR) signalling pathway involves activation of cyclic AMP (cAMP) downstream of  $\beta$ -AR activation. This then leads to activation of protein kinase A (PKA) which has several phosphorylation sites. These include; L-type calcium channels (LTCC) leading to  $\text{Ca}^{2+}$  influx, ryanodine receptors (RyR) activating calcium induced calcium release, phospholamban (PLB) which relieves inhibition of sarcoplasmic reticulum  $\text{Ca}^{2+}$ -ATPase (SERCA) thus causing sequestering of  $\text{Ca}^{2+}$  back into the sarcoplasmic reticulum (SR), and myofilaments assisting relaxation.

### ***$\beta$ -AR activation and heart failure***

Heart failure (HF) has a very high mortality rate and can lead to death as a result of failure of the cardiac pump function or due to arrhythmias leading to SCD (Packer, 1985). HF has been associated with chronic  $\beta$ -AR activation as a result of excessive sympathetic nervous system activity, which can result in abnormal  $\text{Ca}^{2+}$  handling (Bers, 2008, Oгородnik and Niggli, 2010, Wehrens et al., 2005). The resulting abnormal  $\text{Ca}^{2+}$  release from the SR can lead to arrhythmia initiation due to reduced SR load and increased  $\text{Ca}^{2+}$  transients (Wehrens et al., 2005, Pereira et al., 2013, Bers et al., 2003, Shannon et al., 2003).

SR  $\text{Ca}^{2+}$  leak occurs via the RyR's and is thought to be as a result of high calmodulin kinase II (CaMKII) dependent phosphorylation of RyR's (Guo et al.,

2006). This may also account for the  $I_{To}$  and delayed afterdepolarisations (DADs) involved in ventricular tachycardia development (Guo et al., 2006). Spontaneous  $Ca^{2+}$  waves are induced due to the SR  $Ca^{2+}$  leak and this leads to activation of the inward NCX. This can also result in DADs and eventually arrhythmia (Curran et al., 2010). NCX expression is increased in HF which increases  $Ca^{2+}$  efflux and  $Na^+$  influx, depolarising the cell (Curran et al., 2010) These effects can lead to triggered activity and increase the risk of arrhythmia (Pogwizd and Bers, 2004).

Although clinically sympathetic activity is mediated by beta blocker action on  $\beta$ -AR, this is an oversimplification as alpha adrenergic receptors also play an important role in cardiac electrophysiology and arrhythmias (Schwartz, 1984, Corr et al., 1981). They are also activated by adrenaline and noradrenaline and are associated with the  $G_q$  protein signalling cascade. Binding of catecholamines to the G-protein coupled receptor (GPCR) activates phospholipase C (PLC) which cleaves  $PIP_2$  in to  $IP_3$  and DAG.  $IP_3$  causes  $Ca^{2+}$  release via  $IP_3$  receptors, subsequently activating protein kinase C (PKC) which has several phosphorylation targets (Sheridan et al., 1980, Corr and Crafford, 1981). Alpha adrenergic receptors are important for smooth muscle contraction of blood vessels. Furthermore, alpha adrenergic receptor blockade also produces a degree of protection against ventricular arrhythmias (Sheridan et al., 1980), particularly in the presence of ischemia where there is a two-fold increase in alpha adrenergic receptors (Corr et al., 1981, Corr and Crafford, 1981). Therefore clinical treatments that target sympathetic activity directly, and thus all adrenergic receptor activity, could potentially be more effective especially when utilized in conjunction with drug treatment such as beta blockers.

## **1.2 The autonomic nervous system**

The autonomic nervous system (ANS) is responsible for the neuronal control of the heart. It consists of two branches; the sympathetic nervous system and the parasympathetic nervous system. Each have two populations of neurones arranged in series. They synapse in the periphery and those that innervate the target tissue are located outside the central nervous system (CNS). The axons of

the sympathetic and parasympathetic nervous systems project from ganglia, which are grouped cell bodies of these autonomic neurons, to their target tissues or organs and are known as postganglionic neurones. Preganglionic neurones are efferent neurones that project axons from the spinal cord or brain stem into the ganglia and form synapses. The preganglionic cell bodies are located within the spinal cord or brainstem (Jänig, 2006).

The ANS supplies every organ with one or both of the sympathetic or parasympathetic outflows (fig 1.4). The heart is one of the target tissues that is innervated by both the sympathetic and parasympathetic outflows and they each elicit specific and sometimes opposing effects on each organ system.

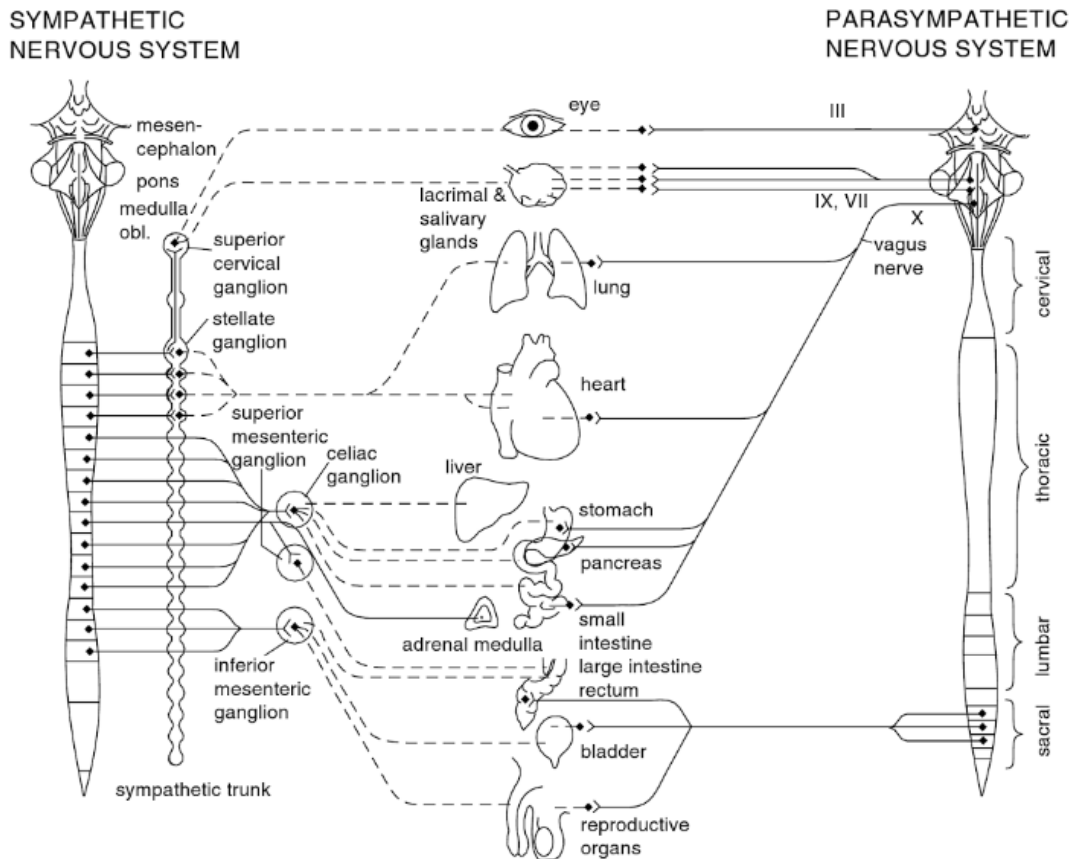


**Figure 1.4. Sympathetic and parasympathetic outflows to target organs.** Continuous lines represent preganglionic neurones and dotted lines represent postganglionic neurones (Jänig, 2006).

Chemical transmission of signals from sympathetic preganglionic neurones is cholinergic and thus requires the neurotransmitter acetylcholine. Some

sympathetic postganglionic transmission appears to be cholinergic and contain the enzyme choline acetyltransferase (ChAT) (Keast et al., 1995). Some also seem to be mediated by co-transmitters such as nitric oxide (NO) and vasoactive intestinal polypeptide (VIP). However, sympathetic postganglionic transmission is mostly adrenergic with noradrenaline as a transmitter. Adrenaline or noradrenaline are released from the adrenal medulla (an endocrine gland) in response to synaptic activation by sympathetic preganglionic neurones with tonic sympathetic discharge reported as 2 to 3 pulses/sec in the anaesthetised dog (Vassalle et al., 1968). Catecholamine content was measured from conductile and contractile tissues by Spurgeon et al (1974) in control and extrinsically denervated dog hearts. Control hearts showed greater levels of adrenaline in conductile tissues rather than contractile and noradrenaline levels were in higher concentrations in the SAN and atria. Sympathetic denervation almost completely removed noradrenaline, with only 1 to 5% remaining in sites surviving neural degeneration. Thus, noradrenaline appears to be entirely associated with nerve terminals. On the other hand, 40-50% of adrenaline remained in contractile tissue and 73% in conductile tissue post denervation. They suggested non-neuronal stores of adrenaline, possibly in chromaffin cells, specialised cells or cardiac analogs of chromaffin cells (Spurgeon et al., 1974), although the functional significance remains unknown (Van Stee, 1978). It has however been suggested that this could play a role in spontaneous pacemaker activity (Pollack, 1977). In HF, cardiac release of noradrenaline stores is increased and noradrenaline stores are depleted, associated with defective uptake in the nerve terminals (Liang, 2007). Neuropeptide Y (NPY) is a neurotransmitter that has also been suggested to be released by sympathetic neurones (Lundberg et al., 1991), with the role of mediating inhibition of vagal acetylcholine (Ach) release during periods of long sympathetic stimulation (Serone and Angus, 1999).

Regional distribution of the principle cardiac nerves has been reported by Randell et al (1972) in which the effects of electrical stimulation at specific points were recorded using strain gauges. Most cardiac nerves were composed of both parasympathetic and sympathetic fibres, excluding the purely sympathetic stellate cardiac nerves (fig 1.5). These principle cardiac nerves identified in

canine studies can be organised into 4 groups (Norris and Randall, 1977). The nerves that carried both sympathetic and parasympathetic fibres to all four heart chambers were labelled Type I by Norris and Randall (1977). Type II were those that produced both chronotropic and inotropic responses for example the innominate and ventromedial nerves. Nerves with only sympathetic efferent fibres were Type III (increased rate and force e.g. ansa subclavian and ventrolateral nerves) or Type IV (increased rate predominantly e.g. the stellates) (Van Stee, 1978).

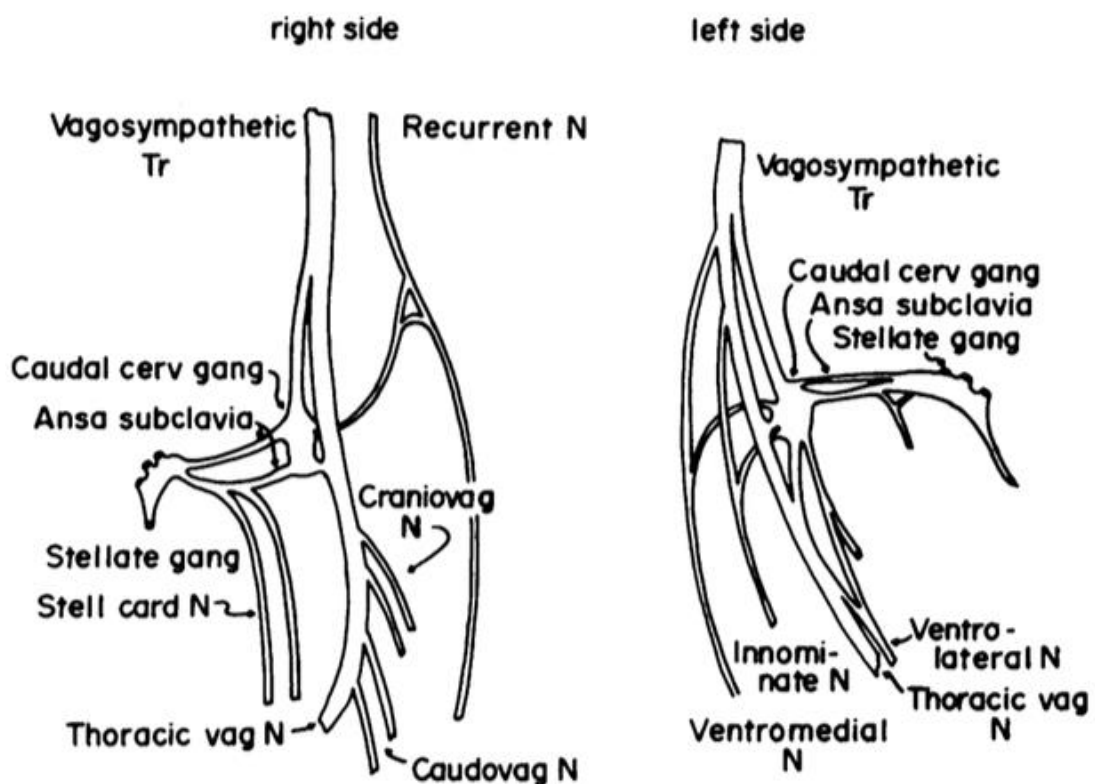


**Figure 1.5. Regional distribution of the principle cardiac nerves.** The principle sympathetic nerves on the right side stellate cardiac, craniovag, caudovagal, and recurrent cardiac nerves. On the left side the principle sympathetic nerves are the innominate, ventromedial, and ventrolateral nerves. All except the stellate cardiac nerve have both parasympathetic and sympathetic components (Van Stee., 1978).

### 1.2.1 Sympathetic and parasympathetic activity in the heart

In the heart, sympathetic and parasympathetic nerve stimulation have different and often opposing effects. Stimulation of sympathetic nerves releases

adrenaline or noradrenaline from nerve terminals which bind to  $\beta$ -AR receptors. This activates cAMP which results in a positive shift in the voltage dependence curve of  $I_f$  and faster depolarisation of the pacemaker cells. This consequently increases SAN firing and thus increases heart rate (Mangoni and Nargeot, 2008, Wainger et al., 2001). Downstream of the  $\beta$ -AR pathway, PKA activity is increased which drives phosphorylation of several targets including LTCC, troponin, PLB and SERCA (Madamanchi, 2007, Mangoni and Nargeot, 2008).  $\text{Na}^+$  channels are also reportedly phosphorylated as a result of sympathetic stimulation, which alters their gating and increases opening times. The resulting effect is faster depolarisation during the action potential upstroke, increased cell to cell conduction and shorter action potentials durations (Nathan and Beeler, 1975, Levi et al., 1997). Furthermore, as already discussed,  $\text{K}^+$  channel activity increases resulting in rapid repolarisation and shorter APDs.

Parasympathetic discharge is cholinergic and activates muscarinic receptors coupled to  $G_i$  proteins in the heart which leads to decreased heart rate, contraction and atrio-ventricular (AV) conduction. Binding of Ach to muscarinic receptors causes increase in cyclic guanosine monophosphate (cGMP) and successively activates PKG (Brink et al., 2005). Parasympathetic stimulation gives rise to accentuated antagonism of sympathetic stimulation. High levels of vagal tone have been found to significantly reduce sympathetic heart rate effects compared to low vagal background activity (Uijtdehaage and Thayer, 2000). Ach reportedly inhibits noradrenaline release from sympathetic presynaptic neurones via  $M_3$  receptors thus inhibiting sympathetic drive. It also causes direct decreases in the cAMP levels in the myocardial cells via the alpha ( $\alpha$ ) subunit of the muscarinic receptor (Hartzell 1988) and indirectly via the beta-gamma ( $\beta\gamma$ ) subunit of the  $G_i$  protein (Fleming et al., 1987) which activates  $K_{\text{Ach}}$  leading to membrane hyperpolarisation. Other studies evidenced reduction in LTCC (Sasaki et al., 2000, Dittrich et al., 2001, Yan et al., 2001) and decreased PLB phosphorylation (Bartel et al., 1993, Sulakhe and Vo, 1995).

Studies in many species have suggested that heart rate alone can alter contractile force (Lewartowski and Pytkowski., 1987) with a negative force-

frequency relationship displayed by rats and mice and a positive force-frequency relationship in guinea pig, rabbit, canine and human ventricular myocardium (Bers, 2002). Brack et al (2006) showed that, in the innervated isolated rabbit heart preparation, the force-frequency relationship was biphasic. They found that a positive force-frequency relationship was apparent at heart rates below the mean intrinsic value (200-350bpm) and there was a negative force–frequency relationship at heart rates above the mean intrinsic value (>350bpm). They also showed that sympathetic stimulation increased LVP in a frequency dependent manner even when heart rate was kept constant unlike vagus stimulation which decreased LVP during sinus rhythm but failed to elicit the same response when heart rate was kept constant. This suggests that sympathetic stimulation increases LVP through direct changes in contractility as appose to just chronotropic action. Factors such as an increase in  $I_{Ca,L}$  (Zygmunt and Maylie, 1990), higher diastolic calcium (Lado et al., 1982) and an increase in  $[Na^+]_i$  (Cohen et al., 1982) have been proposed to underlie the positive force-frequency relationship.

As well as increasing sinus rate and shortening AV conduction, sympathetic stimulation shortens APD and increases dispersion of repolarization (Ng et al., 2007, Mantravadi et al., 2007, Winter et al., 2012). In HF patients, sympathetic stimulation can have arrhythmogenic effects due to an enhanced dispersion of repolarization leading to afterdepolarisations (Shen and Zipes, 2014). Parasympathetic stimulation is recognized as anti-arrhythmogenic and has been found to increase the ERP, flatten electrical restitution curves and increase the threshold for ventricular fibrillation, with sympathetic stimulation eliciting opposite effects (Ng et al., 2007).

For a healthy regulation of cardiac performance, the sympathetic and parasympathetic activities act in balance. A shift in this balance can generate abnormal ECG (Yanowitz et al., 1966) and thus increase the likelihood of arrhythmia generation (Ng et al., 2009, Arora, 2012, Tan et al., 2008). Simultaneous increases in both sympathetic and parasympathetic activity has

also been linked to arrhythmia in the form of atrial fibrillation (Amar et al., 2003, Tomita et al., 2003).

## **1.3 The sympathetic neurones**

### **1.3.1 Interneurones**

Interneurons synapse on the dendrite of sympathetic preganglionic neurons (Deuchars, 2007) and provide an excitatory (EPSPs) or inhibitory (IPSPs) influence as shown by intracellular preganglionic recordings (Dun and Mo, 1989, Lewis et al., 1993, Spanswick et al., 1994, Deuchars et al., 2005, Deuchars, 2007). They play an important role in modulating the pattern of discharge of the sympathetic preganglionic neurone (Coote, 2001, Staras et al., 2001, Pierce et al., 2010).

### **1.3.2 Preganglionic neurones**

Sympathetic preganglionic neurones have cell bodies in the thoracic and upper lumbar spinal cord. Efferent, preganglionic fibres are generally myelinated B-type fibres with conduction velocities of 2.5 to 15m/sec (Van Stee, 1978). Cardiac preganglionic cell bodies originate in the thoracic spinal cord (T1-T6) and their axons exit by the ventral roots. They emerge segmentally and are connected by white rami to join the sympathetic chain (Rubin and Purves, 1980). The sympathetic chains lie parallel to the vertebral column on both the left and right sides. From here they may synapse on postganglionic neurones at that spinal segment level or travel rostrally into the stellate ganglion where they join the inferior/middle cervical ganglion and finally synapse with their target postganglionic neuron (fig 1.6) (Coote and Chauhan, 2016). The overall sympathetic tone delivered to the heart is a proportion of each contributing spinal segment (Lichtman et al., 1980, Nja and Purves, 1977, Pracejus et al., 2015).

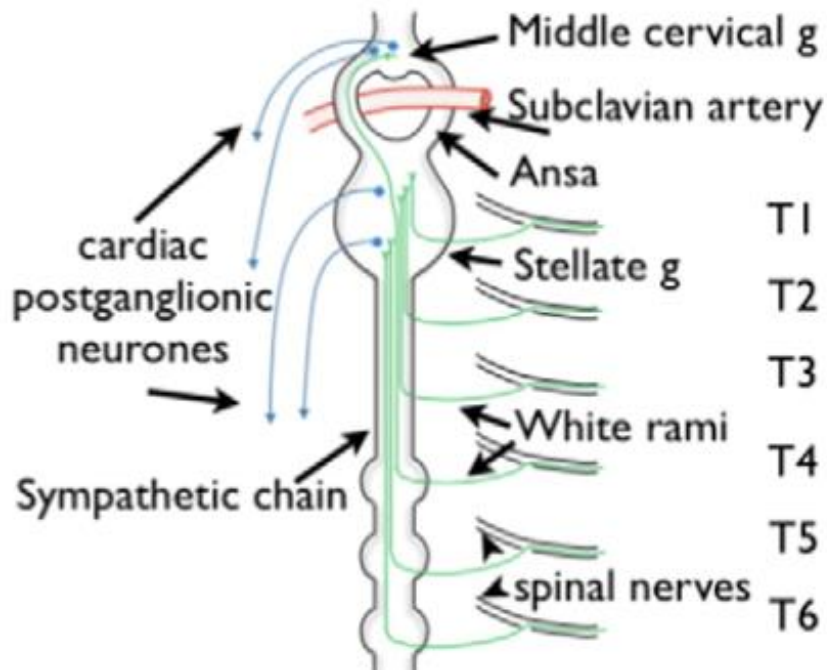


**Figure 1.7. Schematic of the upper thoracic (T1–T6);** showing the path of cardiac sympathetic preganglionic from the spinal cord via the white rami to the sympathetic chain and their synaptic connections in the stellate ganglion and via the ansa subclavian in the middle cervical ganglion. All the cardiac postganglionic neurones lie in these ganglia and project to terminate in different regions of the heart, either as separate nerves or in the vagosympathetic nerve on left and right sides (Coote and Chauhan., 2016).

The segments that contribute most to the cardiac sympathetic supply differ between and within species but mainly arise from the upper thoracic segments. This can be demonstrated experimentally by sequentially cutting the upper thoracic rami and observing the remaining signal. T1-3 are the most dominant in dogs (Kostreva et al., 1977, Norris et al., 1974, Norris et al., 1977), T3 and 4 in cats (Kamosinska et al., 1991, Kocsis and Gyimesi-Pelczer, 1998, Ninomiya et al., 1993, Szulczyk and Szulczyk, 1987), T3 in rats (Ter Horst et al., 1993, Ter Horst et al., 1996, Pracejus et al., 2015), and T1-3 in humans (Randall and McNally, 1960). A third of the 90,000 sympathetic preganglionic efferent neurones in the thoracic spinal cord arise from T1-T3 in humans (Coote, 1988). In another human study, considerable variation of thoracic sympathetic innervation was observed, however the outflows generally arose from the upper 5 thoracic segments (T1-T5)(Randall and McNally, 1960). In all of the species

studied, the upper 3 segments appear to be a key contributors to the cardiac sympathetic nerve supply. The degree of response varies according to which root is stimulated suggesting functional specificity (Norris et al., 1974). However, further investigations are required to determine whether the segmental location of the sympathetic neurones corresponds to a specific cardiac function. Transneuronal tracing has demonstrated projections to distinct regions of the dog heart (Hopkins and Armour, 1984), however thus far there is a lack of electrophysiological evidence of target specificity or selective function (Gilbey, 1997).

### **1.3.3 Cardiac postganglionic nerves**

The sympathetic postganglionic neurones mostly cumulate in the paravertebral or prevertebral ganglia which are interconnected by nerve trunks, forming the left and right sympathetic chains on each side of the vertebral column. The prevertebral ganglia including celiac, aortico-renal, superior mesenteric and inferior mesenteric (Jänig, 2006), are arranged in front of the vertebral column. White and grey rami connect the spinal nerves to the paravertebral ganglia and preganglionic neurones project through the white rami connecting to the sympathetic chains as shown in fig 1.7. The sympathetic chains converge in the stellate ganglion at the rostral end of the sympathetic trunk. The stellate ganglion is composed of the lower cervical and the most rostral thoracic paravertebral ganglia (Jänig, 2006).

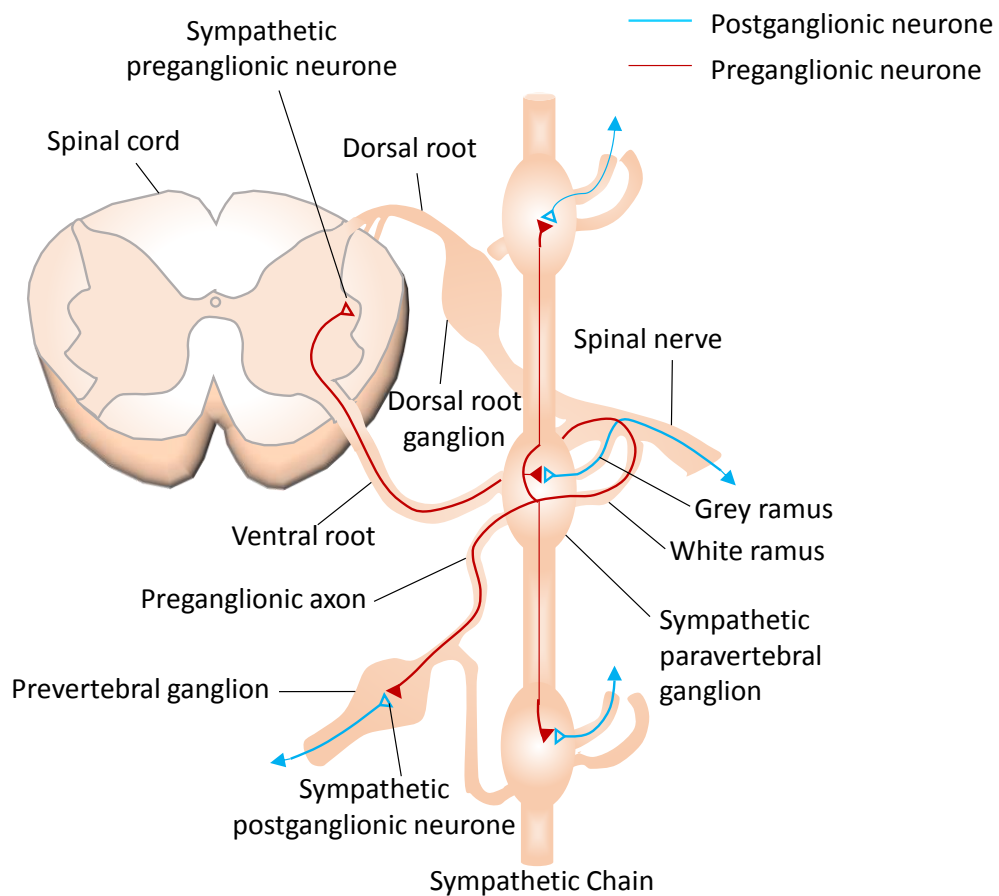


**Figure 1.8. Illustration of sympathetic preganglionic and postganglionic neurone projections**

Efferent, postganglionic fibres are generally unmyelinated C-type fibres with conduction velocities of less than 2.5 m/sec (Van Stee, 1978). The sympathetic postganglionic neurones are generally long as they are located remote from the organs they supply in comparison to parasympathetic neurones which lie closely to their target tissues. At closer proximities to the target cells, the sympathetic postganglionic axons branch multiple times and have numerous varicosities at the nerve terminals, which are essential for synthesis, inactivation, storage, release and reuptake of neurotransmitters (Jänig, 2006).

The heart is innervated by sympathetic postganglionic fibres of which the majority originate from cell bodies in the stellate ganglion or the caudal cervical ganglia (Pardini et al., 1989). They enter the heart alongside the cardiac vagal branches to form the vago-sympathetic trunk (Cooper, 1967). The sympathetic nerve

innervation of the heart is extensive and density varies between chambers of the heart and cardiac muscle layers (Dae et al., 1989, Dae and Botvinick, 1990, Wharton et al., 1990, Gordon et al., 1993, Marron et al., 1994, Chow et al., 1995, Crick et al., 1999a, Crick et al., 1999b). In addition evidence suggests that the sympathetic postganglionic neurons also interact with intrinsic cardiac plexus neuron, residing primarily on the surface of the heart, which can alter the effect of the nerve input alone and produce isolated regional changes (Smith, 1999, Armour, 2008).

#### **1.3.4 Right and left sympathetic chains**

It is suggested that the right stellate ganglion primarily innervates the anterior ventricular surfaces and the left stellate ganglion innervates the posterior (Rogers et al., 1973). This is supported by Yanowitz et al (1966) who reported that the right stellate ganglionectomy prolonged refractory periods on the anterior ventricular surface, whereas the left stellate ganglionectomy was associated with refractory period prolongation on the posterior ventricular surface.

Evidence therefore suggests there is regional and functional specificity of left and right sympathetic nerves. Stimulation of the upper thoracic roots in anaesthetised dogs showed left sympathetic stimulation had greater epicardial effects on the anterior right ventricle and posterior left ventricle, and greater endocardial effects on the basal left ventricle and posterior papillary muscle. Right sympathetic stimulation had more profound epicardial effects on the lateral left ventricular base, anterior left ventricular base and anterior left ventricular apex, and greater endocardial effects on the left ventricular base (Norris et al., 1977). In the rat, removal of either stellate ganglion indicated that left middle/inferior cervical ganglion contributes the majority of noradrenaline fibres to the right ventricle (Pardini et al., 1989). Earlier studies using electrical stimulation of the cardiac postganglionic outflow have repeatedly demonstrated that left sympathetics predominantly have an inotropic response and right sympathetic predominantly display a chronotropic response (Randall and Rohse, 1956, Randall et al., 1968b, Furnival et al., 1973, Van Stee, 1978). Thus, left sympathetics are believed to

have greater innervations of the ventricle whereas right sympathetics are thought to densely innervate the SAN.

In studies in the canine heart, Ardell et al (1988) showed evidence of significant rate changes with right sympathetic stimulation and profound decrease in AV interval with left sympathetic nerve stimulation. Some ventricular electrophysiological differences have also been reported. Prolonged Q-T intervals and increased T-wave amplitude have been observed with right stellate ganglionectomy or left stellate stimulation in anaesthetised dogs. Increased T-wave negativity was evoked by left stellate ganglionectomy or right stellate stimulation without significant Q-T interval changes (Yanowitz et al., 1966). Likewise, in anaesthetised cats, positivity of the T wave was observed with right stellate ganglion stimulation and negativity with left stellate ganglion stimulation (Rogers et al., 1973). Schwartz and Malliani (1975) suggested alternation of the T wave in long QT syndrome was associated with abrupt increases in left sympathetic discharge.

Winter et al (2012) demonstrated differential right and left sympathetic activity further in the isolated innervated rabbit heart preparation, in which stimulation of the right sympathetic chain at T2-T3 showed a greater heart rate increase than stimulation of the left sympathetic chain at T2-T3, which showed a greater change in left ventricular pressure. They also observed a greater shortening of the left ventricle basal APD and apical APD with left sympathetic chain stimulation. Alongside this, there is additional evidence to support that different branches of the cardiac postganglionic nerves effect specific regions of the heart (Szentivanyi et al., 1967, Randall et al., 1968b, Randall, 1977, Armour and Randall, 1975, Ng et al., 2009). This selective control is suspected to arise from the spinal cord. Norris et al (1974) stimulated from several sites between spinal segments T1-T5 and found a variation in the contractile force response depending on which site was stimulated. What remains unanswered is whether the cardiac sympathetic supply is functionally discrete and how the differential left and right innervation contributes to this. Although it is widely acknowledged that the sympathetic fibres have differential innervations, it is unknown whether the pathways for

acceleration and augmented contractions are distinctive. Randal & Rohse (1956) found that although right sympathetic stimulation produced both acceleration and augmentation of contraction, often left sympathetic stimulation was not accompanied by acceleration. This suggests that there are functionally distinct projections of the right and left sympathetic neurones to the heart. Further knowledge of the differential segmental projections of the left and right sympathetic neurones could have implications to understanding impairments in cardiac performance.

## **1.4 Cardiac disease and arrhythmia**

Increased sympathetic drive and parasympathetic withdrawal are associated with development of arrhythmias. Cardiac diseases that exhibit this often have neural remodelling in the form of changes in density, distribution, excitability and neurotransmitter content of autonomic nerve innervations (Ripplinger et al., 2016).

### **1.4.1 Mechanisms of arrhythmia**

A cardiac arrhythmia is an irregularity in the hearts rhythm which is caused by one of three mechanisms; enhanced or suppressed automaticity, triggered activity or re-entry (fig 1.8).

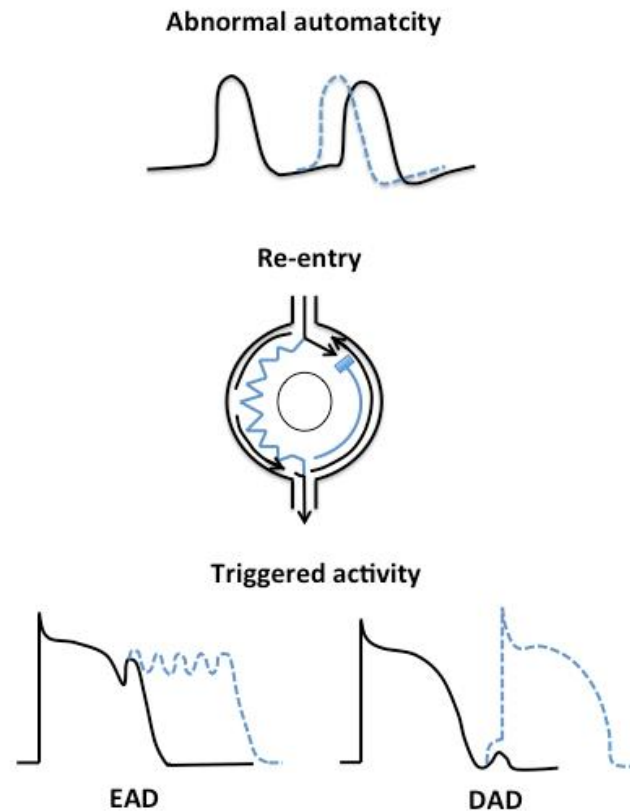


**Figure 1.9. Mechanisms of arrhythmia.** Diagrams displaying the main mechanisms of arrhythmia including abnormal automaticity, re-entry and triggered activity e.g. early afterdepolarisations (EAD) delayed afterdepolarisations (DAD). Adapted from Garratt (2001).

The automaticity of the heart is its capacity to exhibit spontaneous activity. Suppression or enhancement of automaticity can occur as a result of factors such as scarring, ischemia, electrolyte disturbances, medications and advancing age. Suppression can lead to bradycardia whereas enhancement can lead to tachycardia. This occurs as a result of impulses from elsewhere in the heart firing before or concurrently with SAN firing (Gaztanaga et al., 2012).

Triggered activity is caused by afterdepolarisations which are membrane potential oscillations occurring after an action potential, providing they reach the threshold potential. There are two types of afterdepolarisations; early afterdepolarisation (EADs) which occur during phase 2 or 3 of the action potential due to an increased net inward current and prolonged action potentials, and delayed afterdepolarisations (DADs) occurring after the repolarization phase as a result of increased intracellular  $\text{Ca}^+$  ( $[\text{Ca}^{2+}]_i$ ) (Antzelevitch and Burashnikov, 2011, Clusin, 2003). Origin of ventricular tachycardia and fibrillation usually

depends on the first "initiating" ventricular premature beat, and DAD could play such a "trigger" role (Priori et al., 1988). DADs are a likely cause of focal arrhythmias in which the SR becomes overloaded due to increases in cytosolic and SR  $\text{Ca}^{2+}$  and results in spontaneous opening of RyR's and  $\text{Ca}^{2+}$  release. The NCX begins to extrude the  $\text{Ca}^{2+}$  and therefore produces a net inward current due to  $\text{Na}^+$  influx. A large enough inward current will cause the cell membrane to depolarise, causing a triggered action potential (Pogwizd and Bers, 2004, Ripplinger et al., 2016). This must occur in several thousand cells in order to generate propagating action potential. (Xie et al., 2010, Kumar et al., 1996). Focal activity of this sort provides a mechanistic link to investigations of regional hyperinnervation and increased risk of arrhythmia (Myles et al., 2012b, Cao et al., 2000a, Cao et al., 2000b, Li et al., 2004b, Liu et al., 2003).

Re-entry is a common mechanism for arrhythmia generation (Gaztanaga et al., 2012). After activation the cells become refractory preventing immediate re-excitation. The re-entry circuit involves two pathways that join together to form a loop and a unidirectional block in one of these pathways causes slower conduction. By the time the impulse has reached the distal end of the 'fast' pathway, it has already fully recovered and so can be re-excited. The impulse therefore travels in a loop causing retrograde conduction and returns to the site of origin (Gaztanaga et al., 2012, Antzelevitch and Burashnikov, 2011). This can occur due to non-uniform sympathetic activation (i.e. as a result of hyper- or denervation) which effects gradients of repolarisation and therefore increases the likelihood of re-entrant arrhythmia (Ripplinger et al., 2016). This is common in diseased hearts with scar tissue and remodelling. Schwartz et al. (1977) reported dominant effects of the left sympathetic ganglion in increasing refractoriness and that this electrical asymmetry and inhomogeneity in cardiac excitability predisposes to re-entrant arrhythmias.

Dispersion of repolarization, ventricular conduction velocity, intracellular  $\text{Ca}^{2+}$  loading and refractoriness are all factors that affect arrhythmia susceptibility (Gaztanaga et al., 2012). Differences in the recovery properties of neighbouring cells across the heart tissue is known as dispersion of repolarisation (Han and

Moe, 1964). Heterogeneity of ion channel dispersion across the myocardium has direct effects on APD and recovery from excitation (Coronel et al., 2009). Likewise, differential innervation of sympathetic neurones also impacts recovery properties as denser innervations are reported at the base of the ventricle (Ng et al., 2009). Increased dispersion of repolarisation, which is associated with sympathetic stimulation, is proarrhythmic (Han and Moe, 1964, Kuo et al., 1983, Surawicz, 1997, Coronel et al., 2009). One suggested mechanism is, due to the large regional differences in repolarisation times, an impulse generated in a region with early repolarisation fails to propagate to the adjacent region with late repolarisation (Coronel et al., 2009). Thus, the impulse propagates around the refractory tissue and re-enters the starting region, resulting in re-entrant arrhythmias. Another suggestion is that the impulse from the region of late repolarisation propagates to the region of early repolarisation causing depolarisation and initiation of a spontaneous premature beat (phase 2 re-entry) (Lukas and Antzelevitch, 1996). Conditions that favour greater repolarisation heterogeneity are therefore more arrhythmogenic. Coronel et al (2009) reported that initiation of re-entry is not simply due to dispersion of repolarisation but also the time of arrival of the premature activation in relation to the repolarization moment of the tissue. The exact role of repolarisation heterogeneity in initiation of re-entry requires further investigations.

#### **1.4.2 APD restitution**

The three classic mechanisms of arrhythmia described cannot explain the complexity involved in the mechanisms underlying atrial and ventricular fibrillation (Ng, 2016a). Evidence from experimental studies have suggested that fibrillation is created and sustained by the property of APD restitution (Ricchio et al., 1999, Garfinkel et al., 2000, Ng et al., 2007).

The cardiac APD changes in accord with activation rate, with shorter APD's at faster heart rates and longer APD's at slower heart rates. This is known as APD restitution and is important for changes in contraction and relaxation of the heart at faster heart rates (Ng, 2016a, Ng, 2016b). APD restitution is also an important indicator of arrhythmogenesis (Karma, 1994). It is a measurement of the APD

and preceding diastolic interval (DI) and generally APD decreases monotonically as DI decreases (Weiss et al., 2006). Excessive shortening of APD and refractory periods can lead to re-entry arrhythmias and lengthening can lead to after depolarisations (Weiss et al., 2006). The maximum slope of the restitution curves generated from this data, give an indication of arrhythmia susceptibility. Steep curves (maximum slope  $>1$ ) indicate that small changes in DI lead to large changes in APD which further decreases the following DI. When the DI becomes too short to generate another action potential, this causes wavebreaks which degenerate into ventricular arrhythmia (Weiss et al., 2006). In 1968, in frog ventricular muscle strips, Nolasco and Dahlen (1968) demonstrated that the maximum slope of restitution increased when stimulus frequency increased. They also recorded the presence of alternans when slope values were  $>1$ . These alternans can result in the breakup of spiral waves into a fibrillatory state (Karma, 1993). The relationship between APD restitution and VF induction has also been studied. In canines, Riccio et al (1999) demonstrated that drugs that reduced the maximum slope of restitution also prevented induction of VF. Likewise, drugs that did not cause a reduction in maximum restitution slope did not prevent VF initiation, indicating that the kinetics of restitution is a key determinant of VF (Riccio et al., 1999). Similar findings in pig ventricles showed drugs that flattened the restitution curve, also prevented wavebreaks and induction of VF (Garfinkel et al., 2000).

The ionic basis of APD restitution is still not fully understood (Ng, 2017). A simplified model has been proposed by Franz (2003), in which it was suggested that the steepest part of the APD restitution curve is caused by the rapid recovery of APD which is mostly due to the incomplete recovery from inactivation of the  $\text{Na}^+$  channel. Asynchronous recovery of APD and sodium channel activity enhances spatial dispersion of repolarisation and causes regional variations in conduction velocity. The dynamics of a longer DI were proposed to be due to effects from the  $I_{\text{Ca,L}}$  followed by  $\text{IK}_r$  and  $\text{IK}_s$  in the later stages of repolarisation (Franz., 2003). APD shortening during APD restitution can also be explained by the incomplete reactivation of  $I_{\text{Ca,L}}$  at short coupling intervals. This leads to reduction in  $I_{\text{Ca,L}}$  (Gettes & Reuter, 1974) and incomplete deactivation of  $\text{IK}$

(Hauswirth et al., 1972). NCX currents have also been implicated, however it is suggested that all time dependent currents contributing to the action potential are likely to be involved (Janvier et al., 1997). Studies in animal models and humans have reported that sympathetic stimulation increases the maximum slope of restitution (Taggart et al., 1990, Taggart et al., 2003, Ng et al., 2007). In the isolated innervated rabbit heart preparation, Ng et al (2007) found that sympathetic stimulation via the spinal cord both steepened restitution curves and decreased the current required to initiate VF, demonstrating a causal link between APD restitution and VF threshold (VFT). In addition, heterogeneity of sympathetic innervations gives rise to heterogeneities in APD restitution (Ng et al., 2009), which could not be replicated by isoprenaline (Mantravadi et al., 2007). Associations of APD slope and heterogeneity with clinical ventricular arrhythmia and sudden cardiac death have also been demonstrated in patients (Nicolson et al., 2012). APD restitution can therefore be used a strong prognostic marker for arrhythmogenesis.

Mechanisms underlying fibrillation have also been described using the term 'rotors' which are functional re-entrant circuits (Pandit and Jalife, 2013). Rotor sites have been proposed as targets for ablation to eliminate fibrillation (Schricker et al., 2014).

It is clear that the mechanisms that underlie arrhythmia are not fully understood. It is known however that sympathetic stimulation enhances all of the described mechanisms of arrhythmia (Ng, 2016b). In order for clinical treatments to progress, further exploration into the initiation and maintenance of arrhythmia is required.

### **1.4.3 Clinical implications**

ANS dysfunction is a key factor in the progression of most cardiovascular diseases and cardiac electrophysiological abnormalities and it can occur intrinsically, extrinsically or in the higher centres (Ripplinger et al., 2016). In diseased hearts, autonomic imbalance can occur due to adverse remodelling and changes in cardiac innervation density, leading to lethal arrhythmias (Fukuda et al., 2015, Ripplinger et al., 2016). Imbalance in autonomic tone has been related

to ECG waveform abnormalities and prolonged T interval syndromes (Yanowitz et al., 1966, Ueda et al., 1964)

Due to decreases in APD, refractory periods and increases in automaticity, sympathetic nerves are central to the development of arrhythmias (Schwartz and Stone, 1982b, Malliani et al., 1980, Han and Moe, 1964). In HF, changes in sympathetic nerves have been reported including functional changes, axon growth and denervation (Fukuda et al., 2015). An increase in sympathetic efferent activity is observed and is thought to be due to abnormalities in baroreceptor signals (La Rovere et al., 1998). Dysregulation of sympathetic nerve activity in this manner can trigger arrhythmias in HF patients. Activation of the sympathetic nerves has also been shown to induce DAD's in anaesthetised cats, suggesting triggered activity as a possible mechanism (Priori et al., 1988).

Left cardiac sympathetic nerves have been shown to be arrhythmogenic and left cardiac nerve denervation (LCSD) has been demonstrated as anti-arrhythmogenic (Schwartz et al., 2004, Schwartz, 1984). Stimulation of the left sympathetic nerves has been shown to prolong Q-T intervals (Yanowitz et al., 1966), induce T wave alternans (Schwartz and Malliani, 1975) and trigger lethal arrhythmias (Armour et al., 1972, Hageman et al., 1973). Left sympathetic stimulation has also been found to elicit significantly greater EAD amplitudes that reach threshold to cause VT more often than right sympathetic stimulation, attributed to a greater release of noradrenaline in the left ventricle upon left stimulation (Ben-David and Zipes, 1988).

In Long QT syndrome (LQTS), ablation or cooling of the left stellate ganglion in anesthetized and vagotomized dogs increased VFT, whereas with the right stellate ganglion VFT was lowered (Schwartz et al., 1976a). This was observed in the absence of electrical nerve stimulation and thus was a result of resting sympathetic activity. Patients with LQTS had a lower right sympathetic activity and augmented left sympathetic activity and therefore were more at risk of developing VF during sympathetic stimulation (Schwartz et al., 1976a). This further confirms the differential effects of left and right sympathetic nerves on cardiac excitability and increases the rationale for treatment involving LCSD in

LQTS patients. Blockade of the left stellate ganglion in coronary arterial occlusion in anaesthetised dogs also displayed decreased occurrence of arrhythmias (Schwartz et al., 1976b) independent of changes in heart rate or vagal activity. Right stellate ganglion blockade increased the number of ectopic beats and episodes of ventricular tachycardia and fibrillation. This suggests left sympathetic stimulation is predominantly effective at increasing cardiac excitability. However, it is still unclear how LCSD is producing anti-arrhythmic results. Automaticity has been suggested as a likely mechanism rather than re-entry (Janse et al., 1985), however detailed investigations into the left sympathetic innervations and their role in arrhythmia generation are still very much needed.

#### **1.4.4 Neural remodelling**

Remodelling can occur as a result of nerve injury due to local hypoxia or ischemia. It involves nerve sprouting or electrophysiological changes of the nerve membrane and flow of neurotransmitter precursors. Remodelling causes hypo or hyperinnervation, greater neurotransmitter release, target cell super-sensitivity or depression of cardiac parasympathetic activity. Hyperinnervation involves increases in nerve density and commonly occurs in conditions such as MI, heart failure and hypercholesterolemia (Cao et al., 2000b, Li et al., 2004, Liu et al., 2003). Nerve sprouting has been associated with increased nerve growth factor (NGF) and addition of an NGF function-blocking antibody was reported to prevent nerve sprouting post-MI (Hasan et al., 2006). Sympathetic hyperinnervation is associated with ventricular arrhythmias and this has been evidenced in both animal models and in humans (Cao et al., 2000a, Cao et al., 2000b). Sympathetic hypoinnervation or denervation involves axon degeneration triggered by proNGF (Nykjaer et al., 2004) and is also associated with ventricular arrhythmia (Boogers et al., 2010, Fallavollita et al., 2014). It occurs in MI, diabetic neuropathy and heart failure (Gardner and Habecker, 2013, Gardner et al., 2015, Jacobson et al., 2010, Kimura et al., 2010).

As a result of denervation,  $\beta$ -AR can become upregulated or develop increased responsiveness to catecholamines (Vatner et al., 1985). This leads to localised supersensitivity and triggered activity, hence the arrhythmogenic nature of this

condition. Supersensitivity of  $\beta$ -AR has been displayed in GRK2 KO mice and thus GRK2 loss may be responsible (Raake et al., 2012). Nuclear imaging studies have reported that the degree of neural remodelling can predict risk of ventricular arrhythmia (Boogers et al., 2010), predicting cardiac arrest independent of infarct size and ejection fraction (Fallavollita et al., 2014, Ripplinger et al., 2016).

## **1.5 Clinical interventions**

As autonomic tone plays a significant role in the development of lethal arrhythmias, therapies involving modulation of the autonomic nervous system have been explored. Reducing sympathetic input and increasing parasympathetic tone provides an effective treatment for ventricular arrhythmias through therapies such as sympathetic denervation, renal denervation, vagal stimulation and baroreceptor stimulation (Ripplinger et al., 2016).

### **1.5.1 Sympathectomy**

Thoracic sympathectomy is an anti-arrhythmic therapy that involves removing one or both of the stellate ganglia (Shen and Zipes, 2014). Although this therapy has proven to be anti-arrhythmic, there are still problems associated with the removal of normal sympathetic control of the heart (Schwartz, 2010). A more targeted approach would be ideal and is becoming increasingly more feasible as knowledge of the selective function of the sympathetic outflow via each spinal segment progresses. Attempts to limit the extent and side effects of surgical intervention are being investigated in humans (Raskin et al., 2016).

In anaesthetized dogs, using a surgically targeted approach showed the possibility to remove inputs to the paravertebral chain and parts of the stellate without causing significant impairment of non-cardiac viscera supplied by the upper thoracic sympathetic nerves (Buckley et al., 2016, Wu et al., 2016). This more targeted approach is known as left cardiac sympathetic denervation (LCSD).

LCSD involves an incision at the base of the neck and surgical excision of the left stellate ganglion, together with the thoracic ganglia (T2 to T4) (Coleman et al.,

2012). It was first performed in a patient by Jonnesco in 1916 and successfully eliminated angina and ventricular arrhythmias (Jonnesco, 1921). It has since been used to effectively treat various conditions associated with lethal arrhythmias. With LCSD, the upper half of the stellate ganglion is preserved to prevent incidence of Horner's syndrome (loss of sympathetic nerve supply to the eye). The resulting reduction in catecholamine release gives antiarrhythmic effects (Schwartz, 2014) without causing post-denervation supersensitivity (Schwartz and Stone, 1982a). Importantly, LCSD is a preganglionic excision and therefore re-innervation does not arise (Wilde et al., 2008). Furthermore, myocardium contractility is not impaired after LCSD due to compensation by the right sympathetics (Schwartz and Stone, 1979). LCSD has been demonstrated to prolong ventricular refractoriness (Schwartz et al., 1977) and increase VFT (Schwartz et al., 1976a) without disruption to cardiac contractility (Schwartz and Stone, 1979). The antiarrhythmic effects of LCSD have been observed in patients and canines following MI, LQTS patients (Schwartz et al., 2004), catecholaminergic polymorphic ventricular tachycardia (CPVT) patients (Wilde et al., 2008), non-long-QT syndrome arrhythmogenic channelopathies and cardiomyopathies (Coleman et al., 2012) and patients with drug refractory ventricular arrhythmias (Bourke et al., 2010) .

The use of LCSD has been proposed for CPVT patients with drug refractory ventricular arrhythmias. CPVT arises through mutations of RYR2 (Laitinen et al., 2001, Priori et al., 2001) and calsequestrin (CASQ2) (Lahat et al., 2001) genes, resulting in intracellular  $Ca^{2+}$  overload and ventricular arrhythmias triggered by adrenergic stimulation (Priori et al., 2002). Current treatment involves use of ICD's which often deliver multiple shocks or beta blockers which do not provide full protection and can have off target effects. The use of LCSD together with ICD's and beta blockers has been suggested as most beneficial solution for minimising the arrhythmias (Wilde et al., 2008).

LQTS is a prolongation of the QT interval due to abnormalities in  $K^+$  or  $Na^+$  channels. Adrenergic stimulation in these patients can lead to life threatening arrhythmias. LCSD has been proposed as effective treatment for LQTS for those

who are refractory to beta blockers alone. A significant reduction in the incidence of aborted cardiac arrest and syncope was reported in high-risk LQTS patients who had undergone LCSD (Schwartz et al., 2004). However, several studies have indicated that although LCSD is effective at reducing occurrence of cardiac events, it did not eliminate them completely during long term follow up (Schwartz et al., 2004).

Heightened sympathetic activity, for example during exercise or stress, is often the trigger of the cardiac events experienced in these conditions. This was investigated further in dogs during exercise (Schwartz and Stone, 1979). Removal of the right stellate ganglion increased the occurrence of arrhythmia during exercise with 86% of dogs experiencing arrhythmia. Furthermore, cardiac performance was reduced after the right stellate ganglion was removed but increased after left stellate ganglion removal. Similar results were reported in patients affected by Raynaud's syndrome who were treated with unilateral stellectomy (Austoni et al., 1979).

In contrast, Vaseghi et al (2014) suggested that bilateral cardiac sympathetic denervation (CSD), which involves denervation of both the left and right sympathetics, is more beneficial than LCSD in patients with ventricular tachycardia (VT) storm. They found that patients that had undergone bilateral CSD had beneficial effects that lasted beyond the acute hospitalisation period and survival free of ICD shocks was more likely. They suggested that this was due to significant ventricular innervation from the right sympathetic nerve still remaining with LCSD alone. However, bilateral CSD patients experienced side effects such as extreme sweating in the lower extremities, Horner's syndrome and significant skin sensitivities on parts of their chest, back, shoulders and/or arms e.g. numbness, neuropathic pain, tingling (Vaseghi et al., 2014, Ajjola et al., 2012). In addition, due to nature of the study the patients were not randomised. They also showed that both LCSD and bilateral CSD were equally successful at significantly reducing ICD shocks. Other studies have shown that bilateral stellectomy resulted in fatigue during exercise (Hodes, 1939) and impairment in

control of heart rate (Brouha et al., 1936, Samaan, 1935, Schwartz and Stone, 1979).

Denervation supersensitivity to noradrenaline has also been reported in studies using complete bilateral denervation (Cooper, 1965) and those using extensive unilateral stimulation (Priola, 1969). Denervation supersensitivity is an increase in sensitivity to chemical mediators post denervation. One of the reasons for this is increases in the number of receptors (Schwartz and Stone, 1982a). Supersensitivity results in the onset of arrhythmias in both animals (Fleming, 1962, Westfall and Fleming, 1968) and humans (Lown et al., 1961). Priola et al (1969) showed that unilateral denervation in the canine heart elicited supersensitivity however the technique used eliminated all autonomic fibres (both sympathetic and parasympathetic divisions). LCSD on the other hand provides only partial denervation. Moreover, LCSD does not result in depletion of catecholamine stores; a likely cause of denervation supersensitivity (Donald, 1974, Goodall and Kirshner, 1956, Hertting and Schiefthaler, 1964, Hikosaka, 1966). Left denervation also causes less noradrenaline depletion than right denervation, however studies have shown supersensitivity can occur in the absence of catecholamine depletion (Priola, 1969, Kirpekar et al., 1962, Trendelenburg and Weiner, 1962). In 1982, Schwartz et al investigated supersensitivity to noradrenaline in the dog heart after LCSD and reported denervation supersensitivity is not induced and there was a significant decrease in the arrhythmias generated by noradrenaline injection. Thus, LCSD is still an important potential treatment worth exploring for patients at high risk of life-threatening arrhythmias.

Lidocaine has been used clinically to pharmacologically block the left stellate ganglion in order to deduce the potential effectiveness of LCSD in the patient. Successful results are confirmed by the presence of Horner's syndrome. However, this indicates that lidocaine has reached the upper regions but one cannot not assume from this that it has reached the lower regions and it therefore does not accurately reflect LCSD (Schwartz, 2010). Schwartz (2010) suggested that LCSD should be considered before ICD placement in patients on beta

blockers with breakthrough syncope. It has also been suggested to conduct both ICD placement and LCSD to prevent sudden death and the likelihood of electrical storms and multiple shocks (Schwartz, 2010).

LCSD has however been associated with side effects due to the removal of sympathetic supply to the forelimbs and head causing palmer and facial anhidrosis, loss of vasomotion, and poorer visual and salivary control. Other less frequent side effects include paresthesia and bursts of pain in the left arm or shoulder (Schwartz, 1984). These however usually reduce after a few days.

### **1.5.2 Spinal cord stimulation**

Spinal cord stimulation involves a non-focused stimulation of the dorsal spinal cord which has been found to suppress atrial fibrillation (Wang et al., 2016), reduce symptoms of angina pectoris (Foreman et al., 2000), reduce ventricular arrhythmias (Grimaldi et al., 2012), remove cardiac pain (Hautvast et al., 1998) and partially restore ventricular function in HF (Tse et al., 2015). One electrode is placed in the midline and the other laterally on the left side of the spinal cord and high frequency electrical pulses stimulate T1-T4 of the spinal cord. Smith et al (2016), suggested that spinal cord stimulation causes remodelling of the membrane and synaptic properties of autonomic neurons. After several weeks of dorsal spinal cord stimulation, cardiac parasympathetic activity was augmented (Olgin et al., 2002, Smith et al., 2016). Spinal cord stimulation has been found to increase central vagal tone and decrease sympathetic tone (Ripplinger et al., 2016). It has been suggested to reduce sympathetic drive induced by pacing, suppress activity of intrinsic sympathetic afferents and suppress atrial fibrillation (AF) inducibility (Mannheimer et al., 1993, Lopshire et al., 2009). Spinal cord stimulation has possible application in protection against ischemic ventricular arrhythmias (Ripplinger et al., 2016), but again further investigations are required.

It is suggested that inhibition of sympathetic remodelling is a likely explanation for the effects of dorsal spinal cord stimulation (Ajijola et al., 2013, Smith et al., 2016, Wang et al., 2016). Another explanation is modification of the changes caused by remodelling as observed in rabbits where dorsal spinal stimulation

reduced the size of infarcts by increasing catecholamine and galanin release (Southerland et al., 2007). There is still much that is unexplained and it is unclear why such a high stimulation frequency (50hz) is required.

### **1.5.3 Thoracic epidural anaesthesia**

Thoracic epidural anaesthesia (TEA) is antiarrhythmic and has been beneficial in the management of electrical storm in patients with ischemic cardiomyopathy (Mahajan et al., 2005). It has been suggested to reduce both afferent and efferent sympathetic nerve impulses to the heart (Bourke et al., 2010) and lengthen repolarisation and refractory periods (Meissner et al., 2001). However, LCSD was found to be a more effective treatment than TEA with longer lasting effects (Bourke et al., 2010).

### **1.5.4 Other methods**

Carotid baroreceptor stimulation has also been suggested as a method to modulate sympathetic imbalance (Ripplinger et al., 2016). Low-level carotid baroreceptor stimulation inhibited ganglionic plexus activity and thus suppressed AF inducibility (Liao et al., 2015). This is in contrast to high-level carotid baroreceptor stimulation which reportedly increased AF inducibility (Linz et al., 2013b).

Another suggested method is renal denervation, which resulted in a reduction in heart rate, reduction in AV conduction velocity and shortening of AF episodes in pigs (Linz et al., 2013a), and resulted in a 37% reduction in firing of single sympathetic nerves (Hering et al., 2013).

Inhibition or suppression of sympathetic activity to treat ventricular arrhythmias appears to be producing promising results and hence warrants further investigations into differential left and right sympathetic innervations and effects on cardiac electrophysiology and arrhythmia. Clearly, more information into the regionally and functionally discrete innervations of sympathetic neurones is essential for establishing a more targeted clinical intervention. This is a clinically

significant question as currently left or bilateral stellectomy is being utilized for treatment of ventricular arrhythmia (Schwartz et al., 2004, Wilde et al., 2008, Bourke et al., 2010, Vaseghi et al., 2012b).

## **1.6 Summary**

More knowledge of the anatomy and physiology of cardiac nerves is required in order for this to be translated into clinical interventions and the advancement of surgical therapies. Many of the previous studies on differential right and left sympathetic control were conducted in open chested dogs and cats in which it is difficult to assess physiological significance due to the unphysiological state (Van Stee, 1978). The novel adaptation of the innervated rabbit preparation used by Winter et al (2012) is therefore an ideal model to explore this further. It is necessary to establish the regional and functional selectivity of the sympathetic preganglionic neurones to improve the understanding of spinal sympathetic control of the heart. Furthermore, the mechanisms underlying the greater proarrhythmic effects of left sympathetic neurons are still unknown despite their major contribution to the ventricular arrhythmias leading to SCD. In conclusion, there are still necessary further insights to explore including improved understandings of the innervation pathways of the sympathetic nerves and how this can be exploited in order to develop arrhythmia prevention therapies.

## **Chapter 2**

### **Thesis aims**

## 2 Aims

Sympathetic activity has a significant influence over the development and maintenance of arrhythmias and is often upregulated in cardiac disease. It therefore poses as a target for treatment, however a better understanding of the regional and functional selectivity of the sympathetic nerves is required for clinical treatments to advance. Functional selectivity exists between the right and left sympathetic neurones, with left sympathetics proposed to be proarrhythmic. Detailed investigations of the differential right-left sympathetic innervations and effects on ventricular electrophysiology are lacking.

This study aims to investigate the differential effects of the right and left sympathetic chains using a novel adaptation of the innervated isolated rabbit heart preparation. Specifically, effects on ventricular electrophysiology will be examined by measuring effects on ventriculo-atrial conduction, effective refractory period, electrical restitution and ventricular fibrillation threshold.

Secondly, studies have shown a regional and functional selectivity of cardiac postganglionic neurones indicating there might exist a similar heterogeneity in the spinal segmental preganglionic neurones. This physiologically and clinically important characteristic has not yet been shown and the present study aims to investigate this by stimulating the sympathetic chains at several spinal segmental levels between T1-T6, and measuring effects on functional parameters and ventricular electrophysiology.

Finally, by optically mapping action potentials over multiple sites, this study will also investigate the regional differences in ventricular electrophysiology during sympathetic stimulation and sequential removal of the sympathetic chains, in order to gauge an understanding of their selective innervations and the mechanisms underlying the anti-arrhythmic effects of stellectomy.

## **Chapter 3**

### **Methods**

## **3 Methods**

### **3.1 Animal model**

New Zealand White rabbits (male, 2.0-3.2Kg) were used for these experiments as rabbits have cardiac action potentials that are physiologically similar to humans and have similar electrophysiological properties. Expression of cardiac ion channels varies between species and affects the ventricular action potential morphology. For example, rats and mice present a triangular action potential morphology, lacking a defined plateau phase, due to greater expression of  $I_{TO}$  and thus a rapid repolarisation and a significantly shorter APD (Varro et al., 1993). The  $Ca^{2+}$  cycling in rats is also different in that  $Ca^{2+}$  removal is predominantly by SERCA as opposed to NCX (Hasenfuss, 1998). Larger animals including guinea pigs, rabbits and dogs have a dome like shaped action potential and are therefore more representative of a human action potential. Rabbit action potentials have a prominent phase 1 and  $I_{TO}$  expression, unlike guinea pigs. Rabbit myocytes have also been found to express inward rectifier currents and delayed rectifier currents (Varro et al., 1993). Hence, the rabbit model is ideal for investigating cardiac electrophysiology in this study.

All procedures conformed to the ethical guidelines in the Animal Scientific Procedure Act 1986 (ASPA), in accordance with Guide for the Care and Use of Laboratory Animals published by the US National Institute of Health (NIH Publication No. 85-23, revised 1985), and followed the criteria of the EU legislation on the protection of animals used for scientific purposes (Directive 2010/63/EU, 2010).

### **3.2 The dual innervated isolated heart preparation**

The Langendorff heart preparation involves perfusion via the aorta which closes the aortic valve and allows the perfusate to enter the coronary vasculature to maintain cardiac function. It was first pioneered in 1895 (Langendorff, 1895) and has since been used in numerous whole heart studies in various species (Bell et al., 2011). Ng et al in 2001, developed a novel adaptation of the Langendorff preparation; the dual innervated isolated rabbit heart preparation with intact

autonomic innervation. This allows for direct nerve stimulation which is important because experimental use of catecholamines to mimic nerve activity is limited as the heterogeneous distribution of activity from nerve stimulation cannot be adequately represented. This preparation also overcomes the limitations of *in vivo* studies as it is not confounded by the influences of haemodynamic reflexes and circulating catecholamines and hence was used in this study.

Rabbits were sedated with Sedator (Medetomidine Hydrochloride, 0.2 ml/kg, Dechra, UK), Ketaset (Ketamine, 0.15ml/kg, Fort Dodge, UK), and Torbugesic (Butorphanol, 0.01ml/kg, Fort Dodge, UK) via subcutaneous injection, with anesthesia maintained using intravenous, bolus injections of Propofol (10mg/ml, Zoetis, London, UK). The rabbits were deeply sedated after 5-10 minutes, which was confirmed by lack of the pedal and corneal reflex, and were placed onto the surgery table. The ear vein was cannulated with an IF-butterfly infusion needle from which the propofol was administered. The rabbit's limbs were then restrained and its hair clipped from the anterior torso.

After intravenous administration of 1ml Heparin (1000 IU, Wockhardt UK Ltd, UK) via the ear vein to prevent coagulation and thromboembolism, a midline cervical incision was made from the thoracic region to the sternum. Layers of fat and the superficial muscle were then dissected until the trachea was located. After further blunt dissection, the trachea was isolated and intubated with a 5mm diameter plastic tube, and then secured with silk sutures (size 0-0, Harvard apparatus, UK) to enable ventilation. The rate of ventilation, maintained via a small animal ventilator (Harvard Apparatus Ltd, Edenbridge, Kent, UK; O<sub>2</sub> –air mixture), was 50-60 breaths/min on a volume controlled mode delivering about 15 cc of air/cycle. The carotid arteries were then located on both sides and surrounding tissues dissected before they were tied off with silk sutures.

Lateral incisions were made at the level of the lower intercostal spaces to expose the ribcage. In order to expose the subclavian vessels, the pectoral muscles were subsequently dissected. Once exposed, each of the subclavian vessels were tied off individually with silk sutures and cut. The jugular vein was also identified and ligated as were the sternocleidomastoid muscles, taking care not to damage the

vagus nerves lying beneath. The intercostal vascular bundle located below the trapezius muscle, although only containing one small artery and several smaller vessels, was also ligated to prevent decreases in perfusion pressure. Animals were then heparinized (1000 IU, Wockhardt UK Ltd, UK) and euthanized with an overdose of Pentoject (Pentobarbitone sodium, 111 ml/kg, Animalcare Ltd, UK) via the ear vein. Death was confirmed by the absence of respiration and termination of circulation. Ventilation was switched off and incisions were made to open up the thoracic cavity. The anterior portion of the ribcage was removed, the pericardium was cut and the mammary arteries were tied off with silk sutures. To keep the heart at a low temperature and therefore reduce metabolic rate, ice-cold Tyrode solution was applied to the heart. The lower thoracic portion of the descending aorta was located, connective tissues removed and then it was cannulated with a 5mm plastic tube. The pulmonary artery was cut and the heart was then flushed with ice-cold Tyrode solution via the cannula in the aorta. Following this, the vertebral column was dissected at the 12<sup>th</sup> thoracic vertebra and 1<sup>st</sup> cervical vertebra and surrounding tissues were dissected to separate the preparation. Dissection at this level ensures there is no brain stem activity and removes the influence of afferent inputs and central modulation of the autonomic nervous system. The preparation was then mounted on to a platform on the perfusion rig and perfused with warm Tyrode solution.

### **3.2.1 Langendorff perfusion**

The heart was perfused with Tyrode solution (37°C, pH of 7.4 maintained by bubbling with 95% O<sub>2</sub>/5% CO<sub>2</sub>) via the descending aorta, consisting of Na<sup>+</sup> 138.0, K<sup>+</sup> 4.0, Ca<sup>2+</sup> 1.8, Mg<sup>2+</sup> 1.0, HCO<sub>3</sub><sup>-</sup> 24, H<sub>2</sub>PO<sub>4</sub><sup>-</sup> 0.4, Cl<sup>-</sup> 124, Glucose 11 (mM) at a flow rate of 100ml/min via a Gilson minipulse 3 peristaltic pump (Anachem, Luton, UK). This allowed for retrograde perfusion, forcing the aortic valve shut and Tyrode solution into the coronary arteries. The temperature of the Tyrode solution was maintained by water baths and, once in the perfusion system, heat loss was prevented by supplying heated water to water-jackets in the glassware. The perfusion system was primed with Tyrode solution before the preparation was mounted and it was important to ensure there were no air bubbles in system to

prevent embolism. The lungs and hilar vessels were tied off to prevent entry of air into the heart. The Thebesian venous effluent was drained from the left ventricle using a 1-2mm wide catheter.

### **3.2.2 Haemodynamics**

Certain functional parameters of the heart were assessed in order to monitor the condition and stability of the heart. Two pressure transducers (MLT0380/D ADInstruments Ltd, Charlgrove, UK) were removed of all air bubbles and calibrated using a sphygmomanometer at the start of each experiment. One transducer was connected in series to the aortic cannula used to measure the perfusion pressure (PP) and the other was attached to a fluid filled latex balloon inserted through the left atrium into the ventricle to measure the left ventricular pressure (LVP). When inserting the balloon, the perfusion flow rate was reduced to 50% and the preparation was cooled with cold Tyrode solution in order to reduce heart rate and contraction and thus limit damage and entrance of air bubbles. The balloon was inflated with distilled water to reach an end diastolic pressure of 0-5mmHg. Heart rate was calculated using cyclic measurements from the LVP. Hook electrodes are attached to the right atria in order the measure the atrial electrogram. This enabled measurement of the retrograde ventriculo-atrial conduction by measuring the delay from the right ventricular pacing spike the atrial electrogram. The final set up is displayed in fig 3.1.

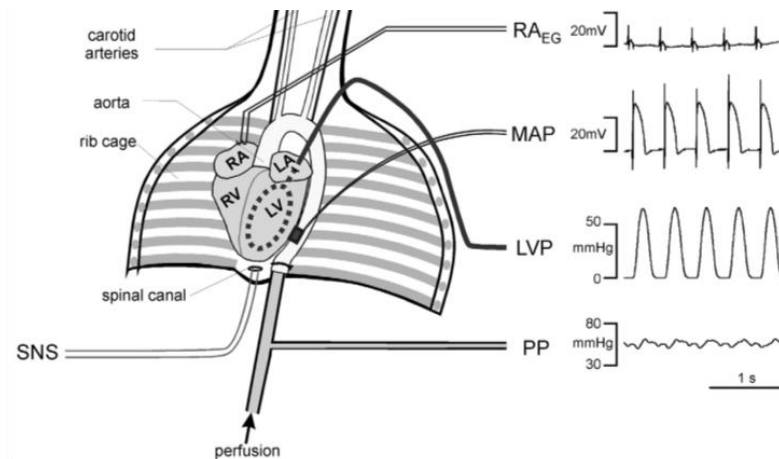


**Figure 3.1. The dual innervated isolated rabbit heart preparation.** Diagrammatic representation of the dual innervated isolated rabbit heart preparation. Tyrode solution is perfused via the cannula at 100ml/min. The pacing electrode is inserted into the right ventricle and allows pacing of the heart via a current stimulator (RA<sub>EG</sub>). The LVP balloon is inserted into the left ventricle and gives a measure of the left ventricular pressure and also a calculation of heart rate. The MAP electrodes allow recordings of monophasic action potentials from the left ventricular epicardial surface at basal and apical sites (LA, left atrium; LV, left ventricle; RA, right atrium; PP, aortic perfusion pressure. Adapted from Ng et al, 2001)

### 3.3 Cardiac electrophysiology and pacing

#### 3.3.1 Ventricular pacing

A pacing catheter (ADInstruments Ltd, Chalgrove, UK) was inserted into the right ventricle (fig 3.1) which delivers a current to the heart at double the current of the diastolic pacing threshold (to ensure capture of ventricles) using a constant current stimulator. The pacing protocols used included constant pacing where the heart is paced at a steady state at a cycle length (CL) of 240 ms (250bpm). This CL was chosen as it is above the range of the rabbits average heart rate (120-150bpm at rest) to ensure stable pacing. Action potential restitution and ventricular fibrillation pacing protocols were used as they serve as an important predictor of arrhythmogenesis.

### 3.3.2 Monophasic action potentials

Monophasic action potentials (MAP) are representative of the repolarization time course of transmembrane action potentials (Franz, 1999). They were recorded extracellularly from the left ventricular epicardial surface of the heart at the base and apex, by pressing two MAP electrodes (Harvard Apparatus Ltd, Holliston, Massachusetts, US. Model number 73-0150) gently on the surface. The myocardium cells directly below the electrode become depolarized to -30 to -20mV due to the pressure exerted. These cells are unexcitable due to inactivated  $\text{Na}^+$  channels, whereas the surrounding cells activate as normal. This gives rise to a time-varying electrical gradient allowing current flow between the unexcitable and excitable cells (Franz, 1999) as shown in fig 3.2.

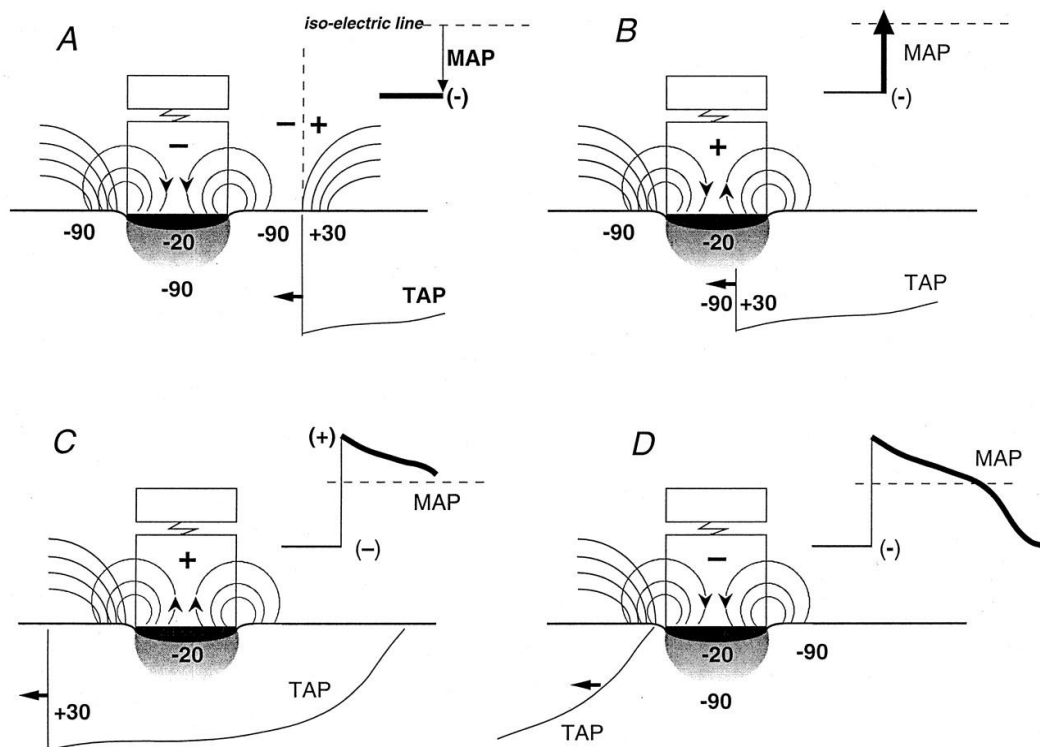


**Figure 3.2. Diagram illustrating the generation of MAP recordings by contact electrodes.** (A) Electrical diastole (late). Cells beneath the electrode are depolarised (-20mV) and unexcitable due to the pressure it exerts. Surrounding cells have a potential of -90mV and so current flows from these cells to the depolarised cells. This forms the base of the MAP recording. (B) Electrical systole (early). An action potential arrives carrying a potential of +30mV. There is a change in current flow and the MAP upstroke is recorded. (C) Electrical systole (mid). There is a gradual repolarisation and the plateau phase is observed on the MAP recording. (D) Electrical diastole (end). Potentials become repolarised, returning to their pre-existing states and the cycle is complete. A completed MAP recording is observed (Franz, 1999).

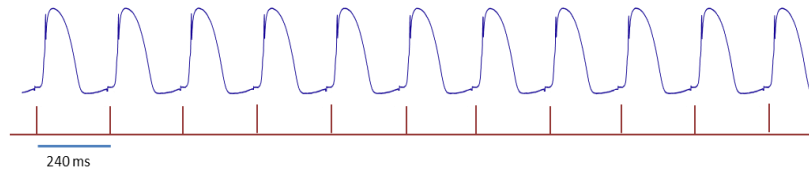
The MAP signal does however differ from the intracellular action potential as it is not representative of the absolute voltage, has a slower phase 0 upstroke and represents an averaged signal from a group of cells over an area. Care must also be taken when placing the MAP electrodes because if the pressure is too great then this can cause ischemia in the cells directly beneath it. MAP signals do however accurately represent the onset of depolarisation and repolarisation phase (Hoffman et al., 1959) and have the advantage of being able to record from intact beating hearts.

### **3.3.3 Restitution protocol**

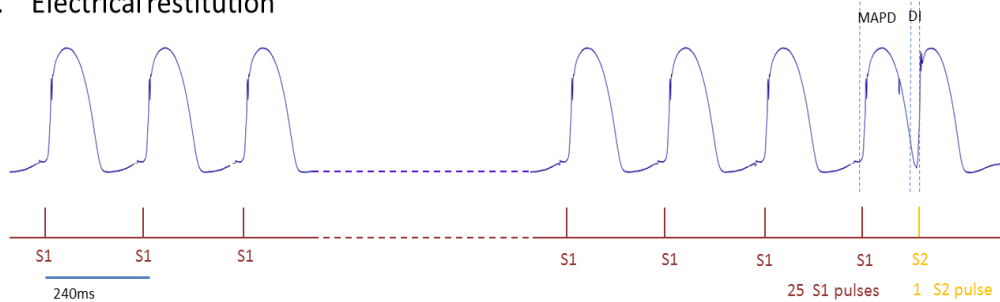
The restitution protocol used consisted of pacing at a CL of 240 ms for 25 S1 drive train beats, followed by a single extra stimulus (S2). S2 had an initial CL of 240 ms which was decreased in increments of 10 ms until an S2 CL of 200ms was reached, and then it was decreased in 5 ms increments until the effective refractory period (ERP) was reached (fig 3.3). The ERP is defined as the longest S1-S2 interval that fails to capture the S2 beat.

These measurements allow construction of APD restitution curves allowing arrhythmia susceptibility to be measured from the slope of the curve. This was produced by plotting S2 MAPD<sub>90</sub> vs. DI (DI = interval between the S1-and S2-MAP signals minus S1-MAPD<sub>90</sub>). APD was identified from time of activation ( $T_{act}$ ) to 90% of repolarization (MAPD<sub>90</sub>) using the programme NewMap (Francis Burton, Glasgow University, UK). Using Microcal Origin (v 6.0, Origin, San Diego, CA, US), the data were fitted to an exponential curve using the formula  $MAPD_{90} = \text{maximum } MAPD_{90}[1 - e^{-DI/\tau}]$  where  $\tau$ =time constant and the maximum slope of the curve ( $RT_{maxSlope}$ ) was acquired by measuring the first derivative.

### 1. Constant pacing



### 2. Electrical restitution



### 3. Ventricular Fibrillation Threshold

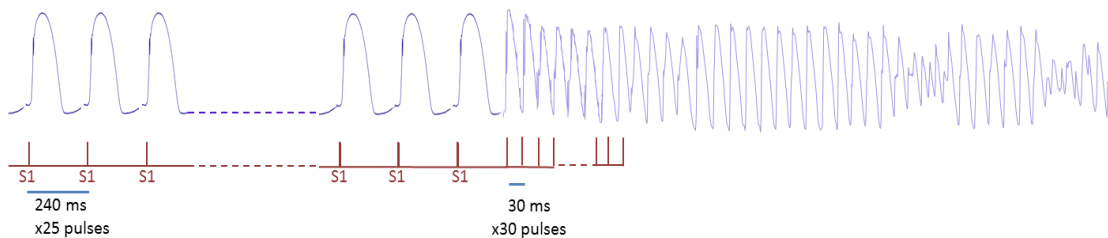


**Figure 3.3. Pacing protocols.** (a) Constant pacing protocol. Involves pacing the heart at a steady state at a cycle length of 240 ms (b) Electrical restitution protocol. The heart is paced at 240 ms for 25 pulses (S1). Following this an extrastimulus is applied (S2). The S1-S2 interval initially has a 240 ms cycle length and then this is decreased in 10 ms increments until 200 ms is reached. From then S1-S2 interval is decreased in 5 ms intervals until ERP is reached. (c) Ventricular fibrillation threshold protocol. The heart is paced with 25 pulses at 240 ms cycle length followed by burst pacing with 30 pulses with 30ms cycle length. This is repeated and current is increased each time from 0.5 mA in 0.5 mA increments until VF is induced.

#### 3.3.4 Ventricular fibrillation threshold protocol

The heart is paced with 25 pulses at 240 ms cycle length followed by burst pacing with 30 pulses with 30ms cycle length. This is repeated and current is increased each time from 0.5 mA in 0.5 mA increments until VF is induced (fig 3.3). The minimum current that induces VF is measured as ventricular fibrillation threshold (VFT).

### **3.3.5 Data recording and statistical analysis**

The Powerlab 16/30 system (AD Instruments Ltd, Chalgrove, UK) was used to record the signals, which were processed at 2 kHz. Data analysis was performed using both Origin Lab software (v.2015; OriginLab, Northampton, MA, USA) and GraphPad Prism 6 software (v6.04, GraphPad, CA, USA). Data are Mean  $\pm$  standard error of mean (SEM). Data were compared using one way ANOVA with a Bonferroni post-test and paired t-tests for left versus right sympathetic stimulation studies. Two way ANOVA with a Bonferroni post-test was used for comparing left and right sympathetic stimulation at different spinal segmental levels. Statistical significance was taken at 5% level ( $p < 0.05$ ).

## **3.4 Optical mapping technique**

Optical mapping allows us to study the action potentials across the surface of the heart with adequate spatial and temporal resolution. This will enable a greater understanding of regional changes in ventricular APD from sympathetic stimulation whereas the MAP electrodes record from only two discrete sites of the left ventricle at the base and apex.

### **3.4.1 Principles of optical mapping**

Commonly, microelectrode techniques are used to measure intracellular membrane potentials however these are limited as they are unable to record from multiple cells simultaneously or intact organs (Efimov et al., 2004). In 1968, the first optical recordings of membrane potential were obtained although there was a poor signal to noise ratio (Cohen et al., 1968). Many dyes were screened in order to improve signals (Cohen and Salzberg, 1978). Salama and Morad (1976) recorded optical action potentials from mammalian hearts. They used the dye Merocyanine 540, which bound to the cardiac membrane without causing detrimental changes and when excited at 540nm, allowed measurement of membrane potential. Optical mapping techniques have advanced with availability

of better dyes and scanning equipment, and are used to study the electrophysiological measurements of many tissues including the heart and neurones.

The ideal optical mapping system should provide high spatial and temporal resolution, high signal to noise ratio and limited side effects such as photobleaching. The major components of a cardiac optical mapping system are; the heart stained with a voltage or calcium sensitive dye, the optics system which filters and focuses the light before the emitted fluorescent light is collected by photodetectors, and the photodetector which measures the emitted fluorescent light (Attin and Clusin, 2009).

### **3.4.2 Voltage sensitive dyes**

Voltage sensitive dyes bind to the cardiac cell membrane with high affinity and fluoresce light in direct proportion to transmembrane voltage (Arora et al., 2003). In this way the dyes are able to act as highly localised transducers, in which change in membrane potential is transformed into change in fluorescent signal intensity. The emission spectra represents the range of wavelengths of light emitted by voltage sensitive dyes or any given constant excitation light intensity and wavelength. Changes in the membrane potential result in changes in the emission spectra for the voltage sensitive dye molecule (fig 3.4).

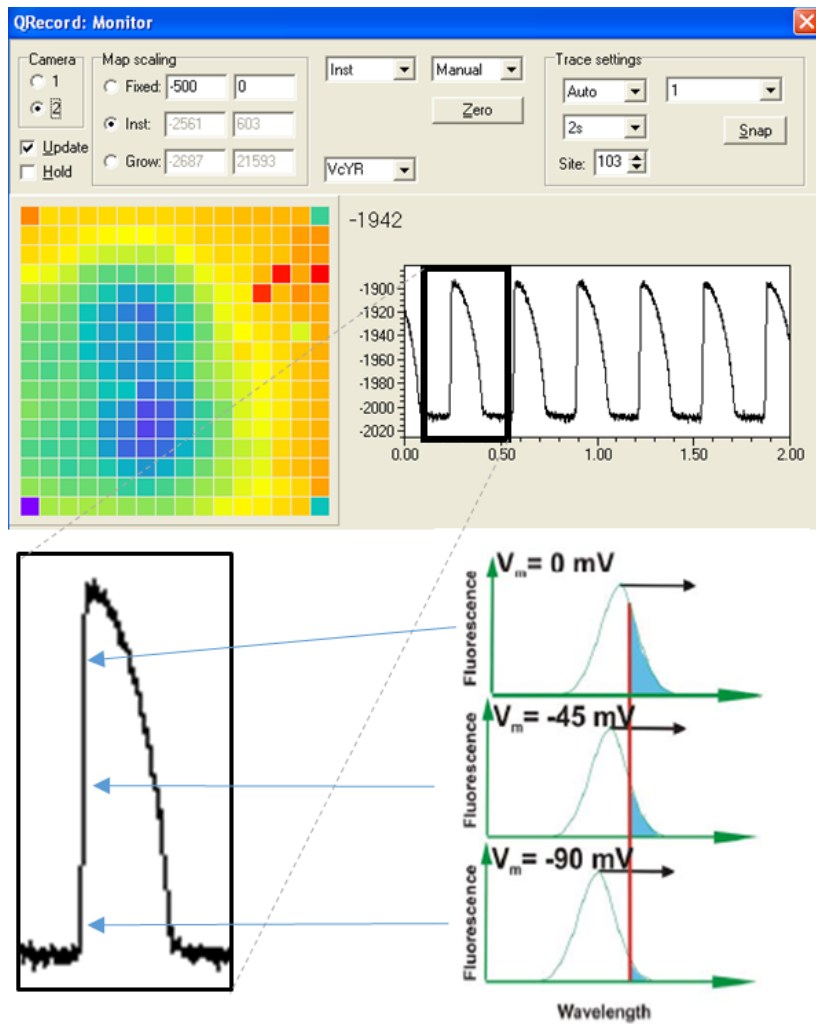


**Figure 3.4. Voltage-dependent changes in emission spectra of a typical electrochromic dye.** Changes in membrane-voltage correspond with changes in the emission spectrum of the dye molecule. Developed from Rosenbaum (2001).

As shown in fig 3.5, the filter allows only light above a specific wavelength to pass through. As the membrane potential changes, the amount of light that passes through the filter varies thus producing the optical action potential. It is important to note that only relative potential change is recorded not absolute voltage. It is possible that at low magnifications, a decrease in the rate of rise of the optical action potential upstroke may occur. This is due to multicellular spatial averaging of the transmembrane potential (Girouard et al., 1996). At higher magnifications, the rate of rise of the optical action potential is closer to that measured from a

single cell (Laurita and Singal, 2001). In this way the optical action potential is in fact an average potential from small group of neighbouring cells.

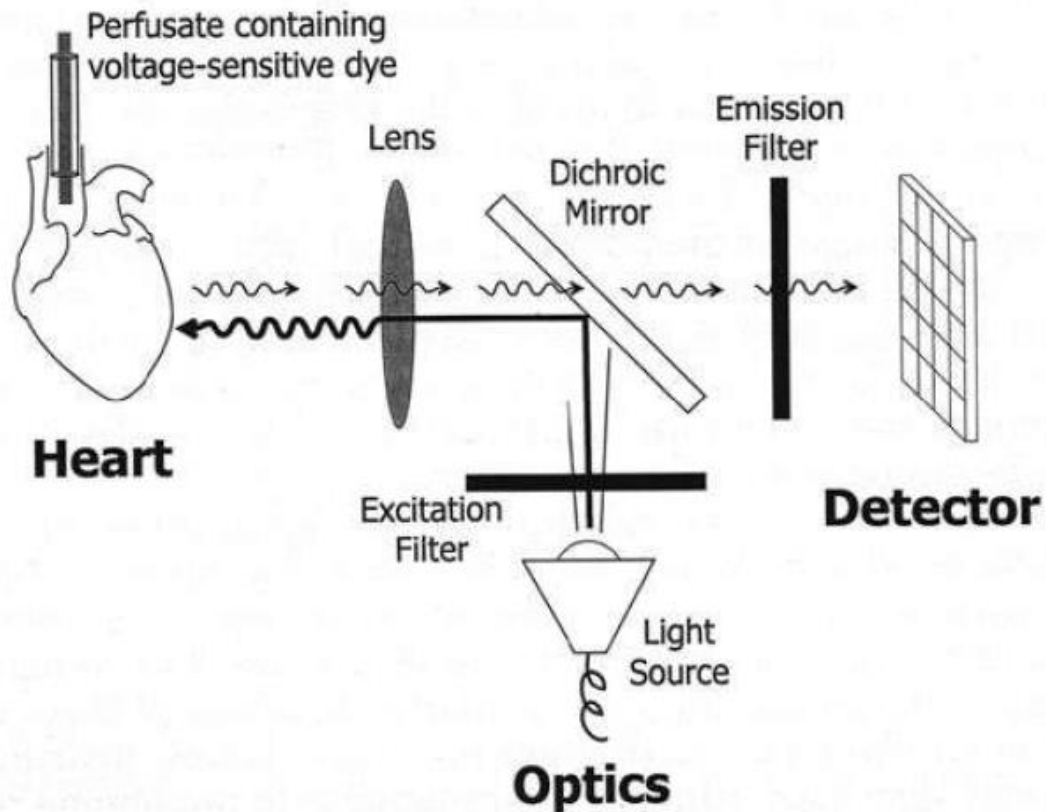


**Figure 3.5. Major components of optical mapping apparatus.** Selected wavelengths of light from the light source pass through the excitation filter. The dichroic mirror then reflects selected wavelengths onto the heart preparation. This excitation light that reaches the heart causes cell bound voltage sensitive dye molecules to fluoresce light in proportion to the membrane potential. The emitted light is of a longer wavelength and passes through the dichroic mirror, is filtered and then received by the detector (Rosenbaum, 2001).

In this set of experiments, the styryl dye Di-4-ANEPPS (fig 3.6) was used to study optical action potentials from the rabbit whole heart. Fig 3.7 illustrates the mechanism of Di-4-ANNEPS better known as the principle of electrochromism. After binding to the cardiac cell membrane, the dye molecule exhibits a charge shift from the ground state to the excited state as electrons shift from their stable valance band to higher energy bands in response to excitation light of a specific wavelength. Fluorescence occurs as the excited state returns to the ground state

and a photon is emitted. The photon is usually of a lower energy and longer wavelength than the excitation light (Rosenbaum, 2001) and its wavelength is determined by the change in molecular energy when changing from the excitation state to the ground state. The intensity of fluorescence is directly proportional to the transmembrane potential.

Di-4-ANNEPS was chosen for this study as it holds many advantages over other voltage sensitive dyes; large changes in fractional fluorescence during the cardiac action potential (8-15%), low toxicity and photobleaching, 2-4 hours of stable signal before re-loading of the dye is required (Loew et al., 1992).

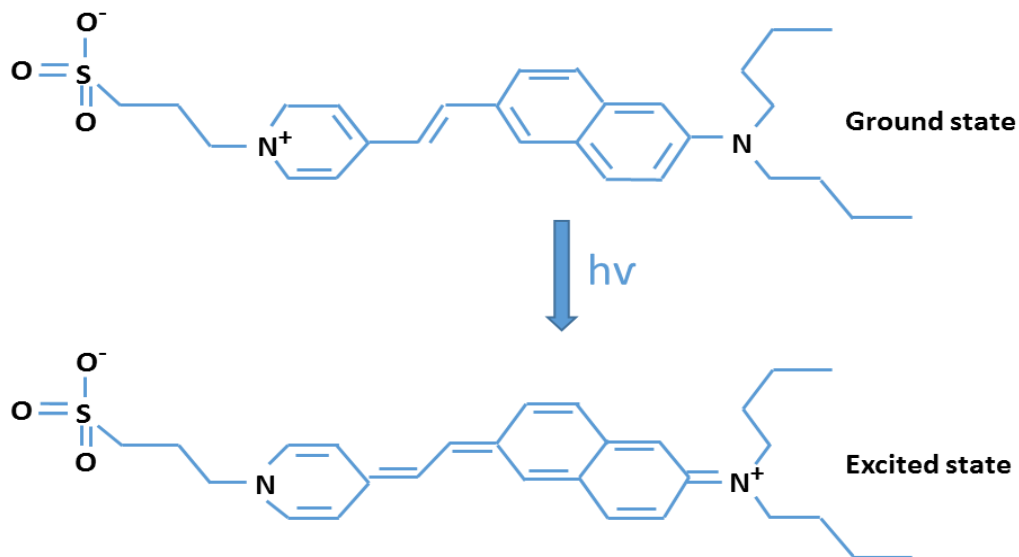


**Figure 3.6. Ultrastructural changes in the Di-4-ANNEPS molecule.** Charge shift of Di-4-ANNEPS from the ground state to the excited state as electrons shift from their stable valance band to higher energy bands in response to excitation light of a specific wavelength.  $h\nu$ : light of excitation wavelength

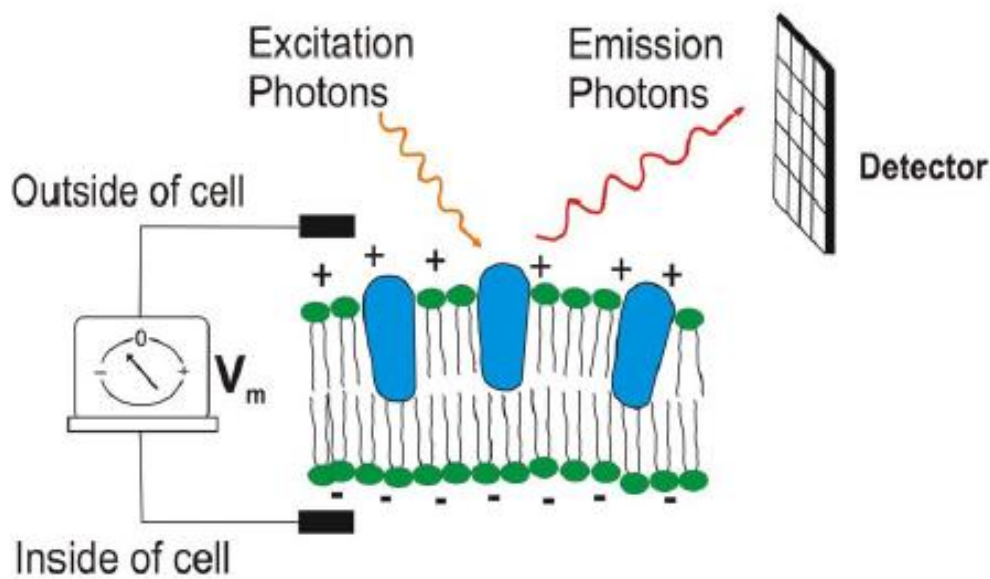


**Figure 3.7. Mechanism of Di-4-ANNEPS.** Di-4-ANNEPS (shown in blue) binds to the cell membrane. When excited by the excitation wavelength of light, a fluorescent light is emitted with a longer wavelength and is collected by the detector which converts it into an electrical signal. The intensity of the fluorescent light emitted is proportional to the membrane potential. Modified from (Rosenbaum 2001).

### 3.4.3 Optical mapping apparatus

Optical signals come from no deeper than 500 $\mu$ m into the tissue due to poor penetration and exponential decay of the light inside the tissue (Knisley, 1995). The optical apparatus set up can be seen in fig 3.8. Its major components are the light source, excitation and emission filters, a dichroic mirror, a lens and a photodiode array (PDA) detector.

The excitation light that excites the dye molecule comes from a light source of a specific wavelength such as tungsten-halogen lamps, mercury arc lamps and argon ion lasers (Arora et al., 2003). Tungsten-halogen lamps, a non-laser light source, are most commonly used with a power of 100-250W and the ability to emit a smooth, continuous spectrum with shorter wavelengths (Attin and Clusin, 2009). They can operate at high temperatures and have a long life due to small amounts of halogen gas inside. The other advantages of using this light source

are its low noise characteristics and its spectrum within the visible range that allows for flexibility when choosing the excitation wavelength. Laser light (which is monochromatic) can also be used for optical mapping however it is high cost, has a short lifetime, and high power consumption (Parker, 2003).

Light-emitting diodes (LEDs) as used in these experiments, are appealing alternatives to the light sources mentioned above as they provide fewer imaging artefacts and a low power consumption (Moe et al., 2005). They also offer a wide range of wavelengths with narrow spectral output, thus reducing the need for optical filtering which can distort signals. It is important to note that continuous illumination can lead to photobleaching so it is necessary to keep the preparation in the dark and use only the amount of light required to produce a good image (Lichtman and Conchello, 2005).

The excitation light from the LED light source is collimated and can be focused with an excitation filter ( $535\pm 12.5\text{nm}$ ). The dichroic mirror, positioned at a 45-degree angle, reflects the shorter wavelength excitation light by 90 degrees onto the rabbit heart preparation. The emitted fluorescent light from the preparation has a longer wavelength and passes through the dichroic mirror and through the long-pass emission filter (630nm) to the detector. The optics filters only allow through selected wavelengths of light. They remove background light and reduce the likelihood of photobleaching (Lichtman and Conchello, 2005). Excitation filters only transmit wavelengths of light that excite the dye, whilst emission filters transmit the emitted light and block the excitation light (Yuste & Konnerth, 2005).

PDA detectors and charged coupled device (CCD) cameras are the most common types of photodetectors used for optical mapping. They comprise of a two dimensional arrays of silicon elements with the ability to transfer light photon energy into electrical charge (Fast, 2005). The light collection onto the PDA detector (Hamamatsu, Cairn Research Ltd, Faversham, UK) is optimised by the lens of x1 magnification to ensure maximal collection and focus of emitted light. Both photographic lenses and microscopic lenses can be used for low magnification studies and high magnification studies (for specimens  $<4\text{mm}^2$ )

respectively. By improving the light collection, the signal fidelity is improved without having to increase the light intensity (Laurita and Singal, 2001).

The PDA comprises of a 16x16 grid of diodes (256 individual diodes) spanning a total area of just under 9cm<sup>2</sup>, with each individual diode covering 0.95x0.95mm<sup>2</sup> of the left ventricle. The pitch, which is a measure of the distance between the centre points of two adjacent diodes, was 1.1mm. The role of the PDA is to act as a semiconductor junction and convert the light intensity into electrical signal so the current can be transmitted to a current-to-voltage convertor where it is amplified and digitized and sent to the data acquisition computer. The photons reach the detector and electron-holes are generated, known as the photoelectric effect. The photons are converted to charge, the charge is converted to current flow and then voltage via a pre-amplifier using a feedback resistor.

The benefit of using a PDA detector is that it allows for rapid rates of digital sampling of action potentials. The CCD camera has high spatial resolution with 10<sup>6</sup> or more pixels (Rosenbaum, 2001), however it has slow frame rates. PDA detectors have better temporal resolution and rates of data acquisition.

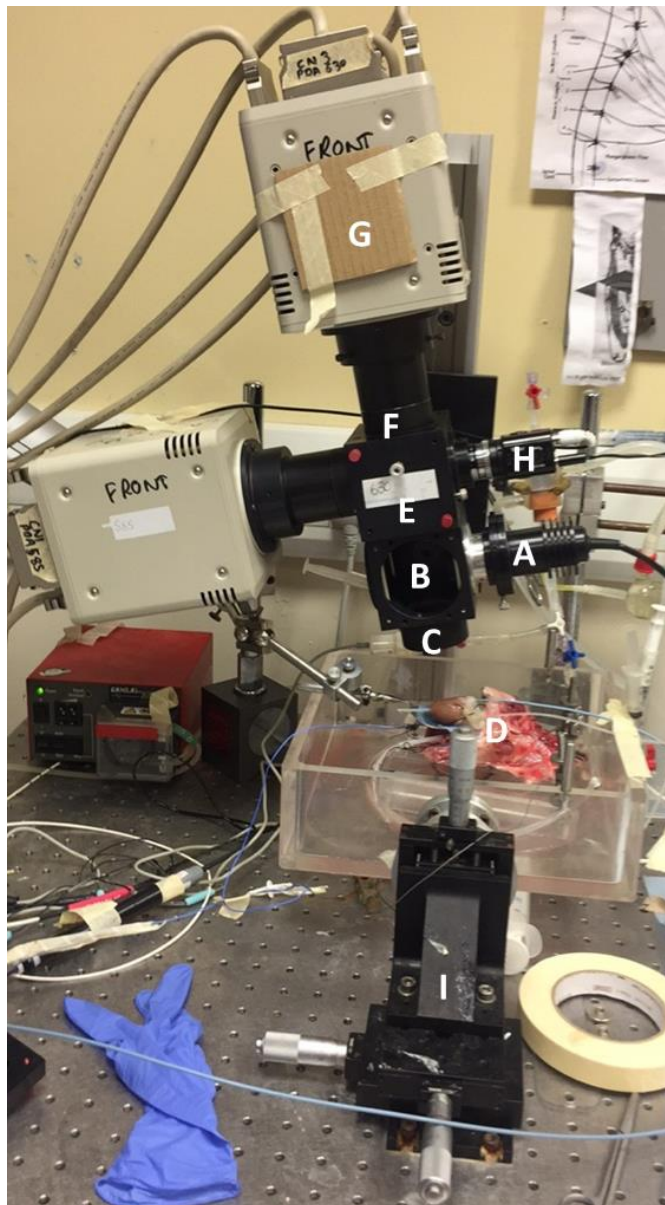


**Figure 3.8. Image of the optical mapping apparatus.** (A) Light source. (B) Excitation dichroic. (C) Object lens. (D) Isolated innervation rabbit heart preparation. (E) Emission dichroic. (F) Focus lens for detector. (G) Detector. (H) Camera. (I) Controls for fine movement of recording chamber with different axis of movement.

#### 3.4.4 Motion artefacts

The myocardial contraction of the heart causes motion artefacts resulting in distortion of the voltage dependent signals; a major limiting factor in optical mapping studies. This results in noisy and poor quality recordings of optical action

potential due to a low signal-to- noise ratio. Several methods have been used in order to limit this.

One method to prevent motion artefacts is the use of mechanical uncouplers. Blebbistatin is a mechanical uncoupler widely used more recently in cardiac electrophysiological studies. It is a small molecule inhibitor with a high affinity and selectivity for myosin II (Bond et al., 2013). It is highly suited to *in vivo* studies due to its rapid cell permeability as well as its ability to be reversed (Straight et al., 2003). Blebbistatin inhibits myosin by binding to the myosin-ADP-Pi complex and interfering with phosphate release. It does so in the actin-detached state preventing rigid actomyosin cross-linking (Kovacs et al., 2004, Allingham et al., 2005). Blebbistatin is limited by its low solubility in aqueous solutions and light sensitivity, as it can be photoinactivated by high levels of blue light (Kolega, 2004). However, its effectiveness has been evidenced in multiple animal models (Farman et al., 2008, Dou et al., 2007, Fedorov et al., 2007, Jou et al., 2010) which supports its use as an ideal candidate for excitation contraction coupling in optical mapping studies.

2,3-Butanedione monoxime (BDM) is also a noncompetitive myosin II inhibitor and acts in the same way as Blebbistatin (Herrmann et al., 1992, McKillop et al., 1994). However BDM has a low affinity for myosin II (Sellin and McArdle, 1994) and there are conflicts over its specificity and significant effects on cardiac electrophysiology have been reported (Blanchard et al., 1990, Liu et al., 1993, Maesako et al., 2000, Kettlewell et al., 2004). Cytochalasin D (cyto-D) is also frequently used in optical mapping studies. It causes failure to contract by depolymerisation of F-actin in cytoskeleton (Wu et al., 1998, Rueckschloss and Isenberg, 2001) with a subsequent reduction of  $Ca^{2+}$  currents (Rueckschloss & Isenberg, 2001). Various electrophysiological effects have been reported in different species. In the canine left ventricle wedge ventricle, Cyto-D did not change repolarization time or transmural propagation (Wu et al., 1998). Electrical restitution curves were significantly flattened by both BDM and Cyto-D (Kettlewell et al., 2004) in rabbit ventricular myocytes, although effects on APD were minimal. Action potential prolongation was however reported by Hayashi et al

(2003) in rabbits and Jalife et al (1998) in mice. Other studies have reported an inability to induce sustained ventricular arrhythmias with Cyto-D in rabbit (Banville and Gray, 2002, Cheng et al., 2004), pig (Qin et al., 2003) and mice hearts (Baker et al., 2004). It is postulated that electrophysiological effects of Cyto-D are as a result of it slowing the rate of inactivation of voltage-dependent Na<sup>+</sup> channels (Undrovinas et al., 1995).

Physical restraints such as containing the preparation in a glass chamber for mechanical stabilization and restriction of movement is another method used to limit motion artefacts (Salama et al., 1987, Brack et al., 2013). However, too much restraint can be detrimental to the preservation of the hearts physiological conditions as it can cause pressure induced cardiac ischaemia (Girouard et al., 1996). Another technique is motion subtraction which involves mathematical corrections and image post-processing methods; for example correcting abnormalities in the action potential shapes (Rohde et al., 2005). The image registration method has been shown to significantly reduce motion-related artefacts and is executed post acquisition (Rohde et al., 2005).

#### **3.4.5 Data recording and statistical analysis**

The Powerlab 16/30 system (AD Instruments Ltd, Chalgrove, UK) was used to record the signals, which were processed at 2 kHz. Data analysis was performed using Origin Lab software (v.2015; OriginLab, Northampton, MA, USA), GraphPad Prism 6 software (v6.04, GraphPad, CA, USA) and MATLAB (v.R2016a. The MathWorks, Inc, MA, USA). Data are Mean  $\pm$  SEM. Data were compared using one way ANOVA with a Bonferroni post-test and paired t-tests and statistical significance was taken at 5% level ( $p < 0.05$ ). 2D plots of recordings from the 16 x 16 diode were mapped using MATLAB.

### **3.5 Sympathetic chain denervation**

Several methods have been employed in previous investigations to remove left and or right sympathetic activity. In studies in which reversible stellectomy was desired, blockage of the right and left stellate ganglion was achieved with thermodes through which coolant, a mixture of ethyl alcohol and propylene glycol at a temperature of -25 C, was circulated (Schwartz et al., 1976a).

In canines, Schwartz et al (1976) performed right or left thoracotomy by first removing the ribs two through five to gain better access to the stellate ganglia. In cats, Rogers et al (1973) located the superior and inferior portions of each stellate ganglia and looped ligatures around them. These ligatures where then pulled to cut the chain and confirmation of stellectomy was confirmed at the end of the experiment by examining the removed stellate ganglia at the site of excision. Similarly, Zaza et al (1991) placed silk sutures under the right and left stellate ganglion and gently pulled them and severed all the preganglionic and postganglionic connections. Stellectomy has also been performed by cutting the rami communicates and the ansa subclavia of the respective stellate ganglia in the dog (Yanowitz et al., 1966).

For these experiments, as reversibility was not required, we used a similar technique to that used by Rogers et al (1973) and Zaza et al (1991). The chains were located and a suture was thread underneath each chain above the T1 segmental level. To remove the chain the suture was pulled causing the chain to snap. Successful chain removal was confirmed at the end of the experiment by observation of no chronotropic changes when the spinal cord was stimulated.

## **Chapter 4**

**Differential effects of right and left  
sympathetic nerve stimulation on  
ventricular electrophysiology and  
arrhythmia inducibility**

## **4 Differential effects of right and left sympathetic nerve stimulation on ventricular electrophysiology and arrhythmia inducibility**

### **4.1 Introduction**

The ANS has a significant influence over the development and maintenance of arrhythmias (Shen and Zipes, 2014). Sympathetic activity is often upregulated during these conditions, for example studies have shown that stellate ganglion stimulation in dogs increased the incidence of VF (Verrier et al., 1974), and hence is a target for treatment. However, a better understanding of the anatomy and physiology of cardiac sympathetic nerves is necessary. Right and left spinal sympathetic neurones differentially innervate specific regions of the heart but whether they exhibit functional selectivity and distinct effects on cardiac electrophysiology has yet to be demonstrated.

The heart is innervated by both left and right-sided sympathetic fibres, which originate from T1-T6 thoracic vertebrae and converge at the cardiac plexus (Armour, 2008, Winter et al., 2012). They then innervate the sinoatrial node (SAN), atrioventricular node (AVN) and atrial/ventricular myocardium (Armour, 2008). Unilateral stimulation of the left and right sympathetic chains has previously been found to have different functional and electrical responses, which are important factors in arrhythmia susceptibility (Anzola and Rushmer, 1956, Randall and Rohse, 1956, Yanowitz et al., 1966, Haws and Burgess, 1978, Ardell et al., 1988, Zaza et al., 1991). But direct studies on differential left vs right effects on electrical restitution and VF inducibility are surprisingly sparse.

Studies in anaesthetised dogs have repeatedly shown that right sympathetic innervations have a preferential influence on heart rate and left sympathetic innervations have a preferential influence on ventricular contractility (Randall and Rohse, 1956, Randall et al., 1968a, Ardell et al., 1988). As well as this, left sympathetic stimulation has been implicated in generation of ventricular arrhythmias as shown in numerous studies in cats and dogs (Armour et al., 1972,

Ben-David and Zipes, 1988, Hageman et al., 1973, Schwartz, 1984, Schwartz and Malliani, 1975, Schwartz et al., 2004, Zaza et al., 1991).

In 2012, our group established an *in vitro* rabbit model to investigate the effects of left and right sympathetic chain stimulation (Winter et al, 2012), which is a modification to the dual innervated isolated rabbit heart preparation as used previously by Ng et al (2001). Each sympathetic chain was isolated and stimulated by electrodes attached between spinal segments T2-T3. The resultant preparation was then used to study the differential effects of each chain on heart rate and left ventricular pressure. The left sympathetic chain had a greater effect on left ventricular contractility, left ventricular monophasic action potentials and conduction through the AVN. The right sympathetic chain had a greater influence on sinus rate. Similar responses have been seen *in vivo* in cats and dogs (Randall & Rhose, 1956, Ardell et al, 1988, Zaza et al, 1991), thereby validating this more recent adaptation to the *in vitro* dual innervated heart preparation.

Transneuronal tracing has demonstrated projections to distinct regions of the dog heart (Hopkins and Armour, 1984), however thus far there is a lack of electrophysiological evidence of target specificity or selective function. The differential innervation of the left and right sympathetic chains is suggested to affect arrhythmia inducibility. For example, *in vivo* stimulation of the left sympathetic chain in cats leads to increased susceptibility of ventricular tachycardia, delayed after depolarizations (DAD) and early afterdepolarizations (EAD) (Priori et al., 1988). Additionally, Schwartz et al (1976b) found that left stellectomy raised the ventricular fibrillation threshold and could pose as a therapy in patients at high risk of SCD from ventricular arrhythmias. Detailed mechanistic studies pertaining to unilateral sympathetic effects are still required.

What remains unanswered is whether the cardiac sympathetic supply is functionally discrete and how the differential left and right innervation contributes to this. This set of experiments aims to answer whether there are specific functional electrophysiological effects of the right and left sympathetic neurones and hence deduce more information about their differential innervations of the heart and their roles in arrhythmia generation.

Using the method described by Winter et al (2012), the effects of left and right sided paravertebral chain stimulation on cardiac electrophysiology and arrhythmogenesis will be explored. APD restitution and ventricular fibrillation threshold protocols will be used as indicators of arrhythmia susceptibility.

## 4.2 Methods

The dual innervated isolated rabbit heart preparation (n=11) was used for the following set of experiments.

### 4.2.1 Right and left sympathetic nerve stimulation

The sympathetic chains which run adjacent and parallel to the spinal column were identified and dissected by gently removing connective tissues from levels T4-T5, where they are more visible, to T1-T2. Bipolar electrodes were carefully positioned between T2-T3 (fig 4.1) and each nerve gently lifted onto them. This was secured and insulated using the silicone adhesive Kwik-Sil (WPI, USA). Left and right sympathetic chains were stimulated between T2-T3 at x2 threshold voltage (1-4V), at a frequency that produced a maximum heart rate increase (5-7Hz). The threshold voltage was defined as the lowest voltage that gave an increase in both LVP (of 3–4mmHg) and heart rate (of 3–4 bpm). Left ventricular pressure changes were recorded during constant pacing at 240ms.

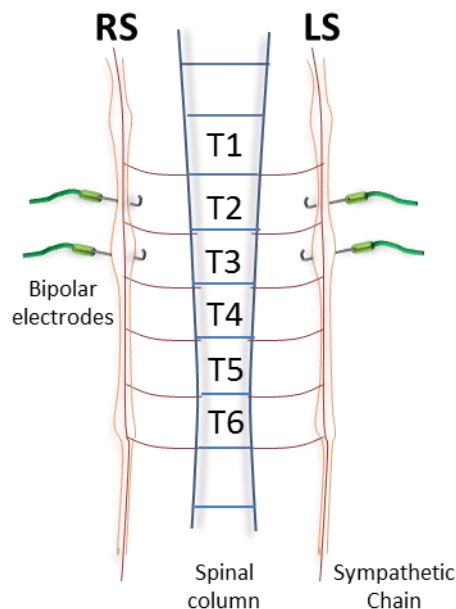


**Figure 4.1.** Diagram showing the placement of electrodes on right and left sympathetic chains parallel to the spinal column at levels between T2-T3.

#### **4.2.2 Method Development**

This method was used by our group previously (Winter et al, 2012), however a few aspects had to be amended. Thinner wired electrodes were made as the previous electrodes were too thick when compared to the width of the sympathetic chain. The thinner electrodes were also easier to manoeuvre into the correct position as they were more flexible.

To insulate the nerve and electrode, dental cement was used previously. However, the length of stimulation was much shorter for these experiments as they did not use the same pacing protocols. The dental cement (Aquasil Ultra LV Fast Set, Dentsply, USA) was not found to be very effective in this study as the nerve response was often lost later on into the experiment, possibly due to the nerve drying out. It was also difficult to sustain a strong nerve response throughout the length of the protocol when this insulator was used. Attempts for insulation were also made using a silicone gel (WACKER SilGel®, Wacker Chemie AG, Germany). Unfortunately this insulator had similar effects as the dental cement and also had a longer curing time.

Hence, Kwik-Sil adhesive was trialled for use as a new insulator. Kwik-Sil is a bio-compatible adhesive for live tissue and nerve studies. It has a short curing time of approximately 1 minute and a low toxicity and so is ideal for this study. Use of this adhesive produced a more stable nerve response which was reproducible throughout the length of the experiment. The Kwik-Sil is also transparent which allowed us to ensure the sympathetic chains were still positioned correctly on the electrode post insulation. We also found that the Kwik-Sil displaced the surrounding fluid and so reduced the chance of fluid contact with the electrodes remaining post insulation. A suction pipette was also made to remove any surrounding fluid during insulation to prevent shunting of electrodes when stimulating.

As seen in the diagram (fig 4.2), cotton wool was used to restrict the Kwik-Sil from running down the preparation while it was curing. To ease the placement of the

sympathetic chain on to the electrodes and to prevent nerve damage, a glass rod with a curved end was made for lifting the nerve.

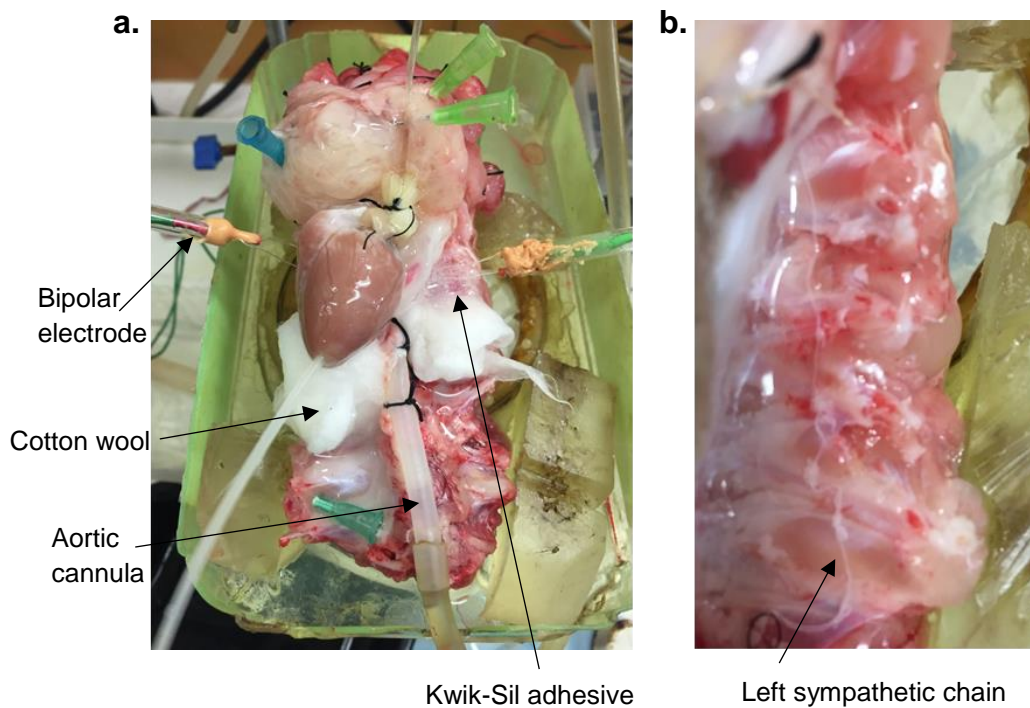


**Figure 4.2.** (a) Image of isolated innervated heart preparation with bipolar electrodes used for right and left sympathetic stimulation. (b) Left sympathetic chain after dissection.

## 4.3 Results

The data below show the differential effects of right and left sympathetic stimulation on ventricular electrophysiology, when stimulated at spinal segment T2-T3 (n=11).

### 4.3.1 Changes in heart rate and left ventricular pressure with right and left sympathetic stimulation

Stimulation of both right and left sympathetic chains caused an increase in heart rate (HR) and left ventricular pressure (LVP). Right sympathetic stimulation showed greater increases in HR whereas left sympathetic stimulation showed greater increases in LVP (Fig. 4.3). These effects of right and left sympathetic chain stimulation on HR and LVP have been noted previously in this model (Winter et al., 2012) at T2-T3. Fig 4.3a shows raw data of HR vs LVP hysteresis loops during right and left sympathetic stimulation in sinus rhythm. During left sympathetic stimulation the loop is shifted towards the left and reaches greater LVP values at lower HR than the right. Right sympathetic stimulation produced a greater HR response with a lower maximum LVP.

#### ***Chronotropic effects***

Right sympathetic stimulation caused a significantly greater HR response than left sympathetic stimulation ( $P < 0.01$ ), from baseline HR of  $144.8 \pm 9.2$  bpm to  $201.5 \pm 6.4$  bpm with right sympathetic stimulation ( $P < 0.0001$ ) and baseline HR of  $139.5 \pm 7.7$  bpm to  $177.7 \pm 5.6$  bpm with left sympathetic stimulation ( $P < 0.001$ ) as shown in fig 4.3b. Right sympathetic stimulation also showed a significant increase in percentage HR change ( $42.6 \pm 7.1$  %) when compared to left stimulation ( $30.0 \pm 5.8$  %,  $P < 0.001$ ) (fig 4.3).

#### ***Inotropic effects***

LVP, measured during constant pacing at 240ms, increased to a greater extent with left sympathetic stimulation compared to right stimulation (fig 4.3d), with baseline values of  $33.7 \pm 4.4$  mmHg to  $43.3 \pm 5.9$  mmHg with right stimulation and a baseline of  $32.0 \pm 3.9$  mmHg to  $49.3 \pm 4.4$  mmHg ( $P < 0.01$ ) with left sympathetic

stimulation. Percentage change in LVP was significantly greater with left sympathetic stimulation ( $57.3 \pm 8.4$  %) than right sympathetic stimulation ( $28.3 \pm 7.3$  %,  $P < 0.05$ ) (fig 4.3e).

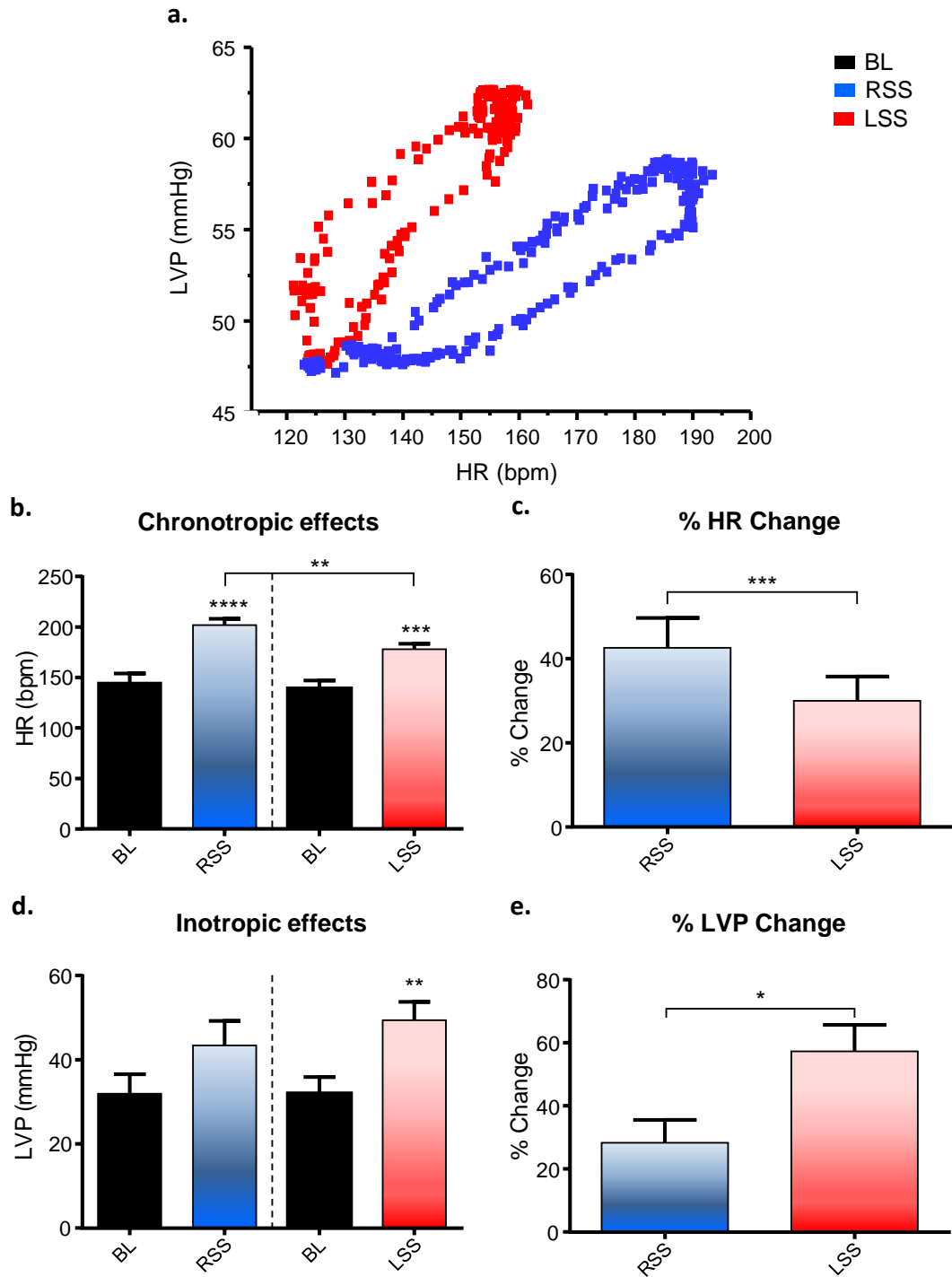


**Figure 4.3. The effect of right and left sympathetic stimulation heart rate and left ventricular pressure.** (a) Raw data from one experiment showing heart rate (HR) vs left ventricular pressure (LVP) changes during right sympathetic stimulation (RSS) and left sympathetic stimulation (LSS) with return to baseline (LVP recorded during sinus rhythm). (b) Heart rate (HR) response under baseline (BL) conditions, RSS and LSS. (c) Percentage change in HR with RSS and LSS. (d) Left ventricular pressure (LVP) response under BL conditions, RSS and LSS recorded during constant pacing at 240ms. (e) Percentage change in LVP with RSS and LSS. Data represent mean  $\pm$ SEM, n=11. \*P<0.05, \*\*P<0.01, \*\*\*P<0.001.

### 4.3.2 Effect of right and left sympathetic stimulation on monophasic action potential duration

Monophasic action potential (MAP) duration, recorded during constant pacing 240ms, was shortened by both right and left sympathetic stimulation at the base and apex as shown in fig 4.4. At the base, left sympathetic stimulation had a greater influence on shortening MAP duration than right sympathetic stimulation (fig 4.5,  $P < 0.05$ ). Left sympathetic stimulation shortened MAP duration from  $126.9 \pm 1.8$ ms at baseline to  $115.8 \pm 2.8$ ms, whereas right sympathetic stimulation shortened MAP duration from  $128.5 \pm 1.5$ ms at baseline to  $122.1 \pm 1.7$ ms at the base. The percentage change in MAP duration at the base was also significantly greater for left stimulation ( $-8.8 \pm 1.4\%$ ) than right ( $-5.0 \pm 0.3\%$ ,  $P < 0.01$ ). At the apex, left sympathetic stimulation shortened MAP duration from  $125.3 \pm 1.6$ ms at baseline to  $114.8 \pm 2.0$ ms, whereas right sympathetic stimulation shortened MAP duration from  $126.6 \pm 2.0$ ms at baseline to  $120.8 \pm 2.0$ ms. There was also a greater percentage change in MAP duration with left stimulation ( $-8.37 \pm 0.9\%$ ) at the apex than with right ( $-4.6 \pm 0.5\%$ ,  $P < 0.05$ ). There was a trend for MAP duration shortening to be greater at the base than apex as shown in fig 4.5e, although this did not reach statistical significance.

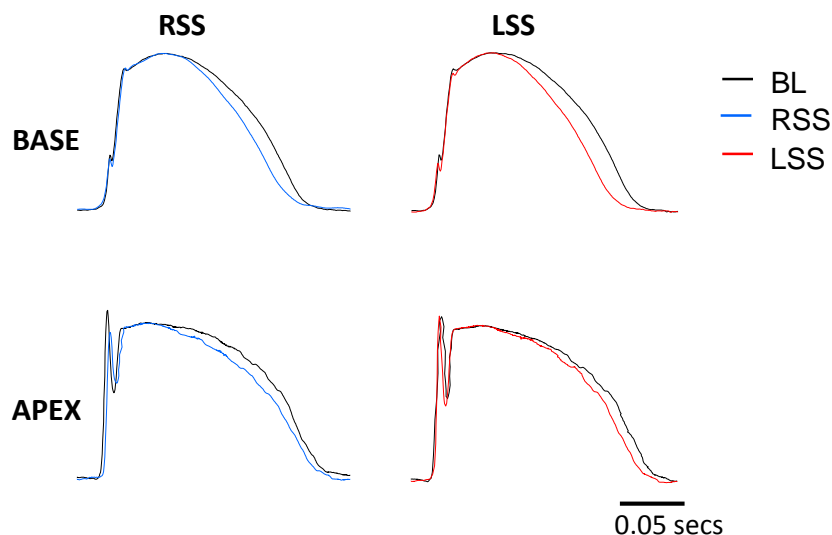


**Figure 4.4. Raw data traces of basal and apical action potentials during constant pacing at 240ms.** Traces are shown for baseline (BL) and during right (RSS) and left sympathetic chain stimulation (LSS).

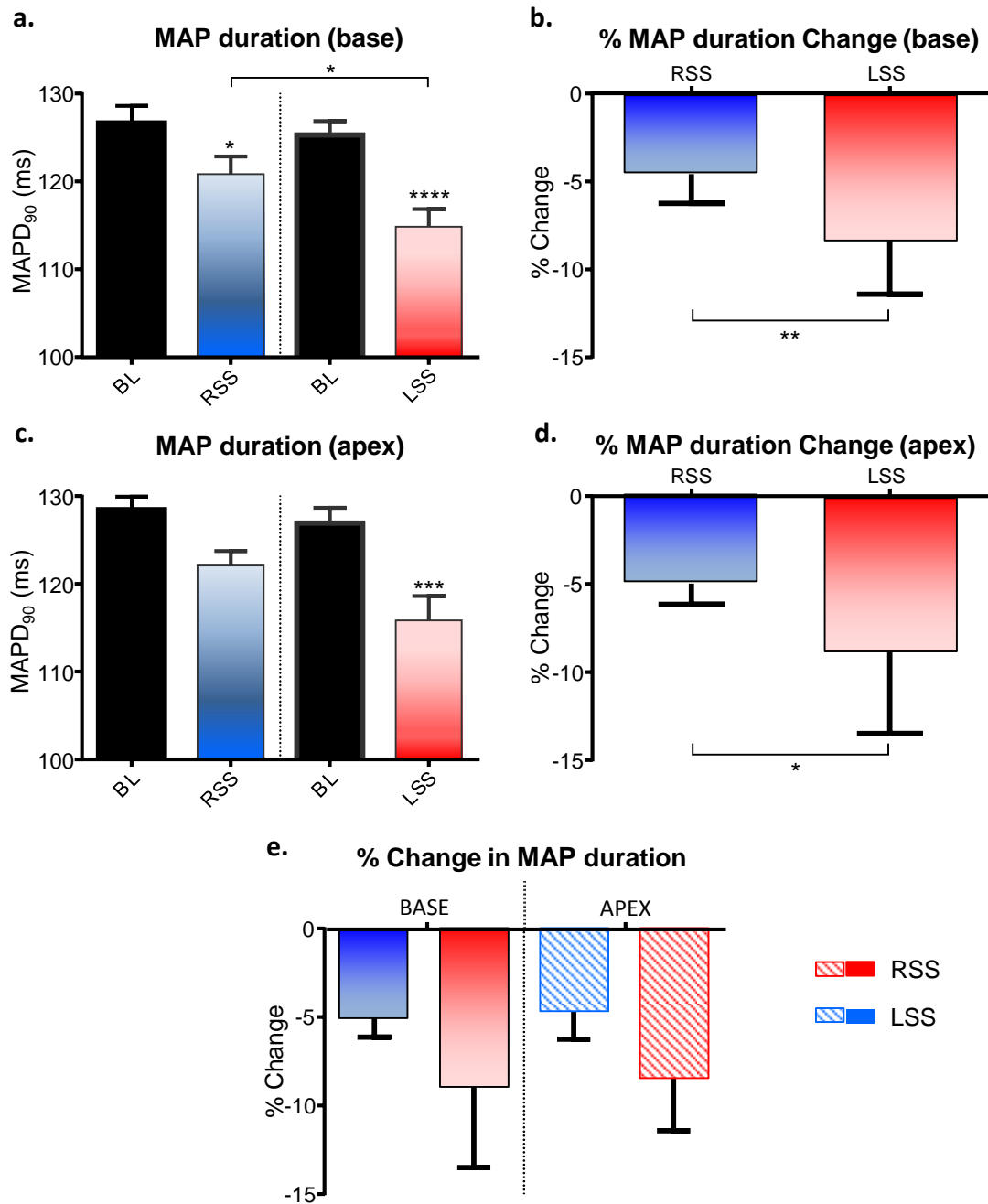


**Figure 4.5. The effects of right and left sympathetic stimulation on monophasic action potential (MAP) duration.** (a) Effects MAP duration from baseline (BL) to right (RSS) and left stimulation (LSS) at the base. (b) Percentage change in MAP duration with RSS and LSS. (c) MAP duration at BL and during RSS and LSS at the apex. (d) Percentage change in MAP duration at the apex during RSS and LSS. (e) Percentage change in MAP duration at both base and apex. Data represent mean  $\pm$ SEM, n=11. \*P<0.05, \*\*P<0.01, \*\*\*P<0.001, \*\*\*\*P<0.0001.

Fig 4.6 shows restitution loops which map the change in MAPD with DI from the start to the end of stimulation during sinus rhythm. As shown in fig 4.7, left sympathetic stimulation shortened the MAPD to a greater extent than right sympathetic stimulation at the base. This effect was less evident at the apex.

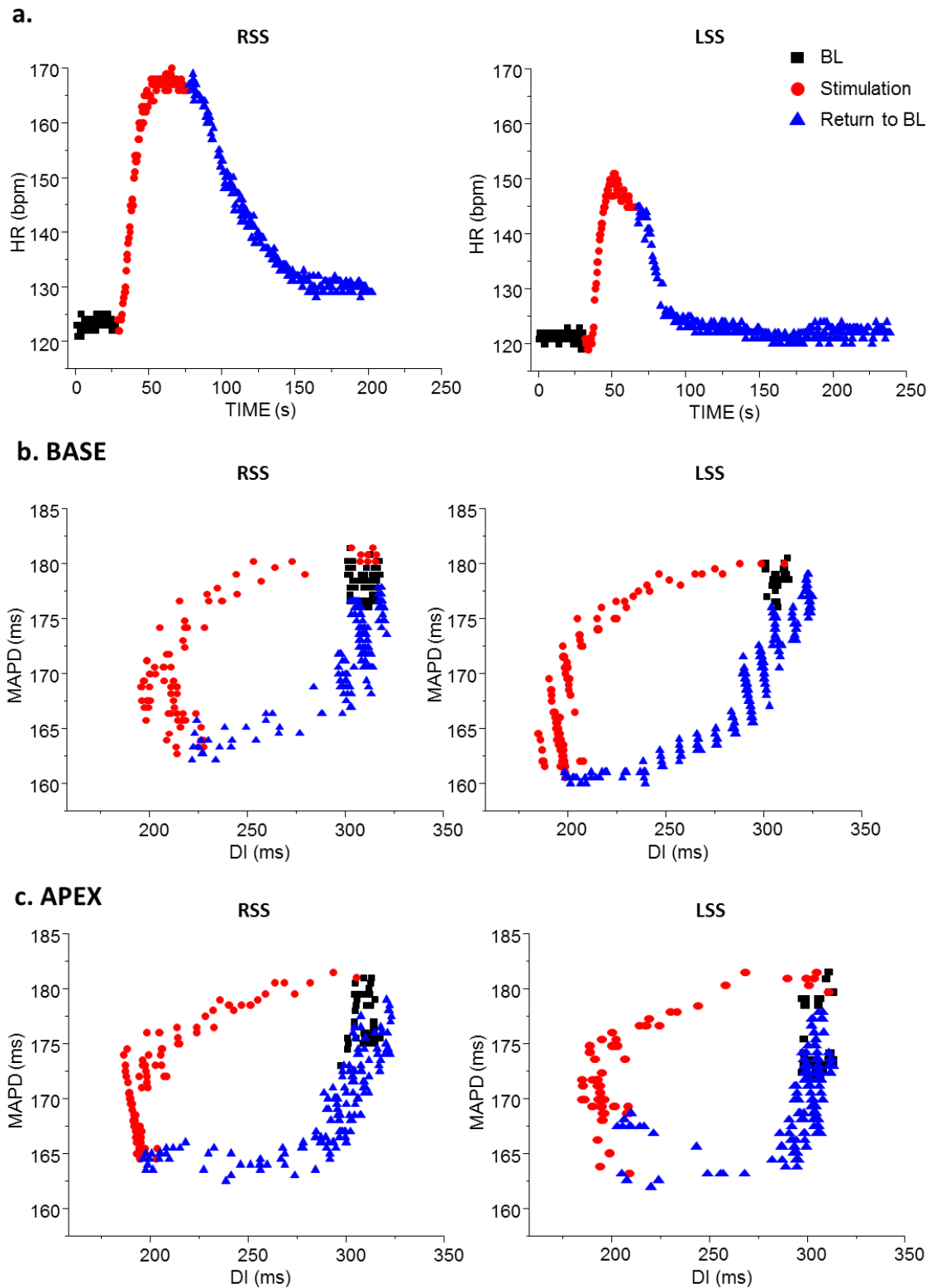


**Figure 4.6. Effects of left and right sympathetic stimulation on APD restitution.** (a) Heart rate trace displaying heart rate during baseline (BL), left (LSS) or right (RSS) stimulation and return to BL. (b) Restitution loops at the base during RSS and LSS.

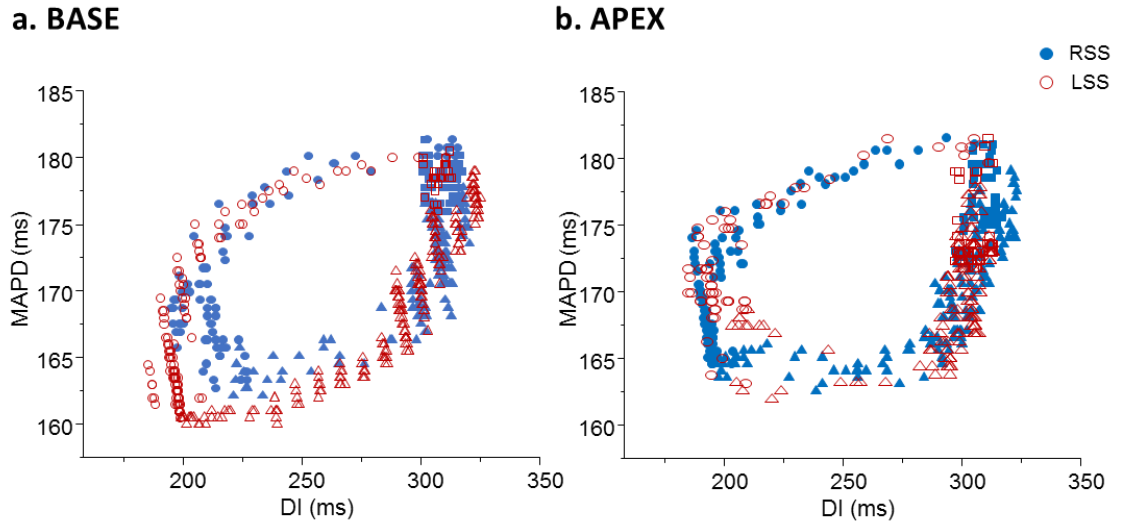


**Figure 4.7.** Restitution loops during left and right sympathetic stimulation at (a) the base and (b) the apex.

### 4.3.3 Effect of right and left sympathetic stimulation on effective refractory period

Effective refractory period (ERP) shortened with both right and left sympathetic stimulation (fig 4.8a). Left sympathetic stimulation was found to shorten ERP more than right sympathetic stimulation. The ERP shortened from  $156.4 \pm 6.3$  ms at baseline to  $130.5 \pm 7.6$  ms with left stimulation ( $P < 0.0001$ ), in comparison to  $152.3 \pm 6.7$  ms at baseline to  $136.4 \pm 7.3$  ms with right stimulation ( $P < 0.01$ ). There was also a significantly larger percentage change in ERP with left sympathetic stimulation ( $-17.1 \pm 2.0\%$ ) than with right sympathetic stimulation ( $-10.6 \pm 2.2\%$ ,  $P < 0.01$ ) (fig 4.8b).

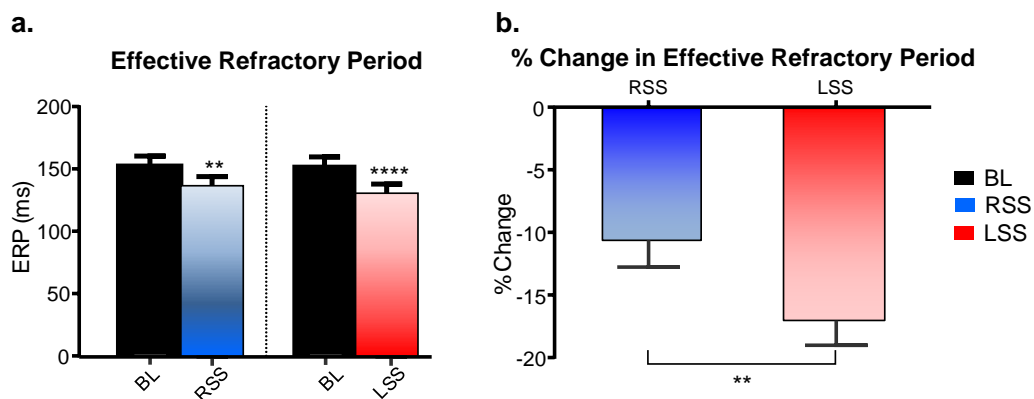


**Figure 4.8. Changes in effective refractory period (ERP) with right and left sympathetic stimulation.** (a) ERP values during baseline (BL) conditions and during right (RSS) and left sympathetic stimulation (LSS). (b) Change in ERP from BL to RSS and from BL to LSS. Data represent mean  $\pm$  SEM,  $n=11$ . \*\* $P < 0.01$ , \*\*\*\* $P < 0.0001$

#### **4.3.4 Action potential duration restitution and the effects of right and left sympathetic stimulation**

Fig 4.9a shows restitution curves during baseline, right sympathetic stimulation and left sympathetic stimulation. The maximum slope of restitution was steepened by both right and left sympathetic stimulation, with a dominant effect of left stimulation which caused significantly greater steepening at the base ( $P<0.05$ ) and the apex ( $P<0.05$ ) (fig 4.9). At the base, the maximum slope of restitution increased from  $0.6 \pm 0.1$  to  $1.5 \pm 0.1$  ( $141.5 \pm 13.3\%$ ) with right sympathetic stimulation ( $P<0.0001$ ) and from  $0.7 \pm 0.1$  to  $2.1 \pm 0.1$  ( $170.8 \pm 22.9\%$ ) with left stimulation ( $P<0.0001$ ). At the apex, the maximum slope of restitution increased from  $0.7 \pm 0.1$  to  $1.4 \pm 0.1$  ( $114.7 \pm 6.7\%$ ) with right stimulation ( $P<0.01$ ) and from  $0.9 \pm 0.1$  to  $2.0 \pm 0.1$  ( $144.6 \pm 23.3\%$ ) with left stimulation ( $P<0.0001$ ). Fig 4.10 shows the changes elicited at the base and apex and a trend for greater steepening of the maximum slope of restitution can be seen at the base. However, this did not reach statistical significance.

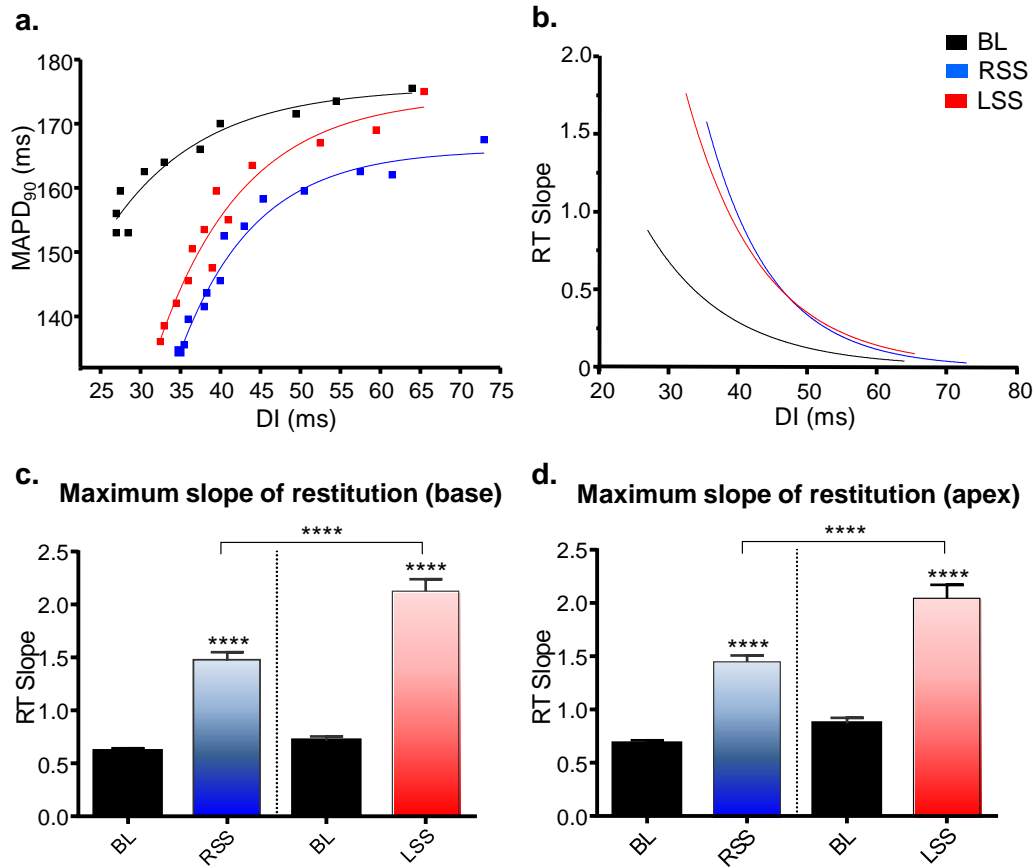


**Figure 4.9. The effects of right and left sympathetic stimulation on action potential duration restitution.** (a) RT curves displaying S2 data for baseline (BL), right sympathetic stimulation (RSS) and left sympathetic stimulation (LSS) with exponential curve fit ( $MAPD_{90} = \text{maximum } MAPD_{90} [1 - e^{-DI/\tau}]$ ). (b) Derivative of fitted curves for BL, RSS and LSS. (c) RT slope values at base and apex. Data represent mean  $\pm$  SEM,  $n=11$ . \* $P < 0.05$ , \*\* $P < 0.01$ , \*\*\*\* $P < 0.0001$

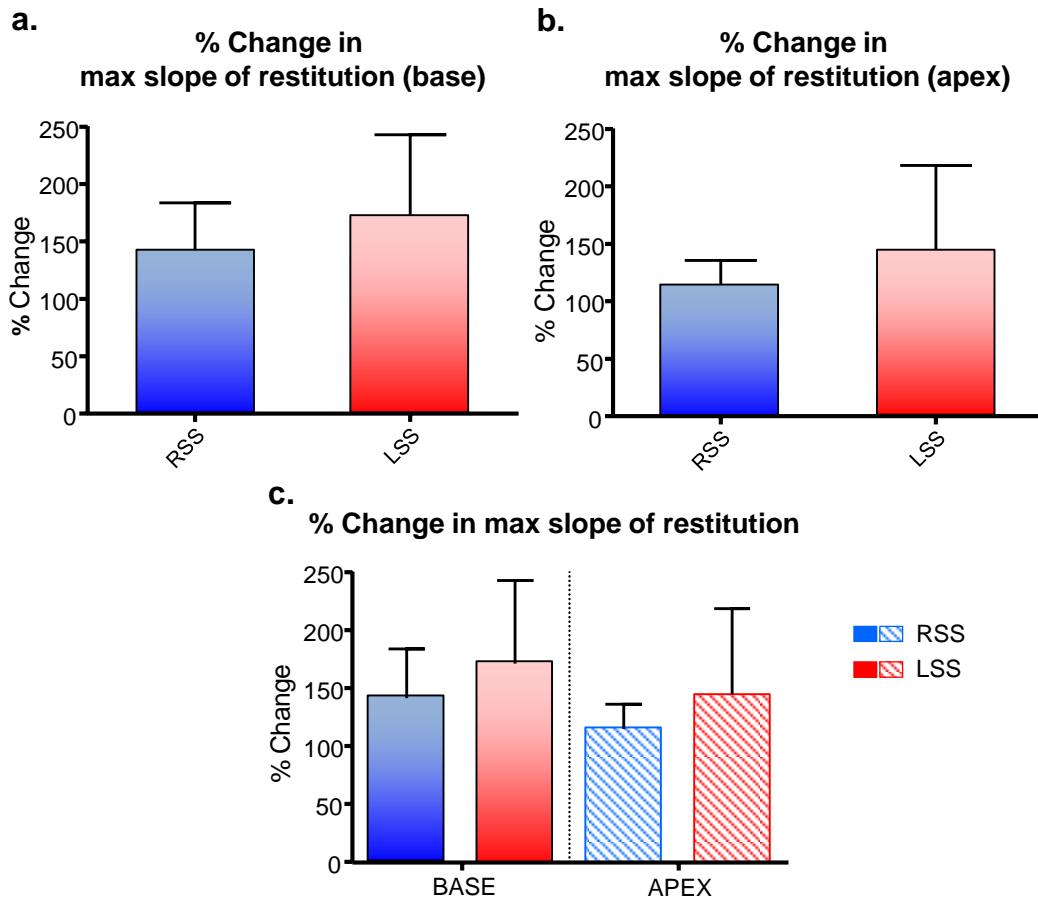


**Figure 4.10. Changes in maximum slope of restitution with right and left sympathetic stimulation.** Percentage change in maximum slope of restitution at (a) the base and (b) the apex. (c) Percentage change in maximum slope of restitution at base and apex with right (RSS) and left sympathetic stimulation (LSS). Data represent mean  $\pm$ SEM,  $n=11$ .

#### 4.3.5 Effect of right and left sympathetic stimulation on ventricular fibrillation threshold

Both right and left sympathetic stimulation caused a decrease in VF threshold from baseline (fig 4.11a), however left sympathetic stimulation showed a larger decrease. VF threshold decreased from  $6.0 \pm 0.5$  mA to  $4.1 \pm 0.6$  mA with right stimulation ( $P < 0.001$ ) and from  $6.2 \pm 0.5$  mA to  $3.2 \pm 0.4$  mA with left sympathetic stimulation ( $P < 0.0001$ ). Percentage change in VF threshold was significantly greater with left stimulation ( $-47.8 \pm 4.8\%$ ) compared to right ( $-34.4 \pm 6.1\%$ ,  $P < 0.05$ ) as shown in fig 4.11b.

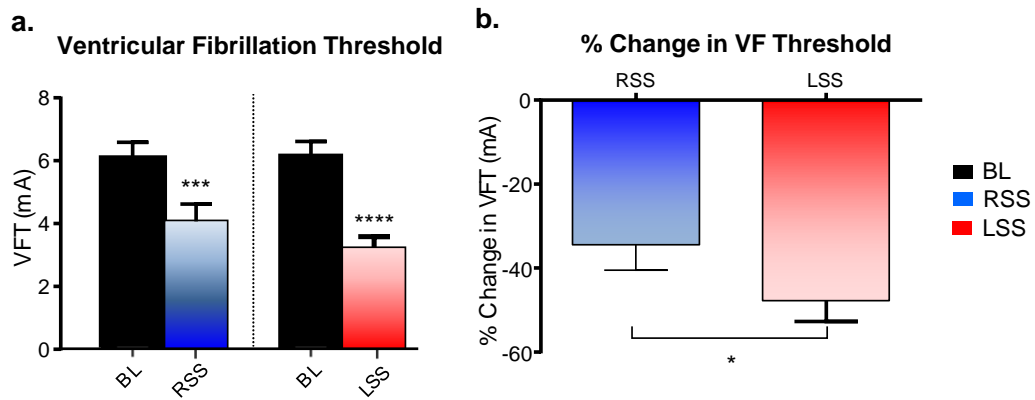


**Figure 4.11. The effects of right and left sympathetic stimulation of ventricular fibrillation (VF) threshold.** (a) VF threshold values under baseline (BL) conditions and with right sympathetic stimulation (RSS) and (left sympathetic stimulation (LSS). (b) Change in VF threshold from BL to RSS and BL to LSS. Data represent mean  $\pm$ SEM, n=11. \*P<0.05, \*\*\*P<0.001, \*\*\*\*P<0.0001

#### 4.3.6 Correlation between sympathetic modulation of ERP and VF threshold

In Fig 4.12, VF threshold is plotted against the corresponding ERP at baseline, and also for left sympathetic stimulation and right sympathetic stimulation. There is a significant relationship between the two cardiac parameters with the effects of left sympathetic stimulation shifted more towards the left.

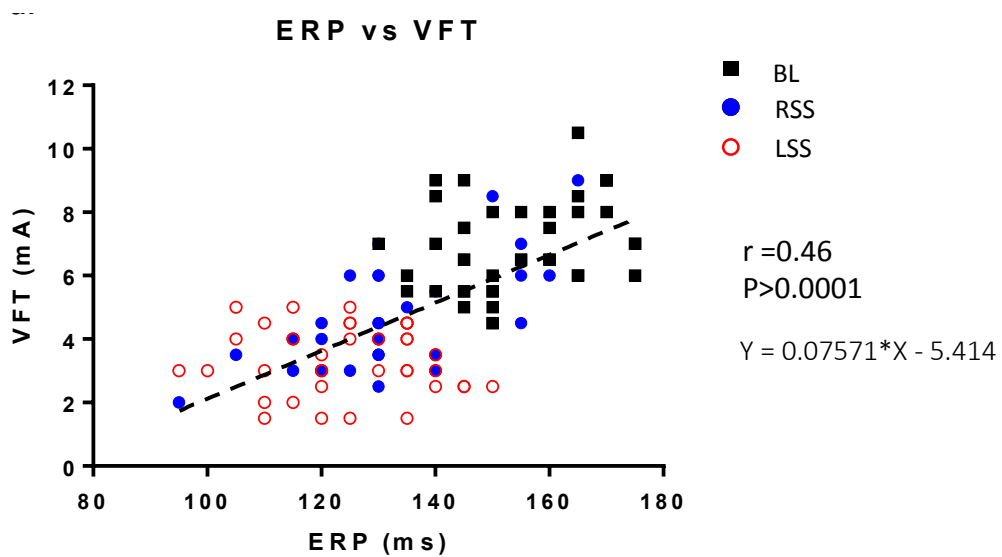


**Figure 4.12. Relationship between ventricular fibrillation threshold (VFT) and effective refractory period (ERP).** Individual symbols represent values obtained at baseline (BL), with left sympathetic stimulation (LSS) and with right sympathetic stimulation (RSS).

#### 4.3.7 Correlation between sympathetic modulation of maximum slope of restitution and VF threshold

In Fig 4.13, maximum slope of restitution is plotted against the corresponding VF threshold at baseline, and also for left sympathetic stimulation and right sympathetic stimulation. There is a significant relationship between the two cardiac parameters. The graph shows the more right shifted effects of left sympathetic efferent nerves and indicates that they have a greater influence on the stability of rhythm than the right sympathetic population.

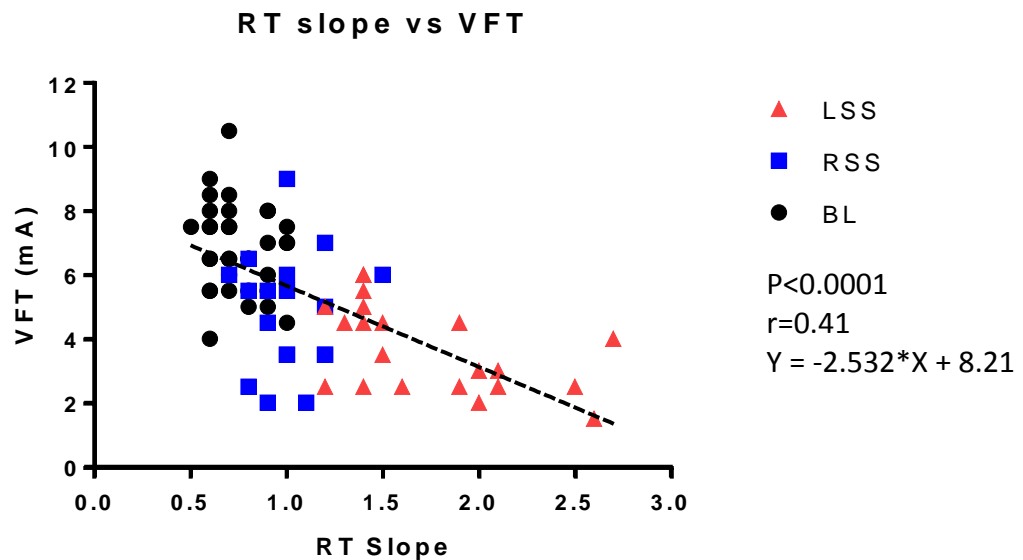


**Figure 4.13. Relationship between maximum slope of restitution and VF threshold with linear regression analysis.** Individual symbols represent values obtained at baseline (BL), with left sympathetic stimulation (LSS) and with right sympathetic stimulation (RSS). Equation of the line is  $y = -2.532 * X + 8.21$ ,  $P < 0.001$ .

## 4.4 Discussion

Previous studies have investigated the differential effects of right and left sympathetic stimulation in different species. The general trend of previous data has shown the preferential effect of right sympathetic stimulation on the chronotropic response, and left sympathetic stimulation on the inotropic response (Randall and Rohse, 1956, Randall et al., 1968a, Ardell et al., 1988). Similarly, in the isolated innervated rabbit model, Winter et al (2012) showed the same of right and left sympathetic stimulation. In the present study we have expanded on these findings to explore further the effects of right and left sympathetic stimulation on electrophysiological parameters and cardiac rhythm, and what the distinct effects of each sympathetic chain can tell us about their selective innervations. These data have shown for the first time in the rabbit heart that the left sympathetic preganglionic neurones have a greater effect on the electrophysiology of the ventricle and hence a dominant effect on cardiac rhythm and excitability.

As seen previously in dogs (Ardell *et al*, 1988; Randall & Rohse, 1956b; Randall et al, 1968; Furnival *et al*, 1973), cats (Zaza *et al*, 1991) and rabbits (Winter et al, 2012), right sympathetic stimulation has shown to have a preferential effect on heart rate and hence is likely to densely innervate the SAN. This is supported by the data in the present study. Likewise, left sympathetic stimulation has shown to have a greater inotropic response (Randall and Rohse, 1956, Randall et al., 1968a, Ardell et al., 1988, Winter et al., 2012) as reported in these results in the rabbit heart. Left sympathetic neurones are therefore thought to have denser innervations of the ventricle. Previous studies have shown that the degree of increase in these parameters is dependent on the thoracic spinal segment that is stimulated and that in most species levels T1 to T3 displayed the most significant responses (Kostreva et al., 1977, Norris et al., 1974, Norris et al., 1977, Kamosinska et al., 1991, Kocsis and Gyimesi-Pelczer, 1998, Ninomiya et al., 1993, Szulczyk and Szulczyk, 1987, Ter Horst et al., 1993, Ter Horst et al., 1996). This is yet to be investigated in the rabbit model and would provide important insights into the differential segmental innervations of the right and left sympathetic neurones.

The findings from this study also support the notion that there is differential basal and apical innervation of the sympathetic nerves on the ventricles. Both right and left sympathetic stimulation showed a greater shortening of the MAP duration at the base. This complies with the study by Ng et al (2009) and supports the notion that there is a denser innervation of the sympathetic nerves at the base where there is more  $I_{K_s}$  activation. A greater density and activation of  $I_{K_s}$  leads to faster repolarisation during phase 3 of the action potential and hence the APD is shorter at the base. The left sympathetic preganglionic neurones had a dominant effect on shortening MAP duration than the right sympathetics which therefore supports that there is a greater density of innervation of left sympathetic neurones over the ventricle.

Previous studies have shown the parasympathetic and sympathetic effects on effective refractory period (ERP). Vagal stimulation was shown to increase the ERP whilst sympathetic stimulation via the spinal cord was found to shorten the ERP (Ng et al., 2007). This observation was seemingly due to the distinct heart rate changes they each elicit. In this study, we found that right and left sympathetic preganglionic neurones each have different effects on the ERP, which has not been shown before in this model. Interestingly, left sympathetic stimulation had a greater influence on the reduction of ERP than right sympathetic stimulation even though right stimulation elicited greater heart rate effects. Therefore, the ERP changes appeared to be independent of heart rate changes. This could be due to the greater innervation density of the ventricles by the left sympathetics and the greater shortening of MAP duration displayed by left sympathetic stimulation. Our data suggest that the ERP involves an interaction between heart rate and ventricular electrophysiology and therefore is a dynamic response involving the interaction of several factors. This is illustrated further by the restitution loops which show that the APD changes in accord with activation rate, with left stimulation eliciting shorter APD's at slower heart rates and right stimulation producing longer APD's at faster heart rates. This effect was more prominent at the base of the ventricle.

ERP changes can give an indication of the likelihood of reentrant arrhythmias occurring and hence this data suggest that left sympathetics have a greater potential to generate an arrhythmia of this sort. Conversely, Yanowitz et al (1966) measured the effects on the ECG after removing or stimulating the left and right stellate ganglia in anaesthetized dogs. They found that left sympathetic activity had less influence than right sympathetic activity on the functional refractory period of the anterior surface of the left ventricle. However, these conclusions were based on interpretation of changes in the T wave, which are dependent on temporal and spatial variations. They are not comparable to the present study in which measurements were confined to electrical changes to the MAP in two more discrete areas at the base and apex of the anterior surface of the myocardium.

Another study in anaesthetised dogs by Haws & Burgess (1978) located 55 sites that were innervated by both the left and right stellate ganglia. Refractory period shortening was studied and in over half of these sites refractory periods were shortened more by left stellate stimulation than right. They suggested that in overlapping sites of innervation of the left and right stellate ganglia, increases in left sympathetic tone are more significant than increases in right sympathetic tone. This was proposed to be due to a greater density of left innervation in these sites as we have also suggested in this study. Uniform increases in sympathetic tone during bilateral sympathetic stimulation should therefore ensure homogenous distribution of recovery properties. Similar effects on ventricular refractory periods have been evidenced previously (Kralios et al., 1975).

Sympathetic stimulation is known to steepen the maximum slope of restitution whereas parasympathetic stimulation causes it to flatten (Ng et al., 2007). Differential effects of right and left stimulation on maximum restitution were investigated for the first time in this study. Both right and left sympathetic stimulation steepened maximum slope of restitution but left sympathetics had a clear dominance. This was more apparent at the base where left and right sympathetic stimulation showed greater steepening of the slope in comparison to apex. This response mirrors the response observed for MAP duration and thus suggests the response is due to greater basal innervations of the sympathetic

nerves. It is therefore not surprising that stimulation of the left preganglionics produced greater slope steepening as they have a denser ventricular innervation. The steeper slopes elicited by left sympathetic stimulation indicate the greater likelihood of wavebreaks occurring and developing into ventricular arrhythmias (Weiss *et al*, 2006). Hence, this data suggest that stimulation of left sympathetic preganglionic neurones has a greater tendency to generate arrhythmias.

In accordance, VF threshold was found to decrease more with left sympathetic stimulation than right, meaning a smaller current was required to induce VF with left stimulation. In anaesthetised or vagotomised dogs, Schwartz *et al* (1976a) investigated the effects of ablation or blockade of the left and right stellate ganglion on VF threshold. Their results showed that right stellate ganglion ablation or blockade significantly decreased VF threshold whereas left stellate ganglion ablation or blockade increased VF threshold in comparison to control. The arrhythmic tendencies of left sympathetic stimulation have also been observed in previous studies in cats (Priori *et al*, 1988) and other dog studies (Zhou *et al*, 2008). This supports what we have observed in the present study and suggests right and left sympathetics have specific effects on cardiac excitability.

#### **4.4.1 Clinical implications**

These data provide a plausible mechanistic basis underlying the value of left stellectomy as therapy in patients at high risk of sudden death from ventricular arrhythmias. In patients with VT refractory to medical therapy and catheter ablation, left cardiac sympathetic nerve denervation (LCSD) effectively reduced the arrhythmia burden with lasting effects (Bourke *et al*, 2010). This study supports the rationale for use of left stellectomy in patients at high risk of sudden death from ventricular arrhythmias for example LQTS patients who are resistant to medical therapies. Furthermore, patients with LQTS have a lower than normal right sympathetic activity and stimulation of the left stellate ganglion or ablation of the right stellate ganglion in dogs, has been shown to prolong Q-T interval (Schwartz *et al.*, 1976a, Schwartz *et al.*, 2004). Hence, these patients have a greater likelihood of developing ventricular arrhythmias due to sympathetic

discharges during emotion stress or exercise. Stimulation of the left sympathetic nerves has also been shown to prolong Q-T intervals (Yanowitz et al., 1966), induce T wave alternans (Schwartz and Malliani, 1975) and trigger lethal arrhythmias (Armour et al., 1972, Hageman et al., 1973).

The antiarrhythmic effects of left cardiac sympathetic denervation (LCSD) have been observed in patients and canines following MI, in LQTS patients (Schwartz et al., 2004), CPVT patients (Wilde et al., 2008), non-long-QT syndrome arrhythmogenic channelopathies and cardiomyopathies (Coleman et al., 2012) and patients with refractory ventricular arrhythmias (Bourke et al., 2010) and VT storm (Vaseghi et al, 2014).

Whilst such treatment has proven to be successful, it is accompanied by serious side effects such as loss of vasomotion, and poorer visual and salivary control. Thus, removing such a large portion of sympathetic input may not be the most effective treatment and further investigations are necessary to determine a more targeted approach.

#### **4.4.2 Limitations**

This *in vitro* preparation has the advantages of allowing measurements in the absence of confounding influences such as tonic autonomic nervous activity, spinal reflexes or changes in haemodynamic loads or circulating hormones, in comparison to an *in vivo* experiment. The use of direct nerve stimulation is also a benefit as we have previously demonstrated novel data showing that the effects of nerve stimulation on ventricular repolarisation gradient were different from perfusing with neurotransmitter analogues due to the heterogeneous innervations of nerves (Mantravadi et al., 2007). However, isolation from confounding factors may represent an over-simplification of the basic control mechanisms in intact animals and humans, although it would be surprising if the functional anatomy is greatly different as similar findings have been shown in various models and the rabbit electrophysiology is very close to that of a human.

Another limitation is that this study was confined to the segmental level T2-T3 as studied previously by Winter et al (2012). However to gain further insights into the distinct functional effects of right and left stimulation, there is a need to investigate the differential inputs from each spinal segmental level from T6 to T1.

#### **4.4.3 Conclusions**

Using a unique refinement of the isolated innervation rabbit heart, this study shows previously unidentified characteristics of the right and left sympathetic preganglionic neurons and their distinct functional effects. These results show the left sympathetic preganglionics have a dominant effect on cardiac electrophysiology and excitability and hence could be used as a target for treatment for ventricular arrhythmias.

More knowledge of the anatomy and physiology of cardiac nerves is required in order for this to be translated into clinical interventions and the advancement of surgical therapies. It is also necessary to establish the regional and functional selectivity of the sympathetic preganglionic neurones to improve the understanding of spinal sympathetic control of the heart. Further investigations are required to determine whether the segmental location of the sympathetic neurones corresponds to a specific cardiac function and thus potentially highlight a more targeted method of clinical treatment.

## **Chapter 5**

### **Functional selectivity of right and left spinal segmental preganglionic neurons**

## **5 Functional selectivity of right and left spinal segmental preganglionic neurons**

### **5.1 Introduction**

Previous studies have shown a regional and functional selectivity of cardiac postganglionic neurones. Hence, the spinal segmental preganglionic neurons may exhibit similar heterogeneity and clinically important characteristics which have not yet been investigated.

When excited, small distal branches of cardiac postganglionic nerve bundles produce highly localized changes in the heart (Szentivanyi et al., 1967, Randall et al., 1968a, Furukawa et al., 1990). In the canine heart, stimulation of the more distal the branches of the stellate ganglion caused fewer test regions on the heart to respond (Szentivanyi et al., 1967). This suggested that as larger nerves successively branch, distribution of smaller bundles of fibres become more restricted to specific portions of the ventricle. Similarly, although a large fraction of the ventricles receive sympathetic supply, distribution appears to be in the form of discrete projections to localized regions rather than syncytial (Randall et al., 1968a).

Randall (1977) suggested regionally specified innervation of the preganglionic neurones from the spinal cord in accordance with their arrangement in series. The cardiac postganglionic innervations originate from the stellate-ansa complex, and signalling to localized portions of the myocardium is dependent on the extent of the discharge zone and spread of synaptic excitation (Chung et al., 1975, 1979, Pardini and Wurster, 1984, Szulczyk and Szulczyk, 1987, Strack et al., 1989, Sundaram et al., 1989a). It would also require projections of spinal axons onto discrete ganglion cells, a notion supported by several studies (Larrabee and Bronk, 1947, Tatarchenko et al., 1990). By stimulating fascicles of preganglionic nerves (Tatarchenko et al 1990) or splitting postganglionic nerves into small strands to allow observation of impulse discharge by a single ganglion cell (Larrabee and Bronk 1947), these studies showed that discharge of a single ganglion cell is governed by a single preganglionic fibre. Hence it is likely that

functionally discrete sympathetic preganglionic efferents synapse with regionally and functionally discrete ganglions that go on to innervate the heart.

This idea has been researched previously in rats by chemically exciting spinal cord neurones (Sundaram et al., 1989a, Sundaram et al., 1989b) and in dogs by electrically stimulating the left and right upper thoracic ventral roots (Norris et al., 1974). The influence of different spinal segments on chronotropic or inotropic functions was however not studied. Therefore evidence of selective regional targets was unobserved.

Differential effects of the left and right sympathetic chains has been previously studied by Norris et al (1974) in which the first five ventral thoracic roots in dogs were stimulated and increases in contractile force were measured. They found that the responses of specific areas of the myocardium varied between ventral roots as did the magnitude of the response. Additionally, Koshtreva (1977) revealed differences in the contribution of different ventral roots in dogs to responses in specific cardiac postganglionic nerves like the ventrolateral cervical cardiac nerve, the ventromedial cervical cardiac nerve and the vagosympathetic trunk, each of which has branches to different regions of the heart. Distinct projections of sympathetic neurones to autonomic, conductile and contractile tissues were shown by Ardell et al (1988) and stimulation of branches of some of these postganglionic nerves had preferential functional cardiac effects. Injections into the sympathetic ganglia of horshradish peroxidase in cats (Chung et al., 1975, Chung et al., 1979, Pardini and Wurster, 1984) and pseudorabiesvirus in rats (Strack et al., 1989), enabled immunohistochemically detectable retrograde viral infections of sympathetic preganglionic neurons. Mapping projections of the preganglionic neurons to the stellate ganglion in this manner found high density of labelling at T1-T2. Similarly, maximum response to electrical stimulation was observed at T2 in cats (Szulczyk and Szulczyk, 1987). Furthermore, experiments in human patients showed a decline in the intensity of chronotropic and inotropic responses elicited by stimulation between T1-T5, with T1-T3 evoking the largest responses and hence containing more fibres (Randall and McNally, 1960). It is therefore likely that there may be differential responses from different spinal

segmental preganglionic neurons as well as a right-left difference described in the previous chapter. Supporting this notion, there is additional evidence to support that different branches of the cardiac postganglionic nerves effect specific regions of the heart (Szentivanyi et al., 1967; Randall et al., 1968; Randall 1977; Armour and Randall, 1975; Randall, 1984; Ng et al., 2009).

Thus far, in all the species studied, T1-T3 appears to be a key contributor to the cardiac sympathetic nerve supply. However, current research does not show direct evidence for selective functional influences of the sympathetic preganglionic nerves arising from different spinal cord segments. Such information is vital for the understanding of cardiac disease in relation to impairment of sympathetic function. What remains unanswered is whether the cardiac sympathetic supply is functionally discrete and how the differential left and right innervation contributes to this. Further investigations are required to determine whether the segmental location of the sympathetic neurones corresponds to a specific cardiac function.

The previous study (Winter et al., 2012) was limited to the T2-T3 level of the sympathetic chain which could not answer the question regarding functional influence. In this study, the left and right sympathetic chains were stimulated at different levels between T1-T6 using the innervated Langendorff rabbit heart model and effects on sinus rate, left ventricular pressure, retrograde ventriculo-atrial conduction, monophasic action potential duration, effective refractory period, ventricular fibrillation threshold and electrical restitution were recorded.

## **5.2 Methods**

The Langendorff innervated rabbit heart preparation was set up as previously described (Ng et al., 2001) and following this, the sympathetic chains were set up for stimulation (n=18).

### **5.2.1 Sympathetic nerve stimulation**

The sympathetic chains were identified lying on either side of midline and parallel to the spinal column. Each chain was dissected free of connective tissue, transected below T6 and decentralized by sectioning the rami from levels T5-T6 to T1-T2. Custom made electrodes consisting of a strip of 6 electrodes, were positioned between T1-T6 on both the left and right sides. Such an arrangement meant that each successive pair of electrodes, from T5-T6 to T1-T2, stimulated all the preganglionic axons from each preceding segment as well as those at which the electrodes were positioned as shown in Fig 5.1. The nerves were lifted gently onto to each electrode and insulated from surrounding tissue and fluid with Kwik-Sil adhesive (WPI, USA). The left and right sympathetic chains were stimulated with a train of square wave pulses at the frequency that produced the maximum heart rate response (5-7 Hz). They were stimulated via pairs of electrodes (cathode proximal to stellate ganglion) at five sites, T1-T2, T2-T3, T3-T4, T4-T5 and T5-T6, at x2 threshold voltage for each segment. The threshold voltage was defined as the lowest voltage that gave an increase in both LVP (of 3–4mmHg) and heart rate (of 3–4 bpm). Caudal to these segments, stimulation in trial experiments failed to get effects on any recorded functional parameter. The five electrode pairs were stimulated from rostral to caudal, caudal to rostral and in a randomised order.

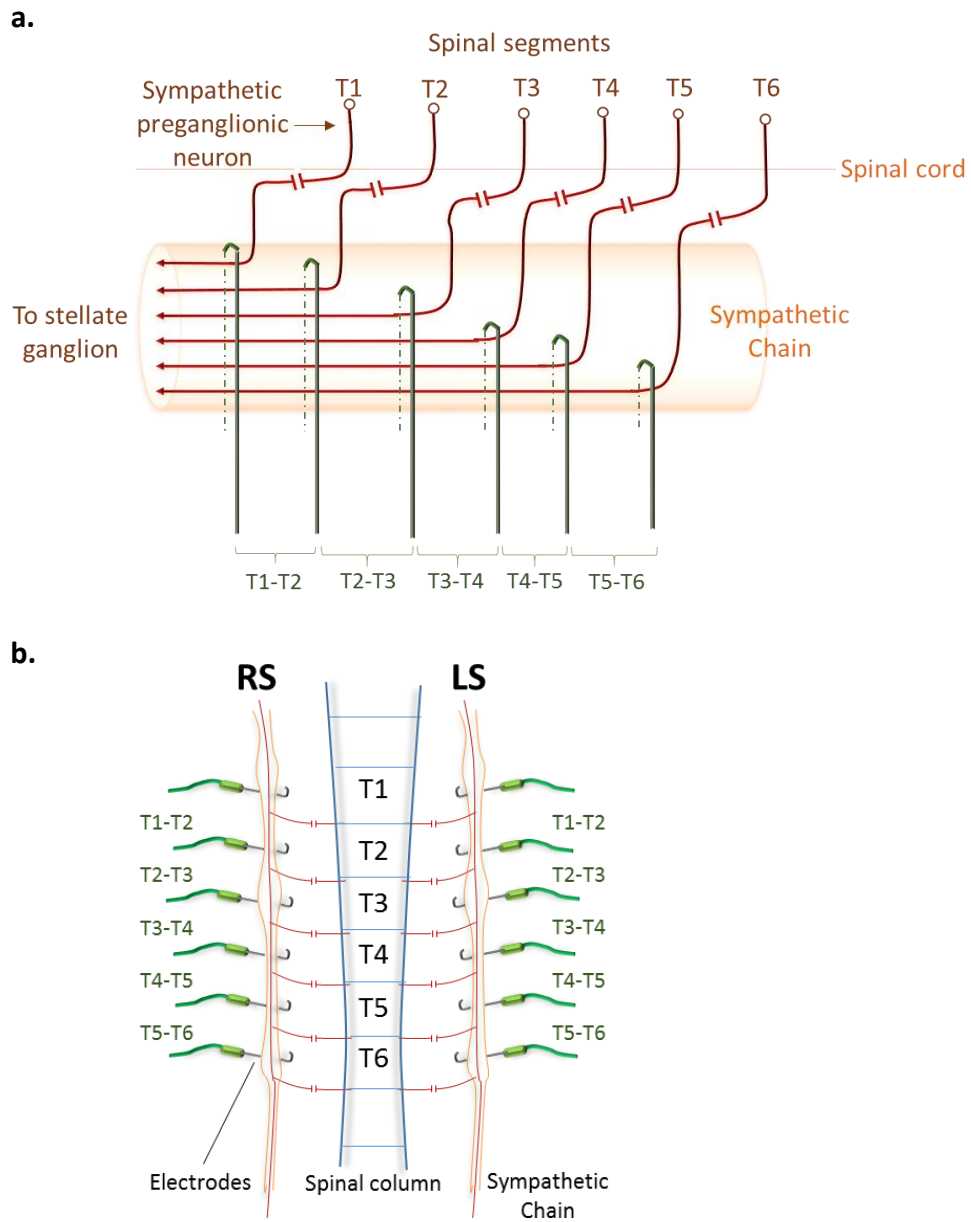


**Figure 5.1. Diagram to illustrate the methods used to stimulate the cardiac sympathetic preganglionic neurones projecting to the stellate ganglion from that upper thoracic spinal cord.** (a) Schematic to show the theoretical basis underlining the experimental approach whereby the placement of the stimulating electrodes activates an increasing contribution of sympathetic preganglionic axons from successive spinal cord segments. (b) Drawing showing the placement of electrodes on right and left sympathetic chains parallel to the spinal column at levels between T1-T6. These six electrodes were carried on a narrow plug attached to the posterior chest wall and the whole arrangement was insulated with Kwik-Sil adhesive.

### **5.2.2 Method Development**

As this is a new technique, it required much development. Initially, bipolar electrodes were used for stimulation and were moved to each segmental level as required. However, there were concerns of the nerve drying out using this method and the nerve response was short lived or non-existent. Movement of the electrode also required moving the heart, which meant the position of the MAP electrodes were lost and new MAP signals had to be found each time. Thus, it was evident that multiple fixed electrodes were needed and insulation with Kwik-Sil adhesive would be required.

A strip of 6 electrodes was made for each chain. For this it was necessary to measure the preparation for exact size and spacing distance, to ensure electrode placement at the correct levels. These were remade several times with small amendments. Firstly, with use of a thicker wire for the electrode to allow for more stability and to minimise positional changes. Secondly, a second layer of wire was added above the first. This was because the sympathetic chain was lifting off the electrodes during the process of insulation. Once the sympathetic chain was placed on the first layer of hooked electrodes, the second layer was gently maneuvered closer to the first. The purpose of this was so that the nerve chain would still be touching an electrode even if it lifted up slightly. The final electrodes are displayed in fig 5.2.

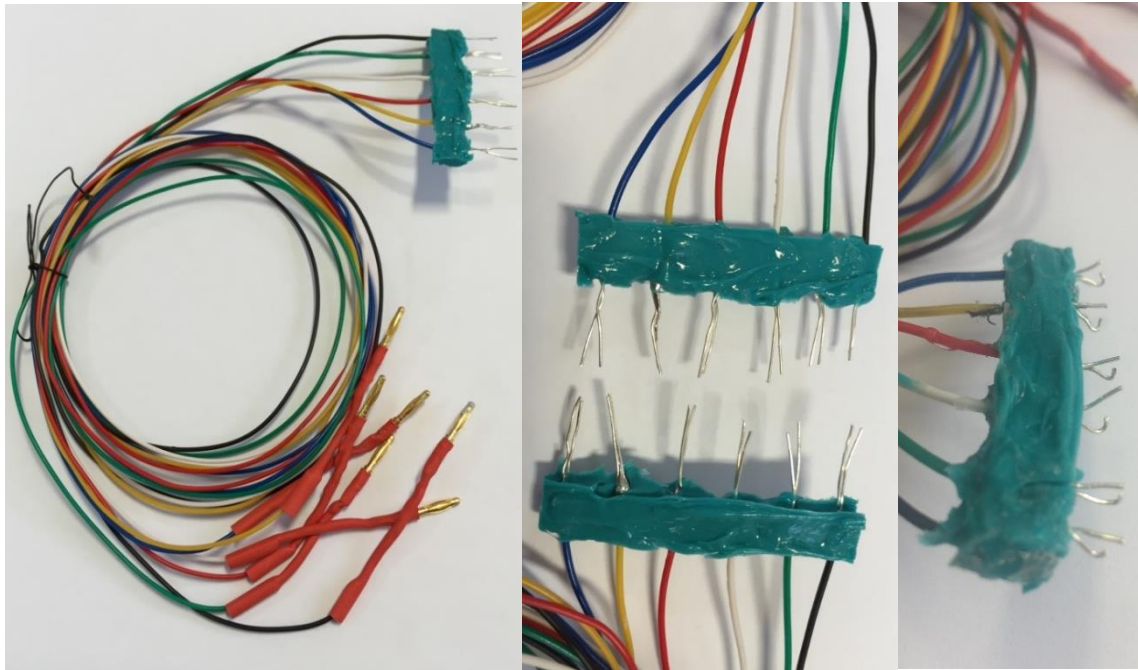


**Figure 5.2.** Custom made electrodes used for stimulation of the left and right sympathetic chains.

During the development of this method it became apparent that it was necessary to cut the rami from levels T5-T6 to T1-T2. This enabled easier lifting of the nerve for placement on the electrodes throughout which care must be taken not to stretch or damage the nerve. As well as this, the rami contain both efferent and afferent fibres and cutting the rami was important in insuring there was no afferent input to the spinal cord upon stimulation, which would complicate the neuronal input. It did not however affect the neuronal input to the heart. Once the electrode placement was at the same level on both left and right sides, the electrode strip was tied to the prep with sutures to prevent movement. The sympathetic chain was then correctly position on the electrodes and insulated with Kwil-Sil adhesive. The surrounding fluid was removed using a suction pipette to prevent electrode shunting. Fig 5.3 shows the final preparation.

In previous studies the sympathetic nerves were stimulated via the spinal cord at a voltage that produced 80% of the maximum response (at 5Hz) and a frequency that gave a heart rate of less than 200bpm (Ng et al., 2007). However, with the sympathetic chains, repeated stimulation of this magnitude was at risk of overheating and damaging the chain. For stimulating the sympathetic chains we

followed similar protocols to the Winter et al (2014) study. Each chain and spinal segment was stimulated using incremental voltages from 0.5V at 5 Hz (2ms pulse width) until there was an increase in both LVP (of 3–4mmHg) and heart rate (of 3–4 bpm). The voltage that gave this change was regarded as the threshold voltage and was doubled. This method reduced the chance of nerve damage by overstimulation at high voltages. Once the threshold voltage was determined, the frequency was increased from 5Hz in increments of 1Hz until the maximum heart rate response was achieved. If the frequency was increased further past this point then the initial response from nerve stimulation began to diminish suggesting nerve damage at high frequencies.

For this preparation, it was also necessary to slightly modify the surgery and cannulate the ascending aorta at a lower level to remove the chance of damaging the left sympathetic chain which runs closely parallel to it.

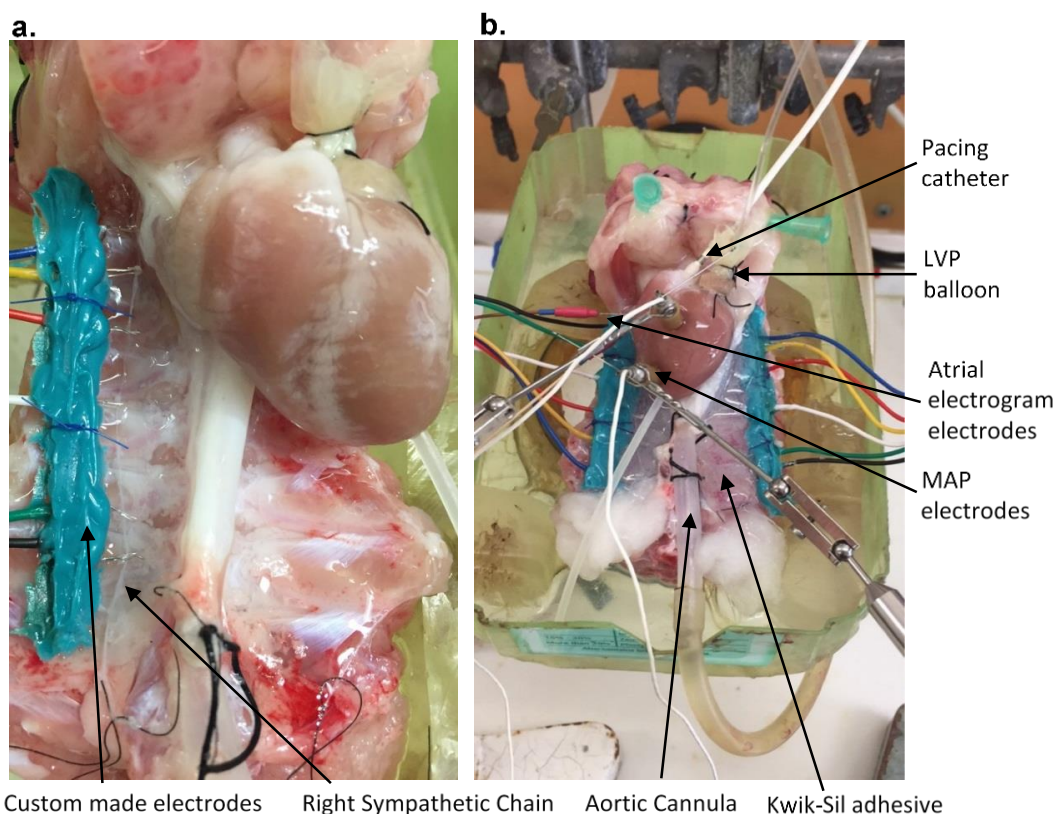


**Figure 5.3.** Final set up of preparation with isolated sympathetic chains and fixed electrodes

## **5.3 Results**

This data displays the differential effects of right and left sympathetic stimulation on ventricular electrophysiology, when stimulated at different spinal segments from T1-T6 (n=18).

### **5.3.1 Effect of left or right sympathetic chain stimulation on Heart Rate (HR) and Left Ventricular Pressure (LVP).**

At each of the electrode pairings between T1-T5, both right and left chain stimulation augmented HR and LVP as seen in figure 5.4. T5-T6 on the left side also increased both HR and LVP however, the right side stimulation at this level was ineffective. A greater response was observed at successive rostral levels due to more sympathetic preganglionic axons activated at these levels. Right chain stimulation elicited greater HR effects than left chain stimulation. In contrast, left sympathetic chain stimulation evoked greater LVP effects than right stimulation.

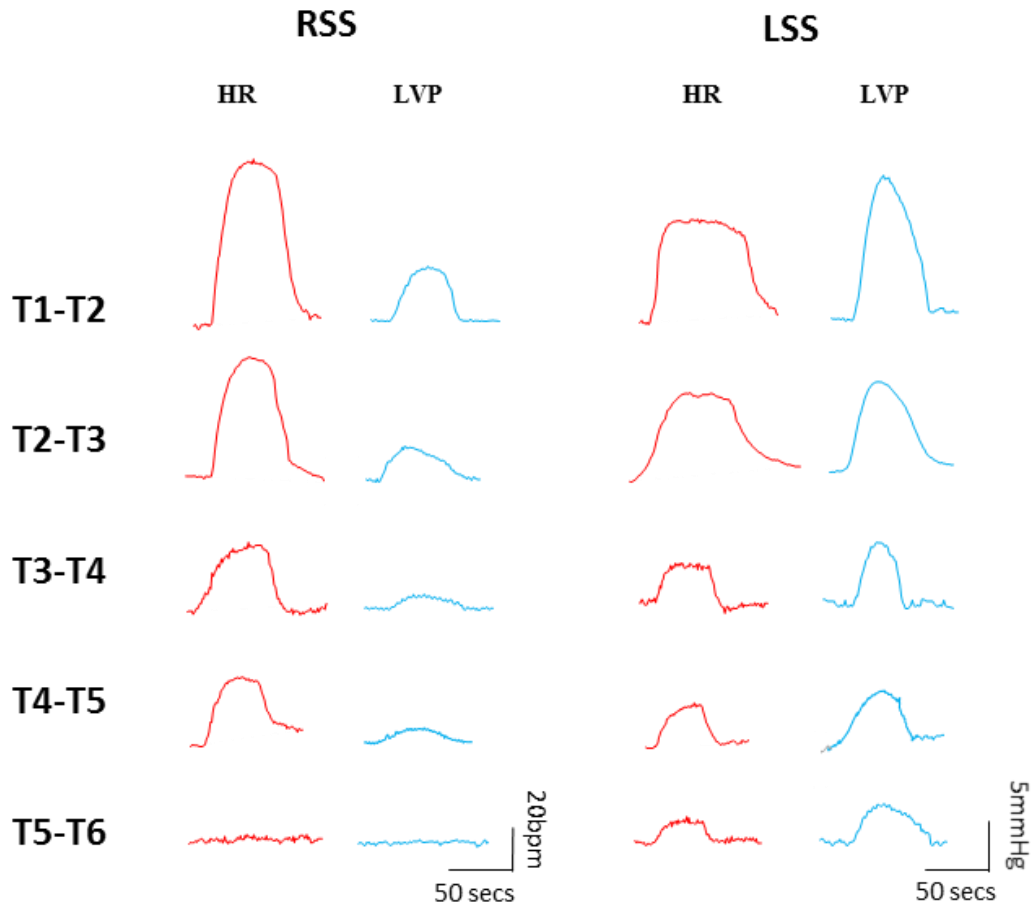


**Figure 5.4.** Raw data heart rate and left ventricular pressure traces recorded during right and left sympathetic chain stimulation, a spinal segmental levels between T1-T6. The left panel shows heart rate response (red) and left ventricular pressure (blue) during right sympathetic stimulation at each segmental level. The right panel shows heart rate response (red) and left ventricular pressure (blue) during left sympathetic stimulation at each segmental level.

### ***Chronotropic effect***

Fig 5.5 illustrates the effects on HR. Stimulation of the left sympathetic chain at T5-T6 increased HR to  $136.5 \pm 4.6$  bpm ( $11.2 \pm 6.1\%$  change from baseline). Subsequently, comparing the mean increases in HR from left with those from right sympathetic stimulation at successive levels, at T4-T5 the increase in HR from left sympathetic stimulation was  $145.4 \pm 3.9$  bpm ( $15.1 \pm 2.7\%$ ), and to right sympathetic stimulation  $167.6 \pm 11.5$  bpm ( $25.9 \pm 7.5\%$ ); T3-T4, left sympathetic stimulation increased HR to  $155.0 \pm 6.5$  bpm ( $19.0 \pm 4.4\%$ ), right sympathetic to  $170.4 \pm 7.0$  bpm ( $29.0 \pm 4.3\%$ ); T2-T3, left increased to  $171.3 \pm 5.3$  bpm ( $29.4 \pm 4.6\%$ )

and right to  $189.5 \pm 5.7$  bpm ( $43.6 \pm 4.7\%$ ); T1-T2, the left sympathetic stimulation elicited an increase to  $181.8 \pm 7.6$  bpm ( $41.1 \pm 5.6\%$ ) and the right sympathetic an increase to  $211.8 \pm 6.9$  bpm ( $59.9 \pm 6.0\%$ ). Notably, the largest HR response was evoked at T1-T2 where all the preganglionic axons are stimulated, yet this was less than the sum of the sequence of increases from T5-T6.

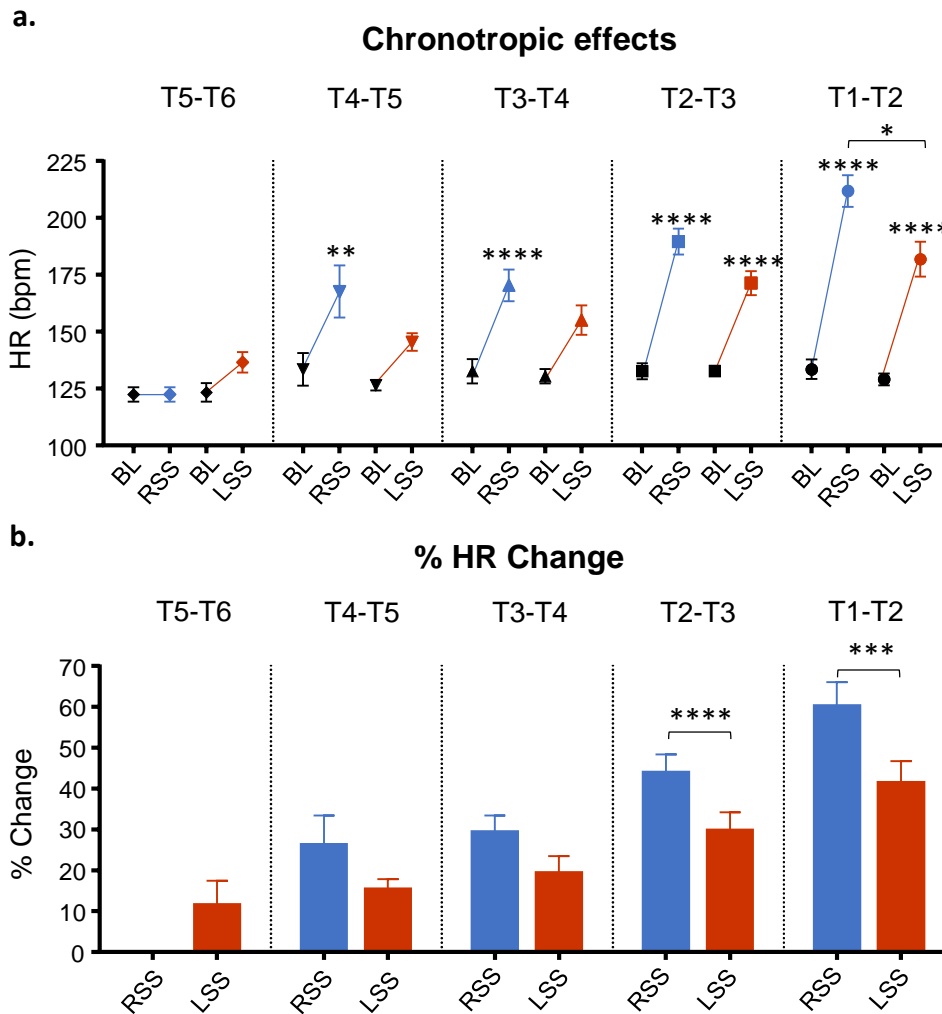


**Figure 5.5. The effect on heart rate (HR) with right and left sympathetic stimulation at different spinal segments.** (a) HR response from baseline (BL) to right sympathetic stimulation (RSS) and BL to left sympathetic stimulation (LSS) at spinal segments T1-T6. (b) Percentage HR change for RSS and LSS at spinal segments T1-T6. Data represent mean  $\pm$  SEM. \* $P < 0.05$ , \*\* $P < 0.01$ , \*\*\* $P < 0.001$ , \*\*\*\* $P < 0.0001$ .

### ***Inotropic effects***

The effects of right and left sympathetic stimulation on left ventricular pressure (LVP) were measured during constant ventricular pacing and are shown in Fig. 5.6. An increase in LVP to  $38.8 \pm 6.1$  mmHg ( $13.0 \pm 2.1\%$  from baseline) was observed at T5-T6, but there was no effect on LVP with right stimulation at this level. Stimulation at successive levels elicited a greater LVP response from left sympathetic chain stimulation when compared to right sympathetic chain stimulation as follows: T4-T5, left side effect was  $40.5 \pm 4.0$  mmHg ( $17.4 \pm 3.0\%$ ), right was  $36.8 \pm 4.0$  mmHg ( $5.6 \pm 1.5\%$ ); T3-T4, left was  $43.6 \pm 4.0$  mmHg ( $20.9 \pm 2.6\%$ ), right was  $38.6 \pm 4.0$  mmHg ( $7.0 \pm 1.6\%$ ); T2-T3 left was  $45.3 \pm 3.5$  mmHg ( $28.8 \pm 2.4\%$ ), right was  $38.5 \pm 3.4$  mmHg ( $15.1 \pm 2.3\%$ ); T1-T2 left was  $51.3 \pm 3.9$  mmHg ( $40.3 \pm 5.4\%$ ), right was  $40.7 \pm 3.7$  mmHg ( $20.7 \pm 3.2\%$ ). As seen with the HR changes, the largest response to stimulation of all the preganglionic axons from each of the segments in the sympathetic chain at T1-T2 was less than the sum of the sequence of increases from T5-T6. The greatest effects were observed at T1-T2 with a dominant effect of left sympathetic chain stimulation at all levels.

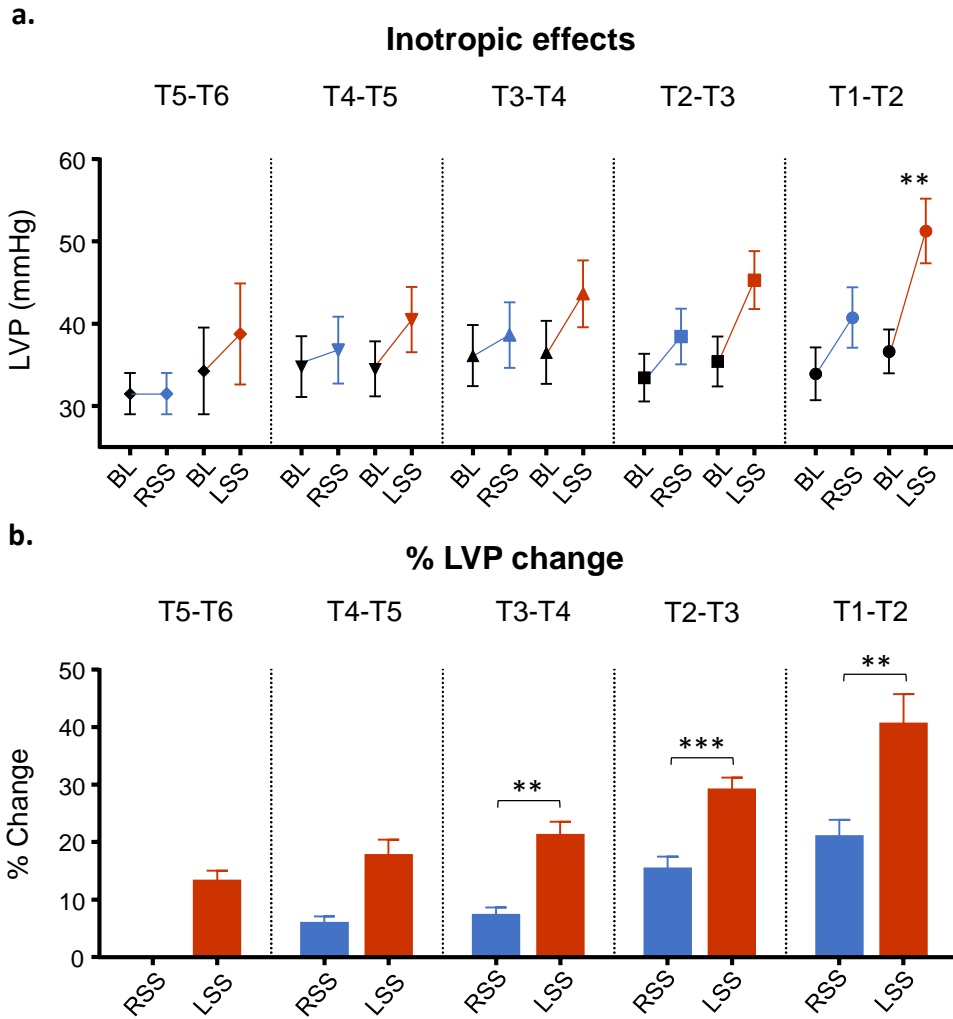


**Figure 5.6. The effect on left ventricular pressure (LVP) with right and left sympathetic stimulation at different spinal segments. (a) LVP response from BL to RSS and BL to LSS at spinal segments T1-T6. (b) Percentage LVP change for RSS and LSS at spinal segments T1-T6. Data represent mean  $\pm$ SEM. \*\*P<0.01, \*\*\*P<0.001.**

### 5.3.2 Effect on atrioventricular (AV) conduction

At each electrode pairing between T1-6, dromotropic effects were measured during constant pacing of the right ventricle with left and right sympathetic chain stimulation (fig 5.7). This allows measurement of retrograde ventriculo-atrial (VA) conduction. Both left and right chain stimulation caused a shortening in VA conduction time although left stimulation elicited the largest changes at all levels. Left sympathetic stimulation decreased VA conduction time from  $143.7 \pm 1.8$ ms to  $137 \pm 1.7$ ms ( $-4.6 \pm 0.2\%$ ) at T5-T6, but right stimulation was ineffective. A similar reduction was also seen at T4-T5 and T3-T4 by left and right sympathetic chain stimulation. Larger reductions were elicited at more rostral levels; at T2-T3 left side was  $130.1 \pm 6.7$ ms ( $-12 \pm 5.0\%$ ) and right was less at  $137.2 \pm 3.5$ ms ( $-6.4 \pm 1.7\%$ ). At T1-T2 the reduction in VA conduction was largest where left side stimulation caused a change to  $125.6 \pm 6.6$ ms ( $-15.5 \pm 0.2\%$ ) whereas the right side was  $135.6 \pm 1.9$ ms ( $-6.8 \pm 1.1\%$ ).

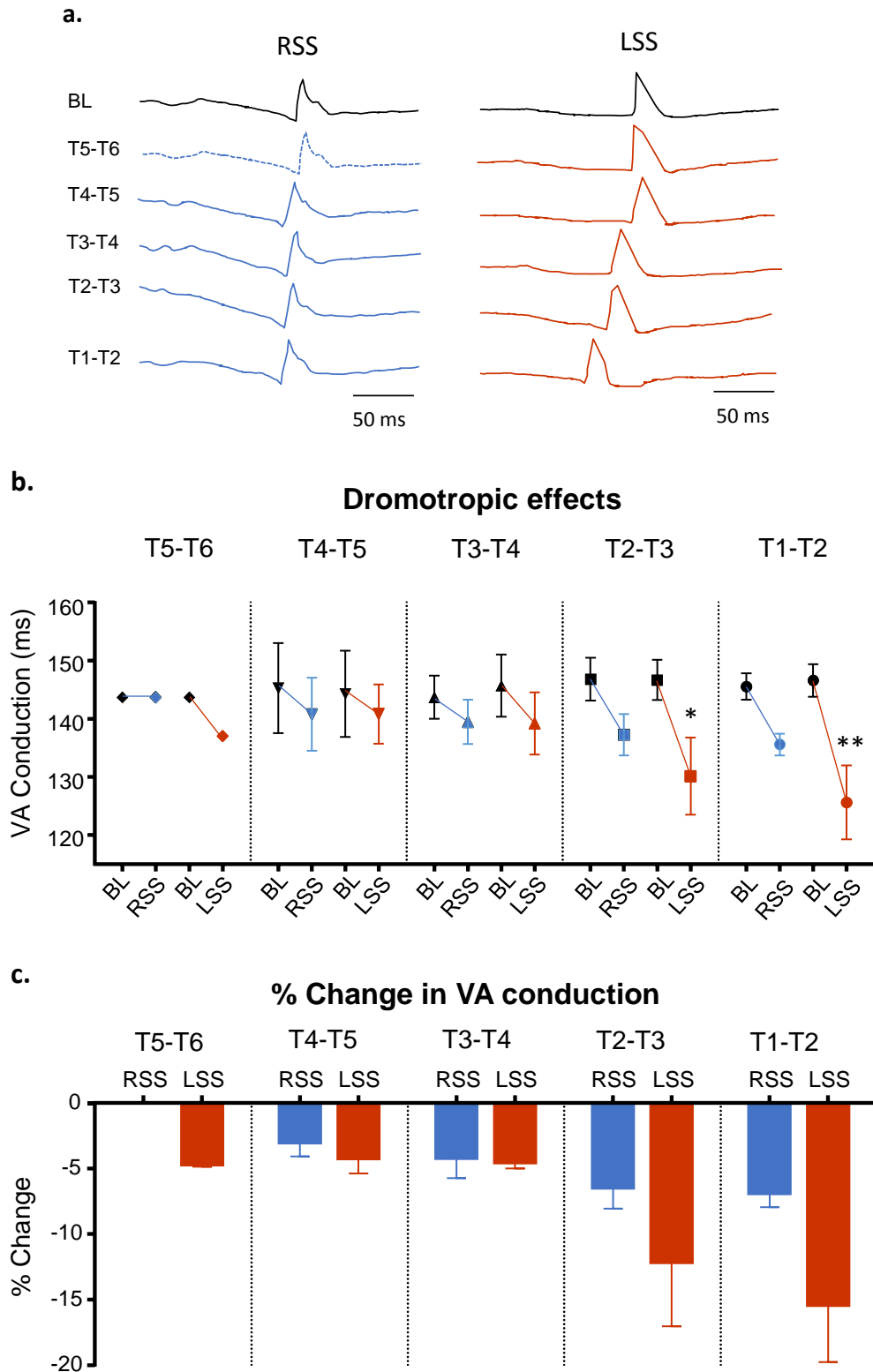


**Figure 5.7. Dromotropic effects upon right and left sympathetic stimulation between T1-T6.** (a) Raw data traces of the right atrial electrogram during baseline (BL) and right sympathetic stimulation (RSS) and left sympathetic stimulation (LSS) between T1-T6. (b) Dromotropic effects from BL to RSS and BL to LSS at spinal segments T1-T6. (c) Percentage change in retrograde ventriculo-atrial (VA) conduction for RSS and LSS at spinal segments T1-T6. Data represent mean  $\pm$  SEM. \* $P < 0.05$ , \*\* $P < 0.01$ .

### 5.3.3 Monophasic action potential (MAP) duration changes

MAP duration changes were measured from the anterior surface of the left ventricle during constant ventricular pacing. MAP duration was shortened by both left and right stimulation at the base and apex, with greater changes observed by left sympathetic chain stimulation. At T5-T6, left sympathetic stimulation decreased MAP duration from 128.2 to  $117.0 \pm 4.1$  ms ( $-8.7 \pm 1.6\%$ ) at the base and from 124.3 to  $113.3 \pm 11.7$ ms ( $-9.2 \pm 2.9\%$ ) at the apex (Fig 5.8). At subsequent levels decreases in MAP duration were similar to T5-T6 for base and apex. No response was observed with right sympathetic stimulation at T5-T6, but a change was seen first at T4-5 at base  $119.3 \pm 2.7$  ms ( $-6.1 \pm 1.3\%$ ) and apex  $118.8 \pm 1.2$  ms ( $-4.9 \pm 1.2\%$ ) and this was little changed by stimulation at subsequent sites. Left sympathetic chain stimulation displayed a considerable dominance on shortening of the MAPs, mainly due to preganglionic fibres at the T5-T6 level. When comparing base and apex data as shown in fig 5.9, left sympathetic stimulation showed a greater change in MAP duration at the base although the difference is small. This effect is particularly evident at the caudal segment T4-T5, where even right stimulation displays dominant changes at the base (fig 5.9c).

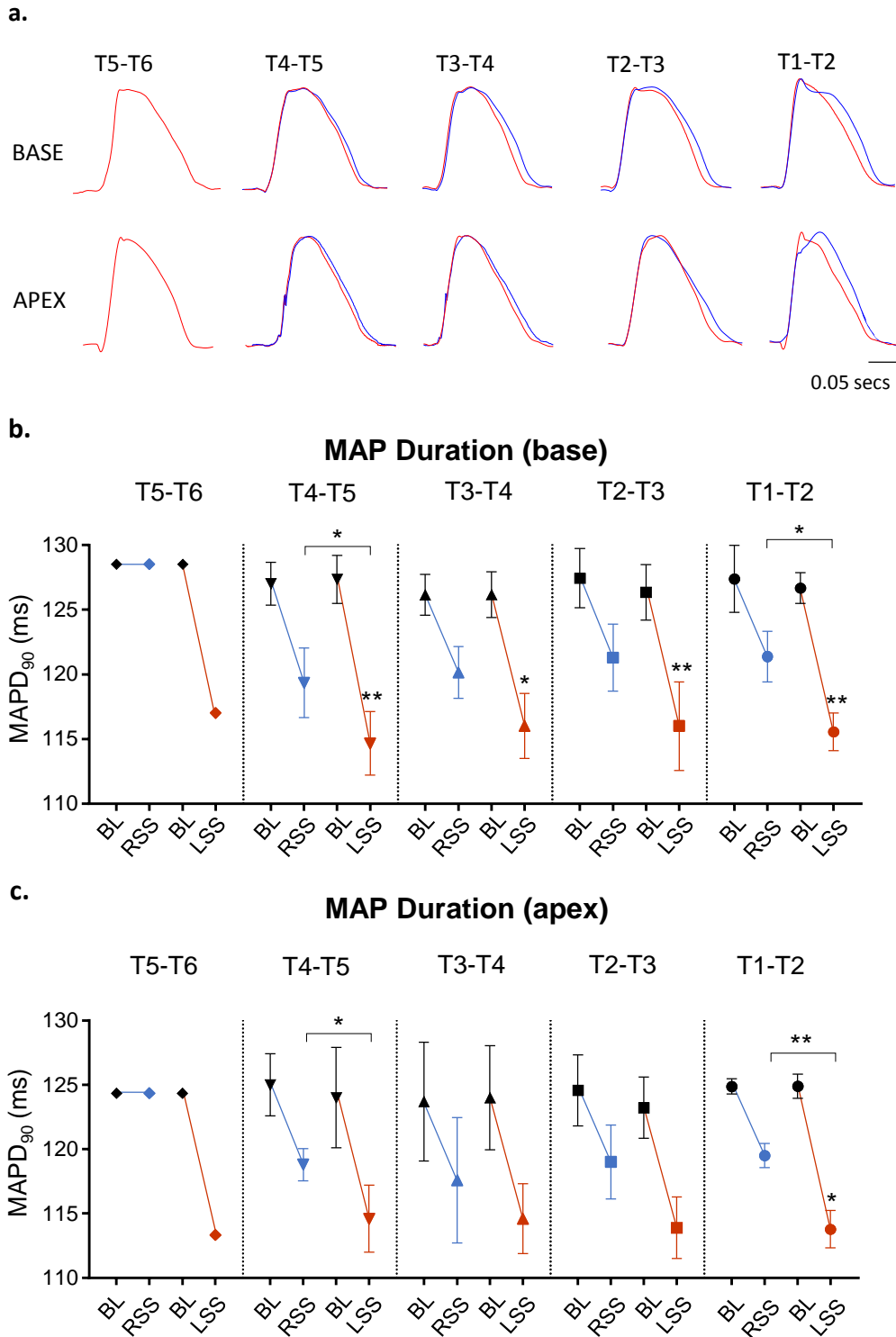


**Figure 5.8. Effects of right and left chain stimulation on monophasic action potential (MAP) duration.** (a) Basal and apical MAP traces during right sympathetic stimulation (RSS) and left sympathetic stimulation (LSS) at the levels stimulated between T1-T6. (b) Basal MAP duration during baseline (BL) and RSS and LSS between T1-T6. (c) Apical MAP duration during BL and RSS and LSS between T1-T6. Data represent mean  $\pm$  SEM. \* $P < 0.05$ , \*\* $P < 0.01$ .

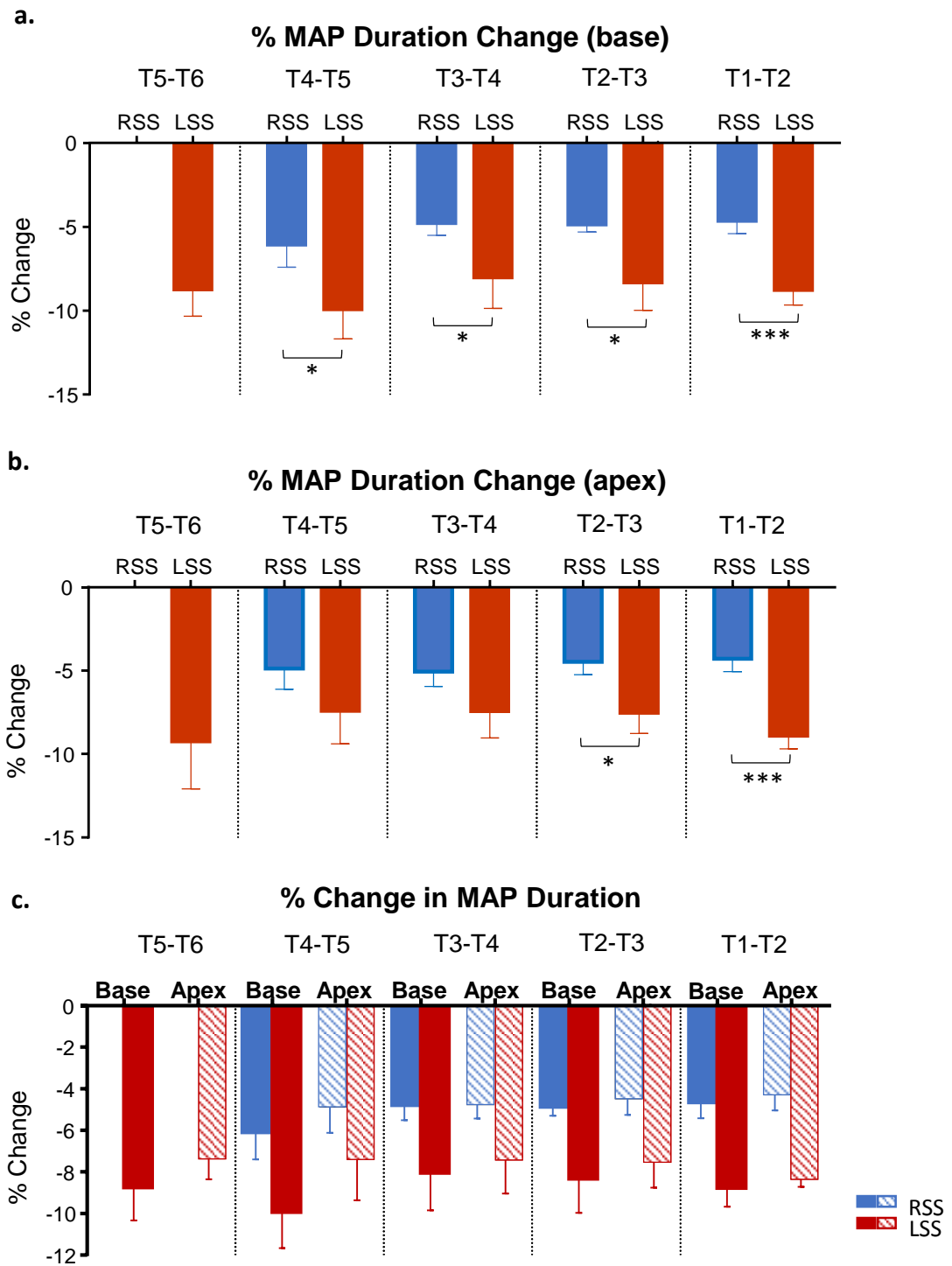


**Figure 5.9.** (a) Percentage change in basal MAP duration for RSS and LSS at spinal segments T1-T6 (b) Percentage change in apical MAP duration for RSS and LSS at spinal segments T1-T6. Data represent mean  $\pm$  SEM. \* $P < 0.05$ , \*\*\* $P < 0.001$ .

#### **5.3.4 Changes in effective refractory period with right and left sympathetic stimulation at different spinal segments**

At T5-T6, left sympathetic stimulation decreased the effective refractory period (ERP) from  $147.5 \pm 12.5$  ms to  $131.7 \pm 4.4$  ms, a change of  $-8.1 \pm 4.4\%$  (Fig 5.10) but there was no effect of right sympathetic stimulation at this level. ERP was further shortened by stimulation of each sympathetic chain at subsequent levels. At T4-T5 on the left the ERP was reduced to  $131.5 \pm 4.5$  ms ( $-7.7 \pm 1.8\%$ ) similar to T5-T6; right at T4-T5 was  $133.3 \pm 2.5$  ms ( $3.6 \pm 1.3\%$ ); T3-T4 left was  $129.5 \pm 4.9$  ms ( $-11.0 \pm 1.9\%$ ), right was  $133.5 \pm 3.7$  ms ( $-9.6 \pm 1.7\%$ ); T2-T3 left was  $128.9 \pm 4.1$  ms ( $-12.6 \pm 2.5\%$ ), right was  $131.6 \pm 4.3$  ms ( $-9.9 \pm 1.8\%$ ); T1-T2 left was  $121.5 \pm 2.6$  ms ( $-17.6 \pm 2.0\%$ ), right was  $131.5 \pm 4.3$  ms ( $-11.3 \pm 1.7\%$ ).

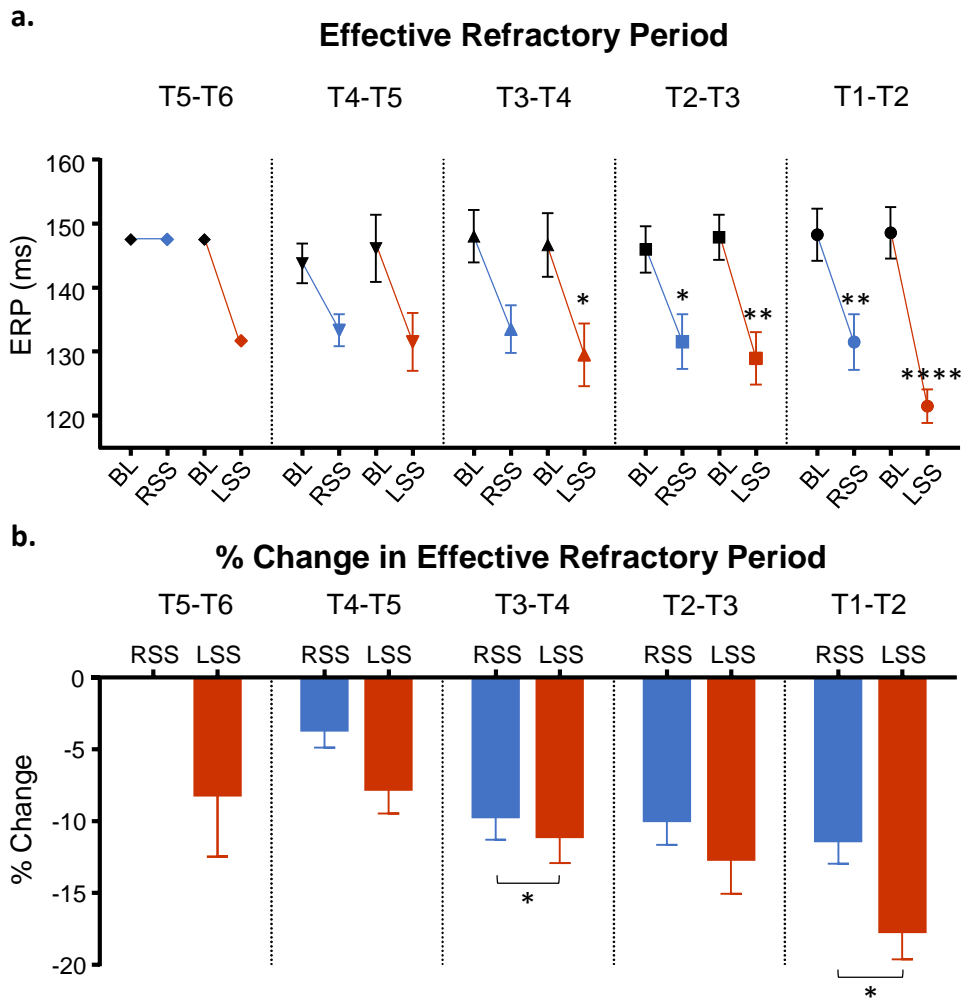


**Figure 5.10. Changes in effective refractory period with right and left sympathetic stimulation at levels stimulated between T1-T6.** (a) Effects on effective refractory period (ERP) from baseline (BL) to right sympathetic stimulation (RSS) and BL to left sympathetic stimulation (LSS) at spinal segments T1-T6. (b) Percentage ERP change for RSS and LSS at spinal segments T1-T6. Data represent mean  $\pm$ SEM. \* $P < 0.05$ , \*\* $P < 0.01$ , \*\*\*\* $P < 0.0001$ .

The relationship between ERP and heart rate is plotted in fig 5.11, illustrating the differential relationships between right and left stimulation.

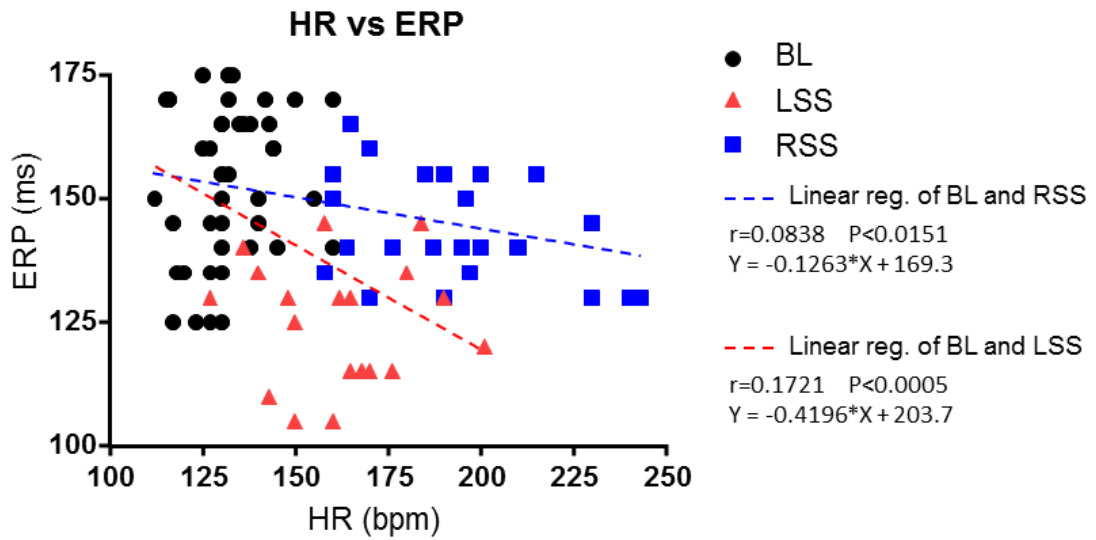


**Figure 5.11. Relationship between heart rate and effective refractory period.** Heart rate (HR) is plotted against effective refractory period (ERP) for baseline (BL) left sympathetic stimulation (LSS) and right sympathetic stimulation (RSS). Linear regression analysis is plotted for the relationship between BL and LSS and between BL and RSS

### 5.3.5 Electrical restitution MAP duration and the effects of right and left sympathetic stimulation at different spinal segments

Fig 5.12 shows restitution curves of the MAP duration at corresponding diastolic intervals, during baseline, left sympathetic stimulation and right sympathetic stimulation. At T5-T6, the maximum slope of restitution was steepened by left sympathetic stimulation by  $18.3 \pm 1.6\%$  at the base but had little effect at the apex  $1.4 \pm 6.1\%$  (fig 5.13). Right sympathetic stimulation had no effect at this level. At subsequent segments, left sympathetic stimulation steepened the maximum slope of restitution at the base to a greater degree than right sympathetic stimulation: T4-T5 left was  $1.8 \pm 0.2$  ( $147.8 \pm 21.7\%$ ), right was  $1.2 \pm 0.1$  ( $69.9 \pm 11.3\%$ ), T3-T4 left was  $1.6 \pm 0.3$  ( $111.5 \pm 25.4\%$ ), right was  $1.1 \pm 0.1$  ( $53.7 \pm 25.7\%$ ), T2-T3 left was  $1.6 \pm 0.1$  ( $121.4 \pm 19.2\%$ ), right was  $1.1 \pm 0.1$  ( $56.9 \pm 17.8\%$ ), T1-T2 left was  $1.8 \pm 0.2$  ( $140.9 \pm 34.4\%$ ), right was  $1.2 \pm 0.2$  ( $67.8 \pm 18.0\%$ ). At the apex, left sympathetic stimulation also steepened the maximum slope of restitution more than right sympathetic stimulation: T4-T5 left was  $1.7 \pm 0.2$  ( $118.2 \pm 21.4\%$ ), right was  $1.0 \pm 0.2$  ( $43.0 \pm 24.0\%$ ), T3-T4 left was  $1.5 \pm 0.1$  ( $120.6 \pm 10.4\%$ ), right was  $1.1 \pm 0.1$  ( $58.2 \pm 14.3\%$ ), T2-T3 left was  $1.4 \pm 0.1$  ( $101.4 \pm 17.3\%$ ), right was  $1.3 \pm 0.2$  ( $39.6 \pm 10.2\%$ ), T1-T2 left was  $1.5 \pm 0.2$  ( $125.5 \pm 22.0\%$ ), right was  $1.0 \pm 0.1$  ( $72.4 \pm 20.8\%$ ). For both base and apex left side preganglionic neurones in the caudal segment T4- T5 were more effective in increasing the slope of restitution, since there was little additional change during stimulation of successive rostral segments. At most levels, left stimulation was shown to have a dominant effect at increasing maximum slope of restitution at the base in comparison to apex (fig 5.14). This was more apparent at caudal levels.

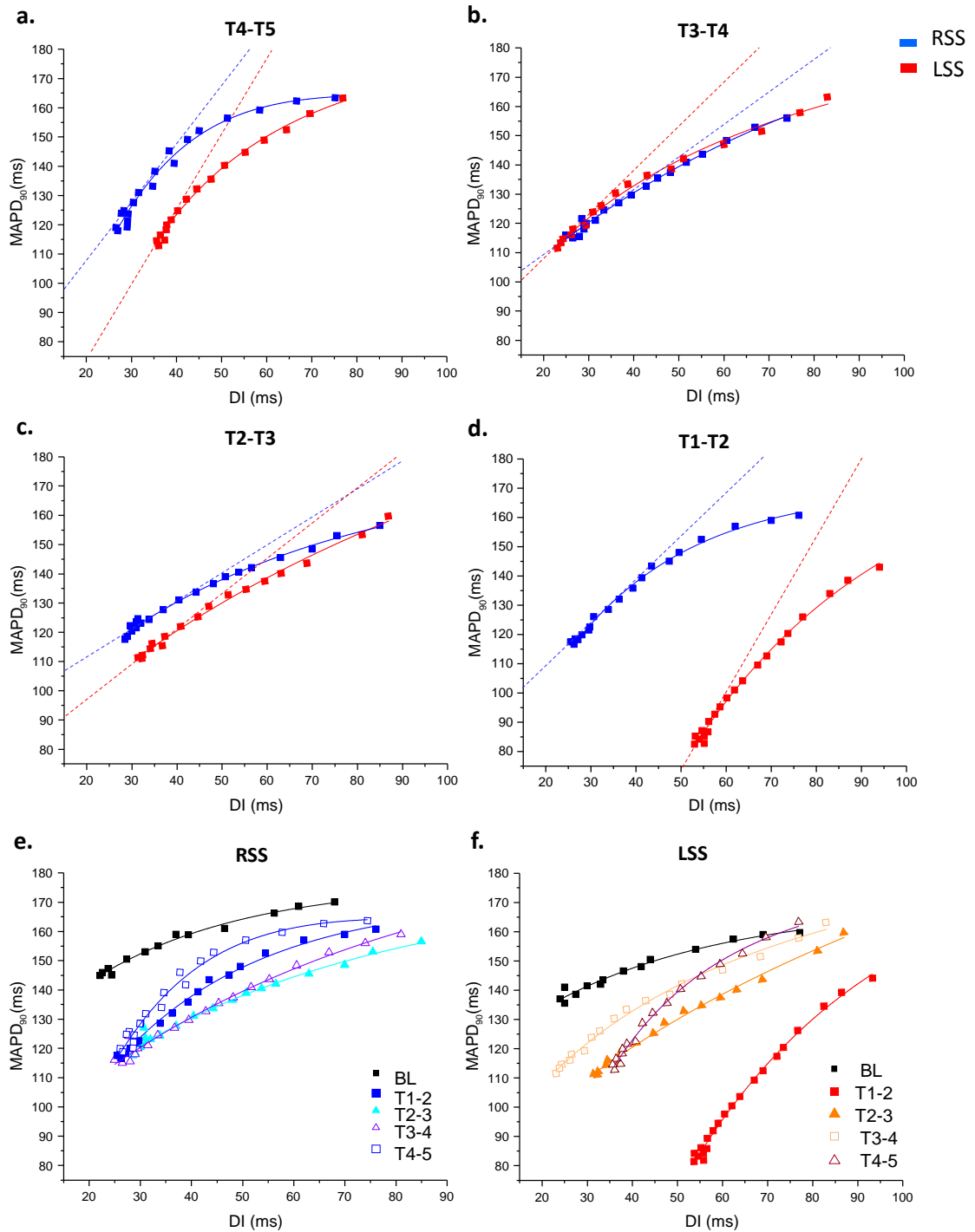


**Figure 5.12. Electrical restitution of monophasic action potential (MAP) duration and the effects of right and left sympathetic stimulation at the levels stimulated between T1-T6.** Restitution (RT) slopes for right sympathetic stimulation (RSS) and left sympathetic stimulation at (a) T4-T5, (b) T3-T4, (c) T2-T3 and (d) T1-T2 with exponential curve fit ( $MAPD_{90} = \text{maximum } MAPD_{90} [1 - e^{-DI/\tau}]$ ). Dotted lines represent the maximum slope of restitution. RT slopes at the levels stimulation between T1-T6 during (e) RSS and (f) LSS with exponential curve fit ( $MAPD_{90} = \text{maximum } MAPD_{90} [1 - e^{-DI/\tau}]$ ).

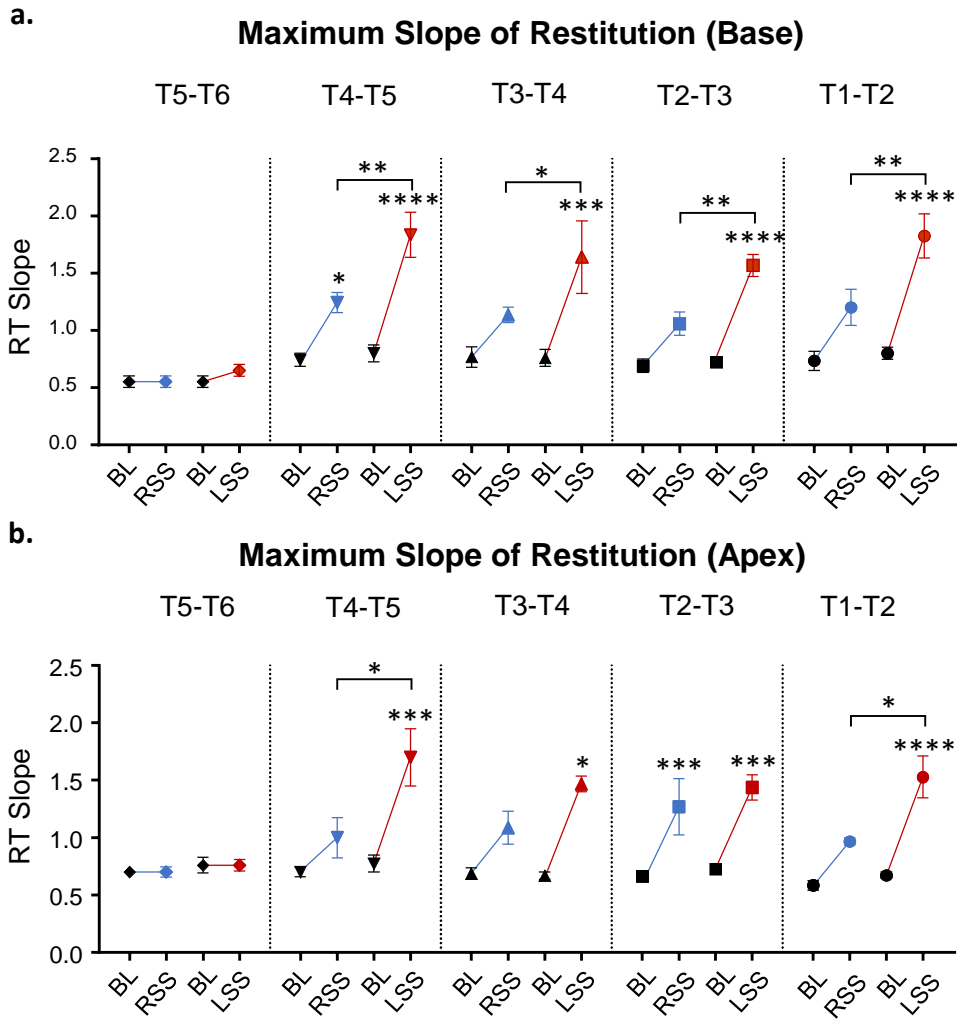


**Figure 5.13. Effect of right and left sympathetic stimulation on maximum slope of restitution.** (a) Maximum slope of restitution at the base from baseline (BL) to right sympathetic stimulation (RSS) and BL to left sympathetic stimulation (LSS) at the levels stimulated between T1-T6. (b) Maximum slope of restitution at the apex from BL to RSS and BL to LSS at the levels stimulated between T1-T6. Data represent mean  $\pm$ SEM. \* $P < 0.05$ , \*\* $P < 0.01$ , \*\*\* $P < 0.001$ , \*\*\*\* $P < 0.0001$ .

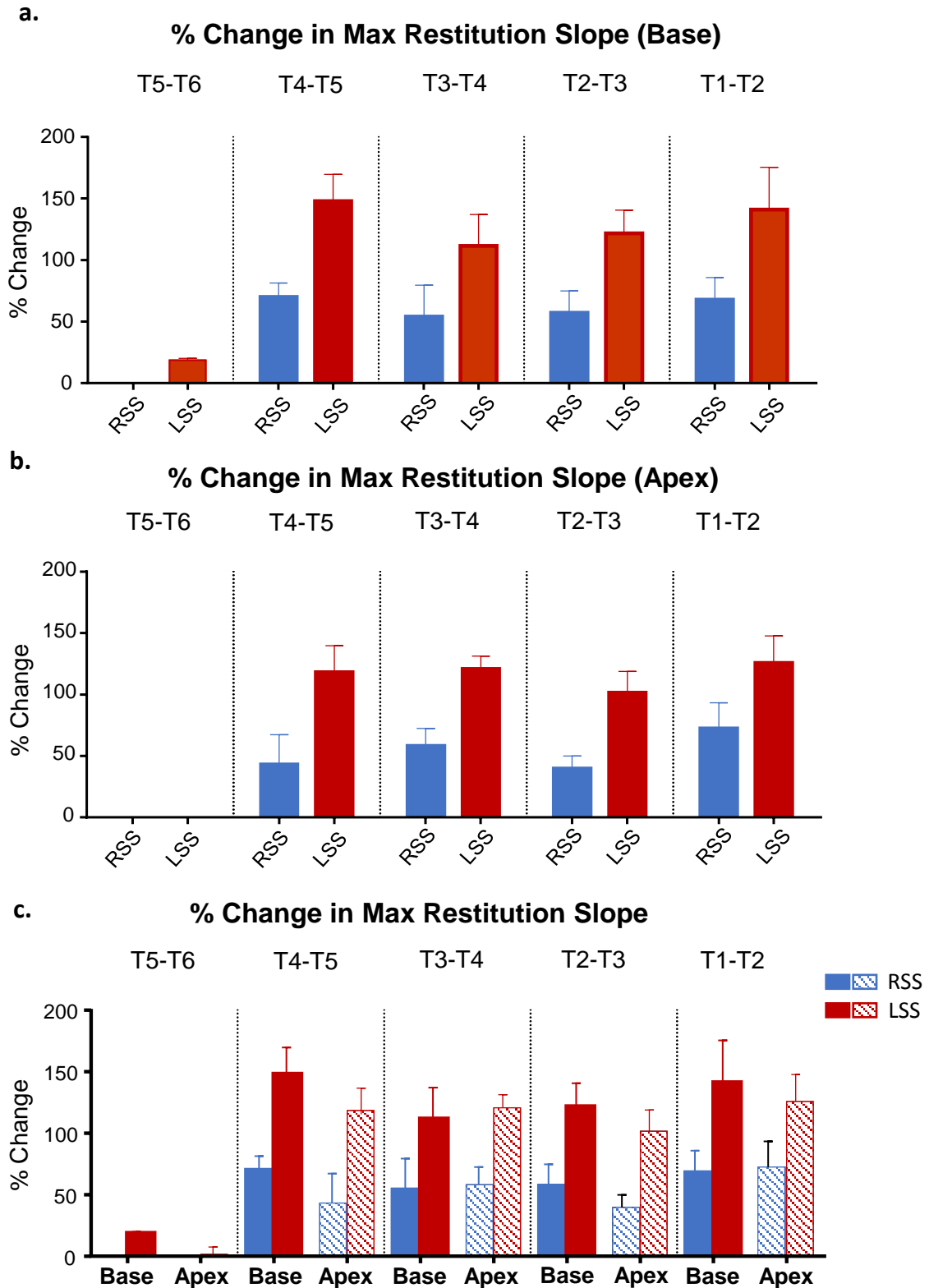


**Figure 5.14.** (a) Percentage change in the maximum slope of restitution at the base for RSS and LSS at spinal segments T1-T6. (b) Percentage change in the maximum slope of restitution at the apex for RSS and LSS at spinal segments T1-T6. Data represent mean  $\pm$ SEM.

### **5.3.6 Effect of right and left sympathetic stimulation at different spinal segments of ventricular fibrillation threshold**

Ventricular fibrillation (VF) threshold decreased with both right and left sympathetic stimulation at electrode pairs between T1-T5 as seen in fig 5.15. Left sympathetic chain stimulation elicited larger decreases in VF threshold compared to right sympathetic chain stimulation at each segment. There was no effect of right stimulation on VF threshold at T5-T6 but left sympathetic stimulation decreased VF threshold to  $2.8 \pm 0.3 \text{ mA}$  ( $-25.9 \pm 11.6\%$ ) at this level. Thereafter, both left and right stimulation caused a decrease as follows: T4-T5 left was  $2.9 \pm 0.6 \text{ mA}$  ( $-39.0 \pm 1.7\%$ ), right was  $3.6 \pm 0.9 \text{ mA}$  ( $-22.3 \pm 6.8\%$ ); T3-T4 left was  $3.6 \pm 0.6 \text{ mA}$  ( $-30.1 \pm 7.7\%$ ), right was  $3.9 \pm 0.5 \text{ mA}$  ( $-29.8 \pm 4.1\%$ ); T2-T3 left was  $3.4 \pm 0.4 \text{ mA}$  ( $-46.4 \pm 5.5\%$ ), right was  $4.5 \pm 0.6 \text{ mA}$  ( $-33.9 \pm 5.1\%$ ); T1-T2 left was  $3.2 \pm 0.3 \text{ mA}$  ( $-50.7 \pm 3.9\%$ ), right was  $3.8 \pm 0.6 \text{ mA}$  ( $-37.7 \pm 6.0\%$ ). A large proportion of the maximum response (76.8% of maximum response) arose from segment T4-T5. These effects were repeatable and consistent at each level and suggest that high amounts of sympathetic drive from the most caudal segments are strongly arrhythmic.

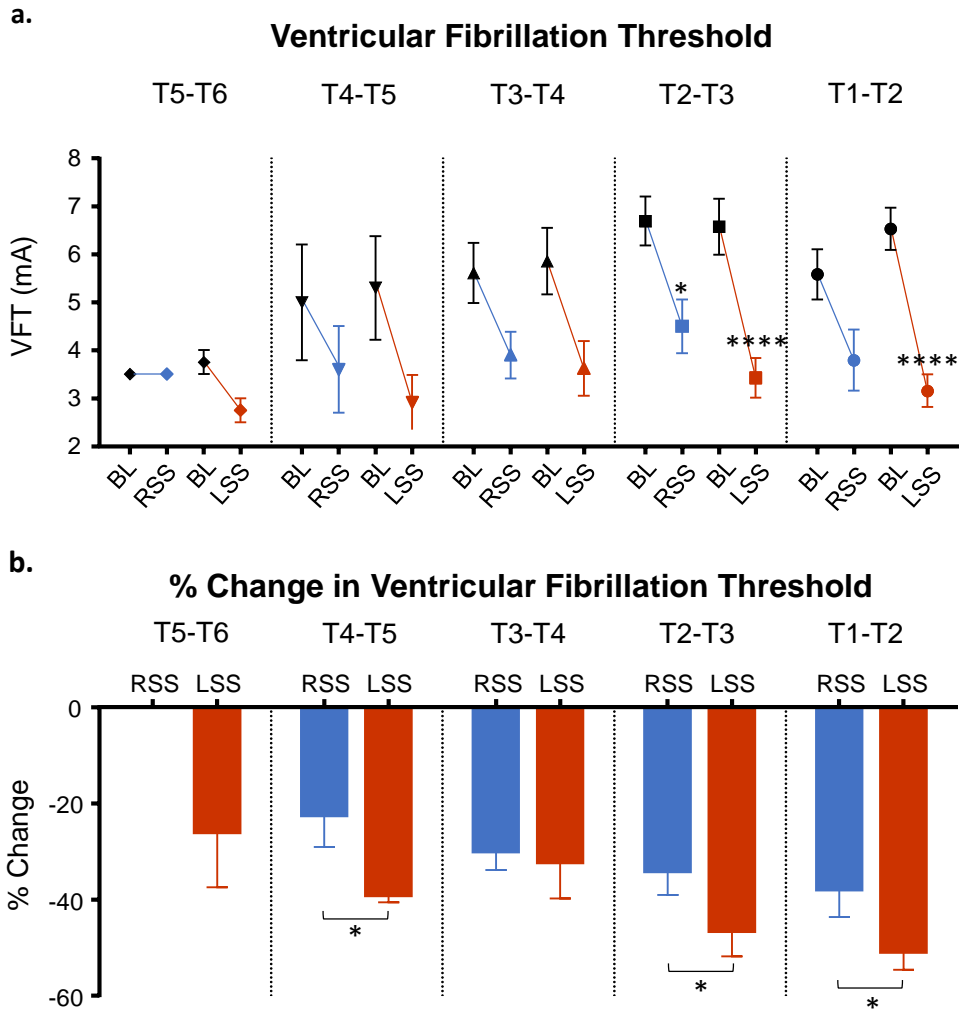


**Figure 5.15. Effect of right and left sympathetic stimulation on ventricular fibrillation threshold (VFT).** (a) VFT changes from baseline (BL) to right sympathetic stimulation (RSS) and BL to left sympathetic stimulation (LSS) at the levels stimulated between spinal segments T1-T6. (b) Percentage change in VFT for RSS and LSS at spinal segments T1-T6. Data represent mean  $\pm$ SEM, \* $P < 0.05$ , \*\*\*\* $P < 0.0001$ .

## 5.4 Discussion

Using a novel refinement of the original isolated innervated heart preparation that allows controlled segmental stimulation, this study demonstrates that there are groups of preganglionic neurones in different spinal segments with distinctly different actions on cardiac cells. Therefore, they must selectively target functionally distinct cardiac postganglionic neurones in the stellate ganglia. Right-left differences in the degree of the functional effects were also observed. Dominant effects on electrophysiological parameters were elicited by the left sympathetic chain as seen previously, however a more novel finding was that there was also a dominance at caudal levels. For the first time, we note the importance of caudal left sympathetic stimulation in cardiac excitability and its potential to induce arrhythmia.

Assuming there are functionally similar groups of preganglionic neurons at each segment, as we stimulate electrode pairs from caudal to rostral we would expect that more axons will be stimulated, resulting in a progressive increase in the size of the cardiac response. This was true for the chronotropic and inotropic responses which displayed an additional increase in rate and force from caudal to rostral electrode pairs. This was not as a result of simple summation as the size of the response at T1-T2 was less than the sum of the sequence of increases from T5-T6. The size of the compound action potential is a reflection of the number of postganglionic neurons activated (Ninomiya et al., 1993). Therefore, the data suggest that the preganglionic neurones arising from each spinal segment converge onto groups of neurones in a single functional pool of postganglionic neurones in the stellate ganglion, a typical characteristic of all autonomic ganglia (Jänig, 2006).

As seen in previous studies (Randall and Rohse, 1956, Randall et al., 1968a, Furnival et al., 1973, Winter et al., 2012) the right sympathetic chain elicited a greater chronotropic response and the left sympathetic chain elicited a greater inotropic response. The largest of these responses was elicited from the first to

third segments (T1 to T3). This suggests that the largest proportion of preganglionic neurones governing the chronotropic and inotropic responses arise from T1-T3 as seen in earlier literature in various species (Randall and McNally, 1960, Norris et al., 1974, Norris et al., 1977, Kostreva et al., 1977, Pracejus et al., 2015). The first of these studies was in anaesthetized open chest dogs by Norris et al (1974) in which left and right stimulation of the ventral roots from T1-T5 showed the second root as the most effective in increasing heart rate, and ventricular force at several discrete areas on the anterior surface of the right and left ventricles. Our study extends these findings in the isolated innervated rabbit heart model which excludes effects of spinal reflexes, haemodynamic changes or circulating hormones. In contrast to the study in dogs, we found the largest response was observed at T1-T2 suggesting spinal segment T1 was of greatest influence. Furthermore, a dominance of left sympathetic stimulation on ventricular force was observed whereas Norris et al (1974) reported that the degree of positive inotropism measured at five sites on the anterior surface of the left ventricle was on average similar for both left and right ventral root stimulation. We measured intraventricular pressure as a representation of force of contraction over the whole left ventricle and found that the effect of the left sympathetic nerves was virtually double that of the right sympathetic nerves at every segmental level.

The ventricular pressure data was collected during constant pacing of the ventricle, thus eliminating the possibility that inotropic increases were produced by changes in heart rate. Interestingly, at T5-T6, only left sympathetic preganglionic neurons produced a chronotropic and inotropic response and hence must be selectively cardiac. No changes in rate or force were present when stimulating this outflow on the right.

Left sympathetic stimulation had a greater effect on AV conduction, particularly at the more rostral segments. Sympathetic stimulation has been shown previously to have direct effects on the AVN and hence AV conduction (Ardell et al., 1988, Winter et al., 2012). Our data show that left sympathetics caused a greater reduction in AV conduction and suggests greater innervation of the AVN

by the left sympathetics as proposed by Ardell et al (1988). A similar effect of left stimulation was seen by Winter et al (2014) however this was restricted to T2-T3. It is important to note that stimulating at this level would also have included axons of neurons from the more caudal segments hence the importance of this study where different levels with more or fewer fibres were stimulated.

Simulation of the left sympathetic chain displayed a more dominant effect with regard to ventricular electrophysiological effects. As seen by Winter et al (2012), left sympathetic stimulation caused greater shortening of MAP duration both at the base and the apex of the anterior ventricle surface when compared to right sympathetic stimulation. This study goes further by showing this effect at the other segmental levels between T1-T6 that were stimulated. The most caudal segments between T4-T6 showed large effects on MAP duration with both left and right sympathetic stimulation, with little additional change in response when successive segments were stimulated. Hence, the effect on MAP duration shortening is likely to be mainly an action of preganglionic neurons located in the caudal spinal segments, with left side dominance at T5-T6. A previous study using optical mapping of the innervated isolated rabbit heart showed a differential gradient of base to apex APD with bilateral sympathetic stimulation (Mantravadi et al., 2007). Although there was a trend for a greater change in MAP duration at the base in comparison to apex, here we have shown that these effects were small. None the less, these results provide evidence of spatial heterogeneities of sympathetic effects and indicate that there may be a greater innervation of sympathetic fibres and a higher density of  $IK_s$  at the base of the ventricle (Ng et al., 2009). The differences observed between base and apex were particularly evident at T4-T5 for both MAP duration and maximum slope of restitution suggesting regional innervation and preferential supply to the base at caudal levels. This merits further investigation into the regional differences in sympathetic innervation of the left ventricle.

These changes were accompanied by reductions in the effective refractory period. The effective refractory period (ERP) was shortened to a greater extent by left sympathetic stimulation than right sympathetic stimulation. Notably the

response from lower thoracic segments was remarkably large when considering how small the heart rate changes were at these levels. We could conclude from this that the changes in ERP observed at this level were independent of heart rate changes. At T1-T2, the reduction in ERP was largest which could partly be explained by the greater effects on heart rate at this level. However, this does not appear to conform to the larger heart rate changes elicited by right sympathetic stimulation and lesser effects on ERP compared to left sympathetic stimulation. Left side preganglionic neurones had a clear dominance over right sympathetic nerves in shortening the ERP even though right sympathetics had a dominant heart rate effect. This was demonstrated in fig 5.11 whereby the left sympathetic response displayed a steeper relationship between heart rate and ERP. This could be explained by the greater MAPD changes evoked by the left sympathetics and their more dense innervations of the left ventricle. ERP therefore appears to be a dynamic response involving the interaction between several factors including heart rate and ventricular electrophysiology.

This study also reveals that in the rabbit, a major influence on the electrical stability of the heart arises from a group of sympathetic preganglionic neurons from the caudal spinal segments. At both the base and apex, a large proportion of the maximum restitution slope change arose from T4-T5 with right and left sympathetic stimulation. A similar effect was seen with changes in VF threshold at the caudal segments in which a large proportion of the maximum response arose. This is an interesting finding considering that the chronotropic and inotropic changes were small at this level. As seen with MAP duration, there is a trend for a greater steepening of maximum slope of restitution at base in comparison to the apex. Again this effect is more apparent at the caudal levels and more dominant with left sympathetic stimulation.

The caudal segments appear to selectively activate cardiac postganglionic neurons that strongly influence APD, APD restitution and VF threshold as stimulation of successive levels did not significantly increase the responses and thus showed no statistical difference. Moreover, left cardiac sympathetic spinal nerves had a larger influence over left ventricle electrophysiology than right side

preganglionics. Of each parameter measured, a degree of difference was observed both between left-right stimulation and differential spinal segment stimulation. Therefore, a functional difference of preganglionic neurons is apparent.

An important novel finding of this study is the high potential for the caudal spinal sympathetic neurons to cause abnormal cardiac rhythms and hence reveals potential for development of more focused clinical treatments. Understanding the implications of cardiotoxic innervation of the sympathetic nerves and regional electrophysiological effects requires detailed knowledge of innervation, ion channel distribution and dynamic behaviour of the heart. This merits further investigation and would require mechanistic insight on regional APD changes in both activation and repolarization. This would be possible with optical mapping, which is a line of investigation our laboratory is pursuing with this refined preparation.

#### **5.4.1 Clinical implications**

Clinical treatment for LQTS and other chronic cardiac arrhythmias includes removal or pharmacological block of the stellate ganglion. Although successful, this form of treatment is not without its serious side effects for example palmer and facial anhidrosis, loss of vasomotion, and poorer visual and salivary control. The reason for such extreme side effects is that removal of the stellate ganglion also leads to removal of the sympathetic supply to the forelimbs and head. A more focused treatment is necessary to eliminate these side effects whilst still successfully reducing arrhythmia in these patients. A suggestion for this could be to remove the T4-T6 sympathetic outflow on the left side instead of removing the stellate ganglion. This may be surgically challenging but is an approach worth exploring in humans as an alternative treatment for chronic cardiac arrhythmias.

#### **5.4.2 Limitations**

The electrophysiological properties of preganglionic synapses in thoracic ganglia have been well documented (Lichtman et al., 1980, Jänig, 2006). The aim of this

study was to test the idea that functionally distinct cardiac sympathetic preganglionic fibres are located in different segments of the upper thoracic spinal cord. In light of this, we stimulated all axons present in the sympathetic chain at different segmental levels and based our interpretation on changes in the magnitude of the cardiac effect. We used a supramaximal stimulation to moderate effects of subliminal fringe, spatial and temporal facilitation, occlusion, convergence and divergence. Our electrophysiological tests were limited to the anterior surface of the left ventricle but stellate stimulation in pigs and humans suggests that similar actions are likely to have occurred on the posterior aspect of the left ventricle (Ajjola et al., 2013, 2015, Vaseghi et al., 2013). To address the issue of order of testing, we randomized the order of the test series between right and left, and rostral to caudal or vice versa or a random order of segment stimulation.

As mentioned previously, the rabbit was used as the experimental model due to the similarity of its cardiac electrophysiological behaviour to humans. It is however understood that extrapolation of this data to humans must be done with caution. Furthermore, the innervated heart preparation is in isolation from confounding physiological factors and could have aspects of over-simplification of the basic control mechanisms in intact animals and humans. Nonetheless there is plenty of evidence for similarity in the anatomy and function of the autonomic innervation of all mammals studied so far (Janig, 2006) and hence it would be surprising if the functional anatomy is different to what we describe in this study in the rabbit.

### **5.4.3 Conclusion**

These results provide evidence for functionally distinct and dominant sympathetic preganglionic pathways to the heart and reveal previously uncharacterized properties of the preganglionic innervation of cardiac neurones in the rabbit heart. It is apparent from this data that the preganglionic sympathetic neurones target functionally distinct cardiac postganglionic neurons. Further supporting this concept, studies in the brain showed that electrical and chemical stimulation of specific sites led to a distinct response i.e. pathological ECG changes (Delgado,

1960; Manning and Cotton, 1962; Ueda et al., 1962; Openheimer 1994) and brain lesions at different sites are associated with specific ECG abnormalities (Hugenholtz, 1962; Srivastava and Robson, 1964; Fukada et al., 2015; Taggart et al 2016). This is consistent with studies that stimulated the stellate ganglia or branches of the cardiac postganglionic sympathetic nerves (Yanowitz et al., 1966; Szentivani et al., 1967; Randall et al., 1968). These features would require the spinal sympathetic neurones to most densely terminate on postganglionic neurones with a specific regional and functional identity, which is demonstrated by these results for the first time experimentally. As well as this, the results show that the caudal spinal segments (T4-T6) may have a dominant action over cardiac rhythm and be more arrhythmogenic, with the left sympathetic chain more so than the right.

## **Chapter 6**

### **Regional heterogeneities of the cardiac sympathetic neurones**

## **6 Regional heterogeneities of the cardiac sympathetic neurones**

### **6.1 Introduction**

The electrical heterogeneity of the heart is well documented, and factors that cause an amplification of the heterogeneities, such as sympathetic stimulation, can be proarrhythmic. The sympathetic nerves are suggested to have heterogeneous innervations with higher densities of innervation at the base of the ventricle (Ng et al., 2009). The left and right sympathetic neurones, as described in the previous chapters, have different effects on heart rate, left ventricular pressure and cardiac electrophysiology. Differences were also observed between the base and apex of the ventricle, with left sympathetic stimulation eliciting a greater response at the base. Hence, it is suggested that the left and right sympathetics exert these functional differences due to differential innervations in distinct regions of the heart. Although electrical heterogeneity of the heart is well recognised, detailed studies into differential sympathetic innervations and effects on cardiac electrophysiology are lacking. Understanding these differences can provide valuable insight into the predominant effects of left sympathetic neurones on cardiac excitability, and the mechanisms behind its proarrhythmic tendencies.

In order to fully understand the implications of heterogeneity on function of the heart, detailed knowledge of nerve innervation and ion channel distributions is required. Previous studies have shown that there are regional differences in ion channel distribution across the ventricle. Epicardial and endocardial differences have been observed using the left ventricular wedge preparation of the canine heart in which epicardial and endocardial transmembrane action potentials and ECGs were recorded from perfused ventricular wall tissue (Antzelevitch, 2001, Antzelevitch, 2005, Antzelevitch and Belardinelli, 2006). APD was found to be shorter in the epicardium than endocardium, suggested to be due to higher levels of  $I_{TO}$  in the epicardium. The M cell (midmyocardial cell), located in the deep subendocardium to midmyocardium in the anterior wall, has the longest APD (Antzelevitch, 2007). This has been attributed to smaller contributions of  $I_{Ks}$  to

the action potential (Viswanathan and Rudy, 2000) and larger  $I_{Na}$  (Zygmunt et al., 2001, Liu and Antzelevitch, 1995). NCX has also been implicated (Zygmunt et al., 2000).

Regional differences between ion channel distributions at the apex and base have also been identified. Heterogeneous  $K^+$  channel distributions in particular have been studied. In situ hybridization and immunofluorescence studies showed abundance of ERG, which has a role in the rapid component of the delayed rectifier  $K^+$  current ( $I_{Kr}$ ), throughout the ventricular epicardium apart from the base (Brahmajothi et al., 1997b). They also found a wide distribution of different voltage gated  $K^+$  channel transcripts throughout the heart (Brahmajothi et al., 1997b). In the rabbit heart, high densities of  $I_{Ks}$  were identified at the base of the left ventricle as well as high levels of tyrosine hydroxylase (provides indication of sympathetic innervations) (Ng et al., 2009). Also in the rabbit heart, at the apex, high levels of the fast component of the delayed rectifier  $K^+$  current,  $I_{Kr}$  were found (Cheng et al., 1999).

It is generally acknowledged that the right sympathetic nerves preferentially innervate the sinus node and the left sympathetic nerves preferentially innervate the ventricles (Randall and Rohse, 1956, Randall et al., 1968a, Ardell et al., 1988). It has also been reported by Yanowitz et al (1966) that the right stellate ganglion primarily innervates the anterior ventricular surfaces and the left stellate ganglion innervates the posterior, however this is controversial and the study was limited by the small number of electrodes and great variability of data across the anterior and posterior walls. Other studies have demonstrated shared left and right sympathetic innervations on the anterior left ventricle (Rubart and Zipes, 2005), with right sympathetic innervations predominating (Kralios et al., 1975, Opthof et al., 1991). However, left sympathetic neurones have been found to significantly increase the dispersion of repolarisation over the anterior surface more than right sympathetics (Vaseghi et al., 2012b). Detailed reports of the innervations of sympathetic nerves have not yet been established.

Investigations in canine hearts reported parallel but distinct projections of the sympathetic efferents to automatic, conductile and contractile tissues. They found

that right sympathetic projections effecting contractile force (atrial and ventricular) mostly converged within the pulmonary artery nerves (PAN), pathways to the pacemaker were focused between the superior vena cava and ascending aorta, and projections to conductile tissue were localised between the common pulmonary artery and proximal pulmonary artery. Similarly, left sympathetic projections to contractile tissues were found within the PAN and in the ventral lateral cardiac nerve (VLCN), heart rate and conductile tissue projections were concentrated at the left pulmonary artery (Ardell et al., 1988). It has also been shown that fibres originating from the left sympathetic chain lead to the ventromedial cardiac nerve (a branch of the left stellate ganglion) and those from the right sympathetic chain lead to the recurrent cardiac nerve (a branch of the right sympathetic ganglion) as illustrated in fig 6.1 (Kralios et al., 1975, Haws and Burgess, 1978). However, there is still a poor understanding of the specificity of left and right sympathetic innervations and the functional effects of their stimulation on the heart. Specifically, there is a lack of data to help understand how the differential innervations effect the cardiac electrophysiology and how this becomes impaired in diseases with sympathetic imbalance.

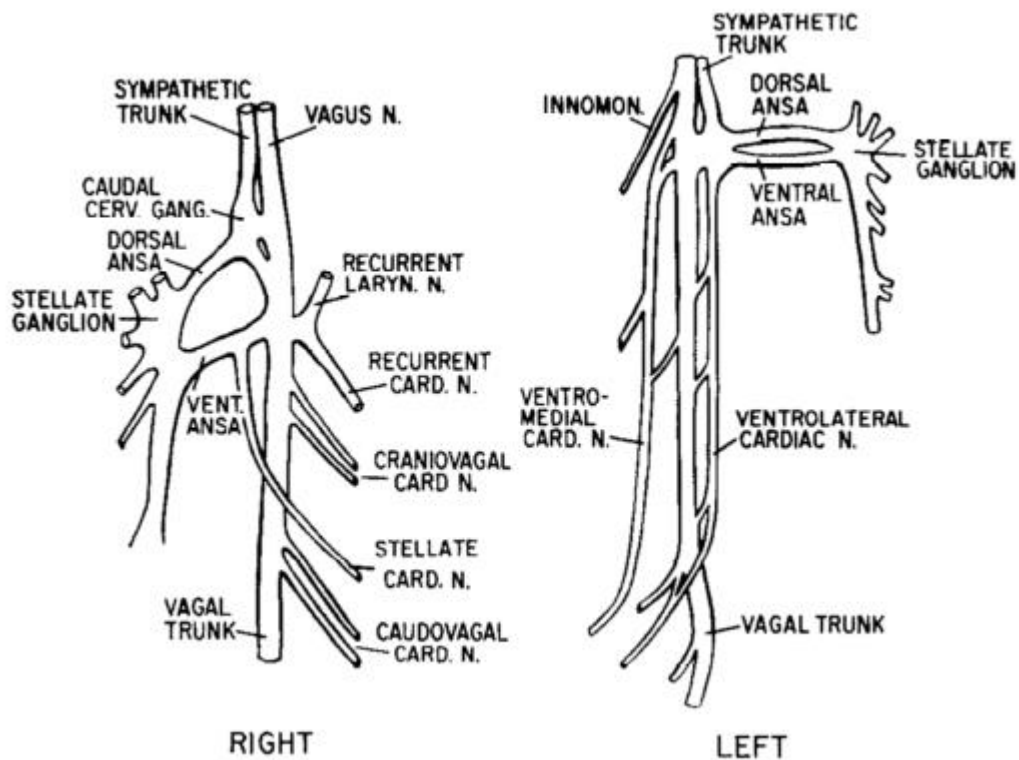


**Figure 6.1.** Distributions of the left and right sympathetic chains (trunks) as described by Kralios et al., 1975.

The distribution and density of sympathetic nerve fibres is heterogeneous and consequently upon stimulation,  $\beta$ -AR over the different regions of the heart are not activated in a uniform fashion. The experimental use of catecholamines to mimic nerve activity is therefore limited as the heterogeneous distribution of activity from nerve stimulation cannot be adequately represented when perfusing the heart with catecholamines, which will affect all regions. It also does not account for the contribution of co-transmitter release and the variations in signalling between intrajunctional and extrajunctional  $\beta$ -ARs (Ripplinger et al., 2016). An approach to investigate the local effects of catecholamines was explored by Myles et al (2012) in which subepicardial injections of noradrenaline in rabbits hearts was used to measure localized  $\beta$ -AR stimulation and induction of focal arrhythmia. However, the relevance to the actual innervation dependent regional changes is arguable.

Optical mapping of the Langendorff perfused rabbit heart highlighted the heterogeneity of sympathetic innervations (Mantravadi et al., 2007). It displayed that sympathetic stimulation increased the dispersion of repolarisation and reversed the direction of repolarisation from apex to base seen in sinus rhythm, to base to apex after sympathetic stimulation. Isoproterenol increased the dispersion of repolarisation but did not change the direction of repolarisation. This represents spatial heterogeneities of sympathetic effects and their results indicated that there may be a greater innervation of sympathetic fibres at the base of the ventricle.

Stimulation of the left sympathetic neurones has been demonstrated previously to be arrhythmogenic, and removal of the left stellate ganglion has anti-arrhythmic effects (Armour et al., 1972, Ben-David and Zipes, 1988, Hageman et al., 1973, Schwartz, 1984, Schwartz and Malliani, 1975, Schwartz et al., 2004, Schwartz et al., 1976a). This suggests that the left and right sympathetic chains have differential regional distributions and hence different effects on cardiac rhythm and electrophysiology, which has not been adequately characterised. However, there is very little data on the mechanisms underlying the proarrhythmic nature of the left sympathetics. Heterogeneity of sympathetic innervations give rise to heterogeneities in APD restitution (Ng et al., 2009). A better understanding of the cardiotoxic innervation of sympathetic nerves and regional electrophysiological effects require detailed knowledge of innervation, ion channel distribution and APD dispersion.

In order to understand the mechanisms behind the initiation and maintenance of arrhythmia, it is important to understand the spread of electrical activity. Single cell experiments using microelectrodes are often used to investigate cellular electrophysiology however, this does not allow simultaneous action potential recording from several sites (Efimov et al., 2004, Ideker et al., 1989). Surface electrodes have also been utilized to measure spread of excitation and repolarisation but there are limits to the number of recording sites and interpretations of data (Ideker et al., 1989, Haws and Lux, 1990).

Hence, this study will use optical mapping to investigate the possible regional heterogeneities of ventricular electrophysiological effects from stimulating left and right sympathetic neurones. This will add further knowledge to the regional heterogeneities of sympathetic innervation and will gain mechanistic insight into cardiotoxic effects of sympathetic stimulation on regional APD changes in both activation and repolarisation. For this set of experiments, the spinal cord was stimulated to measure effects of bilateral sympathetic stimulation, and then the chains were successively removed in order to gauge an understanding of the functional and electrophysiological changes upon denervation. This will improve our knowledge of the role of each sympathetic chain in shaping APD, dispersion of repolarization, effective refractory period and electrical restitution by observing the responses during bilateral spinal cord stimulation, spinal cord stimulation after left sympathetic chain removal and spinal cord stimulation after additional right sympathetic chain removal. Removal of the left sympathetics has been shown by many studies to reduce arrhythmia generation (Schwartz et al., 2004, Bourke et al., 2010, Coleman et al., 2012, Wilde et al., 2008), however the underlying mechanisms are not understood. Importantly, we hope to improve the understanding of the mechanisms behind the preferential influence of the left sympathetic neurones on cardiac excitability and arrhythmia generation by measuring the change in electrophysiological responses after the left sympathetic chain is removed.

## **6.2 Methods**

### **6.2.1 Mounting Isolated innervated rabbit heart preparation**

The isolated innervated rabbit heart preparation was set up as described earlier (n=12). Once the preparation is mounted on to the dish, it is perfused via the cannula in the ascending aorta with Tyrode solution at 100ml/min. As described previously, the vent and LVP balloon are inserted into the left ventricle. A pair of platinum electrodes were attached to the right atria and rib cage in order to record a simplistic ECG.

### **6.2.2 Preparation of sympathetic chains**

The left and right sympathetic chains were identified and traced up to just above T1 by gently removing surrounding tissues. Once the chains were located a suture was thread underneath the chain above the T1 segmental level. Both ends of the suture were then threaded through a 4cm (2-3mm diameter) tube of plastic and tied to secure the tube (fig 6.2).

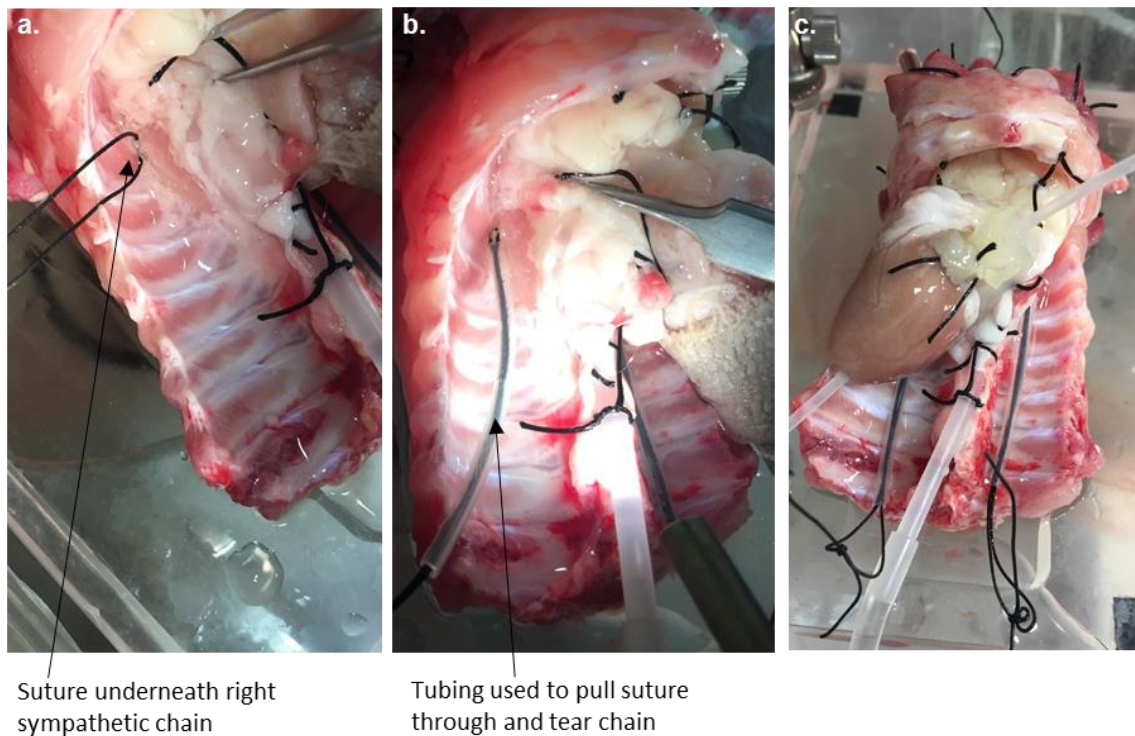


**Figure 6.2.** (a) Image showing right sympathetic chain with suture thread underneath. (b) Suture threaded through tubing and later used to pull suture through and tear the sympathetic chain. (c) Image showing preparation after both sympathetic chains have been prepared.

### 6.2.3 Positioning and stabilising the preparation

Blebbistatin was prepared by dissolving in DMSO (2mg/ml) and adding to the Tyrode solution to make up a 5 $\mu$ M Blebbistatin concentration. Blebbistatin was used to reduce motion artefacts. Contraction of the heart seized within half an hour of perfusion of the Tyrode solution containing Blebbistatin. A plastic slide was placed on the surface of the left ventricle and secured to the dish to prevent further positional changes so the recording field remained the same throughout the experiment. It also slightly flattened the ventricular surface so that a clean signal could be obtained from all 256 diodes.

The preparation had to be carefully positioned to ensure it was within the recording field and in focus. The focus could be improved by lifting or lowering the optics camera.

#### **6.2.4 Loading the dye**

During the surgical procedure, a cannula was used to pierce the carotid artery and was then advanced slowly and secured with sutures. 40 $\mu$ L of Di-4-ANEPPS (Fisher Scientific Ltd, UK) was loaded via the carotid artery in 15 $\mu$ L boluses. The dye was stable for 2-4 hours before further loading was necessary.

#### **6.2.5 Optical Mapping**

Optical action potentials were recorded from the anterior left ventricular surface. An LED light source (535nm) was projected on to the heart using a dichroic mirror (570nm). Emitted light was filtered through a 630 nm long-pass filter and collected using a Hamamatsu 16  $\times$  16 element photodiode array (Cairn Research, Faversham, UK).

### **6.3 Sympathetic nerve stimulation**

For bilateral sympathetic stimulation, a quadripolar catheter (2.0mm outside diameter, Biosense Webster Inc. Diamond Bar, USA) was inserted into the spinal cord and advanced upwards. It was inserted at the level of the twelfth thoracic vertebra and slowly advanced to the second thoracic vertebra at the level of the stellate ganglion as performed previously (Ng et al., 2007). An increase in heart rate upon insertion due to mechanical stimulation confirmed correct positioning of the catheter. The catheter was connected to a constant voltage stimulator (SD9, Grass Instruments, Astro-MedInc., Slough, UK), which stimulated the sympathetic nerves at a voltage that produced 80% of maximal heart rate response at a frequency of 5Hz (2ms pulse duration). The frequency was then adjusted to produce a steady state heart rate just less than 250bpm in order to not override the cycle length used in the pacing protocols (240ms). Constant pacing (240ms) and single extrastimulus protocol for electrical restitution

measurement, as described previously, were the pacing protocols used in this set of experiments. The final set up of the preparation is displayed in fig 6.3.

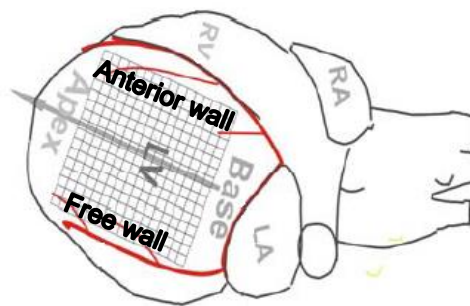
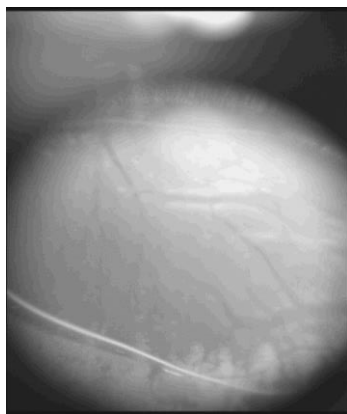
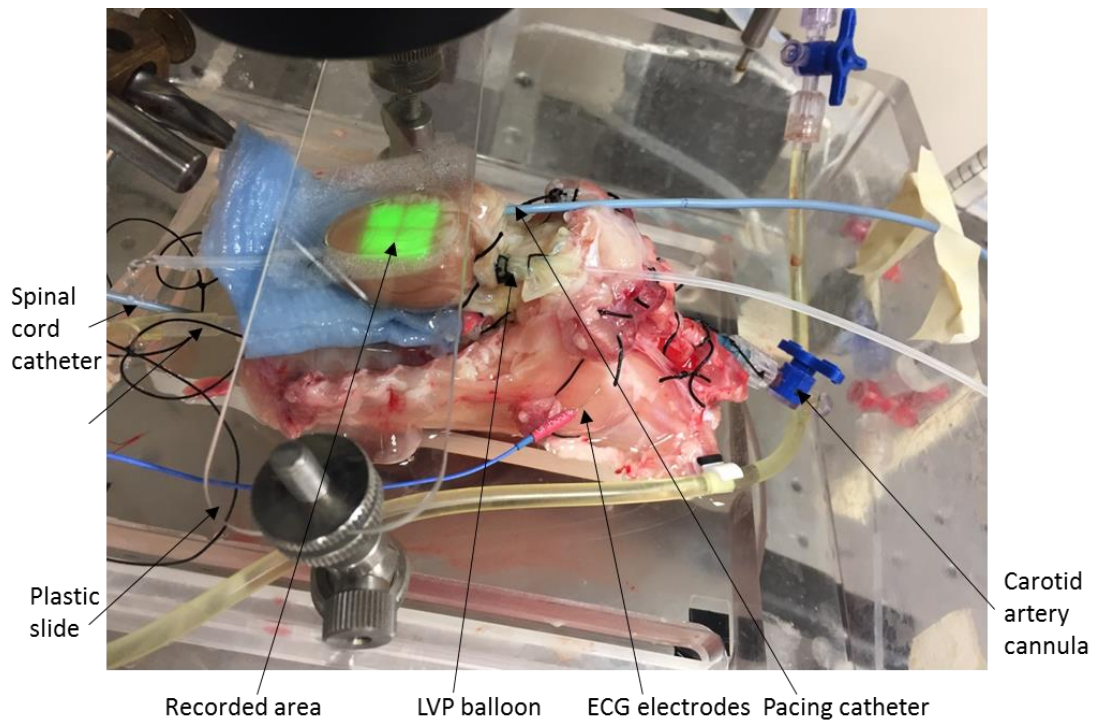


**Figure 6.3.** (a) Image showing final set up of preparation. (b) Image from camera of recorded area of left ventricle with diagram illustrating the orientation of the 256 diode recording grid.

### **6.3.1 Removing the sympathetic chains**

It was necessary to develop a method of removing the sympathetic chains without disrupting the preparation in any other way. It was important that the preparation did not move during this process as then the recorded area would change and not be representative of the data collected prior to the removal of the sympathetic chain. For this reason, the chains were isolated and prepared prior to any optic mapping recordings being made. To remove the chains, the tube that was placed previously was pushed down the suture and close to the chain. The suture was then tugged at through the tube until the nerve snapped. This ensured damage of the nerve without any positional changes of the preparation. To further ensure that all input from the chain was removed, the area in which we damaged the nerve was cauterized. The left sympathetic chain was removed first, followed by the right sympathetic chain, leaving no sympathetic response remaining at the end of the experiments. Successful chain removal was confirmed at the end of the experiment by observation of no chronotropic changes when the spinal cord was stimulated.

### **6.3.2 Data analysis**

Functional parameters were recorded with a PowerLab 8 s system and digitized at 2 kHz using Chart and Scope software (ADInstruments Ltd). Optical action potential signals were digitized at 2 kHz and recorded on a custom designed computer system (National Instruments, USA) using QRecord software (Dr Francis Burton, University of Glasgow, UK). The program Optiq (Dr Francis Burton, University of Glasgow, UK) was used to measure the APDs at each site from the difference between the activation and repolarization time points as described previously (Mantravadi et al., 2007). Using MATLAB, a script was developed which carried out calculations, plotting and fitting of the electrical restitution curves at all 256 recorded sites simultaneously. Calculations of the first derivative were also performed generating the maximum slope of restitution data. Data are mean  $\pm$ SEM; compared using ANOVA or paired t-test for which statistical significance was taken at 5% level ( $p < 0.05$ ).

## 6.4 Results

### 6.4.1 Effect of Blebbistatin

Fig 6.4 shows the effects on left ventricular pressure (LVP), perfusion pressure (PP) and heart rate (HR) when the preparation was perfused with Tyrode solution containing 5 $\mu$ M Blebbistatin. The LVP decreased within 30 minutes of perfusion and the heart stopped contracting. All other parameters were maintained at a stable level.

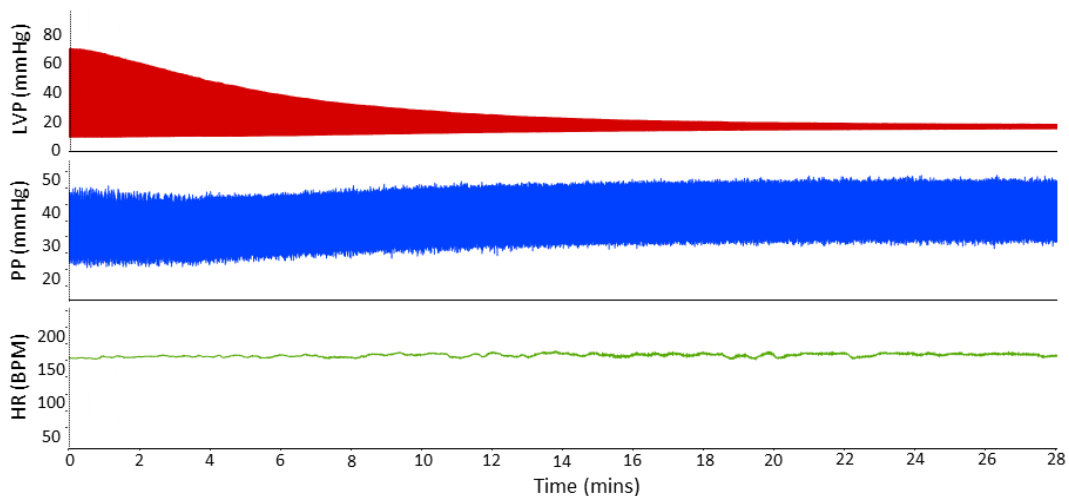


**Figure 6.4. Effect of 5 $\mu$ M Blebbistatin.** Raw data traces displaying the effects of Blebbistatin on left ventricular pressure (LVP), perfusion pressure (PP) and heart rate (bpm).

### 6.4.2 Heart rate

The largest HR response was elicited from bilateral sympathetic stimulation (fig 6.5), which increased heart rate from baseline  $130.9 \pm 7.2$  bpm to  $216 \pm 3.9$  bpm ( $P < 0.0001$ ). Denervation of the left sympathetic chain above T1 caused a significant reduction in heart rate when the spinal cord was stimulated ( $P < 0.0001$ ). Following left denervation spinal cord stimulation evoked a HR increase to  $170 \pm 7.1$  bpm from baseline  $127.5 \pm 5.5$  bpm ( $P < 0.0001$ ). After removal of the right sympathetic chain in addition to the left sympathetic chain, there was no increase in heart rate during spinal cord stimulation ( $P < 0.0001$ ).

Fig 6.5c shows the percentage changes in the HR response. Bilateral sympathetic stimulation increased HR by  $74.5 \pm 10.5\%$ , which was significantly reduced to  $39.2 \pm 8.2\%$  ( $P < 0.01$ ) with left denervation. The HR change was removed by right sympathetic chain denervation ( $P < 0.001$ ).

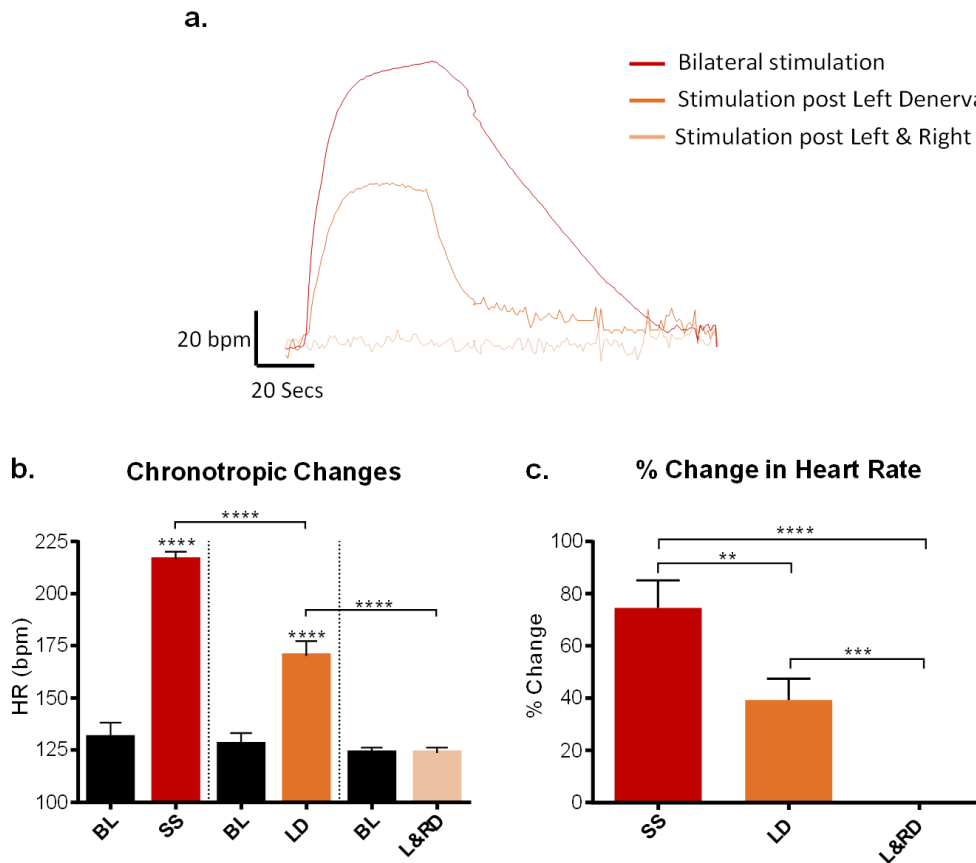
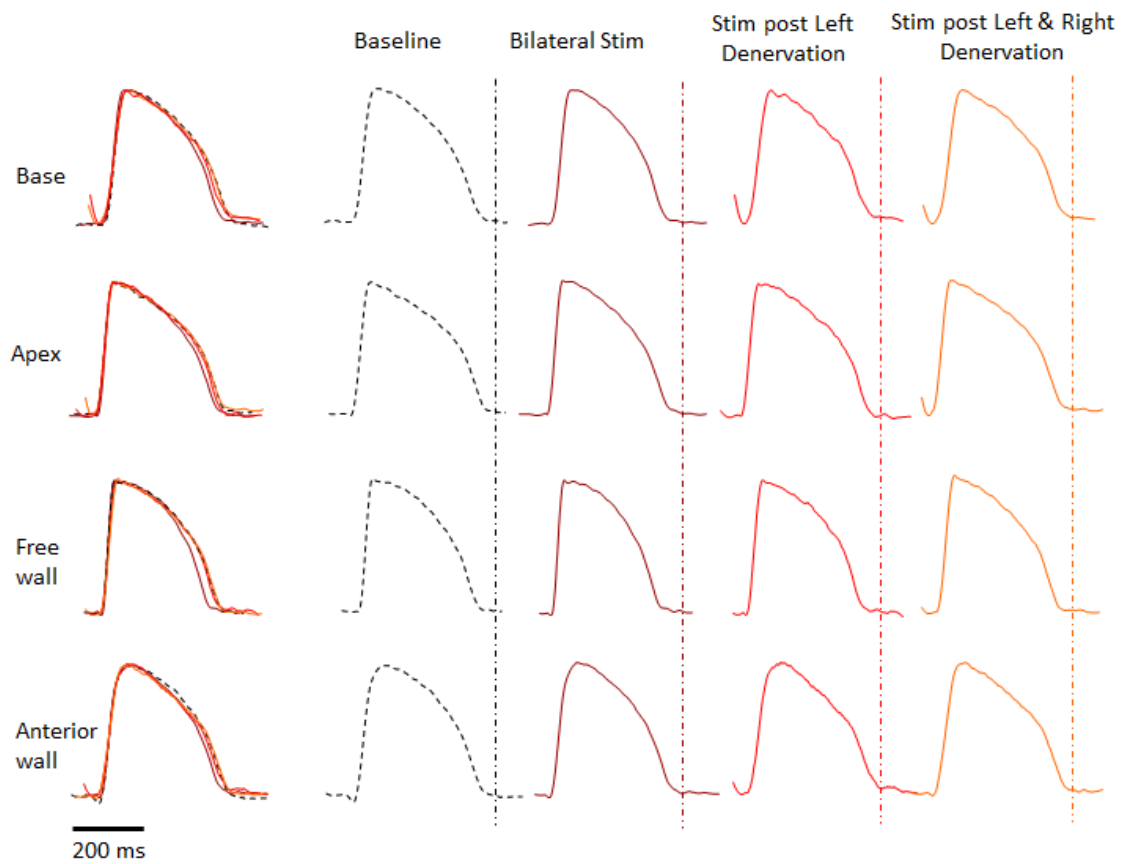


**Figure 6.5. Chronotropic effects of differential sympathetic stimulation.** (a) Raw data traces of heart rate change with bilateral sympathetic stimulation (SS), spinal cord stimulation after left denervation (LD) and additionally right denervation (L&RD). (b) Mean heart rate response (c) Percentage heart rate change from baseline for each condition. Data represent mean  $\pm$  SEM. \*\* $P < 0.01$ , \*\*\* $P < 0.001$ , \*\*\*\* $P < 0.0001$ .

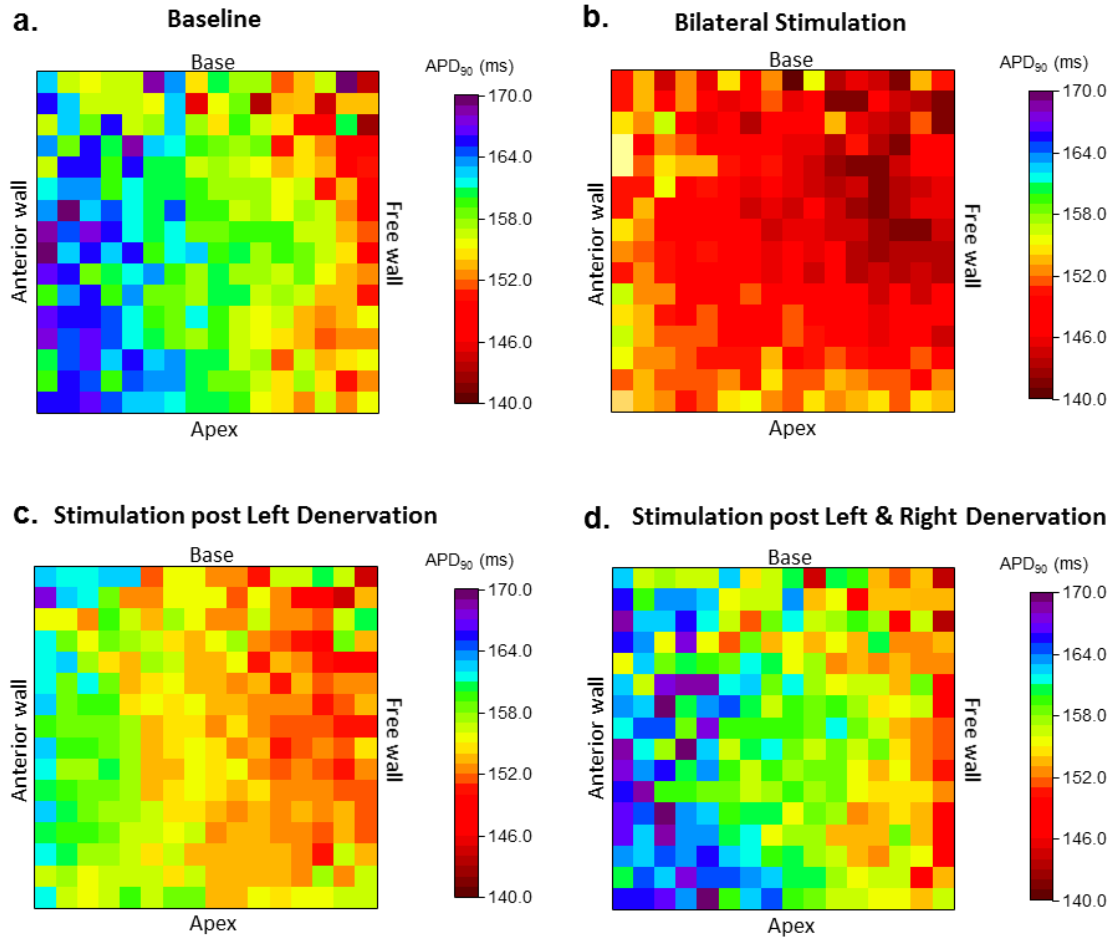
#### 6.4.3 Action Potential Duration

Fig 6.6 shows action potential traces from single sites at the base, apex, free wall and anterior wall during baseline, bilateral sympathetic stimulation, spinal cord stimulation following left sympathetic chain denervation and spinal cord stimulation with additional right sympathetic chain denervation. APD for all the 256 sites measured is shown in the 2D plot in fig 6.7. During baseline conditions,

the shortest APD values were observed at the base and free wall with the majority ranging between 150-158ms. Longer APDs were observed at the apex and anterior wall. Fig 6.7b shows the APDs during bilateral sympathetic stimulation. The APDs were shorter across the sites during bilateral stimulation when compared with baseline, with the shortest APDs in the base-free wall corner ranging between 140-150ms. After spinal cord stimulation following left sympathetic chain denervation, as shown in fig 6.7c, there are longer APDs in the apex-anterior wall region when compared to bilateral sympathetic stimulation. The shorter APDs that were seen at the base-free wall region with bilateral stimulation were also lengthened after spinal cord stimulation following left denervation (150-155ms). Fig 6.7d shows the APDs during spinal cord stimulation after both chains had been denervated and the range and distribution of APDs was very similar to the baseline values. A 2D plot of the percentage change between each condition is shown in fig 6.8. Large changes are evident from baseline to bilateral stimulation. This was greatly decreased after left denervation.



**Figure 6.6. Effects of sympathetic stimulation and denervation on action potential duration (APD).** Raw APD trace from single sites at the base, apex, free wall and anterior wall. APD traces are shown for baseline, bilateral spinal cord stimulation, spinal cord stimulation after left denervation, and after left & right denervation.



**Figure 6.7. Regional action potential duration (APD) changes during differential sympathetic stimulation.** 2D plots displaying APD at 256 sites across the left ventricle, recorded during constant pacing. APDs are shown during (a) baseline, (b) bilateral sympathetic stimulation, (c) stimulation after left denervation, (d) stimulation after left & right denervation.

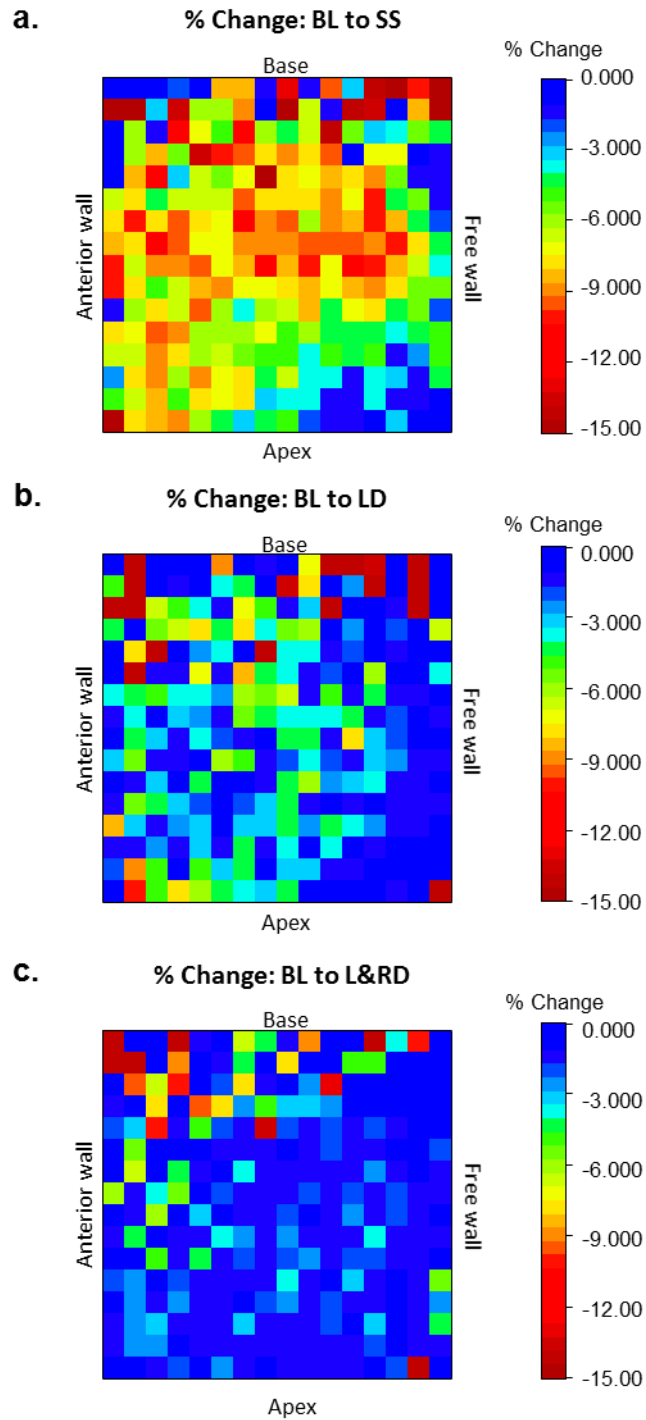


**Figure 6.8. Percentage change in action potential duration (APD).** Percentage change in APD from baseline (BL) to (a) bilateral sympathetic stimulation (SS), (b) spinal stimulation after left denervation (LD) and (c) spinal stimulation after left & right denervation (L&RD).

APD dispersion was measured by two methods. Firstly, by calculating maximum APD ( $APD_{max}$ ) – Minimum APD ( $APD_{min}$ ) for the 256 sites recorded. With bilateral sympathetic stimulation, APD dispersion increased from  $39.1 \pm 1.9$  ms at baseline to  $47.6 \pm 0.9$  ms ( $P < 0.05$ ). After left denervation, spinal cord stimulation caused minimal increase in APD dispersion from  $43.4 \pm 1.2$  ms to  $44.2 \pm 0.8$  ms (NS). After additional right chain denervation, spinal cord stimulation caused no difference in APD dispersion between baseline of  $44.9 \pm 1.0$  ms to  $44.4 \pm 0.7$  ms with stimulation (NS). The second method used to measure APD dispersion was to calculate the standard deviation of the APDs over the 256 recording sites to measure the spread of the data. The mean APD at baseline was  $154.4 \pm 1.5$  ms with an average standard deviation of  $4.1 \pm 0.3$ . APD dispersion significantly increased with bilateral stimulation (mean APD  $148.2 \pm 1.2$  ms) as standard deviation increased to  $5.2 \pm 0.4$  ( $P < 0.05$ ). Spinal cord stimulation produces a small increase (NS) in APD dispersion after left chain removal from baseline  $6.2 \pm 0.8$  (mean APD  $157.3 \pm 1.4$  ms) to  $6.4 \pm 0.8$  (mean APD  $154.7 \pm 1.2$  ms). After both chains were removed, spinal cord stimulation caused no significant change in APD dispersion, from baseline  $5.7 \pm 0.7$  (mean APD  $157.4 \pm 1.2$ ) to  $5.5 \pm 0.6$  (mean APD  $156.6 \pm 1.5$ ).

#### **6.4.4 Effective Refractory Period**

The effective refractory period (ERP) was reduced from baseline  $171.7 \pm 2.4$  ms to  $157.8 \pm 2.2$  ms with bilateral sympathetic stimulation ( $P < 0.0001$ ) as shown in fig 6.9. After left sympathetic chain denervation, spinal cord stimulation evoked a much smaller change in ERP from  $171.1 \pm 2.2$  ms at baseline to  $169.4 \pm 1.9$  ms with spinal cord stimulation, which was significantly less than with bilateral sympathetic stimulation ( $P < 0.0001$ ). In 7 out of 12 hearts there was no change in ERP from baseline to spinal cord stimulation following left denervation. After right sympathetic denervation, there was no change from baseline ERP during spinal cord stimulation.

Percentage change in ERP is displayed in fig 6.9b. Percentage change in ERP was significantly greater with bilateral sympathetic stimulation ( $-8.1 \pm 1.3\%$ ) than

spinal cord stimulation following left sympathetic chain denervation ( $-2.3 \pm 1.0\%$ ,  $P < 0.001$ ) and additionally right sympathetic chain denervation ( $0\%$ ,  $P < 0.0001$ ). There was no significant difference in percentage ERP change with left denervation alone or with the addition of right denervation.

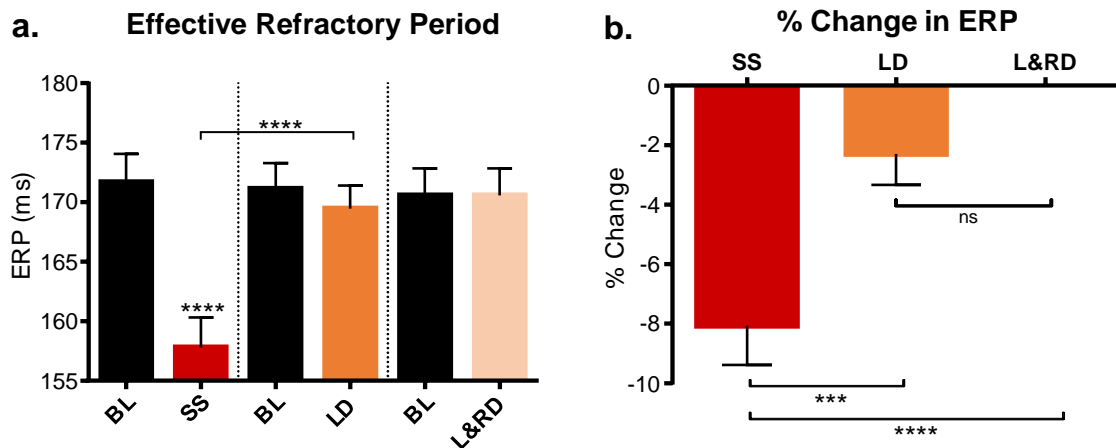
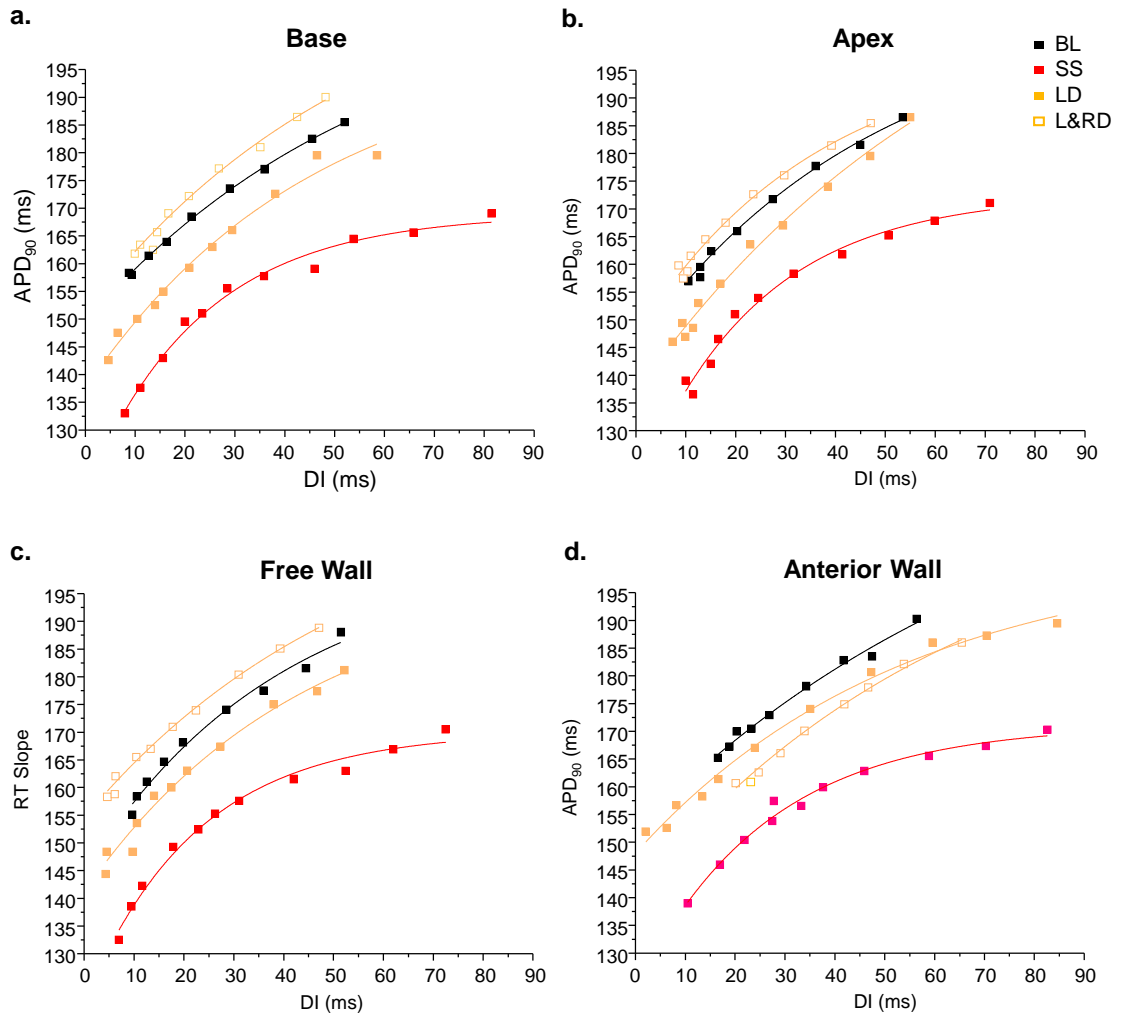


**Figure 6.9. Effects on effective refractory period (ERP).** (a) ERP response with baseline (BL), bilateral sympathetic stimulation (SS), spinal cord stimulation after left denervation (LD) and additionally after left & right denervation (L&RD). Data represent mean  $\pm$  SEM. \*\*\* $P < 0.001$ , \*\*\*\* $P < 0.0001$ .

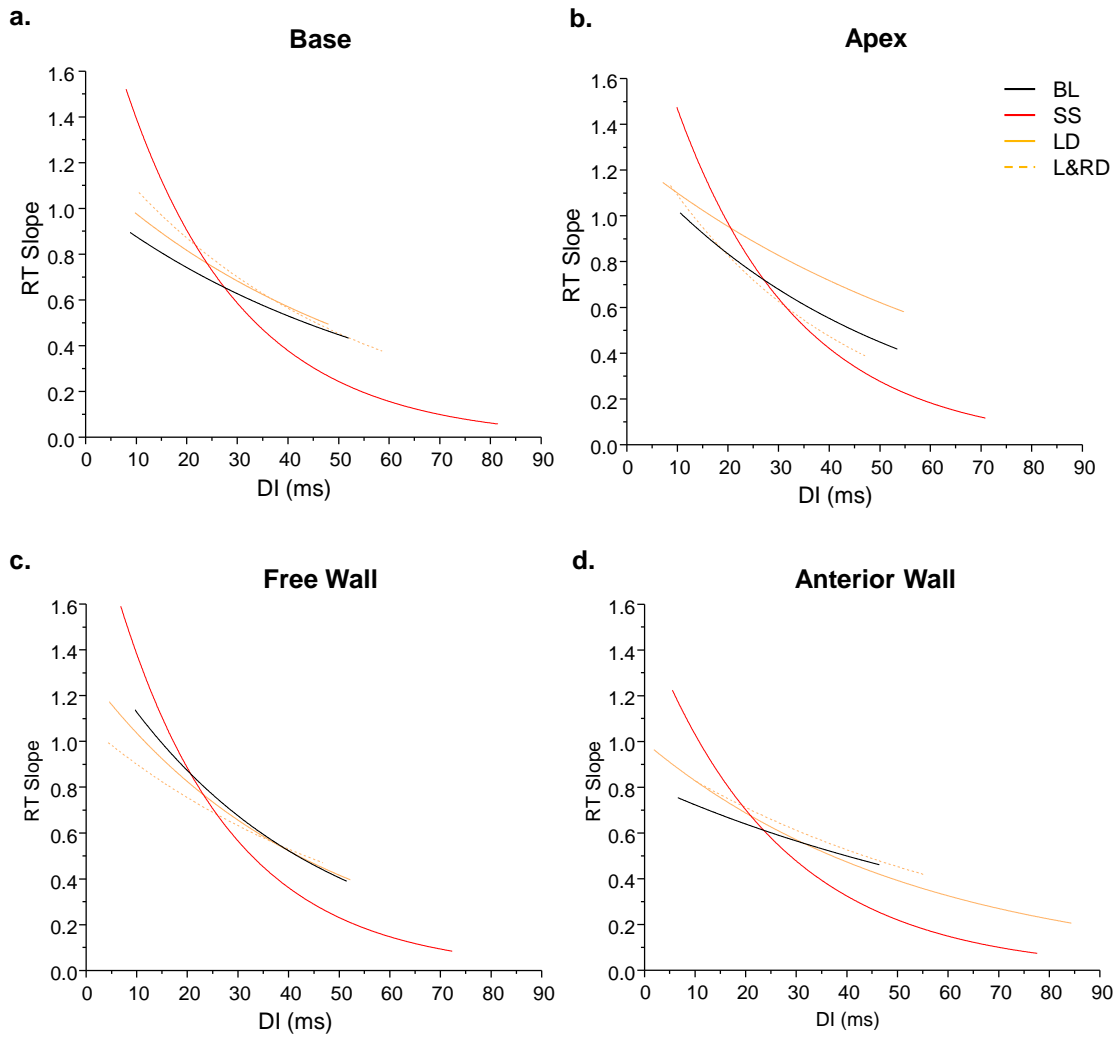
#### 6.4.5 Action Potential Duration Restitution

Fig 6.10 displays APD restitution curves from selected sites at the base, apex, anterior wall and free wall of the left ventricle for each condition in, with the corresponding first derivative curves in fig 6.11. Bilateral stimulation produced the steepest curves and the highest maximum slope of restitution across all regions. Left denervation decreased the maximum slope of restitution achieved with spinal cord stimulation close to baseline values. Likewise spinal cord stimulation following right denervation produced maximum slope of restitution values close to baseline. The restitution curves were generated for each of the 256 recorded sites and can be seen in fig 6.12. The maximum slope of restitution was calculated for each curve and plotted in fig 6.13. Increased slope values were elicited by bilateral sympathetic stimulation in most regions, but particularly in the basal region. The highest slope values were observed at the base with the most dense regions reaching slope values of 2.5. After left denervation there were fewer regions showing high slope values with spinal cord stimulation and a marked decrease in maximum slope of restitution in most areas in comparison to bilateral sympathetic stimulation. Discrete regions at the base and free wall exhibited the steeper slope values with spinal cord stimulation after left denervation and a small number of sites at the apex also retained the higher slope values. However, a large proportion of the response at the base seen during bilateral sympathetic stimulation was lost after left denervation. After the addition of right sympathetic chain denervation the maximum slope of restitution in all regions with spinal cord stimulation was very similar to that observed at baseline.

The percentage change in maximum slope of restitution is shown in fig 6.14. The greatest changes were observed between baseline and bilateral sympathetic stimulation. The base elicited the largest percentage change. A large majority of the response was lost when the spinal cord was stimulated after left denervation, with very little change in maximum slope of restitution observed. Finally, after both left and right sympathetic chains were removed, percentage change was approximately zero in the majority of regions with spinal cord stimulation.



**Figure 6.10. Action potential duration restitution curves.** Restitution curves from single sites at (a) the base, (b) apex, (c) free wall and (d) anterior wall during baseline conditions (BL), bilateral sympathetic stimulation (SS), stimulation after left denervation (LD) and stimulation after left & right denervation (L&RD). All curves are fitted with exponential curve fit ( $\text{MAPD}_{90} = \text{maximum MAPD}_{90} [1 - e^{-\text{DI}/\tau}]$ ).



**Figure 6.11. Derivative of fitted restitution curves.** Derivative curves for baseline (BL), bilateral sympathetic stimulation (SS), stimulation after left denervation (LD) and stimulation after left & right denervation (L&RD) at single sites at the (a) base, (b) apex, (c) free wall and (d) anterior wall. The maximum slope of restitution is determined from the maximum y value of these curves.

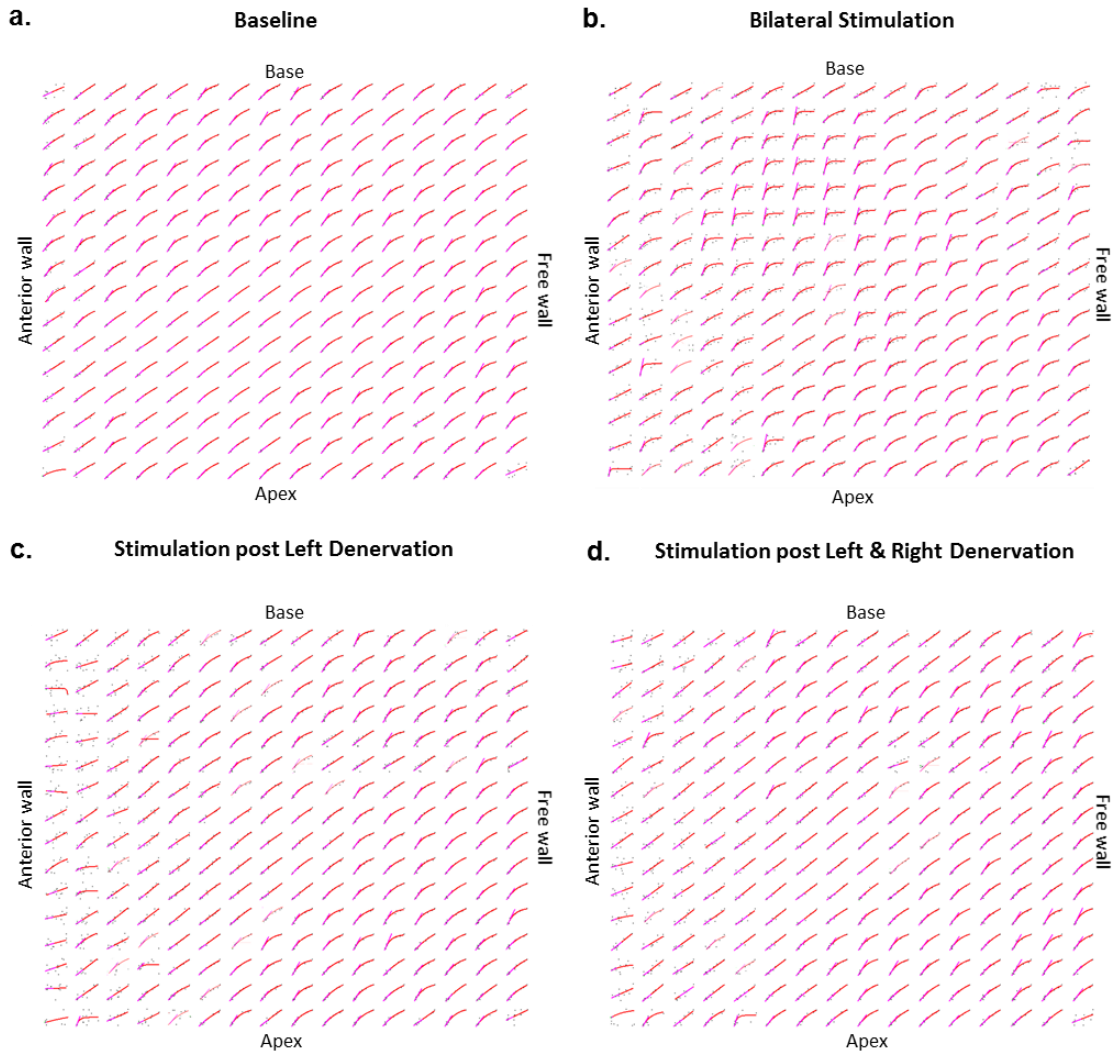


**Figure 6.12. Action potential duration restitution curves at multiple sites over left ventricle.** Restitution curves fitted with exponential curve fit ( $\text{MAPD}_{90} = \text{maximum MAPD}_{90} [1 - e^{-DI/\tau}]$ ) for 256 sites across left ventricle during baseline conditions (BL), bilateral sympathetic stimulation (SS), stimulation after left denervation (LD) and stimulation after left & right denervation (L&RD).

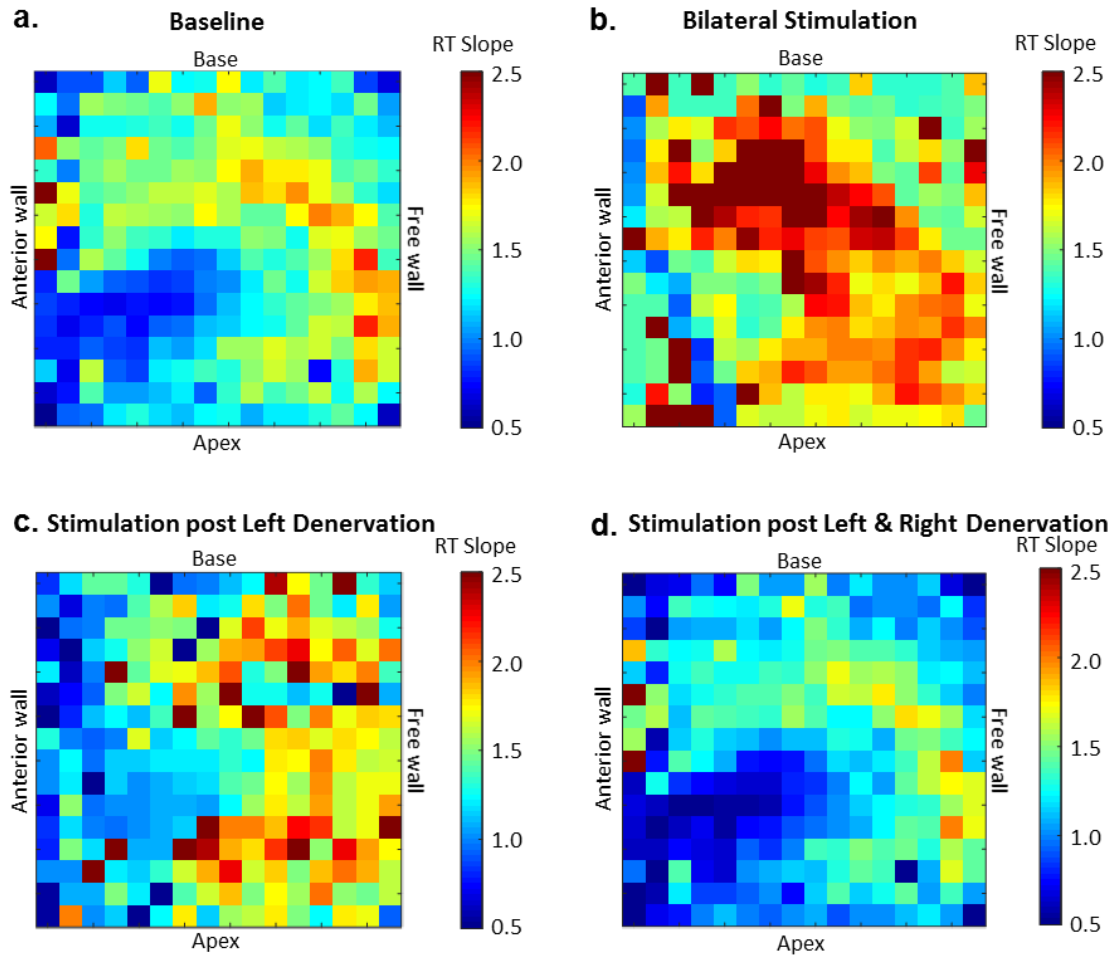


**Figure 6.13. 2D plots of regional differences in maximum slope of restitution across left ventricle.** Maximum slope of restitution displayed at 256 sites across left ventricle during baseline conditions, bilateral sympathetic stimulation, spinal cord stimulation after left denervation and stimulation after left & right denervation.

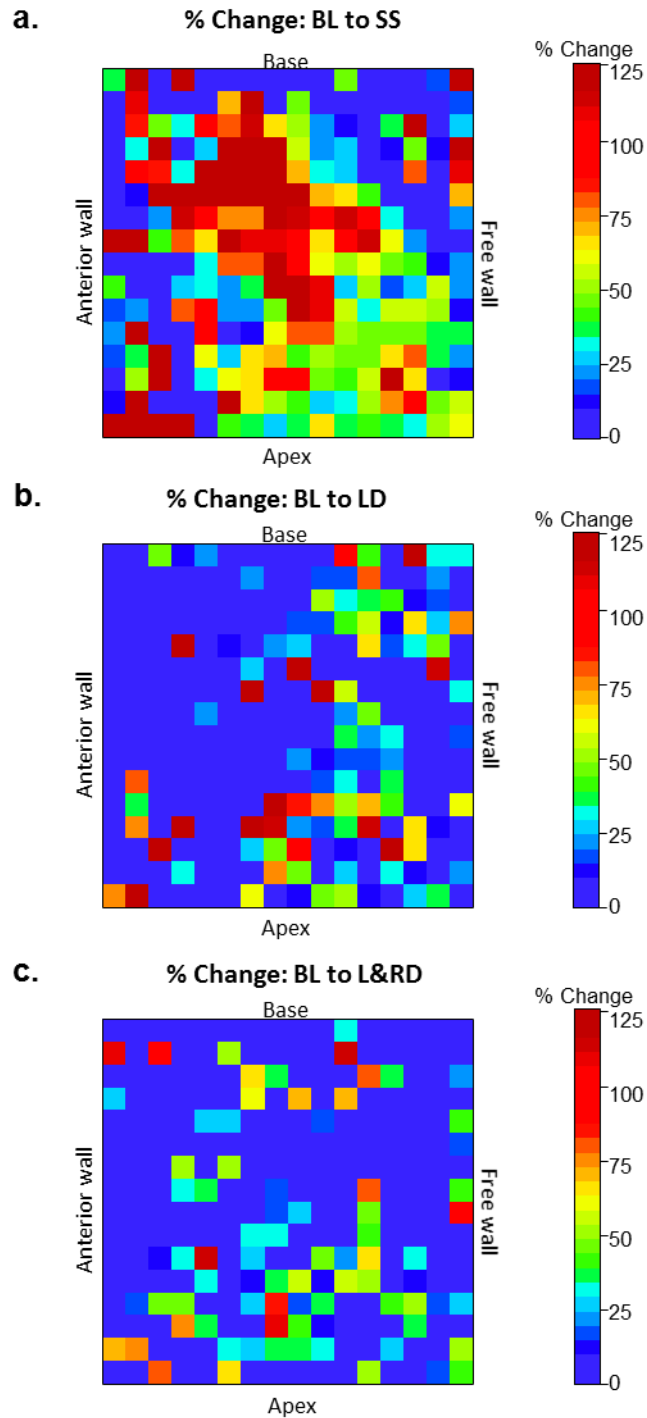


**Figure 6.14. Percentage change in maximum slope of restitution.** Percentage change in maximum slope of restitution from baseline (BL) to (a) bilateral sympathetic stimulation, (b) spinal stimulation after left denervation and (c) spinal stimulation after left & right denervation.

## 6.5 Discussion

It is well established that the heart displays regional electrical heterogeneity, partly due to differential nerve innervations and ion channel distributions. These findings support the notion of higher sympathetic nerve innervations at the base of the ventricle and demonstrate the regional differences in electrophysiological parameters such as action potential duration and electrical restitution. This study highlights for the first time the dominance of the left sympathetic neurons on cardiac electrophysiology and preferential innervation at the base of the ventricle.

Right sympathetic stimulation is known to innervate the sinoatrial node and have a preferential effect on heart rate. It was therefore not surprising that upon removal of the left sympathetic chain, a large proportion of the heart rate response still remained. Although the heart rate still greatly increased with spinal cord stimulation after left sympathetic chain denervation, there was little or no change in effective refractory period (ERP). This suggests that during bilateral sympathetic stimulation, the left sympathetic chain exerts dominance over the ERP. Previous data has shown that sympathetic stimulation decreased ERP and vagal stimulation increased ERP, which correlated with the heart rate changes elicited by each (Ng et al., 2007). However, it is evident from this study that changes in ERP were independent of heart rate changes. This response can be attributed to the greater shortening of action potential duration (APD) during left sympathetic stimulation as demonstrated in the previous chapters. Haws and Burgess (1978) reported that in regions of overlapping innervations, left sympathetic stimulation shortened refractory periods more than right stimulation. Likewise, in open chested dogs, right sympathetic stimulation did not elicit refractory period shortening (Cinca et al., 1985), which supports our observations of no or little ERP change from baseline during spinal stimulation after left sympathetic chain removal. In addition, right stellate ganglion blockade in patients with supraventricular tachycardia did not change the refractory period (Garcia-Calvo et al., 1992) .

It has been suggested previously that the sympathetic nerves have high densities of innervation at the base of the ventricle where they activate  $I_{K_s}$  which are also dominant in this region (Mantravadi et al., 2007, Ng et al., 2009). In support of this, bilateral sympathetic stimulation in this study caused shortening of APD across the ventricle, with the shortest APDs elicited at the base of the ventricle towards the free wall. After removal of the left sympathetic chain, the greatest shortening of APD with stimulation occurred in the free wall region however there was a much lesser response over all regions than observed with bilateral stimulation. Particularly in the basal region, much less APD shortening was observed after left denervation. APD prolongation after left stellectomy has also been observed in anaesthetised cats (Zaza et al., 1991). It is well recognized that the left sympathetics preferentially innervate the ventricle (Randall and Rohse, 1956, Randall et al., 1968b, Furnival et al., 1973, Van Stee, 1978). In this study we report for the first time in the rabbit ventricle that the left sympathetic neurons predominantly innervate the base of the ventricle.

This correlates with previous studies in a number of species showing transmural and base-apex heterogeneities in action potential duration and ion channel distributions (Wolk et al., 1999, Szentadrassy et al., 2005, Cheng et al., 1999, Li et al., 2002, Szabo et al., 2005). In the rabbit heart, the base of the left ventricle was found to have higher levels of tyrosine hydroxylase which is a marker for sympathetic innervation and higher levels of KCNQ1 protein expression, an  $I_{K_s}$  subunit (Ng et al., 2009). Furthermore, inhibition of  $I_{K_s}$  by HMR 1556 eliminated the greater shortening of APD at the base during sympathetic stimulation (Ng et al., 2009). Nerbonne et al (2002) found regional differences in action potential waveforms in the mammalian myocardium which henceforth impacts the normal dispersion of repolarization (DOR). The observed effects also reflected the differential voltage gated  $K^+$  channel expression. In accord, it is understood that regions of the ventricle that activate first will repolarize first and thus have shorter APDs (Spach and Barr, 1975). This allows for synchronous coordination of DOR. These data showed that bilateral sympathetic stimulation increased APD dispersion and thus, as indicated by previous studies (Han and Moe, 1964), has more potential to induce arrhythmia.

Amplification of dispersion of repolarisation underlies the development of ventricular arrhythmias, particularly in conditions of disease such as LQTS and CPVT (Antzelevitch, 2007). Removal of the left sympathetic chain, eliminated the increase in APD dispersion observed with spinal cord stimulation suggesting left sympathetic input plays a dominant role in APD dispersion during sympathetic stimulation. This is supported by previous studies in pigs (Vaseghi et al., 2013). This improves our understanding of the mechanisms underlying the proarrhythmic tendencies of the left sympathetics and suggests increased DOR as a potential mechanism. Vaseghi et al (2012b) studied the contribution of the left and right stellate ganglion to the innervation of the anterior left ventricle in pig hearts, in order to understand the role of the sympathetic nervous system in the genesis of ventricular tachycardias. Left sympathetic stimulation was found to significantly increase activation recovery interval (a surrogate measure of action potential duration), more than right stimulation. They concluded that left sympathetic stimulation is more proarrhythmic due to the greater effect it has on DOR, which is supported by the data in the present study.

During sympathetic stimulation, direction of repolarisation is reversed due to greater innervations of the sympathetic nerves at the base of the ventricle (Mantravadi et al., 2007). This heterogeneity in sympathetic innervation, ion channel distribution and action potential duration also impacts the restitution properties of the heart. The maximum slope of restitution was greatest in the basal and free wall regions and with bilateral sympathetic stimulation the intensity of response in these regions displayed the greatest increases. The base in particular showed the steepest slope values which correlates with data suggesting the sympathetic innervations have high densities in basal regions. Sympathetic stimulation has also been previously demonstrated to give rise to regional variations in restitution kinetics curves as a result of heterogeneous sympathetic innervations and  $K^+$  channel distributions (Ng et al., 2009). Removal of the left sympathetic chain greatly reduced the steepening of the restitution curves predominantly at the base. These data suggest that the increased slope values observed during sympathetic stimulation are largely due to innervations of the left sympathetic neurons, particularly at the base of the ventricle. Again we

evidence here that left sympathetics exert a dominance over cardiac electrophysiology. This also provides an indication of what changes in cardiac electrophysiology occur upon removal of the left sympathetics in clinical treatments such as left cardiac sympathetic denervation (LCSD). As steeper restitution slopes correspond with increased likelihood of developing ventricular arrhythmias (Garfinkel et al., 2000, Ng et al., 2009, Riccio et al., 1999), it can be extrapolated from this study that LCSD would exert anti-arrhythmic effects through flattening of restitution curves.

### **6.5.1 Clinical implications**

APD restitution has been correlated with VF initiation and studies have shown that drugs that reduce the maximum slope of restitution also prevent initiation of VF (Riccio et al., 1999, Garfinkel et al., 2000). Anti-arrhythmic drugs are often limited as they do not provide a preventative solution and can have off target effects. We have shown that removal of the left sympathetic chain resulted in flattening of restitution curves during spinal cord stimulation and thus increases the rationale for LCSD as a clinical treatment to prevent VF initiation. Heterogeneity of sympathetic innervations gives rise to heterogeneities in APD restitution (Ng et al., 2009) and we show here that removal of the left sympathetic nerves reduces the heterogeneity. Associations of APD slope and heterogeneity with clinical ventricular arrhythmia and sudden cardiac death have also been demonstrated in patients (Nicolson et al., 2012). APD restitution can therefore be used a strong prognostic marker for arrhythmogenesis.

Studies have shown that factors known to favour VF initiation, such as sympathetic stimulation, also increase the DOR (Han and Moe, 1964). Heterogeneous sympathetic innervation of the ventricle impacts the DOR as DOR increases during sympathetic stimulation (Han and Moe, 1964); an important mechanism in arrhythmia generation. An increased DOR leads to development of conduction delay which induces sustained arrhythmia (Kuo et al., 1983) and non-uniformity in recovery from excitation can lead to reentry (Han and Moe, 1964). Hence, a better understanding of the differential innervations of the sympathetic nerves is especially important in conditions of sympathetic

imbalance and lethal arrhythmias. Investigations such as those in the present study in healthy hearts can provide important indications of what may occur in disease, for example following myocardial infarction (MI) and heart failure (HF), where remodelling occurs. HF in patients and animal models have shown prolongation of ventricular APD reflecting impaired repolarization (Janse, 2004, Li et al., 2002). This is due to remodelling of ion channels such as downregulation of voltage dependent  $K^+$  currents (Rose et al., 2005, Li et al., 2004a, Li et al., 2002) which causes delayed repolarization and thus promotes generation of EADS (Janse, 2004). Heterogeneous DOR in heart failure provides a substrate for re-entrant arrhythmia. In patients with postinfarct cardiomyopathy (ICM), sympathetic stimulation increased regional differences in repolarisation due to denervation of scar tissue and denervation supersensitivity of regions surrounding scar tissue (Vaseghi et al., 2012a). Thus, understanding of sympathetic innervations and ion channel distributions in healthy hearts is essential to understanding what occurs in diseased states.

Furthermore, these data clearly show that the left sympathetic chain has a dominance over ventricular electrophysiology and hence supports the rationale for left sympathetic cardiac denervation (LCSD). Currently, this treatment is used for patients with chronic cardiac arrhythmias but possesses significant side effects. Importantly, we have shown that removal of the left sympathetics dramatically alters the electrophysiology of the heart in all regions but specifically in the basal regions. Sympathetic stimulation after the removal of the left sympathetic chain largely reduced the shortening of action potentials, the decreases in ERP, the increases in DOR and the steepening of electrical restitution slopes, and hence helps improve the understanding of the mechanisms involved in reducing risk of arrhythmia in LCSD. If a more selective approach was implemented, as suggested in the previous chapters, side effects could be reduced. However, this would require further investigation into the regional innervations of different spinal segments using optical mapping of the left ventricle.

## 6.5.2 Limitations

Optical mapping is generally accompanied by several limitations which vary in extreme depending on the type or how advanced the devices and optical probes are. These include contraction artefacts, spatial and temporal resolution, limitations of surface images, depth of field and field of view (Efimov et al., 2004). We can however be certain that these results are not the product of artefact as we observe augmentation or elimination of the measured parameters between conditions. The study was however limited by low spatial resolution of APD recordings caused by the use of a 16 x 16 element photodiode arrays. In order for continuous recordings to be made without interruption between baseline and stimulation, this photodiode had to be used and outweighed the need for higher spatial resolution.

Studies in a number of species including zebra fish, mouse, rat and rabbit (Fedorov et al., 2007, Farman et al., 2008, Jou et al., 2010, Dou et al., 2007) have reported that Blebbistatin does not significantly alter electrophysiology of the heart. However, previous research from our group in the rabbit heart has suggested Blebbistatin does have significant effects on cardiac electrophysiology (Brack et al., 2013). Blebbistatin was found to prolong basal and apical APDs and ERP, and increase maximum slope of restitution and VFT. This study also reported significant increases in perfusion pressure within 30 minutes of perfusion of Blebbistatin which was not observed in the present study, however we cannot rule out the effects on the electrophysiology. Although there appears to be controversy, Blebbistatin still remains the best way to remove motion artefacts in comparison to alternatives such as BDM which have significant adverse effects (Blanchard et al., 1990, Liu et al., 1993, Maesako et al., 2000, Kettlewell et al., 2004). However, the electrophysiological effects of Blebbistatin should not be ignored when interpreting data. It is also important to note that all recordings including baseline recordings were taken in the presence of Blebbistatin, after 30 minutes of perfusion, when conditions had stabilised. As reported by Brack et al (2013), measurements of action potential duration and electrical restitution remain stable over a period of up to 5 h after Blebbistatin

perfusion, therefore the changes we observed between conditions can still be appropriately interpreted.

### **6.5.3 Conclusion**

This study provides data in support of what was previously elucidated; that left sympathetics have a dominance over cardiac rhythm and electrophysiology. It is important to note that previous studies that performed stellectomy to observe left and right sympathetic differences, did so in anaesthetised dogs or cats (Schwartz et al., 1976b, Schwartz et al., 1977). Furthermore, vagal input was also removed in some studies to eliminate the tonic afferent vagal inhibition on sympathetic nerves (Schwartz et al., 1976a), thus limiting interpretations of data. This highlights the importance of this study as we report data in support of previous findings in the novel isolated innervated rabbit heart preparation.

The novel finding is that left chain denervation removed a significant amount of effects of spinal cord stimulation suggesting that the left chain may exert a more dominant effect, particularly at the base of the ventricle. Innervations of the left sympathetic neurons at the base are the main cause of the shortest APDs and steepest electrical restitution slopes observed in this region. This also helps us to understand why left sympathetics have a greater tendency to induce arrhythmia and how LCSD is producing anti-arrhythmic results. Our findings implicate decreased refractoriness, increased DOR and steepening of restitution curves as possible mechanisms to explain how the left sympathetic nerves have greater tendency to induce arrhythmia. Thus, this study improves our knowledge of the regionally selective innervations of the sympathetic nerves and how this relates to the heterogeneity of cardiac electrophysiology. Further investigations are necessary to understand how these innervations are remodelled in disease and hence provide more focused clinical therapies.

## **Chapter 7**

## **Conclusion**

## 7 Conclusion

ANS dysfunction is a key factor in the progression of most cardiovascular diseases and cardiac electrophysiological abnormalities, with the sympathetic nervous system central to the development of arrhythmias (Schwartz and Stone, 1982b, Malliani et al., 1980, Han and Moe, 1964). Hence, in this study we investigated the sympathetic innervations of the heart and its distinct effects on cardiac electrophysiology, to provide important insights into the mechanisms of arrhythmia generation.

### ***Differential effects of right and left sympathetic nerve stimulation on ventricular electrophysiology and arrhythmia inducibility***

The left and right sympathetic chains have been reported to have differential chronotropic and inotropic effects in various species. Unilateral stimulation of the left and right sympathetic chains has previously been found to have different functional and electrical responses, which are important factors in arrhythmia susceptibility (Anzola and Rushmer, 1956, Randall and Rohse, 1956, Yanowitz et al., 1966, Haws and Burgess, 1978, Ardell et al., 1988, Zaza et al., 1991). The direct effects of the individual sympathetic outflows on cardiac electrophysiology and mechanisms of arrhythmia induction have however been reported in less detail.

Winter et al (2012) were the first to report the differential effects of left and right sympathetic stimulation in the isolated innervated rabbit heart preparation, but further investigation into the electrophysiological differences was required. In this study we report novel findings in the innervated isolated heart preparation of the steepening of restitution curves and decrease in ventricular fibrillation threshold with left sympathetic stimulation at the segmental level T2-T3. Studies have suggested a causal link between APD restitution and VF initiation (Riccio et al., 1999, Garfinkel et al., 2000, Ng et al., 2007). APD restitution can therefore be used as a marker for induction of arrhythmia and thus our data indicate that left sympathetic neurones are more proarrhythmic. These data have shown for the first time in the rabbit heart that the left sympathetic preganglionic neurones have

a greater effect on the electrophysiology of the left ventricle and hence a dominant effect on cardiac rhythm and excitability. These are the first reports of the proarrhythmic nature of left sympathetic neurones in this model, and our findings correlate with previous data from other species including cats and dogs (Armour et al., 1972, Ben-David and Zipes, 1988, Hageman et al., 1973, Schwartz, 1984, Schwartz and Malliani, 1975, Schwartz et al., 2004). This provides important implications for clinical treatment of arrhythmia in which sympathetic stimulation is currently a target for treatment.

### ***Functional selectivity of right and left spinal segmental preganglionic neurons***

Previous findings suggest that there may be regionally specified innervation of the preganglionic neurones from the spinal cord in accordance with their arrangement in series (Randall, 1977). This implies that the left and right sympathetic innervations arising from the spinal cord segments may be functionally discrete (Szentivanyi et al., 1967; Randall et al., 1968; Randall 1977; Armour and Randall, 1975; Randall, 1984).

Further investigations were required to determine whether the segmental location of the sympathetic neurones corresponded to a specific cardiac function. Consequently, we investigated the differential inputs from each spinal segmental level from T6 to T1 for both the left and right sympathetic chains.

Dominant effects on electrophysiological parameters were elicited by the left sympathetic chain as seen previously, however a more novel finding was that there was also a dominance at caudal levels. For the first time in the novel adaptation of the innervated isolated rabbit heart preparation, we note the importance of caudal left sympathetic stimulation in cardiac excitability and its potential to induce arrhythmia. We also observed differences between the base and apex which were particularly evident at T4-T6 for both MAP duration and maximum slope of restitution, suggesting regional innervation and preferential sympathetic supply to the base at caudal levels.

Due to the proarrhythmic effects of left sympathetic neurones, LCSD has been explored as a clinical treatment. Whilst such treatment has proven to be successful, it is accompanied by serious side effects. Removing such a large portion of sympathetic input may not be the most effective treatment and a more targeted approach is required. We report for the first time that, alterations in discharge of neurones in the caudal segments (T4-T6) of the left sympathetic chain had a greater potential for arrhythmia generation and hence could pose a target for more focused clinical treatments for impairments in cardiac function.

### ***Regional heterogeneities of the cardiac sympathetic neurones***

The heterogeneous nature of the heart is well recognised and is attributed to variations in ion channel distribution and nerve innervations. The distributions of ion channels have been well document and their density and expression varies between the epicardium and endocardium and between the base and apex (Antzelevitch, 2001, Antzelevitch, 2005, Antzelevitch and Belardinelli, 2006, Brahmajothi et al., 1997a, Brahmajothi et al., 1997b, Cheng et al., 1999, Ng et al., 2009).

The base of the heart has been reported to have a greater density of sympathetic innervation (Ng et al., 2009). The differential effects of the right and left sympathetic nerves on functional and electrophysiological responses suggest that each outflow must innervate specific regions of the heart. This was elucidated by several studies in cats and dogs (Yanowitz et al., 1966, Ardell et al., 1988, Kralios et al., 1975, Opthof et al., 1991, Rubart and Zipes, 2005), however specific details of the innervations of the sympathetic nervous system are still lacking. The left sympathetic neurones have been reported to be proarrhythmic by many studies (Armour et al., 1972, Ben-David and Zipes, 1988, Hageman et al., 1973, Schwartz, 1984, Schwartz and Malliani, 1975, Schwartz et al., 2004). Therefore, knowledge of the regional heterogeneities of the left sympathetic nerves is important for clinical intervention and will enable a better understanding of the mechanisms underlying its proarrhythmic tendencies.

To our knowledge, this is the first study to use optical mapping to identify the regional changes in ventricular electrophysiology with sympathetic stimulation and removal of the left and right sympathetic chains. We report that the base of the left ventricle elicited the shortest APDs and steepest restitution curves with sympathetic stimulation, which was reversed by removal of the left sympathetic chain. Therefore the data suggest that the left sympathetic neurones primarily innervate the basal regions. We also conclude that although the right sympathetics appear to have a dominant effect on heart rate, cardiac ventricular electrophysiology was predominantly mediated by the left sympathetics.

These results support the rationale for treatments such as LCSD in which left sympathetic supply is removed in order to reduce the risk of arrhythmia initiation in patients following MI, LQTS patients (Schwartz et al., 2004), CPVT patients (Wilde et al., 2008), non-LQTS arrhythmogenic channelopathies and cardiomyopathies (Coleman et al., 2012) and patients with drug refractory ventricular arrhythmias (Bourke et al., 2010). Our findings lead us to suggest that the mechanisms that give rise the antiarrhythmic results of LCSD are prolonged refractoriness, decreased dispersion of repolarisation and flattening of restitution curves.

### ***Future works***

Our data from optical mapping provide evidence of regional differences in left and right sympathetic innervations of the left ventricle and support the notion that left sympathetic nerves innervate more densely at the base. We have also shown that the caudal segments of the left sympathetic chain produced more pronounced effects at the base of the left ventricle. Therefore, in order to progress this study further, it is important to investigate differential regional innervations of the spinal segmental inputs of the left and right sympathetic chains. This will provide insight into the mechanism underlying the predominant proarrhythmic tendencies of the left sympathetic chain at the segmental levels T4-T6. This would require combining the novel technique used to stimulate each spinal segmental level with optical mapping, which has never previously been explored. In addition, using voltage sensitive dyes with different optical properties, there is

the potential to measure APD from different myocardial layers to gain a more detailed understanding of the heterogeneous innervations.

In diseased states, remodelling of the sympathetic nerves can occur which is associated with the development of lethal arrhythmias. The consequences of remodelling are still unclear and it has been suggested that LCSD in these conditions would be insufficient as remodelling would continue with the right sympathetics (Ajjola et al., 2012). An understanding of the changes in left and right sympathetic neurone innervation in diseased conditions is therefore essential for determining adequate clinical treatments. This could be explored using the coronary ligation model of heart failure model previously described by our group (Ng et al., 1998) combined with the same techniques utilized in this study.

Future investigations using the optical mapping technique could also explore the correlation between the regions with large differences in APD and APD restitution slopes, and the sites in which VF is initiated both in healthy and diseased models. This will provide the potential to identify specific sites for therapeutic intervention.

## 8 Appendix

The following study was performed prior to the former studies. In this set of experiments we aimed to investigate the role of Epac, which acts downstream of sympathetic activity and has been proposed to influence arrhythmogenesis. Previous studies were performed in cellular mice and rat models with one previous study in a whole heart mouse model. Hence, we chose to investigate the effects of Epac in the Guinea pig whole heart in which the electrophysiology is more representative of that in humans. The data did not display significant effects of Epac on any of the parameters measured in the Guinea pig. We suggest this was due to the species differences and suggest that Epac may have a more pronounced effect in disease models or with chronic Epac stimulation.

We therefore decided that in order to explore the relationship between the sympathetic response and arrhythmia initiation further, it was necessary to instead investigate effects of direct sympathetic nerve stimulation using the isolated innervated rabbit heart model, and thus moved on from this line of research. The following are the results obtained from the Epac study.

## 8.1 Abstract

### Introduction

The exchange protein activated by cAMP (Epac) highlights a novel pathway downstream of  $\beta$ -adrenergic signalling. Activation of Epac by cAMP has been found to cause abnormal  $\text{Ca}^{2+}$  handling within cardiomyocytes due to spontaneous  $\text{Ca}^{2+}$  transients and sarcoplasmic reticulum  $\text{Ca}^{2+}$  leak. This can lead to arrhythmia generation, highlighting Epac as a potential therapeutic target. This has importance in cardiac disease i.e. heart failure, where there is chronic stimulation of the  $\beta$ -adrenergic pathway and increased Epac expression.

### Methods

Langendorff whole heart perfusion using adult male Dunkin Hartly guinea pigs was used to study the effect of Epac on cardiac physiology. Epac activator 8-CPT was perfused in  $1\mu\text{M}$  and  $10\mu\text{M}$  concentrations. Data was obtained using constant pacing, electrical restitution and dynamic pacing protocols. A positive control of  $1\text{nM}$  isoproterenol was also used.

$\text{Ca}^{2+}$  imaging using the fluorescent dye Fura-2 dye was used to investigate Epac's effect on calcium handling in both rat and guinea pig cardiomyocytes. Data was recorded from both electrically evoked transients and caffeine evoked transients.

### Results

The Epac activator caused no significant changes in  $\text{MAPD}_{50}$  or  $\text{MAPD}_{90}$ . The electrical restitution protocol provide data showing no changes in ERP or steepness of restitution slope with either  $1\mu\text{M}$  8-CPT or  $10\mu\text{M}$  8-CPT. The dynamic pacing protocol displayed no alternans and no changes in the cycle length that induced ventricular fibrillation with the Epac activator. Calcium imaging data showed no changes in systolic or diastolic  $\text{Ca}^{2+}$ , no changes in transient amplitude and no changes in sarcoplasmic reticulum  $\text{Ca}^{2+}$  load that reached statistical significance.

## Conclusions

Epac activation did not induce changes in  $\text{Ca}^{2+}$  handling or initiate arrhythmia in the Guinea pig heart. There may be a greater role for Epac in pathophysiological conditions where Epac is more highly expressed.

## 8.2 Introduction

### 8.2.1 Introduction to the Epac protein

In 1998, de Rooji et al discovered a PKA independent, cAMP induced activation of Ras-related protein 1 (Rap1). Up until this point it was generally accepted that PKA alone was activated downstream of cAMP. Epac is a guanine nucleotide exchange factor (GEF) for Ras like GTPases and is regulated by cAMP. Epac has two isoforms; Epac1 and Epac2, both of which activate GDP for GTP exchange in Rap1 and Rap2 (Ruiz-Hurtado et al., 2013, Holz et al., 2006) and are coded for by the genes RAPGEF3 and RAPGEF4 respectively (de Rooij et al., 1998, Guo et al., 2006). There is also evidence for the presence of splice variants of Epac particularly for Epac2 (Schmidt et al., 2013).

Effects of Epac activation have been evidenced in a variety of cell types and it has many known functions. The following functions have been associated with Epac activation; integrin mediated cell adhesion (Rangarajan et al., 2003), increased myofilament sensitivity (Cazorla et al., 2009), exocytosis (Seino and Shibasaki, 2005), interactions with ion channels e.g.  $K_{ATP}$  channels (Purves et al., 2009), mitogen-activated protein kinase (MAPK) signalling (Wang et al., 2006), PLC activation (Schmidt et al., 2001), formation of vascular endothelial cell barrier (Fukuhara et al., 2005) and also gap junctions via increased connexin accumulation (Somekawa et al., 2005),  $Ca^{2+}$  handling modulation in cardiomyocytes (Oestreich et al., 2009, Oestreich et al., 2007, Pereira et al., 2013, Pereira et al., 2007, Ruiz-Hurtado et al., 2012), cardiac hypertrophy (Metrich et al., 2008, Morel et al., 2005, Ruiz-Hurtado et al., 2013) and increasingly more functions.

The structure of both Epac proteins (fig 8.1) consists of a C-terminal catalytic region, a Ras exchanger motif and a putative Ras associating domain (Gloerich and Bos, 2010, Schmidt et al., 2007). The CDC25 homology domain of the catalytic region exhibits the GEF activity for Rap proteins. Epac has an N-terminal regulatory region consisting of a 'dishevelled Egl-10 pleckstrin' (DEP) domain important for membrane association and a cAMP binding domain. In addition to

the above, Epac2 has an extra cAMP binding domain with a 20 fold lower affinity (Holz et al., 2006, Ruiz-Hurtado et al., 2013). The N-terminal regulatory region has the ability to exert an autoinhibitory effect which is relieved upon cAMP binding and results in Rap activation (Gloerich and Bos, 2010, Ruiz-Hurtado et al., 2013). The structure of Epac suggests it may have multiple binding targets (Ruiz-Hurtado et al., 2013).

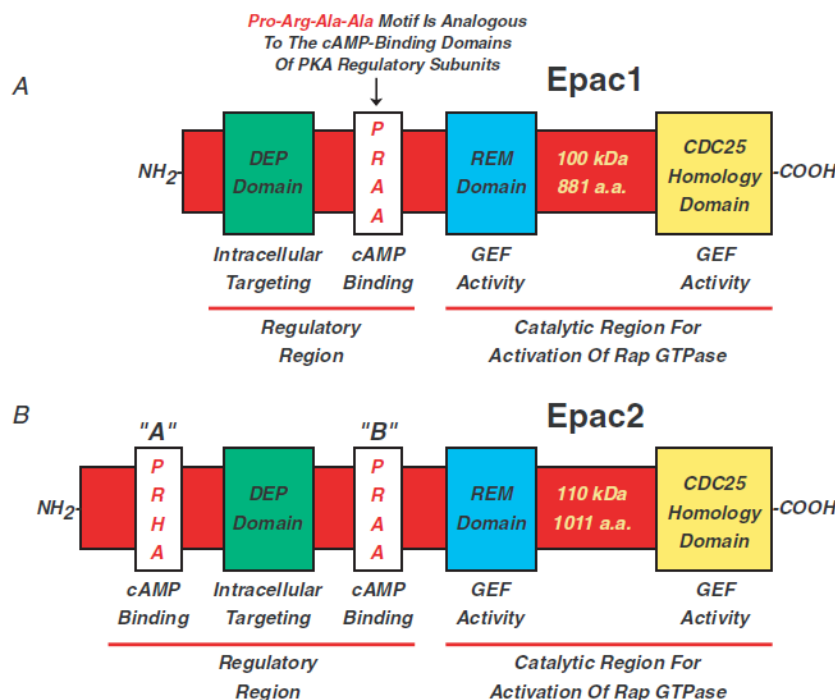


**Figure 8.1. Structure of Epac.** Epac proteins consist of a C-terminal catalytic region and an N-terminal regulatory region. Present within the catalytic region is a Ras exchange motif (REM) and a CDC25 homology domain. The regulatory region consists of a dishevelled Egl-10 pleckstrin (DEP) domain and cAMP binding domain(s) and upon binding the autoinhibition is relieved. (A) Epac1 consisting of 881 amino acids (molecular mass 100 kDa) and one cAMP binding domain. (B) Epac2 structure made up of 1011 amino acids (molecular mass 110 kDa) and two cAMP binding domains (Holz et al., 2006).

Expression of Epac1 is ubiquitous and is found mainly in the brain, adipose tissue, pancreas heart, kidney, ovary, spinal cord, spleen, uterus and blood vessels (de Rooij et al., 1998, Holz et al., 2006, Kawasaki et al., 1998, Schmidt et al., 2013). Epac2 is mostly located in the pancreas, adrenal glands, liver and central nervous system (Holz et al., 2006, Schmidt et al., 2013, Ueno et al., 2001).

Epac1 has high expression in the heart (Metrich et al., 2008, Schmidt et al., 2007) and is thought to be part of a signalling complex involving muscle-specific A-kinase anchoring protein (mAKAP), and PKA in order to regulate the RyR activity (Dodge-Kafka et al., 2005). Within rat cardiac myocytes, Epac distribution is favoured at the nuclear/perinuclear areas and at the plasma membrane (Metrich et al., 2008, Pereira et al., 2012) and it is thought that Epac may be present in microdomains (Ruiz-Hurtado et al., 2013). In addition, different Epac1 and Epac2 expression is found in adult tissues as appose to foetal tissues (Schmidt et al., 2013).

### 8.2.2 Epac activators

8-pCPT-2'-O-Me-cAMP (8-CPT) is the most commonly used Epac activator and has been found to bind to Epac with a threefold higher  $V_{max}$  than that of cAMP (Rehmann et al., 2003). 8-CPT has been used in many Epac studies and at concentrations  $<100 \mu\text{M}$  it activates Epac with high specificity. At concentrations of  $100 \mu\text{M}$  or higher, it begins to activate PKA but not to its full activity (Christensen et al., 2003). Epac analogues such as 8-CPT use a 2'-O-alkyl substitution e.g. 2'-O-Me-cAMP on the ribose ring of cAMP to activate Epac and also weaken the ability to activate PKA (Christensen et al., 2003).

It has been suggested by Schmidt et al (2007), that higher levels of  $\beta$ -AR activation and so higher levels of cAMP are necessary for Epac activation. This would mean that lower levels of  $\beta$ -AR activation might only be recruiting PKA (Bers, 2007, Pereira et al., 2013), complementary with the view that Epac has a lower affinity for cAMP than PKA does (Smrcka et al., 2007). However, Epac1 binds to cAMP with  $K_d$  of  $2.8 \mu\text{M}$  (Christensen et al., 2003), Epac2 with a  $1.2 \mu\text{M}$   $K_d$  value and PKA binds to cAMP with a similar  $K_d$  value to Epac1 of  $2.9 \mu\text{M}$  (Christensen et al., 2003, Dao et al., 2006, Purves et al., 2009). Pereira et al (2013) also found that a lower concentration of isoproterenol ( $30\text{nM}$ ) was able to cause maximal Epac-dependent RyR2 effects then needed for maximal PKA-dependent effects. Ultimately it may be the subcellular location of Epac in comparison to PKA that may determine the extent to which each is activated (Purves et al., 2009).

There are concerns that 8-CPT could have other targets for example inhibition of platelet PDE5 and/or PDE3 leading to activation of cAMP-PKA and cGMP-PKG signalling pathways (Poppe et al., 2008). These results were however found in the presence of 100 $\mu$ M of 8-pCPT, higher than the Epac specific concentrations.

8-CPT has been used in many Epac studies that suggest a role for Epac in the heart due to its effect on ion channel function, Ca<sup>2+</sup> handling, arrhythmia and cardiac hypertrophy.

### **8.2.3 Epac and ion channel function**

Although Epac is known to have effects on Ca<sup>2+</sup> handling (Oestreich et al., 2007, Pereira et al., 2007), many studies have ruled out involvement of L-type Ca<sup>2+</sup> currents ( $I_{Ca,L}$ ) in Epac activation (Brette et al., 2013, Dominguez-Rodriguez et al., 2013, Pereira et al., 2007, Smani et al., 2010). T-type Ca<sup>2+</sup> channels have been implicated via increased Cav3.1 subunit expression (Novara et al., 2004). An Epac dependent recruitment of T-type Ca<sup>2+</sup> channels was observed in rat chromaffin cells upon  $\beta$ -AR stimulation however, this was observed at concentrations of 8-CPT above those selective for Epac (200 $\mu$ M).

Dominguez –Rodriguez et al (2013) did however see a shift in the voltage dependent activation curve of  $I_{Ca,L}$  in the direction of more hyperpolarized potentials. Although there were no significant alterations in  $I_{Ca,L}$ , an increase in  $I_{Ca}$  window current was observed in the presence of Epac activators (fig 8.2). This was accompanied by CaM upregulation. Ruiz-Hurtado et al (2012) also observed an increase in  $I_{Ca}$  window current which contributed to the positive inotropic effect induced by Epac activation.

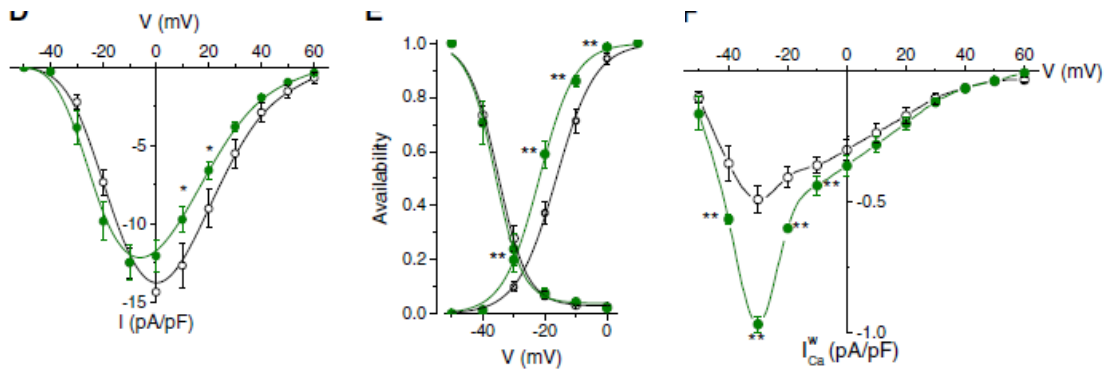


**Figure 8.2. Effects of Epac on  $I_{Ca}$  window current.**  $I_{Ca}$  window current-density voltage relationship, steady state inactivation and activation curves and voltage dependence curves respectively from left to right in cardiac myocytes. Black curves represent control cells. Green curves represent cells incubated with 10  $\mu$ M 8-CPT. Adapted from Ruiz-Hurtado et al (2012).

There is also evidence of  $K^+$  channel modulation upon Epac activation. Kang et al (2008) discovered a reduction in the activity of  $K_{ATP}$  channels in the presence of 8-CPT due to increased sensitivity of the channels to ATP inhibition. This is thought to be due to the interaction of Epac with NBF-1 of the full length SUR1 subunit of  $K_{ATP}$  channels (Kang et al., 2006). It was suggested that interaction with Epac causes SUR1 to act as a scaffolding protein for a Rap and phospholipase  $C_e$  ( $PLC_e$ ) resulting in a decrease in phosphatidylinositol biphosphate ( $PIP_2$ ) and so increased  $K_{ATP}$  channel sensitivity. It has also been proposed that Epac promotes  $PIP_2$  hydrolysis and this may account for the inhibitory effect on  $K_{ATP}$  channels (fig 8.3) (Holz et al., 2006).

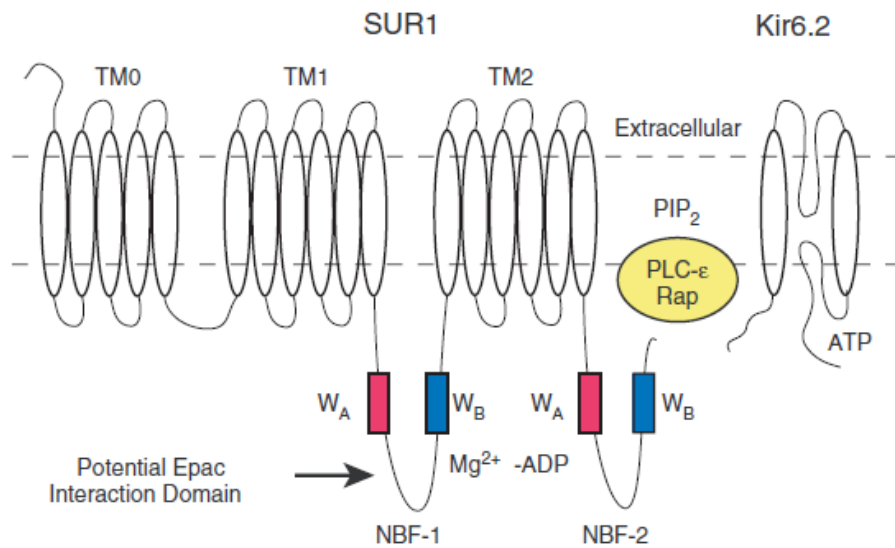


**Figure 8.3. Epac's effect on K<sub>ATP</sub> channels.** It is proposed that Epac is recruited to the plasma membrane by nucleotide-binding fold 1 (NBF-1) of the SUR1 subunit of K<sub>ATP</sub> channels, allowing it to bin with cAMP and activate Rap. Rap then stimulates PLC<sub>ε</sub> which hydrolysis PIP<sub>2</sub> and increases K<sub>ATP</sub> channel sensitivity to ATP and therefore leads to K<sub>ATP</sub> channel closure (Holz *et al.*, 2006).

Purves *et al* (2009) discovered that Epac is able to modulate the activity of K<sub>ATP</sub> channels by activating Ca<sup>2+</sup> sensitive protein phosphatase-2B (PP-2B) in a Ca<sup>2+</sup> dependent manor, acting as a regulator of vascular tone in arterial K<sub>ATP</sub> channels and a regulator of insulin release in pancreatic K<sub>ATP</sub> channels (Shibasaki *et al.*, 2007). It was suggested that Epac and K<sub>ATP</sub> channels form a complex that is in close proximity to the SR (Purves *et al.*, 2009). Epac1 has also been found to immunoprecipitate with Kv4.3 suggesting its involvement in I<sub>TO</sub> (Potapova *et al.*, 2007).

Other evidence using vascular smooth muscle cells has suggested that 8-CPT-AM (a more membrane permeable form of 8-CPT) can increase the open probability of Ca<sup>2+</sup> sensitive K<sup>+</sup> channels (BK, SK and IK channels), implicating Epac in regulation of hyperpolarization and so vasorelaxation due to decreased Ca<sup>2+</sup> entry via voltage gated calcium channels (VGCC) (Roberts *et al.*, 2013). Epac activates BK channels by increasing the frequency of SR Ca<sup>2+</sup> sparks in close proximity to the channel. If this coupling becomes abnormal then

vasorelaxation will become defective and can lead to hypertension (Amberg et al., 2003). Ster et al (2007) also observed an activation of BK channels induced by Epac. The SK and IK channels are activated via the nitric oxide (NO) and Endothelium-Derived Hyperpolarizing Factor (EDHF) pathways, which are triggered by Epac (Roberts et al., 2013).

A decrease in KCNE1 mRNA and membrane protein expression in cardiac myocytes has also been observed upon Epac activation leading to  $I_{K_s}$  downregulation in guinea pig left ventricular myocytes (Aflaki et al., 2014). The observed decrease in  $I_{K_s}$  density has also been seen previously upon sustained  $\beta$ -AR stimulation, reinforcing these findings (Zhang et al., 2002). Downregulation of  $I_{K_s}$  occurs via the  $Ca^{2+}$ /calcineurin (Cn)/ nuclear factor of activated T cells (NFAT) signalling (figure 8.4) which is supported by previous studies displaying NFAT nuclear translocation in cardiac hypertrophy (Morel et al., 2005). As CaMKII was found to be necessary for this response, it was suggested that CaMKII and Rap1 are required for  $Ca^{2+}$  release which in turn is important for  $I_{K_s}$  downregulation (Aflaki et al., 2014).

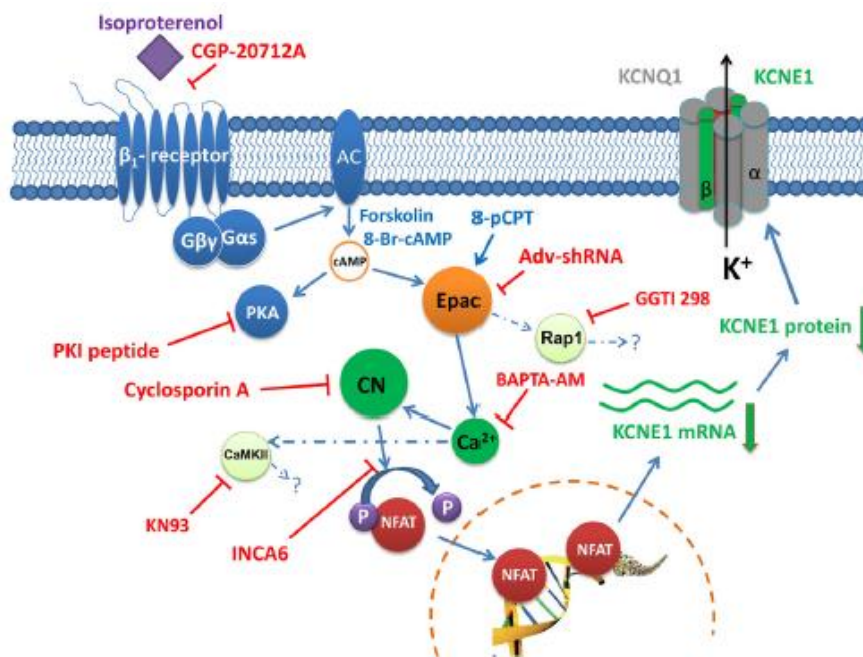


**Figure 8.4. Mechanisms of the downregulation of IKs by sustained  $\beta$ -AR stimulation.** Proposed pathway by which Epac stimulation leads to decreased translation of KCNE1 mRNA and so reduced KCE1 protein expression. Therefore Iks is downregulated as a result of Epac activation by  $6\mu\text{M}$  8-CPT. Blockers (red), Activators (blue). (Aflaki et al., 2014).

Although other studies have suggested that action potential duration (APD) remains unaltered by Epac activation (Aflaki et al., 2014, Hothi et al., 2008, Oestreich et al., 2009, Pereira et al., 2007), Brette et al (2013) saw a significant increase in APD in the presence of 8-CPT-AM with no changes in action potential amplitude, maximum depolarization rate and resting membrane amplitude (fig 8.5). This led them to believe that Epac has no effect on  $\text{Na}^+$  current and inward rectifier  $\text{K}^+$  current. They also found no changes in  $I_{\text{Ca,L}}$  in line with what other studies have shown (Brette et al., 2013, Dominguez-Rodriguez et al., 2013, Pereira et al., 2007, Smani et al., 2010) and  $I_{\text{TO}}$  also remained unaltered. The proposed mechanism for the increased APD was inhibition of the steady state  $\text{K}^+$  current. Inhibiting PKA during  $\beta$ -AR activation produced the same results as direct Epac activation (Brette et al., 2013), implying a physiological relevance of this atypical result.

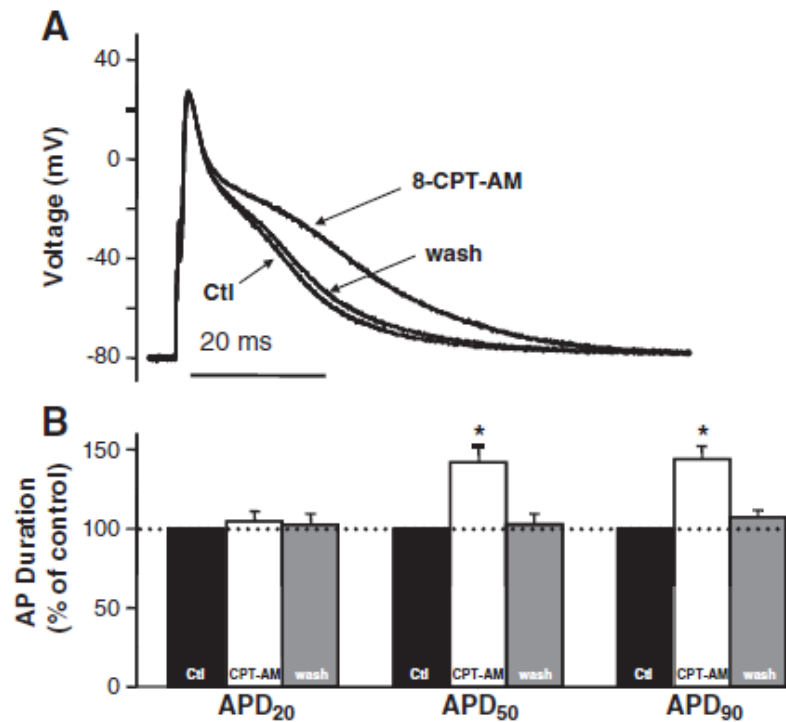


**Figure 8.5. Effect of Epac on action potential duration.** (A) Action potential durations in the absence (Ctl) and presence of 10 $\mu$ M 8-CPT-AM. APD for washout is also shown (wash). (B) Effect on APD<sub>20</sub>, APD<sub>50</sub>, APD<sub>90</sub> in controls, in the presence of 10 $\mu$ M 8-CPT-AM and during washout (Brette et al., 2013).

One reason for the differences observed between APD changes in this study in comparison to the others is the use of a slightly different Epac activator; 8-CPT-AM as opposed to 8-CPT. Brette et al (2013) also did not see increases in APD when just 8-CPT was used. 8-CPT-AM is more membrane permeant with a greater potency (100 to 1000 fold greater) and this could provide an explanation for the discrepancies (Brette et al., 2013). Another explanation is that Epac activation involves compartmentalization of signalling as suggested by Ruiz-Hurtado et al (2012) in cardiomyocytes and the more membrane permeant 8-CPT-AM would interfere with this.

Epac has also been implicated in regulation of epithelial Na<sup>+</sup> channels via dopamine signalling and this also involves compartmentalization (Helms et al., 2006). The suggested mechanism involves activation of Epac via dopamine production of cAMP in compartments where only Epac is available (not PKA).

Recent studies have also shown that Epac can enhance late  $\text{Na}^+$  current upstream of CaMKII $\delta$  (Dybkova et al., 2014).

It has also been proposed that Epac can exert its effects on transporters such as the  $\text{Na}^+$ - $\text{H}^+$  exchanger 3 (NHE $_3$ ) (Honegger et al., 2006) and  $\text{H}^+$  $\text{K}^+$  transporters (Laroche-Joubert et al., 2002).

#### **8.2.4 Epac and cardiac calcium signalling**

In various cell types, it has been evidenced that Epac modulates  $\text{Ca}^{2+}$  handling. The first evidence of this was observed in pancreatic cells whereby Epac mediated CICR (Kang et al., 2001). As well as in pancreatic cells (Kang et al., 2001, Kang et al., 2005, Kang et al., 2003), Epac has also been found to alter  $\text{Ca}^{2+}$  handling in rat and mice cardiac myocytes (Morel et al., 2005, Oestreich et al., 2007, Pereira et al., 2007), aortic myocytes (Purves et al., 2009), inner medullary collecting duct (Yip, 2006), cerebellar neurons (Ster et al., 2007) and the endothelium (Mayati et al., 2012). Abnormal  $\text{Ca}^{2+}$  handling due to Epac activation does not involve LTCC's (Brette et al., 2013, Dominguez-Rodriguez et al., 2013, Oestreich et al., 2007, Pereira et al., 2007, Smani et al., 2010).

In cardiomyocytes, both increases and decreases in  $\text{Ca}^{2+}$  transient amplitude have been observed in response to Epac activation. An enhancement in the electrically evoked  $\text{Ca}^{2+}$  transient amplitude was observed by Oestreich et al (2007) in mice when 8-CPT was applied for no more than 60 seconds. This was found to be PLC dependent (fig 8.6).

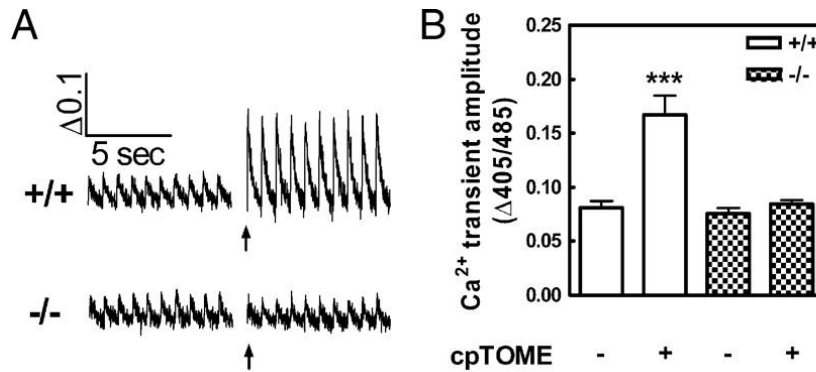


**Figure 8.6. Acute Epac activation increases Ca<sup>2+</sup> transients in a PLC dependent manner.** (A) Ca<sup>2+</sup> transients from PLCε +/+ (+/+) and PLCε -/- (-/-) mice cardiac myocytes in the absence and presence of 10 μM 8-CPT (B) Peak Ca<sup>2+</sup> transient amplitudes. Adapted from Oestreich et al (2007).

In comparison, Pereira et al (2007) applied 8-CPT for 2-5 minutes to rat cardiac myocytes and found a decrease in Ca<sup>2+</sup> transient amplitude and an increase in the frequency of Ca<sup>2+</sup> sparks, which was CaMKII dependent (fig 8.7). This occurred independent of changes in contraction as a result of increased myofilament sensitivity (Cazorla et al., 2009). Purves et al (2009) did not observe an increase in Ca<sup>2+</sup> spark activity but increased Ca<sup>2+</sup> transients were present in human pancreatic β-cells and rat INS-1 cells. Pereira et al (2013) reported that activation of RyR by 8-CPT was due to Epac2 via β1-AR and Epac1 cannot replace this function. As well as this, they reported that Epac2 was the only Epac isoform that was mediating increased SR Ca<sup>2+</sup> leak.

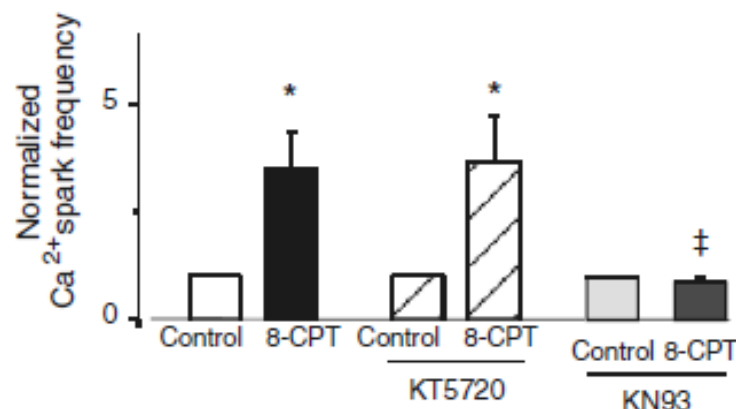


**Figure 8.7. Epac increases Ca<sup>2+</sup> spark frequency.** Application of 10 μM 8-CPT to rat cardiac myocytes under control conditions, in the presence of a PKA inhibitor (2 μM KT5720) and in the presence of a CaMKII inhibitor (1 μM KN93). Adapted from Pereira et al (2007).

It has been suggested that the differences seen between the Oestreich et al (2007) and Pereira et al (2007) papers are due to the application times of the Epac activator however it could also be as a result of species differences due to different patterns of isoform expression (Ruiz-Hurtado et al., 2013). Brief periods of Epac activation used by Oestreich et al (2007) may not have allowed enough time for SR depletion. Furthermore, the Epac dependent  $Ca^{2+}$  responses observed by both papers may not be seen on a longer term basis as the SR stores would become fully depleted in the absence of  $Ca^{2+}$  entry (Ruiz-Hurtado et al., 2013).

Periods of Epac activation of 5 hours, overnight or 4 weeks used by one study generated a strong positive inotropic effect due to  $[Ca^{2+}]_i$  transient increase (Ruiz-Hurtado et al., 2012). The positive inotropic effect was reduced by Epac1 knock down, protein synthesis blockade and inhibition of CaMKII or Cn, the downstream effectors of calmodulin (CaM) (Ruiz-Hurtado et al., 2012). The same study also observed upregulation of CaM expression in cardiomyocytes as a result of Epac activation suggesting CaM's importance in chronic Epac activation. Epac causes CaMKII dependent RyR phosphorylation resulting in increased  $Ca^{2+}$  spark frequency however CaM directly blocks RyR (Yamaguchi et al., 2003). This is possibly why increases in  $Ca^{2+}$  spark frequency are not observed under chronic Epac activation and an increased SR load is observed (Ruiz-Hurtado et al., 2012).

Supporting Epac's activation of PLC suggested by Oestreich et al (2007), Smrcka et al (2007) proposed an Epac-PLC $\epsilon$ -PKA pathway as a result of  $\alpha_1$  adrenergic receptor ( $\alpha_1$ -ADR) stimulation (O-Uchi *et al.*, 2005). This occurs alongside PKA pathways so SR depletion is avoided due to PLB phosphorylation and therefore SERCA activity (Smrcka et al., 2007). Schmidt et al (2001) also found a PKA independent PLC stimulation and  $Ca^{2+}$  mobilization as a result of  $\beta_2$ -AR and forskolin activation of Rap2B. This suggests that Epac may also influence production of IP $_3$ . In the endothelium, it was suggested that Epac may be causing increase in  $[Ca^{2+}]_i$  by targeting IP $_3$  sensitive stores (Mayati et al., 2012, Roberts et al., 2013). However, it was also found that only inhibition of the  $\beta_1$ -AR pathway

blunted Epac's effects on  $\text{Ca}^{2+}$  signalling (Mangmool et al., 2010, Pereira et al., 2013).

Ruiz-Hurtado et al (2013) suggested Epac activation has both acute and chronic effects. The proposed pathway of the acute effects of Epac is demonstrated by fig 8.8a. It has been suggested that Epac activates  $\text{PLC}\epsilon$ , producing DAG and  $\text{IP}_3$ . DAG activates PKC which then phosphorylates CaMKII. CaMKII in turn phosphorylates RyR resulting in  $\text{Ca}^{2+}$  release.  $\text{IP}_3$  activation leads to  $\text{Ca}^{2+}$  release from  $\text{IP}_3\text{R}$ . Chronic activation of Epac may also lead to activation of histone deacetylase (HDAC) and NFAT and so activate transcription (figure 8.8b).

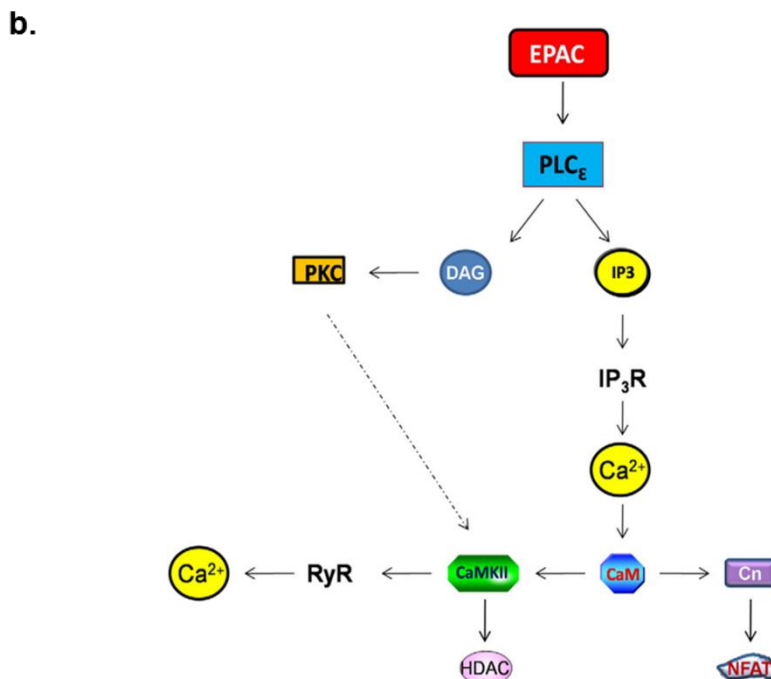
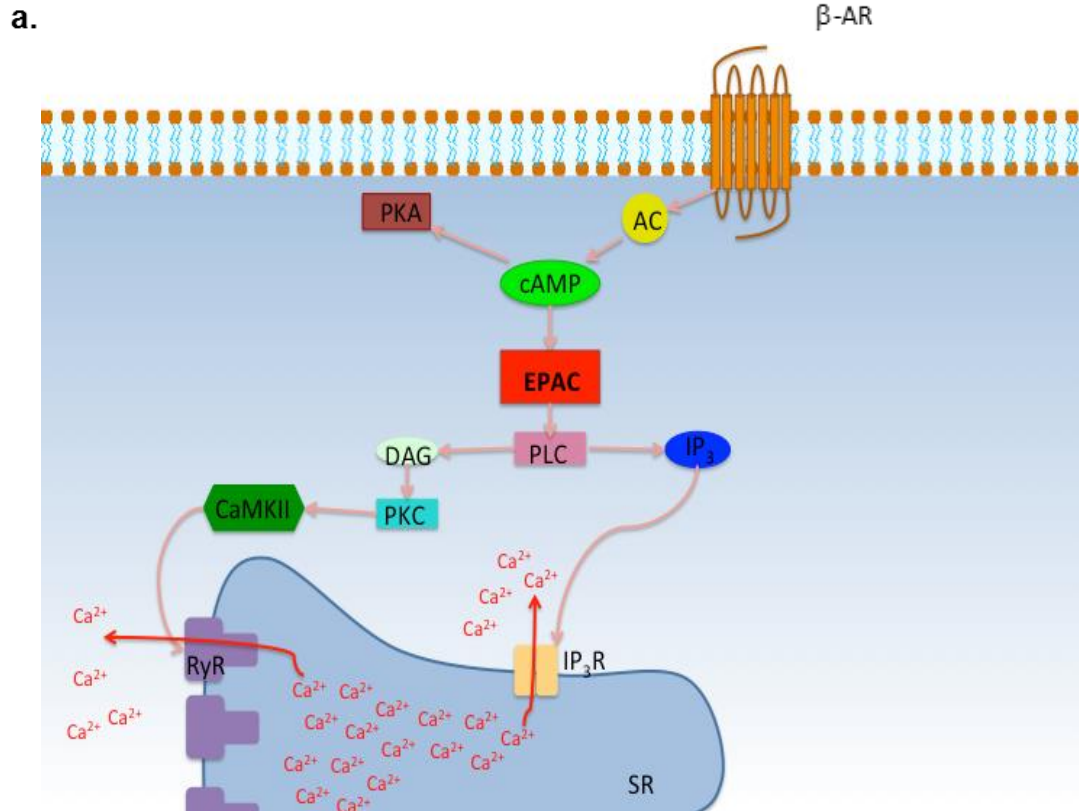


**Figure 8.8. Proposed Epac pathway in cardiac myocytes.** Epac activates PLC, which goes on to produce both diacyl glycerol (DAG) and inositol 1,4,5 trisphosphate (IP<sub>3</sub>). DAG activates PKC which then goes on to phosphorylate CaMKII. CaMKII phosphorylates RyR and HDAC. RyR Ca<sup>2+</sup> release from SR is observed. IP<sub>3</sub> activates IP<sub>3</sub> receptors (IP<sub>3</sub>R) and Ca<sup>2+</sup> may also be released in this way. CaMKII and Cn are activated by Ca<sup>2+</sup>. Cn can cause nNFAT dephosphorylation. Figure 8b from Ruiz-Hurtado et al (2013).

As mentioned previously, an increase in  $\text{Ca}^{2+}$  spark frequency and decrease in the SR  $\text{Ca}^{2+}$  load was observed by Pereira et al (2007). The SR load is decreased as a result of the SR leak via RyR's and this results in decreased  $[\text{Ca}^{2+}]_i$  transients. A similar effect is seen in heart failure stress-induced activation of the sympathetic nervous system leading to leaky RyR's (Reiken et al., 2003). Epac has also been suggested to increase RyR activity possibly through interactions with Rap1 (Kang et al., 2003, Roberts et al., 2013). There is also evidence to suggest that Epac is present in a cAMP regulated macromolecular complex consisting of muscle-specific A-kinase anchoring protein (mAKAP), PKA, cAMP-phosphodiesterase (PDE), and RyR2 (Dodge-Kafka et al., 2005).

Although the  $[\text{Ca}^{2+}]_i$  transient amplitude may be reduced as a result of Epac activation Pereira et al (2007) suggested contraction of the heart may still be favoured. One explanation for this is that the duration of the  $[\text{Ca}^{2+}]_i$  transient is extended, although it has also been proposed that Epac may increase the  $\text{Ca}^{2+}$  sensitivity of myofibrils (Cazorla et al., 2009, Pereira et al., 2007).

8-CPT was found to increase phosphorylation of CaMKII (Kawasaki et al., 1998, Oestreich et al., 2009, Pereira et al., 2007) at Thr286 in a PKC dependent manner (Oestreich et al., 2009). Epac activation has also been suggested to increase phosphorylation of CaMKII (Thr17), RyR (Ser2815) and PLB (Thr17). This was also found to be PKC-dependent (Oestreich et al., 2007). The phosphorylation of RyR and PLB occurs at CaMKII specific sites as a result of Epac activation (Oestreich et al., 2009). The use of PKC and CaMKII inhibitors has blocked the effects of Epac activation (Cazorla et al., 2009).

Intracellular  $\text{Ca}^{2+}$  loading is one of the factors that can affect arrhythmia and thus Epac's modulation of  $\text{Ca}^{2+}$  handling can provide an explanation for its role in ventricular arrhythmogenesis.

### **8.2.5 Epac and arrhythmia**

The initial arrhythmogenic effects as a result of abnormal  $\text{Ca}^{2+}$  handling have been associated with the acute effects of Epac activation, whereas more chronic effects of prolonged Epac activation have been reported to result in cardiac hypertrophy (Metrich et al., 2008). Pereira et al (2013) have however suggested that Epac's acute effects are more significant than its role in hypertrophy.

The increased SR load caused by Epac can lead to DADs, EADs and triggered activity (figure 8.9) and thus cause arrhythmias (Ruiz-Hurtado et al., 2012). Hothi et al (2008) reported abnormal  $\text{Ca}^{2+}$  homeostasis in response to Epac activation, which eventually resulted in ventricular tachycardia in the mouse heart (fig 8.10). This was found to be CaMKII dependent and independent of changes in repolarization gradients, action potential gradients and effective refractory period. Epac activation was found to increase the occurrence of ectopic  $\text{Ca}^{2+}$  release, which could result in the onset of arrhythmias (Hothi et al., 2008).

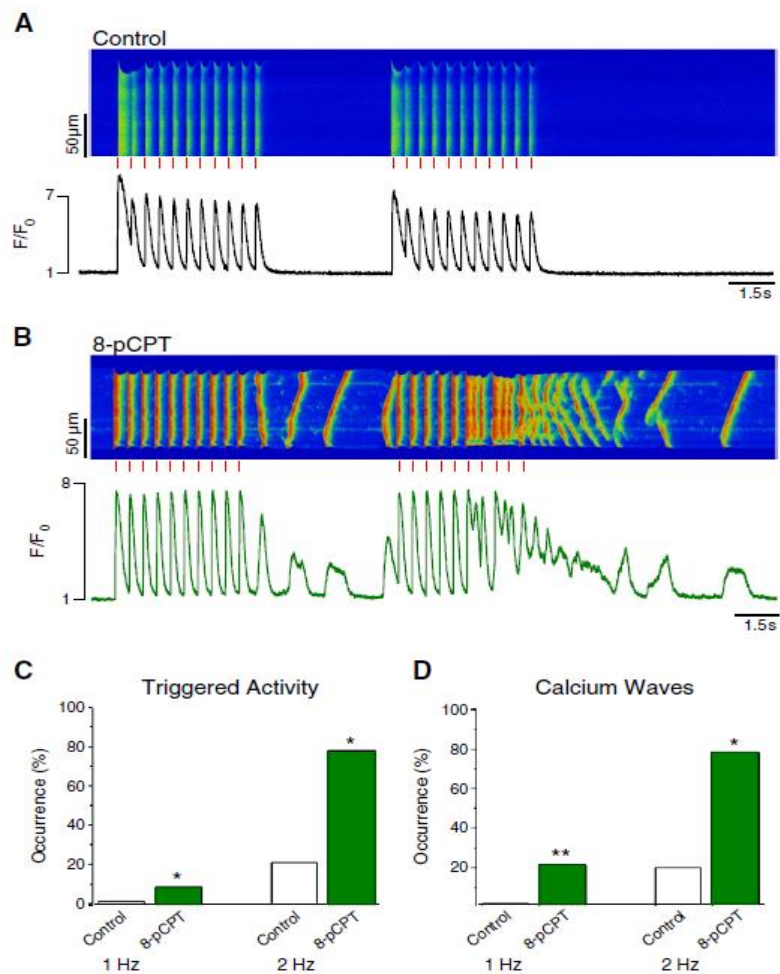


**Figure 8.9. Chronic Epac activation causes triggered activity.** (A-B) Line scan images in the presence and absence of 10 $\mu$ M 8-CPT with fluorescence [Ca<sup>2+</sup>] transient profiles beneath the corresponding traces. (C) Triggered activity with 1Hz and 2Hz pacing, with control and 10 $\mu$ M 8-CPT. (D) % occurrence of spontaneous Ca<sup>2+</sup> waves (Ruiz-Hurtado et al., 2012).

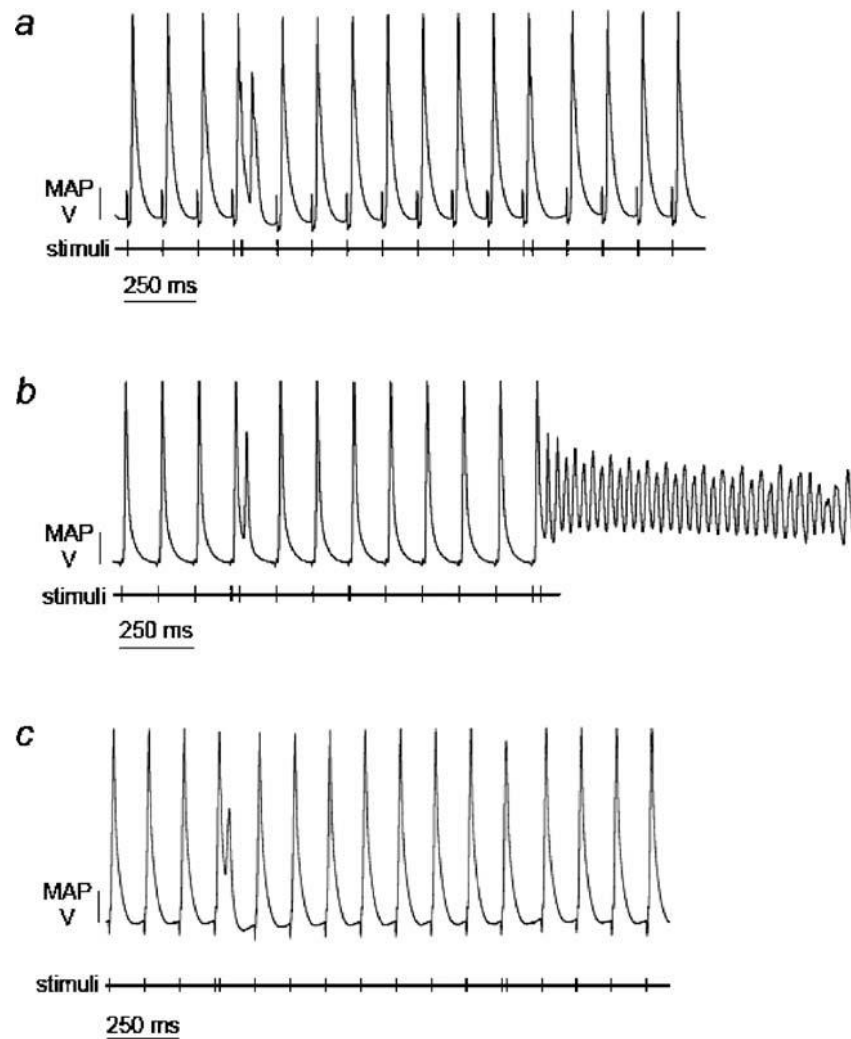


**Figure 8.10. Epac application results in ventricular tachycardia.** Monophasic action potentials from mice hearts during control conditions (a), perfusion with 1 $\mu$ M 8-CPT (b) and perfusion with CaMKII inhibitor KN93 (c). Recorded during programmed electrical stimulation (Hothi et al., 2008).

The SR  $\text{Ca}^{2+}$  release in response to Epac activation has arrhythmogenic potential. Pereira et al (2013) suggested that  $\beta_1$ -AR activates Epac2 in parallel with PKA and downstream of this CaMKII is activated. CaMKII then goes on to phosphorylate RyR at the S2814 site resulting in SR  $\text{Ca}^{2+}$  leak and triggered arrhythmias and reduced cardiac function (Pereira et al., 2013). Arrhythmia susceptibility was reduced in Epac2-KO mice and there was a reduction in abnormal  $\text{Ca}^{2+}$  sparks (Pereira et al., 2013).

This type of abnormal  $\text{Ca}^{2+}$  release from the SR via RyR has been seen in contractile dysfunction and arrhythmogenesis in HF (Pieske et al., 2002). In this case decreased diastolic  $\text{Ca}^{2+}$  transient amplitude and reduced SR load were also observed (Ai et al., 2005). As well as this, CaMKII expression was increased and more CaMKII was found in the RyR2 complex. The SR  $\text{Ca}^{2+}$  release associated with HF was reduced by CaMKII inhibition but PKA inhibition had no effect (Ai et al., 2005). CaMKII inhibition has even been found to reduce cardiac arrhythmogenesis *in vitro* and *in vivo* (Sag et al., 2009). This implicates Epac as a possible activator of this process. In fact, Epac has also been found to have increased expression in human HF (Metrich et al., 2008, Ulucan et al., 2007).

Arrhythmogenesis is seen in patients with HF and reduction in  $\text{I}_{\text{Ks}}$  currents is a potential cause for this. In HF, Epac1 expression is increased ~2 fold in ventricular cardiomyocytes and it has been known to reduce the density of  $\text{I}_{\text{Ks}}$  (Aflaki et al., 2014, Metrich et al., 2008). This impairs repolarisation and is therefore another mechanism by which Epac can cause arrhythmia. Arrhythmia can also be induced due to Epac's effects on  $\text{I}_{\text{Ca}}$  window current, associated with CaM upregulation (Dominguez-Rodriguez et al., 2013). This is due to the effects on the repolarization phase of the action potential caused by the increased  $\text{I}_{\text{Ca}}$  window current, and thus its generation of EADs (Benitah et al., 2010, Ruiz-Hurtado et al., 2013).

As mentioned previously, arrhythmia is associated with Epac's acute effects whereas chronic Epac activation can lead to cardiac hypertrophy.

### **8.2.6 Epac and hypertrophy**

Chronic activation of the  $\beta$ -AR pathway can result in cardiac hypertrophy and eventually HF. Cardiac hypertrophy involves nonmitotic cell growth, sarcomere rearrangement and gene expression (Metrich et al., 2008). Epac expression was found to be upregulated in cardiac hypertrophy and HF (Metrich et al., 2008, Ulucan et al., 2007). In addition, animal models of cardiac hypertrophy and patients with heart failure show increased Epac expression (Metrich et al., 2008, Ulucan et al., 2007).

Metrich et al (2008) discovered that prolonged Epac activation resulted in cytoskeleton reorganization and increased cell surface area. This effect was found to be PKA independent, with the involvement of Ras, Cn and CaMKII.

Similarly, Morel et al (2005) observed morphological changes induced by Epac activation and expression of cardiac hypertrophic markers. Increases in cardiomyocyte size and changes in the sarcomeric organization were also observed. Protein synthesis was increased two fold. Epac stimulation was found activate Rac in a  $Ca^{2+}$  dependent manner thereby activating the calcineurin/NFAT prohypertrophic signalling pathway. Epac's hypertrophic response was inhibited when Rac or Cn were blocked (Morel et al., 2005). Inhibition of protein synthesis by blocking transcription or transduction, and inhibition of CaMKII or Cn eliminated Epac's chronic effects (Ruiz-Hurtado et al., 2012).

After a period of 30 minutes Epac activation, not only was an increase in intranuclear  $[Ca^{2+}]$  seen but also translocation of HDAC and subsequent MEF2 suppression (Ruiz-Hurtado et al., 2012). Therefore, prolonged Epac activation results in CaMKII phosphorylation of HDAC, leading to HDAC translocation out of the nucleus and thus MEF activity is suppressed, activating gene transcription. Cn de-phosphorylates NFAT and forms a complex with it, leading to importation into the nucleus and activation of transcription (figure 8.11). This points to Epac's importance in the cardiac response to stress (Ruiz-Hurtado et al., 2013). As mentioned previously, Epac1 forms part of a signalling complex with mAKAP further indicating its relevance in nuclear signalling and gene expression (Pereira et al., 2013).

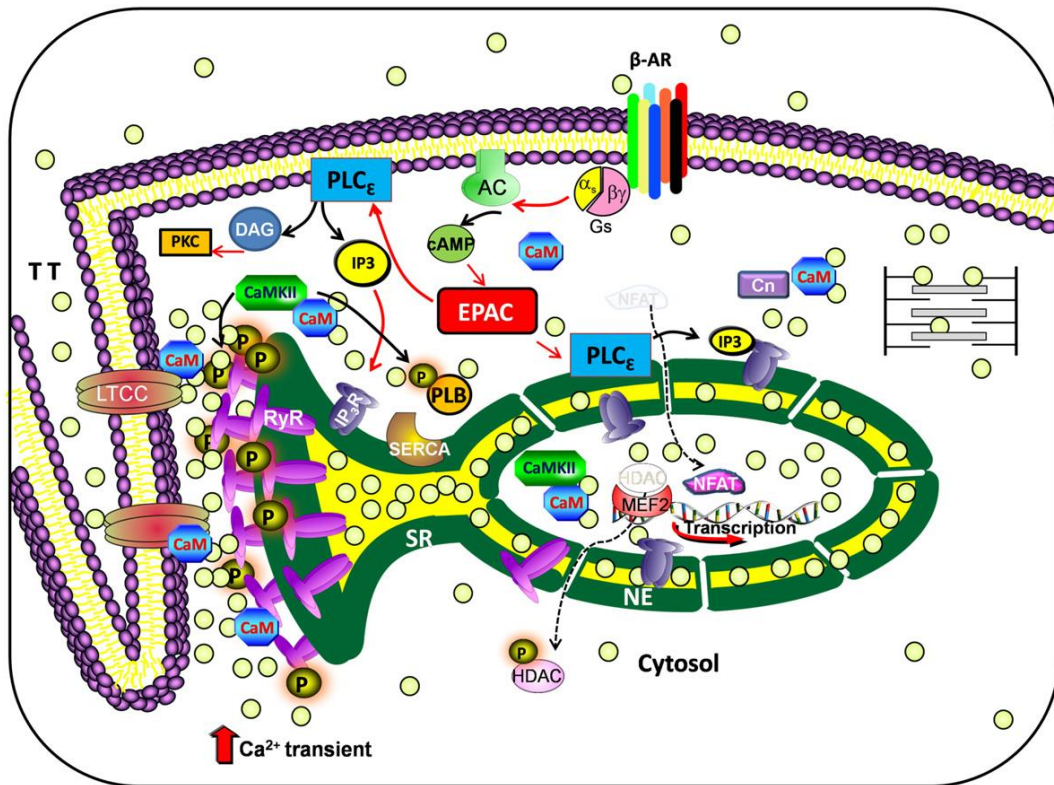


**Figure 8.11. Acute and Chronic Effects of Epac activation.** Both acute and chronic effects of Epac activation displayed in a myocyte. Chronic Epac activation leads to CaMKII phosphorylation of HDAC which then translocates to the nucleus and activates gene transcription. Increased intracellular  $\text{Ca}^{2+}$  due to acute Epac activation effects activates CaM which in turn activates Cn. Cn dephosphorylates NFAT and it gets imported into the nucleus and also activates gene transcription (Ruiz-Hurtado *et al.*, 2013).

The hypertrophic effects induced by Epac were found to be independent of its classical effector Rap1 and dependent on the small GTPase H-Ras, Rac (Morel *et al.*, 2005). The hypertrophic response was also observed by overexpressing Epac in the absence of Epac activators thus implying intracellular levels of cAMP are sufficient to activate Epac physiologically (Morel *et al.*, 2005). It has also been suggested that Epac's activation of PLC could lead to activation of cardioprotective pathways with the ability to balance the hypertrophic effects (Smrcka *et al.*, 2007).

### 8.2.7 Summary

Thus far Epac's effects on Langendorff whole heart physiology have only been studied in one paper in the mouse heart which attributed Epac to arrhythmia generation and therefore has the potential to be a target for treatment (Hothi et al., 2008). Majority of the Epac research mentioned has involved the use of rat or mouse cells and there is only one guinea pig paper which displayed Epac's downregulation of  $I_{K_s}$  (Aflaki et al., 2014). The guinea pig action potential is more representative of the human action potential, therefore the use of the whole heart guinea pig model will allow for more representative data with consideration of factors such as electrical coupling and spatial heterogeneities due to non-uniform ion channel dispersion. The chosen Langendorff preparation also means there will be no interference from haemodynamic reflexes and humoral factors (Ng et al., 2007) as seen in other *in vivo* models.

## **8.3 Aims and hypothesis**

### **8.3.1 Aims**

To investigate the role of Epac in cardiac arrhythmia in guinea pig hearts.

### **8.3.2 Hypothesis**

Epac activation will cause spontaneous calcium transients resulting in ventricular arrhythmogenesis

## **8.4 Methods**

### **8.4.1 Animal model**

Adult male Dunkin Hartley guinea pigs (n=14, 400-850g) were used for Langendorff whole heart perfusion and Ca<sup>2+</sup> imaging. The guinea pig model was chosen as they have an action potential more physiologically similar to humans than rats and mice used in most of the previous Epac studies. Data is also shown for Ca<sup>2+</sup> imaging in rats due to the availability of the rat cardiomyocytes during learning of the technique and for comparison with previous research. All procedures conformed to the ethical guidelines in the Animal Scientific Procedure Act 1986 (ASPA), in accordance with Guide for the Care and Use of Laboratory Animals published by the US National Institute of Health (NIH Publication No. 85-23, revised 1985), and followed the criteria of the EU legislation on the protection of animals used for scientific purposes (Directive 2010/63/EU, 2010).

### **8.4.2 Langendorff whole heart perfusion**

#### ***Isolation of the whole heart***

This preparation has been described previously by Melgari et al (2015). In brief, Guinea pigs were culled by cervical dislocation. Confirmation of death was established by respiratory arrest and absence of the pedal or corneal reflex. To isolate the heart, a bilateral thoracotomy was performed followed by anterior ribcage resection, allowing for clear access to the heart and excision from surrounding tissues. The isolated heart was immediately immersed in cold Tyrode solution with 1000 IU of Heparin to reduce metabolic activity and prevent thrombosis formation.

#### ***Langendorff perfusion***

Once the ascending aorta was identified, it was cannulated and the heart was perfused with Tyrode solution (37°C, pH of 7.4 maintained by bubbling with 95% O<sub>2</sub>/5% CO<sub>2</sub>) consisting of Na<sup>+</sup> 138.0, K<sup>+</sup> 4.0, Ca<sup>2+</sup> 1.8, Mg<sup>2+</sup> 1.0, HCO<sub>3</sub><sup>-</sup> 24, H<sub>2</sub>PO<sub>4</sub><sup>-</sup> 0.4, Cl<sup>-</sup> 124, Glucose 11 (mM) at a flow rate of 20ml/min via a Gilson minipulse 3 peristaltic pump (Anachem, Luton, UK). This allowed for retrograde perfusion,

forcing the aortic valve shut and Tyrode solution into the coronary arteries. The Thebesian venous effluent was drained via the left ventricle using a 1-2mm width catheter.

### **8.4.3 Haemodynamics**

Certain functional parameters of the heart were assessed in order to monitor the health of the heart. Two pressure transducers (MLT0380/D ADInstruments Ltd, Chalgrove, UK) were removed of all air bubbles and calibrated using a sphygmomanometer at the start of each experiment. One transducer was used to measure the perfusion pressure (PP) and the other was attached to a fluid filled latex balloon inserted through the left atrium into the ventricle to measure the left ventricular pressure (LVP). The balloon was inflated with distilled water to reach an end diastolic pressure of 0-5mmHg. Heart rate was calculated using cyclic measurements from the LVP. Hook electrodes are attached to the right atria in order to measure the atrial electrogram. The final Langendorff perfusion set up is displayed in fig 8.12.

### **8.4.4 Cardiac electrophysiology and pacing**

#### ***Ventricular pacing***

A pacing catheter (ADInstruments Ltd, Chalgrove, UK) was inserted into the right ventricle (fig 8.12) which delivers a current to the heart at double the current of the diastolic pacing threshold (to ensure capture of ventricles) using a constant current stimulator. The pacing protocols used included constant pacing where the heart is paced at a steady state at cycle lengths of 200 ms, 250 ms and 300 ms. Standard restitution and dynamic restitution pacing protocols were used as they serve as an important predictor of arrhythmogenesis.

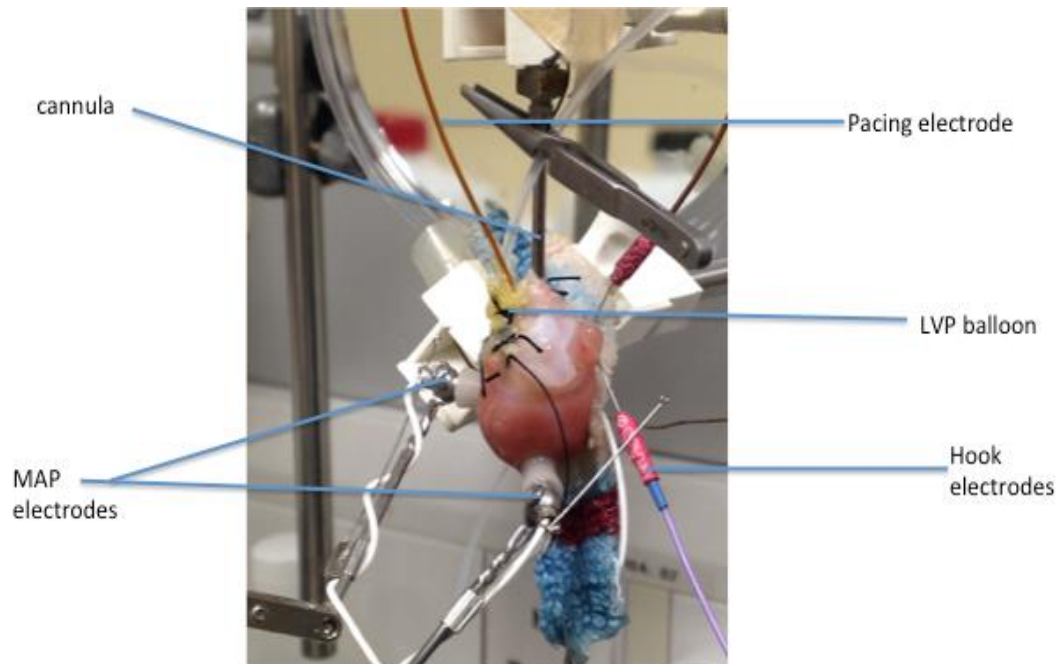


**Figure 8.12. Langendorff whole heart perfusion preparation for guinea pig heart.** Tyrode solution is perfused via the cannula at 20ml/min. The pacing electrode is inserted into the right ventricle and allows pacing of the heart via a current stimulator. The LVP balloon is inserted into the left ventricle and gives a measure of the LVP and also a calculation of heart rate. The hook electrodes record an atrial electrogram from the right atria. The MAP electrodes allow recordings of MAPs from the left ventricular epicardial surface at basal and apical sites.

### ***Monophasic action potentials***

Monophasic action potentials (MAPs) are representative of the repolarization time course of transmembrane action potentials (Franz, 1999). They were recorded extracellularly from the left ventricular epicardial surface of the heart at the base and apex, by pressing two MAP electrodes (Harvard Apparatus Ltd, Holliston, Massachusetts, US. Model number 73-0150) gently on the surface. The myocardium cells directly below the electrode become depolarised to -30 to -20mV due to the pressure exerted. These cells are unexcitable due to inactivated  $\text{Na}^+$  channels, whereas the surrounding cells activate as normal. This gives rise to a time-varying electrical gradient allowing current flow between the unexcitable and excitable cells (Franz, 1999) as shown in fig 8.13.

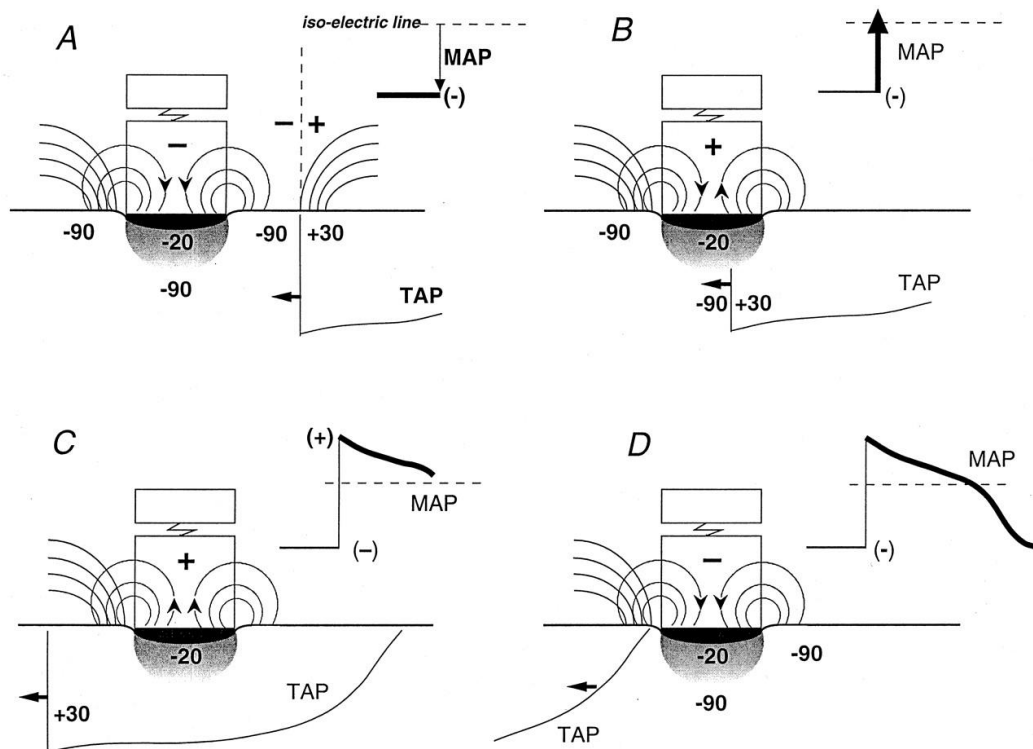


**Figure 8.13. Diagram illustrating the generation of MAP recordings by contact electrodes.** (A) Electrical diastole (late). Cells beneath the electrode are depolarised (-20mV) and unexcitable due to the pressure it exerts. Surrounding cells have a potential of -90mV and so current flows from these cells to the depolarised cells. This forms the base of the MAP recording. (B) Electrical systole (early). An action potential arrives carrying a potential of +30mV. There is a change in current flow and the MAP upstroke is recorded. (C) Electrical systole (mid). There is a gradual repolarisation and the plateau phase is observed on the MAP recording. (D) Electrical diastole (end). Potentials become repolarised, returning to their pre-existing states and the cycle is complete. A completed MAP recording is observed (Franz, 1999).

### ***Restitution protocol***

The restitution (RT) protocol used consisted of pacing at a cycle length (CL) of 250 ms for 25 S1 drive train beats, followed by a single extra stimulus (S2). S2 had an initial CL of 250 ms which was decreased in increments of 3 ms until the effective refractory period (ERP) was reached (fig 8.14). The ERP is defined as the longest S1-S2 interval that fails to capture the S2 beat.

These measurements allow construction of action potential duration (APD) restitution curves allowing arrhythmia susceptibility to be measured from the slope of the curve. This was produced by plotting S2 MAPD<sub>90</sub> vs. DI. APD was identified from time of activation ( $T_{act}$ ) to 90% of repolarisation (MAPD<sub>90</sub>) using the programme NewMap (Francis Burton, Glasgow University, UK). Using Microcal Origin (v 6.0, Origin, San Diego, CA, US), an exponential curve was formulated using the following function:  $MAPD_{90} = \text{maximum } MAPD_{90}[1 - e^{-DI/\tau}]$  where  $\tau$ =time constant and the maximum slope of the curve ( $RT_{maxSlope}$ ) was acquired by measuring the first derivative.

### ***Dynamic pacing protocol***

The susceptibility of the heart to repolarization alternans and VF inducibility was explored using the dynamic pacing protocol, a second method to measure APD RT whereby a drive train of 100 pulses with an initial CL of 250ms was applied to the heart (figure 16). The CL was decreased in increments of 10ms until VF was induced. VF was stabilized by perfusing the heart with small volumes (2-5ml) of potassium chloride (KCl).

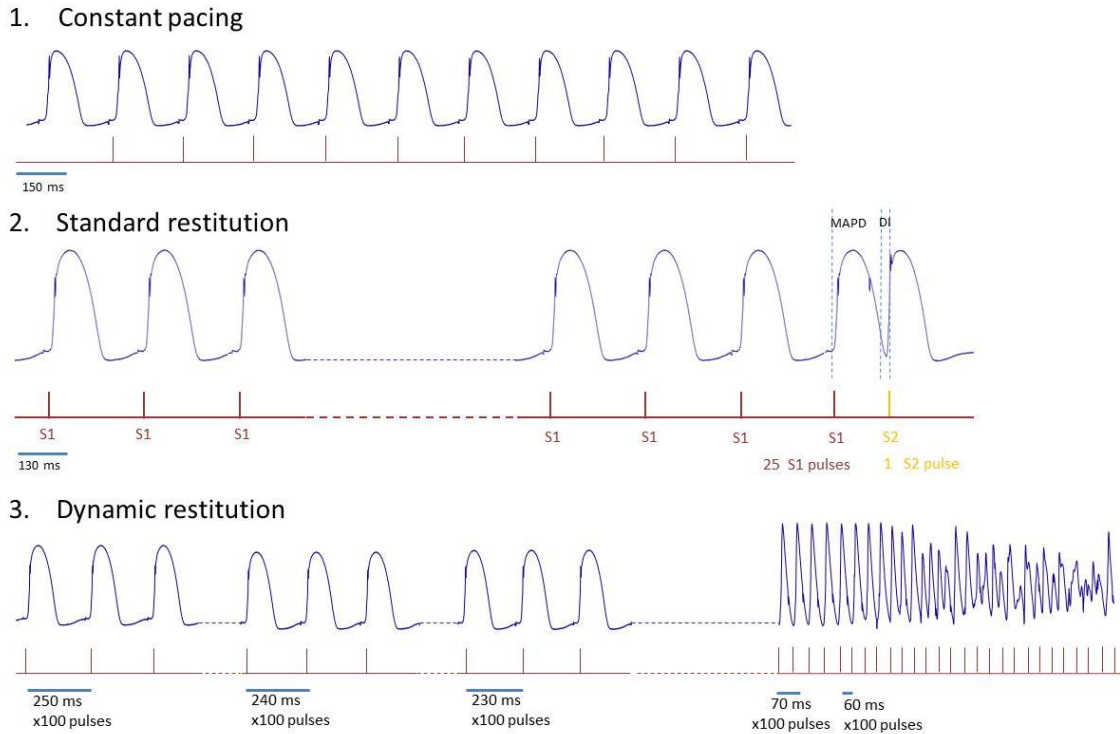


**Figure 8.14. Pacing protocols.** (a) Constant pacing protocol. Involves pacing the heart at a steady state at cycle lengths of 200 ms, 250 ms and 300 ms. (b) Electrical restitution protocol. The heart is paced at 250 ms for 25 pulses (S1). Following this an extrastimulus is applied (S2). The S1-S2 interval initially has a 250 ms cycle length and then this is decreased in 3ms increments until ERP is reached. (c) Dynamic pacing protocol. Involves pacing the heart with 100 pulses at 250 ms cycle length initially. This then decreased in 10ms increments until VF is induced.

#### 8.4.5 Effects of 8-CPT on cardiac function

The Epac activator 8-pCPT-2'-O-Me-cAMP (8-CPT) was perfused through the heart in order to activate the Epac protein. The parameters mentioned above were recorded and the pacing protocols applied at two concentrations of 8-CPT. Initially a 1 $\mu$ M 8-CPT concentration was used in accordance with the mouse whole heart paper (Hothi et al., 2008). This was later increased to 10 $\mu$ M 8-CPT as used by many other Epac studies including Pereira et al (2007) and Oestreich et al (2007) when no significant response with 1 $\mu$ M 8-CPT was observed.

#### **8.4.6 Effects of positive control isoproterenol on cardiac function**

A positive control of isoproterenol (ISO) was used for comparison with results with 8-CPT. Epac has been found to mimic the effects of ISO (Aflaki et al., 2014).

#### **8.4.7 Data recording and statistical analysis**

The Powerlab 16/30 system (AD Instruments Ltd, Chalgrove, UK) was used to record the signals, which were processed at 2 kHz. Paired t-tests were conducted and statistical significance was taken at 5% level ( $p < 0.05$ ).

#### **8.4.8 Calcium Imaging**

##### ***Ventricular myocyte isolation***

The isolation of the whole heart was conducted as mentioned above. After isolation, hearts were immediately immersed in cold  $\text{Ca}^{2+}$ -free Tyrode solution consisting of NaCl 135 mM, KCl 4 mM, Glucose 10 mM, HEPES 10 mM,  $\text{Na}^+$  Pyruvate 5 mM,  $\text{NaH}_2\text{PO}_4$  0.33 mM and MgCl 1 mM. After identifying the aorta it was cannulated and perfused at 12ml/min with  $\text{Ca}^{2+}$ -free Tyrode. The heart was perfused in a retrograde manner, forcing the aortic valve shut and solution into the coronary arteries. This was continued for 4-6 minutes whilst excess tissue surrounding the heart was removed. This was followed by 8-11 minutes perfusion of enzyme solution containing 0.56mg/ml Protease Type XIV, 1.04mg/ml Collagenase Type I and 1.67mg/ml BSA. The atria were then removed and the heart was cut down, dissected into smaller pieces and placed in ~10ml 2mM  $\text{Ca}^{2+}$  Tyrode made up of the same components as the  $\text{Ca}^{2+}$ -free Tyrode with the addition of CaCl 2mM. Gentle shaking of the heart at 35°C at a speed of 15rpm released single myocytes from the tissue. Periodically, the cell suspension is separated from the tissue and more 2mM  $\text{Ca}^{2+}$  Tyrode is added to the tissue and returned to shaking. This was repeated until the cardiac tissue fully dissociated or until there was a decrease in healthy myocytes. A 200 $\mu\text{m}^2$  pore stainless steel sieve was used to sieve the cell suspensions and they were left to sediment. Once a pellet has formed, the supernatant is discarded and the pellet is

resuspended in 2mM Ca<sup>2+</sup> Tyrode. This is repeated for a second time and the final cell suspension is transferred to a petri dish. All solutions were bubbled with oxygen during isolation.

### ***Loading Myocytes with Fura-2***

25µl of 5% Pluronic acid in DMSO was added to 5µg of the Ca<sup>2+</sup> sensitive dye Fura-2 to produce a 2mM stock which was stored at -20°C and concealed from light. 5µl of Fura-2 stock solution was added to 2ml of the myocyte cell suspension. This was left for 20 minutes to load and kept unexposed to light. The Fura-2 acetoxymethyl (AM) ester form of the dye that is initially loaded on to the cells is membrane permeable but Ca<sup>2+</sup> insensitive. Esterases cleave the AM groups once the dye is inside the cell, trapping the Fura-2 within the cell. This cleaved form of the dye is able to bind to Ca<sup>2+</sup> (Hirst et al., 2006). Following this, the cells were washed with 2mM Ca<sup>2+</sup> Tyrode to remove free Fura-2AM-ester and after a five minute period were washed again in the same way.

### ***Measurement of intracellular Ca<sup>2+</sup>***

Fura-2 is a ratiometric dye and upon binding of Ca<sup>2+</sup> there is a shift in the excitation spectrum. At 340nm, excitation of Fura-2 causes an increase in fluorescence whereas at 380nm there is a decrease. During recordings, dual excitation of Fura-2 at 340/380nm was used whilst monitoring at 510nm. At a wavelength of 340nm, maximum Fura-2 fluorescence is observed in the presence of Ca<sup>2+</sup> whereas this occurs at 380nm in Ca<sup>2+</sup> free conditions. This allows for an intracellular Ca<sup>2+</sup> ratio to be measured. These recordings were taken from within a light protective chamber. A PTI bryte box acquisition system collected the fluorescence recordings at a rate of 60Hz. These were calibrated using PTI Felix 32 software using the following equation where K<sub>d</sub>=285mM, R<sub>min</sub>=0.4, R<sub>max</sub>=4.96, F<sub>380max</sub>/F<sub>380min</sub>=6.39 and R=uncalibrated Fura-2 ratio:

$$[Ca^{2+}] = K_d \left( \frac{R - R_{min}}{R_{max} - R} \right) \times \left( \frac{F_{380max}}{F_{380min}} \right)$$

The values used were produced for the rat model however, as there is no evidence to suggest they should be different for the guinea pig model, the same values were used for both species.

Tyrode solution was perfused at a rate of 2-4ml/min via a peristaltic pump into the superfusion chamber which was maintained at  $35 \pm 2^\circ\text{C}$  (Warner Instruments Single Inline Solution Heater SH-27B) for a period of ~5 minutes. A small amount of the Fura-2 loaded cells were pipetted into the superfusion chamber on the microscope stage (Nikon diaphot) and left to settle to the bottom of the chamber for 5 minutes with the perfusion turned off. Tyrode perfusion was continued for 5 minutes allowing cells to reach a steady state. Cells were field stimulated at a rate of 1Hz during this time using two platinum stimulation electrodes connected to a Harvard research stimulator. After a contracting cell was selected, recordings were taken for no more than 30 seconds to avoid photobleaching.

Approximately 6-8 electrically evoked  $\text{Ca}^{2+}$  transients were recorded before the recording was paused. The drug solution was then perfused for a period of 5 minutes into the superfusion chamber before the recording was restarted and recordings were taken in the same manner as before (fig 8.15a).

To record caffeine evoked  $\text{Ca}^{2+}$  transients, 6-8 electrically evoked  $\text{Ca}^{2+}$  transients were recorded before the stimulator was turned off. 20mM Caffeine was then perfused into the superfusion chamber via a separate line to the Tyrode solution. Once a large peak of caffeine evoked transient is observed the caffeine perfusion is switched off. The stimulator is turned back on after this until electrically evoked transients return to their original state (fig 8.15b).

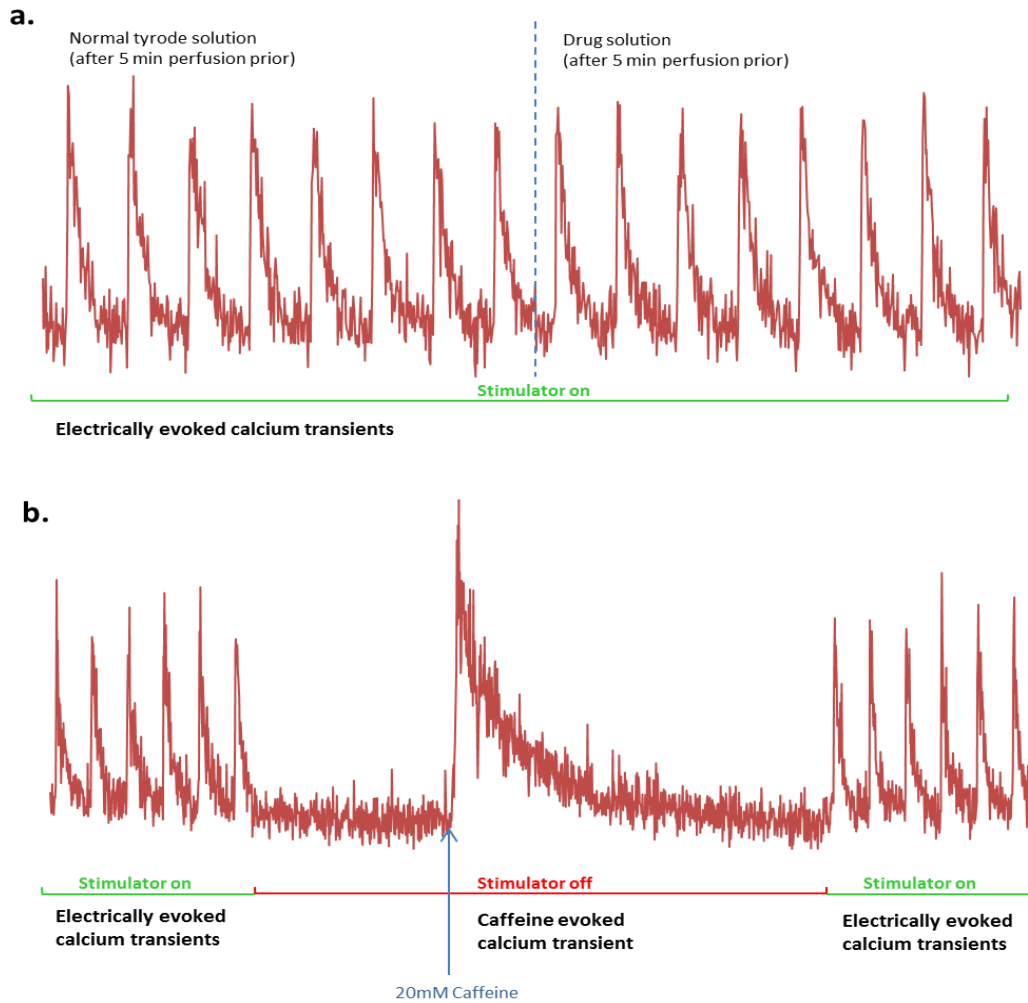


**Figure 8.15. Protocol for recording  $\text{Ca}^{2+}$  transients.** (a) Electrically evoked  $\text{Ca}^{2+}$  transients recorded with the stimulator on, after 5 mins of normal Tyrode perfusion. Dotted line represents pause of recording during 5 min drug perfusion before recording is restarted. (b) To record caffeine evoked  $\text{Ca}^{2+}$  transient, the stimulator is first turned on. The stimulator is then turned off and 20nM caffeine is applied. After the caffeine evoked  $\text{Ca}^{2+}$  transient ends the stimulator is turned back on.

### ***Analysis of $\text{Ca}^{2+}$ transients and statistical analysis***

Once calibrated, the electrically evoked  $\text{Ca}^{2+}$  transients are averaged in sets of three and measurements of systolic  $[\text{Ca}^{2+}]_i$  and diastolic  $[\text{Ca}^{2+}]_i$  were taken. To analyse caffeine evoked  $\text{Ca}^{2+}$  transients, the peak  $\text{Ca}^{2+}$  transient was measured which signifies the SR  $\text{Ca}^{2+}$  load (Bers, 2002). Statistical analysis was carried out using paired t-tests with statistical significance at a 5% level ( $p < 0.05$ ).

## 8.5 Results

### 8.5.1 The effect of Epac on whole heart physiology

#### *LVP, PP, MAP and HR*

Fig 8.16 displays the effects on left ventricular pressure (LVP), perfusion pressure (PP), monophasic action potentials (MAP) and heart rate (HR) with  $1\mu\text{M}$  and  $10\mu\text{M}$  8-CPT. No obvious changes in these parameters were observed with either concentration. There were no changes in LVP or heart rate.

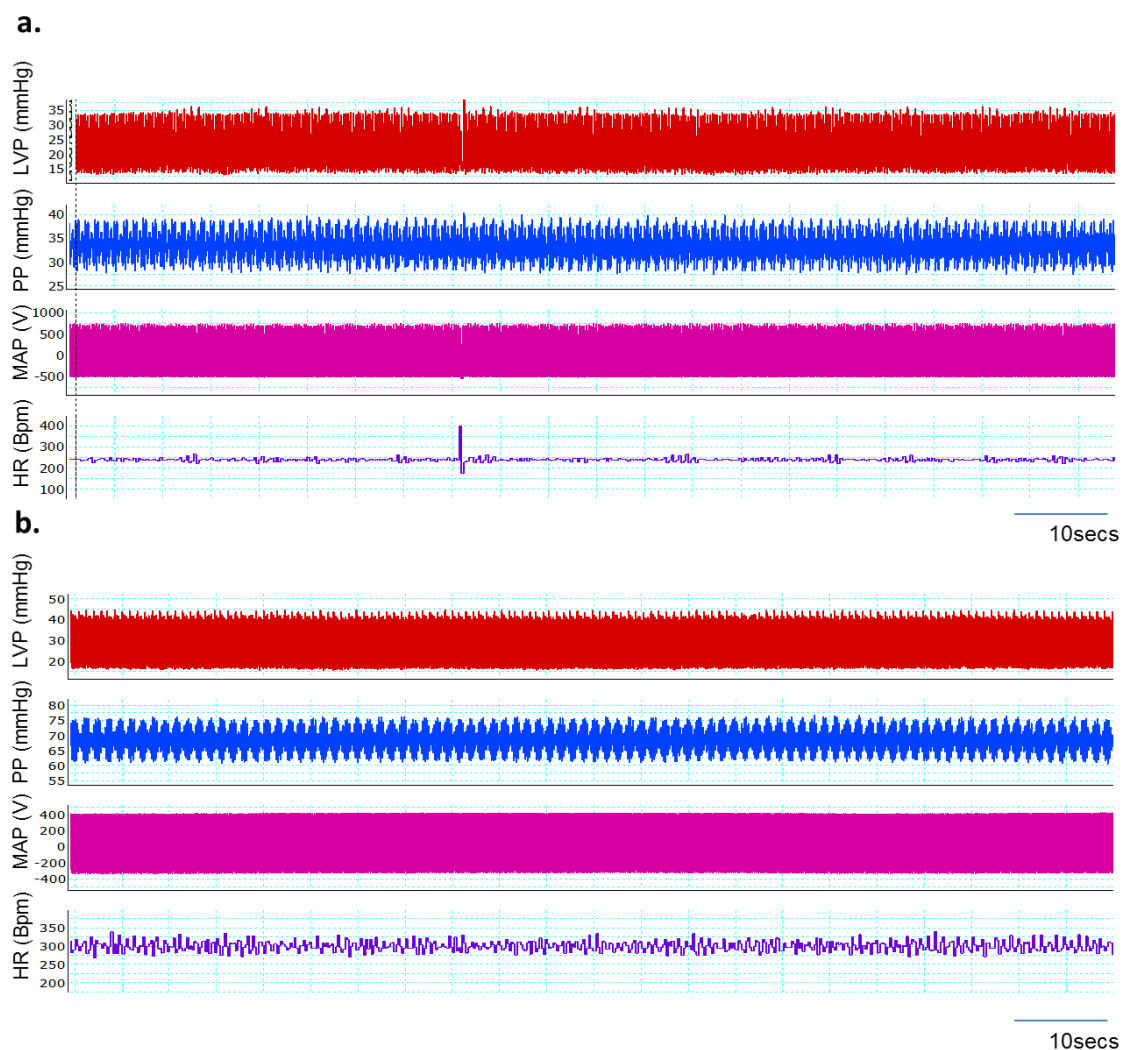


**Figure 8.16.** The effect 8-CPT on LVP, PP, MAPs and HR. Raw trace of left ventricular pressure (LVP), perfusion pressure (PP), basal monophasic action potentials (MAP) and heart rate during perfusion of  $1\mu\text{M}$  8-CPT (a) and  $10\mu\text{M}$  8-CPT (b).

### ***MAPD during constant pacing***

Mean data and representative figures for the effect of 1 $\mu$ M (n=5) and 10 $\mu$ M 8-CPT (n=4) are shown in figure 8.17 and 8.18 respectively. MAPD was measured at two time points; 50% repolarization of the monophasic action potential (MAPD<sub>50</sub>) and 90% repolarization of the action potential (MAPD<sub>90</sub>) as shown in the first basal and apical single trace MAPs of fig 19b & d and fig 12b & d. 30 MAPs were averaged from each of the cycle lengths of 200 ms, 250 ms and 300 ms. Although there appeared to be a trend for increase in MAPD with the Epac activator, mean data demonstrate that there was no significant difference in the MAPD from baseline with 1 $\mu$ M 8-CPT or with 10 $\mu$ M 8-CPT.

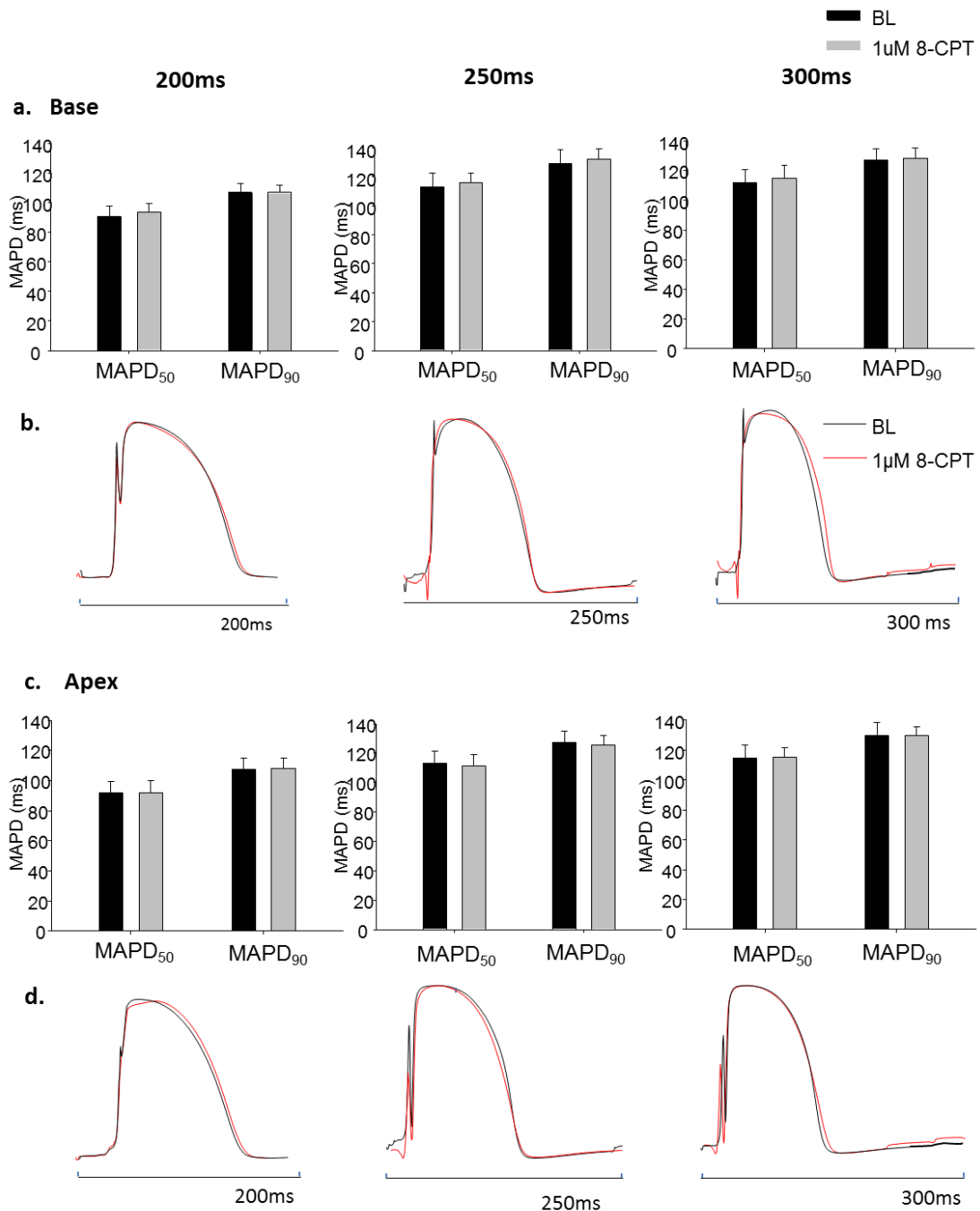


**Figure 8.17. Effect of 1 $\mu$ M 8-CPT on monophasic action potential duration (MAPD).** Mean data of MAPD<sub>50</sub> and MAPD<sub>90</sub> at the base (a) and apex (c) in baseline (BL) conditions and with 1 $\mu$ M 8-CPT during constant pacing at cycle lengths of 200ms, 250ms and 300ms. Raw data of the MAP's at the base (b) and apex (d) at cycle lengths of 200ms, 250ms and 300ms at BL and with 1 $\mu$ M 8-CPT also illustrated. P= ns between BL and 1 $\mu$ M 8-CPT for all conditions, n=5.

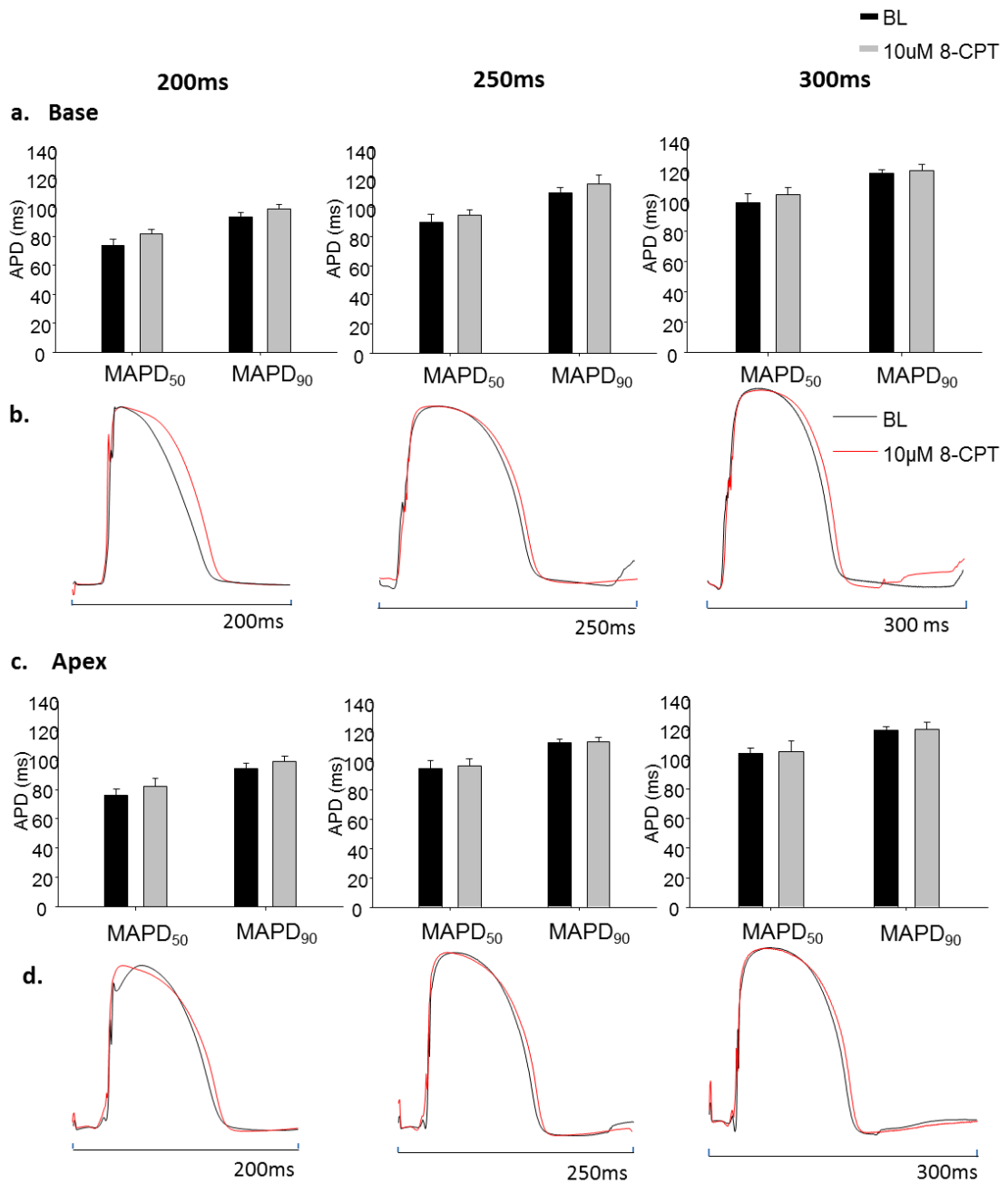


**Figure 8.18. Effect of 10uM 8-CPT on action potential duration (APD).** Mean MAPD<sub>50</sub> and MAPD<sub>90</sub> and SEM illustrated at the base (a) and apex (c) during constant pacing at 200ms, 250ms and 300ms at baseline (BL) and with 10uM 8-CPT. Corresponding raw data MAP's shown at the base (b) and apex (d). P=ns between BL and 10uM 8-CPT for all conditions, n=4.

## ERP

Fig 8.19 shows ERP data at 1 $\mu$ M 8-CPT and at 10 $\mu$ M 8-CPT. The figures also show there was no statistical difference with 1 $\mu$ M 8-CPT or 10 $\mu$ M 8-CPT in comparison to baseline.

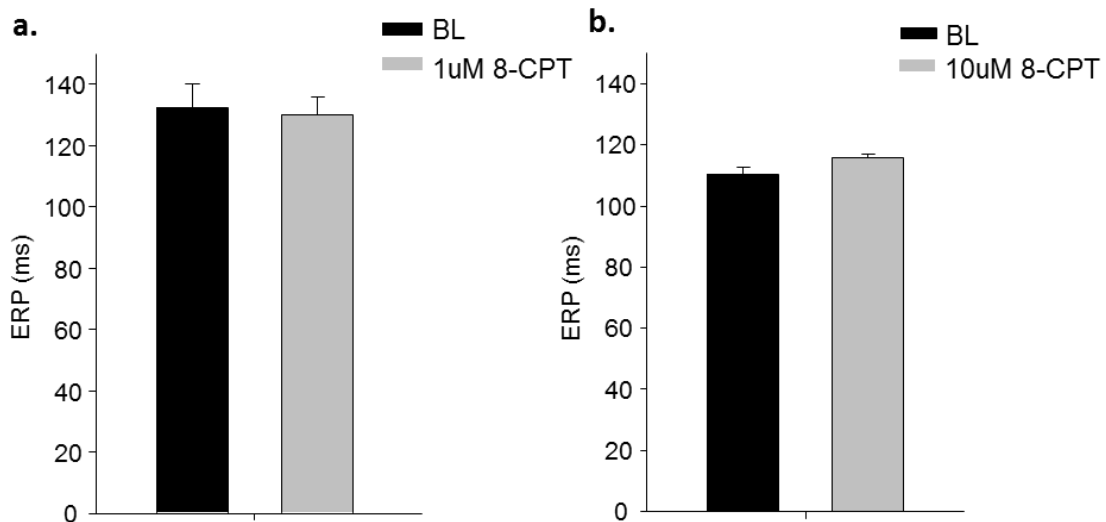


**Figure 8.19. Effect of 8-CPT on effective refractory period.** Effective refractory period (ERP) data at baseline (BL) and in the presence of 8-CPT at 1 $\mu$ M (a)  $n=5$ , and 10 $\mu$ M (b)  $n=4$ .  $P=ns$ .

## Standard restitution

Restitution (RT) curves were plotted from the data obtained from the standard restitution protocol. Fig 8.20 and 8.21 illustrate this data with 1 $\mu$ M 8-CPT ( $n=5$ ) and 10 $\mu$ M 8-CPT ( $n=4$ ) respectively. RT curves displaying both S1 and S2 data are shown in fig 8.20a & b and figure 8.21a & b. The curves in fig 8.20c and fig 8.21c show S2 data baseline and 1 $\mu$ M or 10 $\mu$ M 8-CPT respectively. The straight dotted line represents the maximum slope. Fig 8.20d and fig 8.21d show the maximum slopes of the RT curves ( $RT_{maxslope}$ ) generated by measuring the first derivative. There appeared to be a trend for increase in  $RT_{maxslope}$  with 1 $\mu$ M 8-CPT however t-tests showed no significant difference from baseline and this trend was not replicated with 10 $\mu$ M 8-CPT which also did not reach statistical significance.

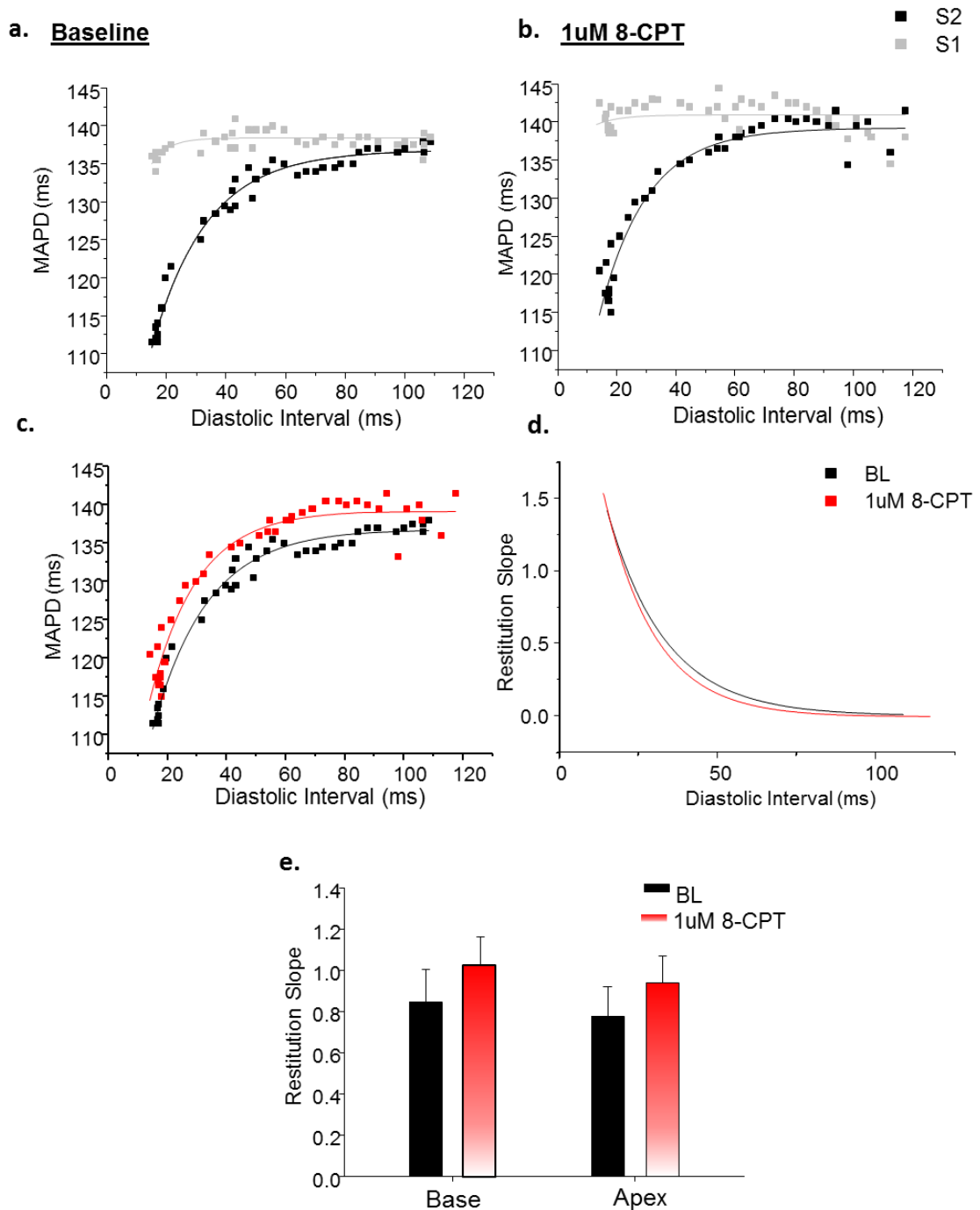


**Figure 8.20 Effect of 1uM 8-CPT on standard restitution curves. (a)** Baseline (BL) and (b) 1uM 8-CPT restitution curves illustrating data from both S1 and S2 MAP's. (c) Restitution curve showing BL and 1uM 8-CPT data with exponential curve fit ( $MAPD_{90} = \text{maximum } MAPD_{90} [1 - e^{-DI/\tau}]$ ). (d) Derivative of fitted curve for BL and 1uM 8-CPT restitution curves. (e) Mean of maximum restitution slope data and SEM at base and apex at BL and with 1uM 8-CPT (n=5), P=ns.

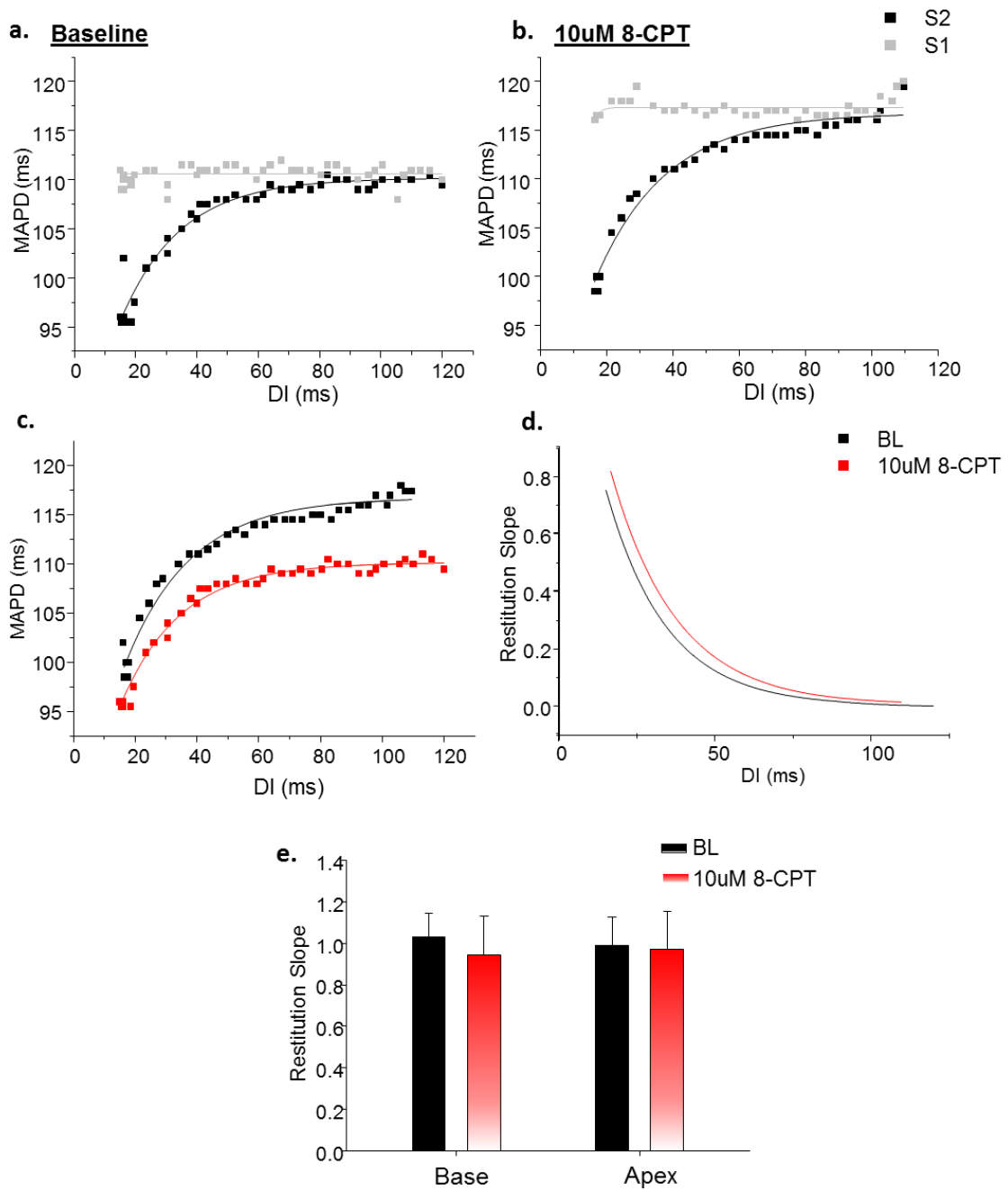


**Figure 8.21. Effect of 10µM 8-CPT on standard restitution curves.** (a) Baseline (BL) and (b) 10µM 8-CPT restitution curves. Both S1 and S2 data are illustrated. (c) Restitution curve showing BL and 10µM 8-CPT data with exponential curve fit ( $MAPD_{90} = \text{maximum } MAPD_{90} [1 - e^{-DI/\tau}]$ ). (d) Derivative of fitted curve for BL and 10µM 8-CPT restitution curves. (e) Mean of maximum restitution slope data and SEM at base and apex at BL and with 10µM 8-CPT (n=5), P = ns.

### ***Dynamic pacing and the effect of Epac activator 8-CPT***

The dynamic pacing protocol induced ventricular fibrillation (VF) in baseline conditions and in the presence of the Epac activator at short cycle lengths varying from 40-70 ms. The cycle length that induced VF at baseline was similar or the same as the cycle length that induced VF with 8-CPT as shown by fig 8.22a with 1 $\mu$ M 8-CPT (n=2) and figure 8.22b with 10 $\mu$ M 8-CPT (n=4) indicating no statistical difference. MAPD<sub>90</sub> was also plotted against DI (fig 8.23a and fig 8.24a) and against cycle length (fig 8.23b and fig 8.24b). For these curves, the last three MAPs of the 100 pulses at each cycle length were analysed. This would allow for detection of alternans which are beat to beat alterations in APD. However, no alternans were observed. The corresponding RT<sub>maxslope</sub> is plotted in fig 8.23c and fig 8.24c. Again this showed no significant difference with 1 $\mu$ M 8-CPT or with 10 $\mu$ M 8-CPT compared to baseline.

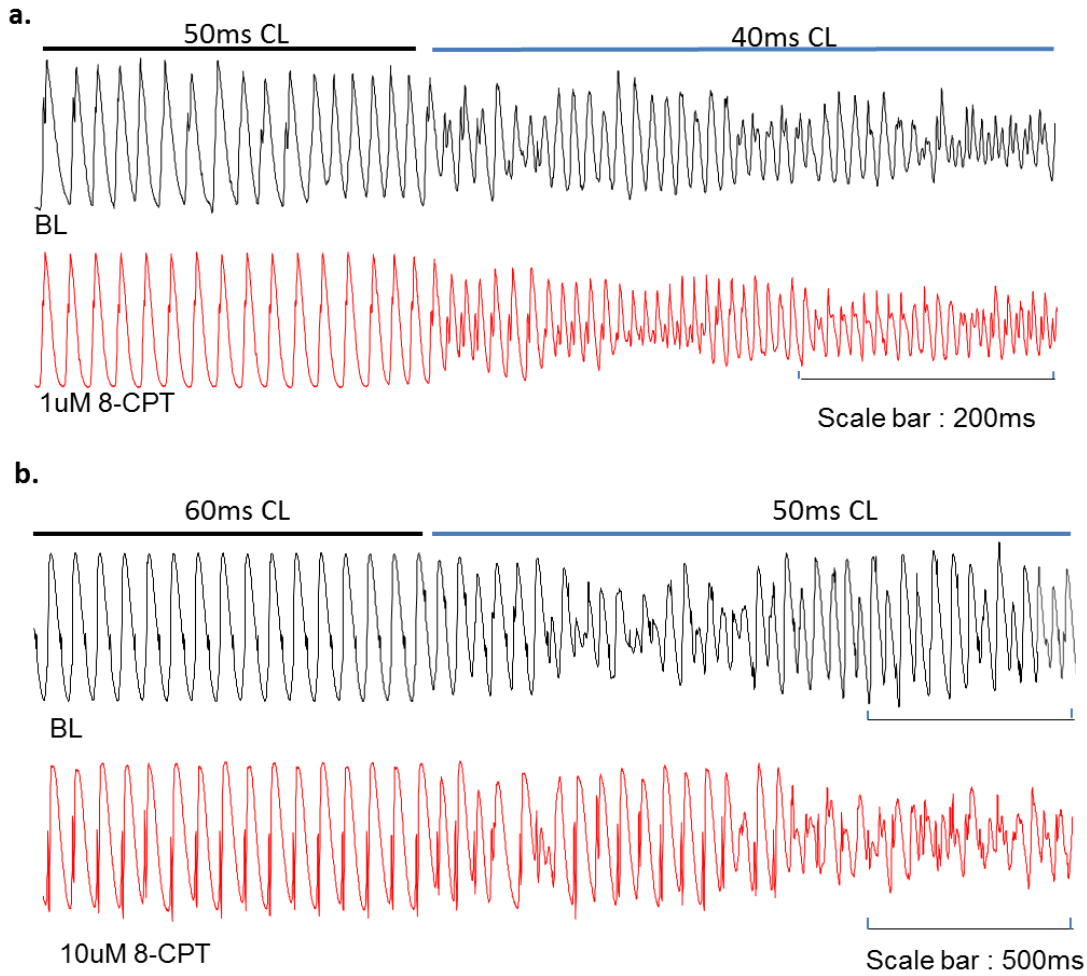


**Figure 8.22. VF induced by dynamic pacing protocol.** VF induced by dynamic pacing protocol at baseline (BL) and with 1 $\mu$ M 8-CPT and 10 $\mu$ M 8-CPT. VF was induced by the same cycle length at BL and with drug in these hearts.

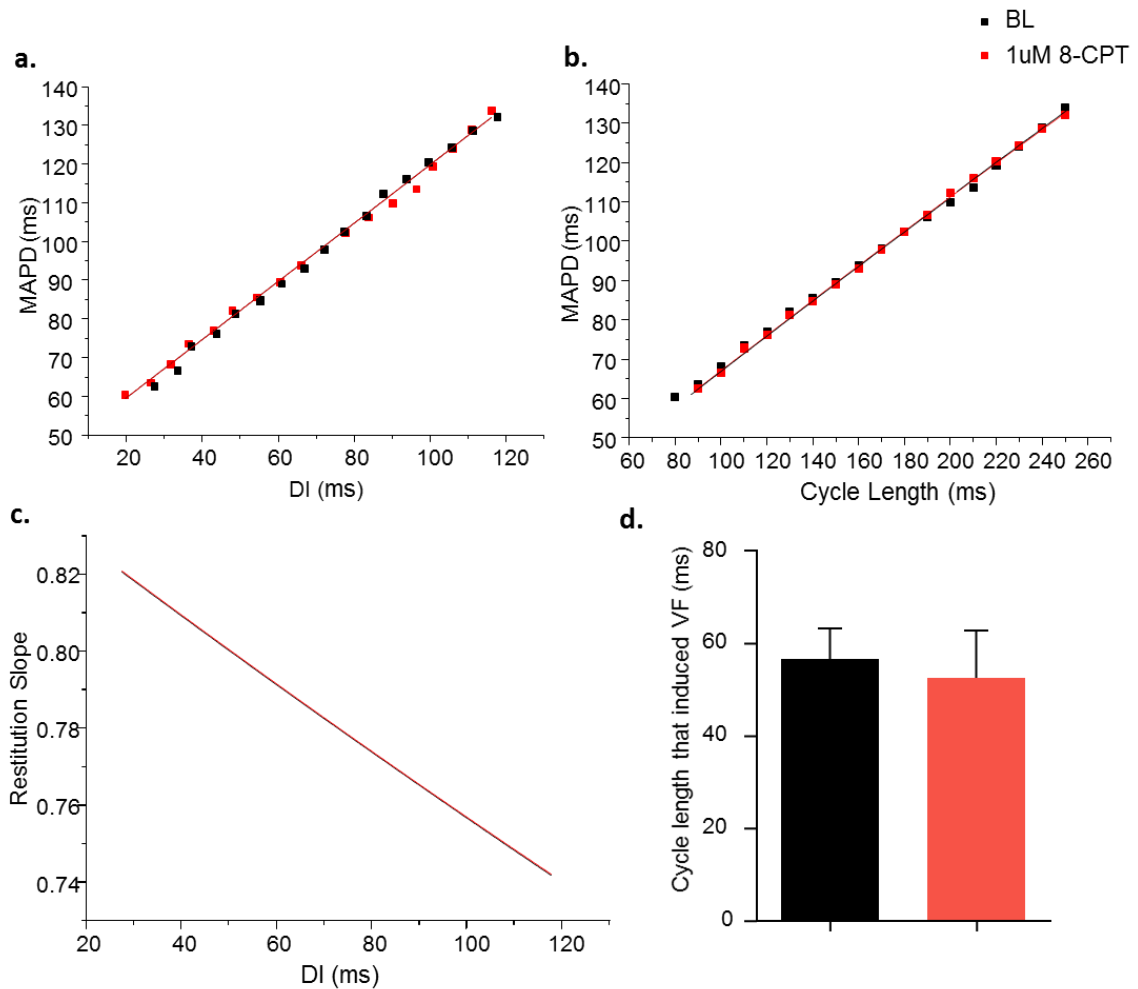


**Figure 8.23. Dynamic restitution data with 1 μM 8-CPT.** (a) Restitution curve of the dynamic restitution data at baseline (BL) and with 1 μM 8-CPT, with exponential fit  $MAPD_{90} = \text{maximum } MAPD_{90} [1 - e^{-DI/\tau}]$  (b) MAPD data at each cycle length during the dynamic pacing protocol. (c) Derivative of fitted curves for BL and 1 μM 8-CPT data. (d) Mean and SEM data illustrating the cycle length at which the dynamic pacing protocol induced VF at BL and with 1 μM 8-CPT (n=2). P = ns.

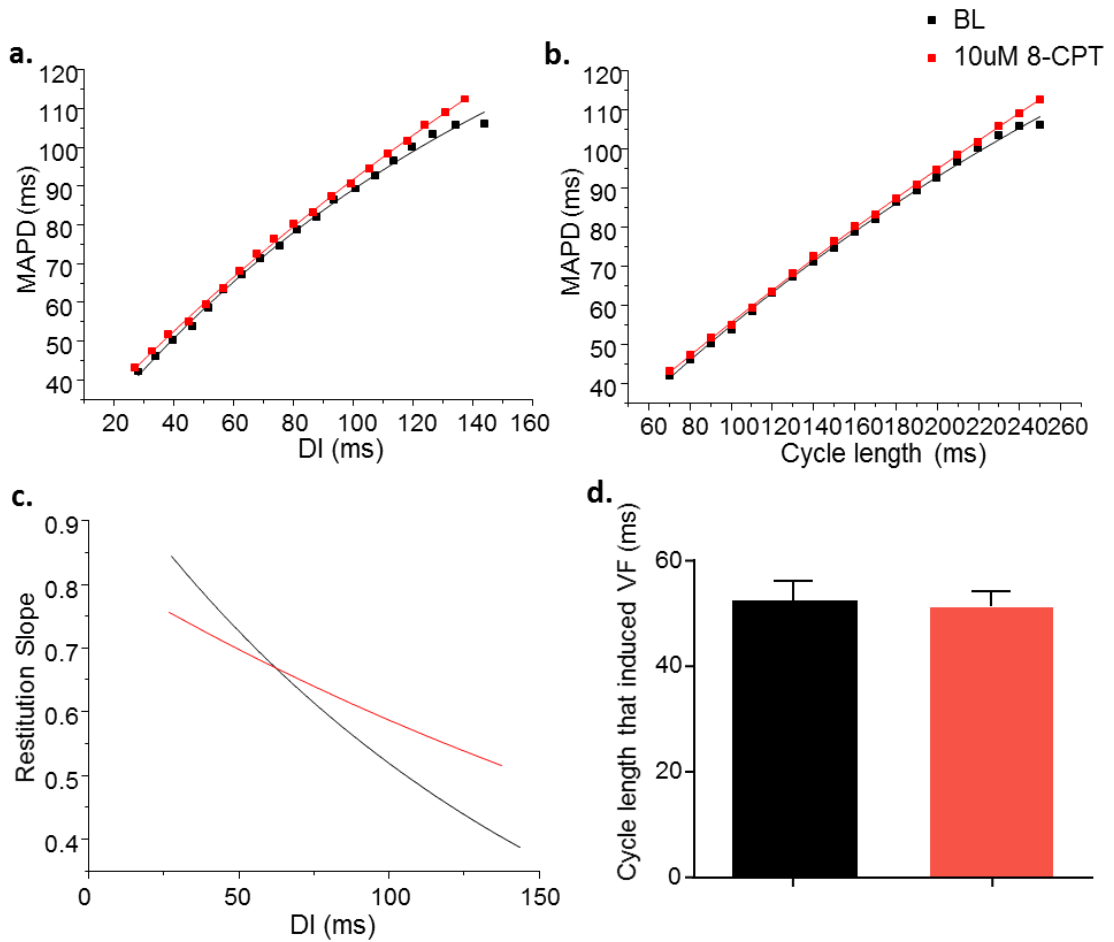


**Figure 8.24 . Dynamic restitution data with 10 μM 8-CPT.** (a) Restitution curve of the dynamic restitution data at baseline (BL) and with 10 μM 8-CPT. Curve fitted with exponential fit  $MAPD_{90} = \text{maximum } MAPD_{90} [1 - e^{-DI/\tau}]$  (b) MAPD data at each cycle length during the dynamic pacing protocol. (c) Derivative of fitted curves for BL and 10 μM 8-CPT data. (d) Mean and SEM data illustrating the cycle length at which the dynamic pacing protocol induced VF at BL and with 10 μM 8-CPT (n=4). P = ns.

### **8.5.2 The effect of positive control isoproterenol on whole heart physiology**

A positive control of 1nM isoproterenol (ISO) was applied to 2 hearts. ISO is a  $\beta$ -AR agonist that causes positive inotropy and chronotropy leading to increased predisposition to arrhythmias (Dodge et al., 1960). Upon perfusion of 1nM ISO, VF was induced after ~2.5 minutes. After a steady state was reached, the protocols were applied. It was difficult to generate data using the protocols as the intrinsic heart rate increased in the presence of 1nM ISO and the heart became difficult to pace, so only one successful run of the protocol was possible.

#### ***LVP, PP, MAP and HR with ISO***

Figure 8.25 illustrates the change in LVP, PP, MAPs and HR during perfusion of 2nM ISO. An obvious change in these parameters was observed, LVP increased, intrinsic heart rate increased and signals eventually deteriorated into VF. LVP increased from 61.74mmHg at baseline to 118.94mmHg with 1nM ISO.

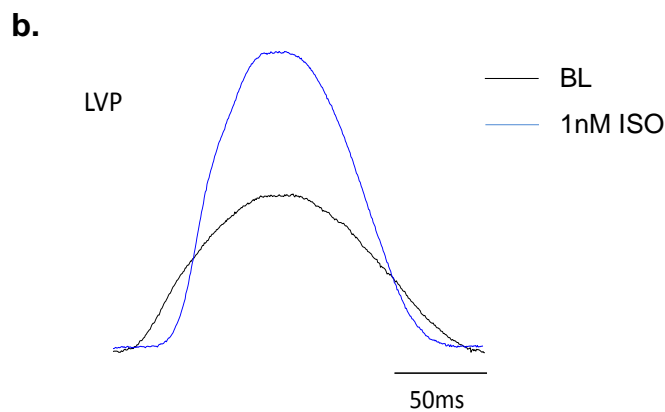
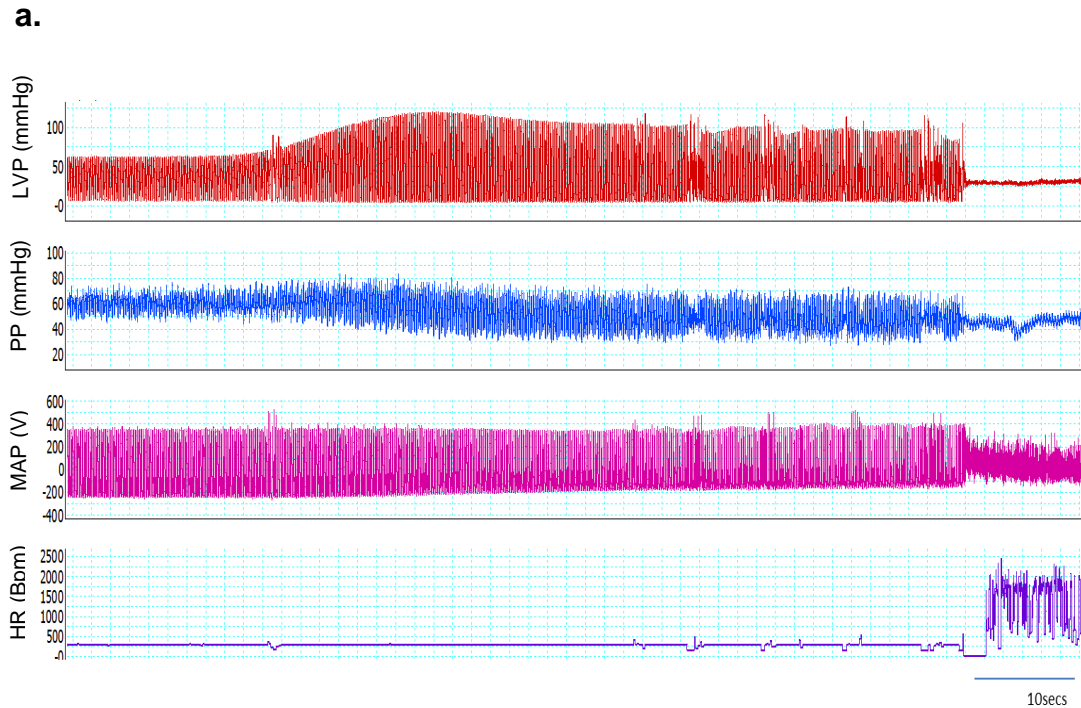


**Figure 8.25. The effect of 1nM ISO on LVP, PP, MAPs and HR.** (a) Raw data trace illustrating left ventricular pressure (LVP), perfusion pressure (PP), basal monophasic action potential duration (MAP) and heart rate during perfusion of 1nM isoproterenol (ISO) and during constant pacing. (b) Single raw data trace demonstrating changes in LVP during 1nM ISO perfusion.

### ***Effect of isoproterenol on MAPD during constant pacing***

MAPD<sub>50</sub> and MAPD<sub>90</sub> were measured at cycle lengths of 200 ms and 250 ms. 300 ms cycle length could not be recorded, as the heart could not be paced at this cycle length in the presence of 1nM ISO due to a high intrinsic heart rate. Figure 8.26 illustrates the effect of 1nM ISO on MAPD.

### ***Effect of isoproterenol on electrical restitution***

The ERP in baseline conditions was 110 ms and with 1nM ISO was 116 ms. Fig 8.27 displays the S1 and S2 RT data at BL and 1nM ISO. Fig 8.27c shows the S2 data for both conditions. The  $RT_{max}$ slope is illustrated in fig 8.27d with  $RT_{max}$  values of 1.29 for control and 2.07 with 1nM ISO.

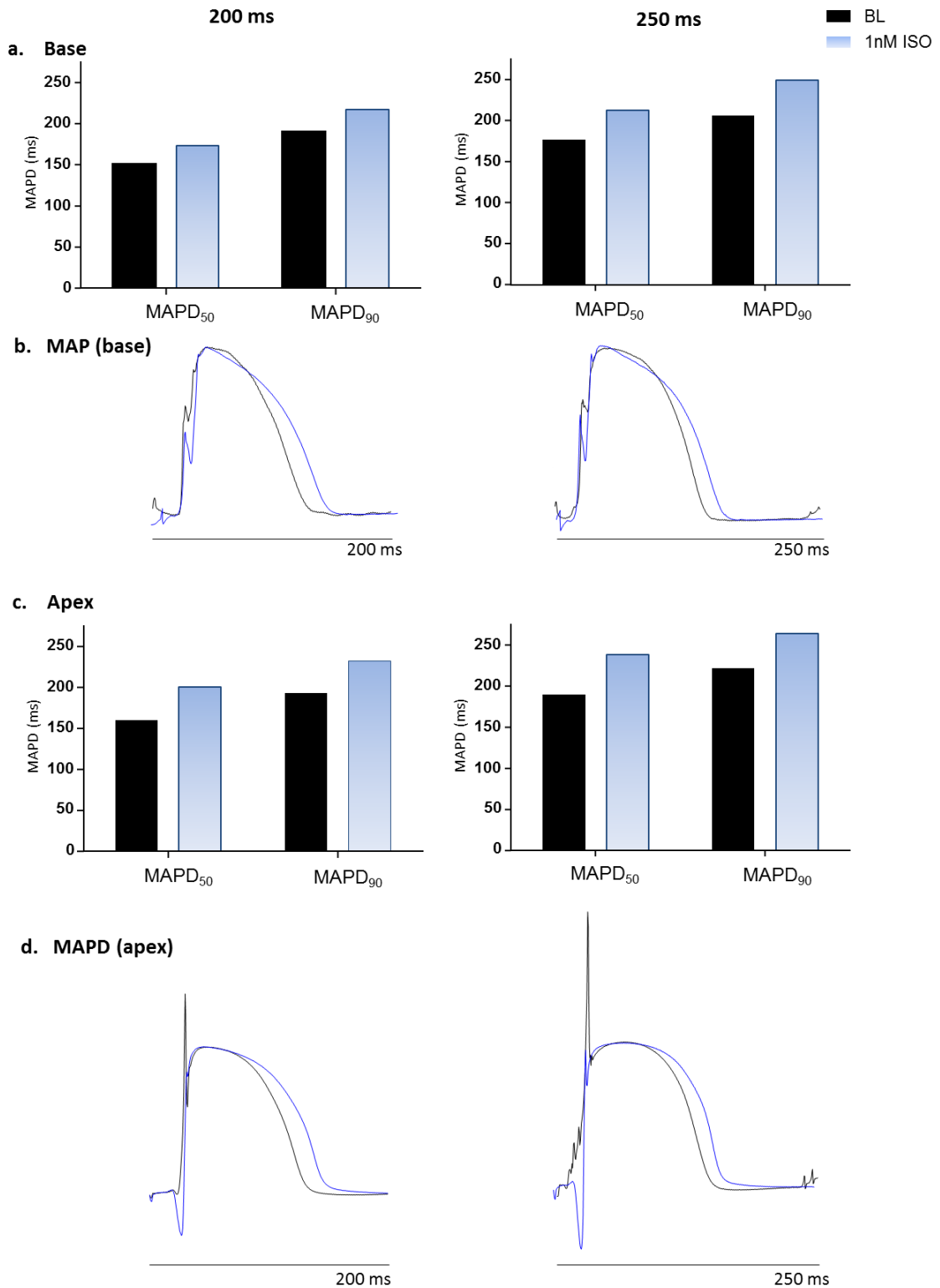


**Figure 8.26. Effect of 1nM ISO on monophasic action potential duration (MAPD).** Mean data of MAPD<sub>50</sub> and MAPD<sub>90</sub> at the base (a) and apex (c) at baseline (BL) and with 1nM ISO during constant pacing at cycle lengths of 200 ms and 250 ms. Raw data of the MAP's at the base (b) and apex (d) at cycle lengths of 200ms and 250 ms at BL and with 1nM ISO also illustrated. n=2.

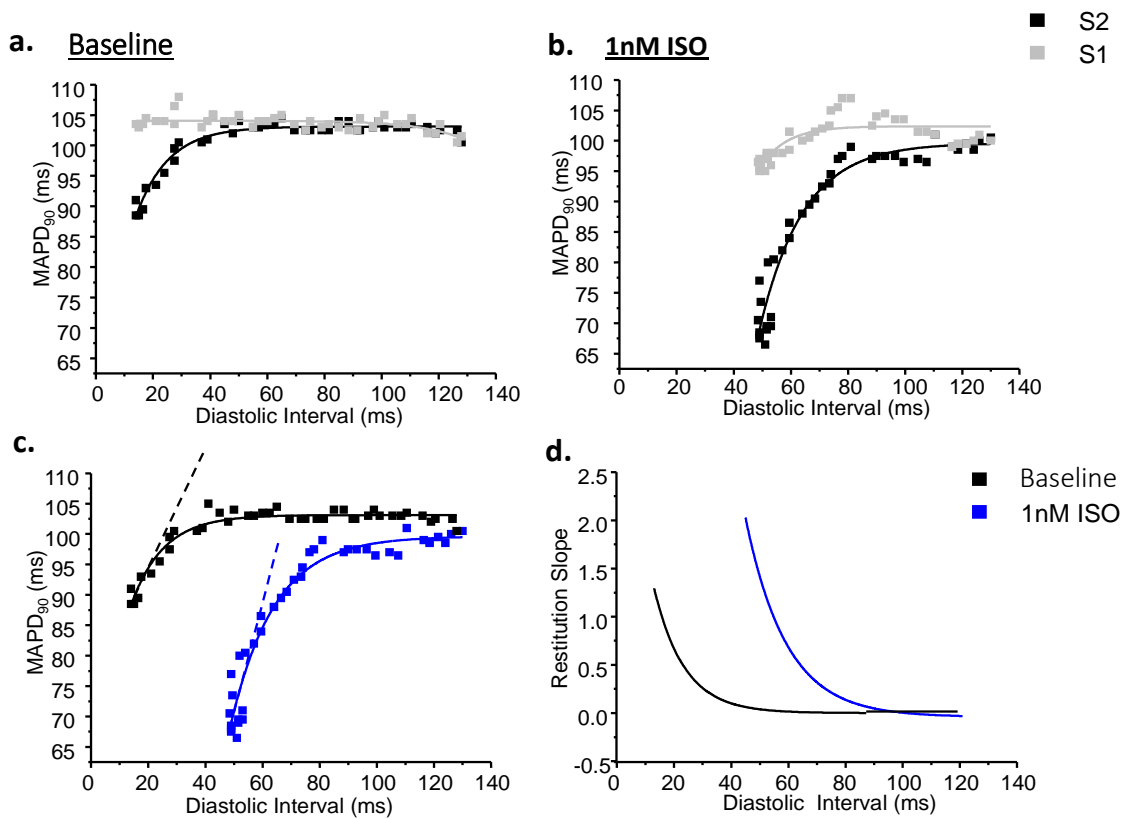


**Figure 8.27. Effect of 1nM Isoproterenol on standard restitution curves.** (a) Baseline (BL) and (b) 1nM isoproterenol restitution curves. Both S1 and S2 data are illustrated. (c) Restitution curve showing BL and 1nM isoproterenol data with exponential curve fit ( $MAPD_{90} = \text{maximum } MAPD_{90} [1 - e^{-DI/\tau}]$ ). (d) Derivative of fitted curve for BL and 1nM isoproterenol restitution curves. (e) Mean of maximum restitution slope data and SEM at base and apex in control conditions and with 1nM isoproterenol ( $n=1$ ).

### ***Dynamic pacing and the effect of isoproterenol***

MAPD<sub>90</sub> was plotted against DI (fig 8.28a) and cycle length (fig 8.28b) in baseline conditions and with 1nM ISO. The last 3 MAPs from the each cycle length were plotted so that alternans could be observed. RT<sub>maxslope</sub> curves were also plotted from this data (fig 8.28c). VF occurred at 60ms in baseline conditions and 40ms with 1nM ISO.

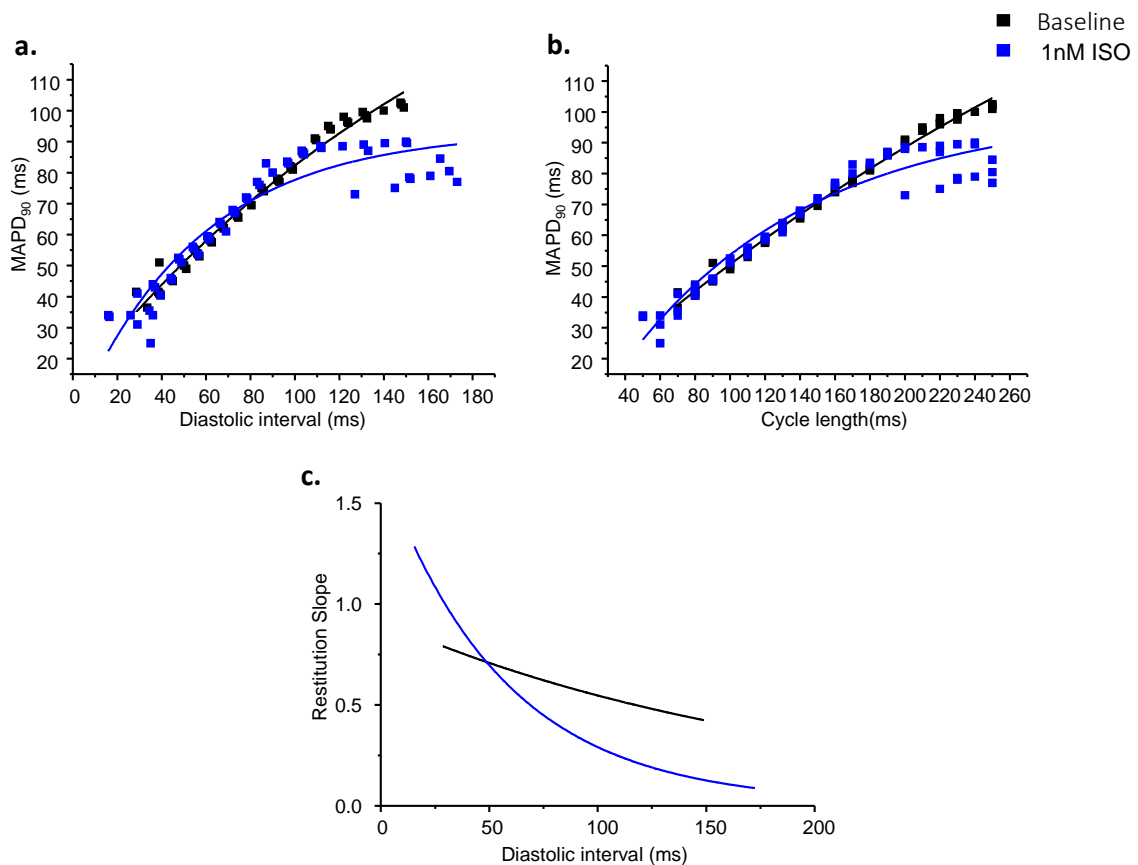


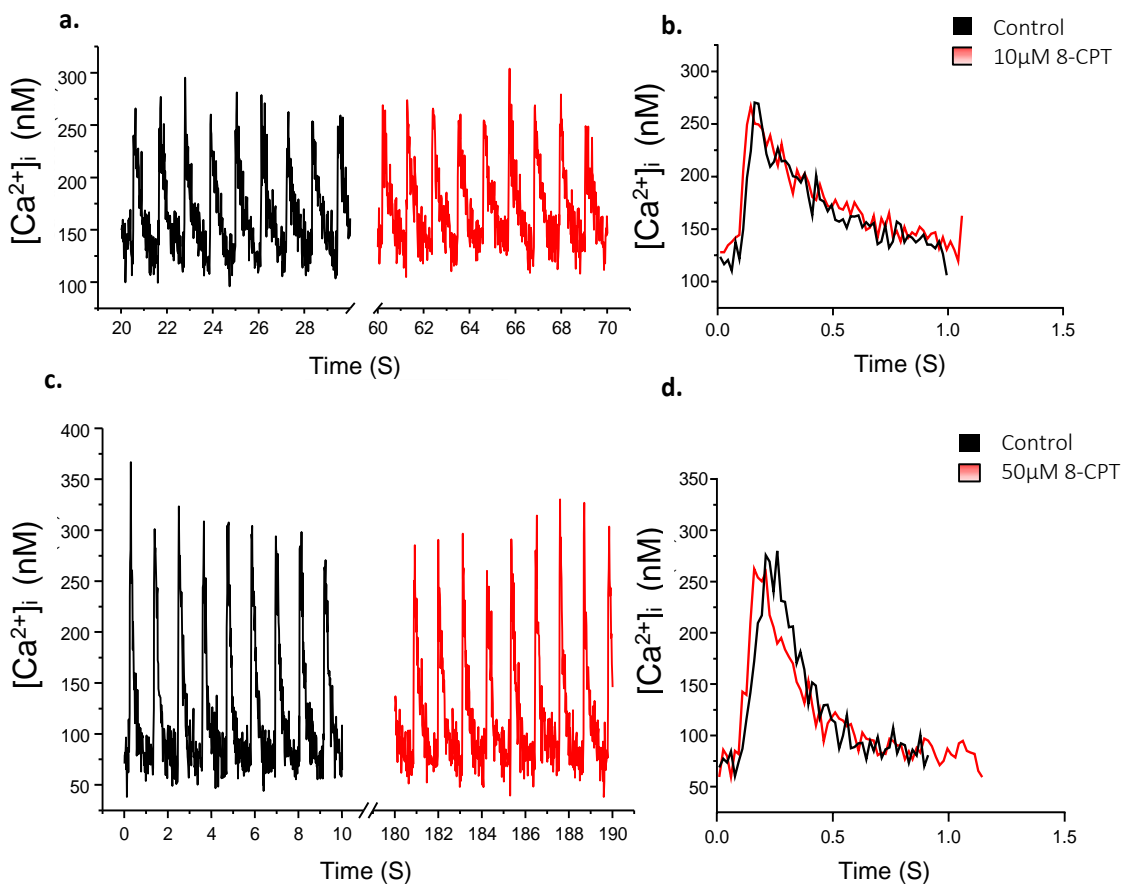
**Figure 8.28. Dynamic restitution data with 1nM isoproterenol (ISO).** (a) Restitution curve of the dynamic restitution data in control conditions and with 1nM ISO, with exponential fit  $MAPD_{90} = \text{maximum } MAPD_{90} [1 - e^{-DI/\tau}]$ . (b) MAPD data at each cycle length during the dynamic pacing protocol. (c) Derivative of fitted curves for control and 1nM ISO data. (d) Mean and SEM data illustrating the cycle length at which the dynamic pacing protocol induced VF in control conditions and with 1nM ISO (n=2).

### 8.5.3 The effect of Epac activator 8-CPT on cardiomyocyte Ca<sup>2+</sup> handling

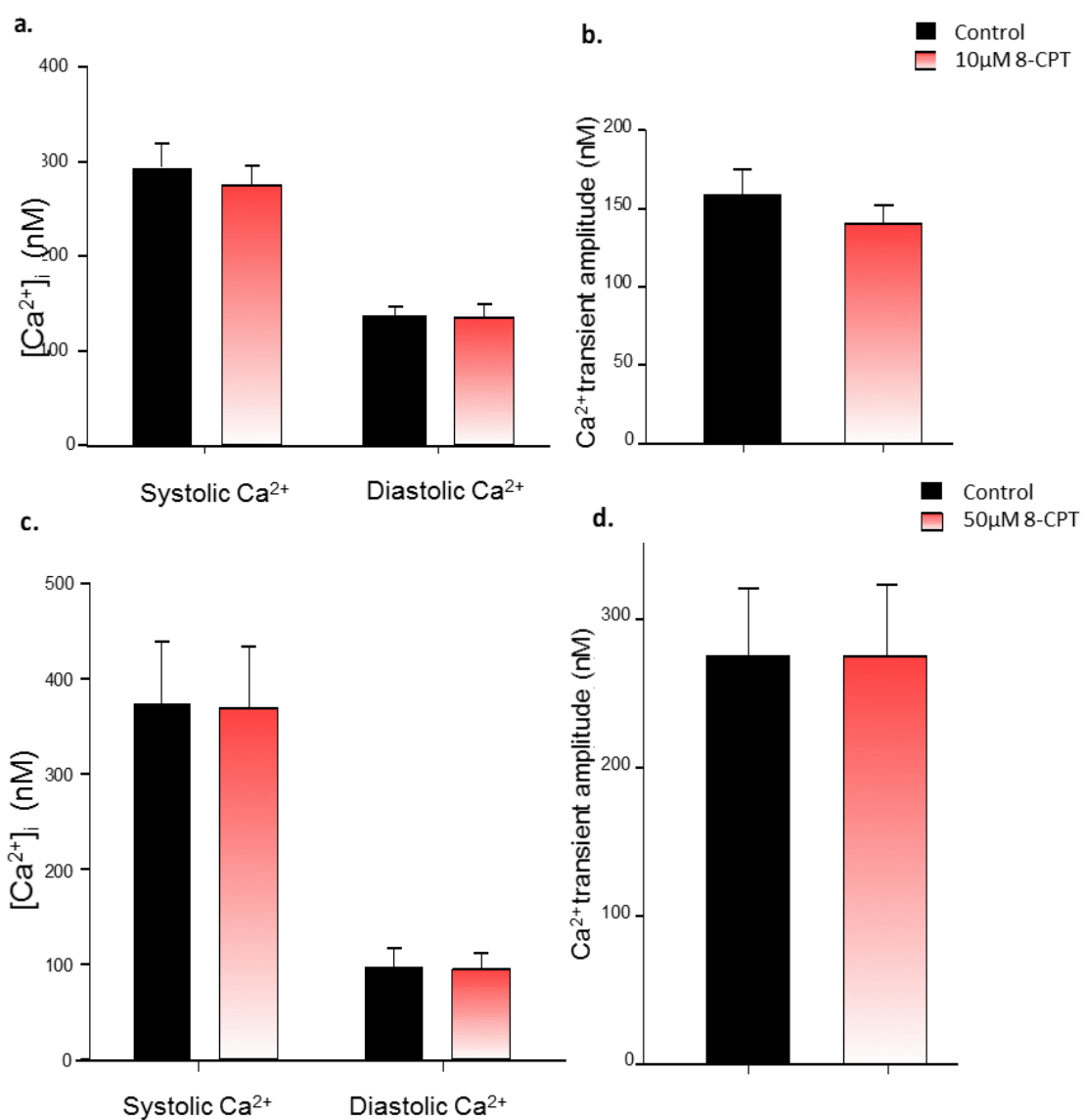
#### *The effect of Epac on electrically evoked Ca<sup>2+</sup> transients in rat cardiomyocytes*

Fig 8.29a displays the electrically evoked Ca<sup>2+</sup> transients rat cardiomyocytes, in baseline conditions and in the presence of 10 $\mu$ M 8-CPT. A trace showing a single averaged transient (5 transients averaged) is illustrated in fig 31b. Similarly, the same data is displayed in fig 8.29c & d with a 50 $\mu$ M 8-CPT concentration.

Data is represented as; n = n of hearts/ n of cells. Systolic and diastolic  $\text{Ca}^{2+}$  mean and SEM data are displayed in fig 8.30a & c for  $10\mu\text{M}$  8-CPT (n= 2 / 8) and  $50\mu\text{M}$  8-CPT respectively (n= 2 / 2). There was no significant difference between systolic or diastolic  $\text{Ca}^{2+}$  with  $10\mu\text{M}$  8-CPT) or with  $50\mu\text{M}$  8-CPT.



**Figure 8.29. Electrically evoked  $\text{Ca}^{2+}$  transient traces and the effect of Epac in rat cardiomyocytes.** Traces showing electrically evoked  $\text{Ca}^{2+}$  transients in (a) Control and with  $10\mu\text{M}$  8-CPT and (c) Control and  $50\mu\text{M}$  8-CPT. Averaged single  $\text{Ca}^{2+}$  transient generated from averaging 5  $\text{Ca}^{2+}$  transients in control conditions and with (b)  $10\mu\text{M}$  8-CPT and (d)  $50\mu\text{M}$  8-CPT.



**Figure 8.30. The effect of Epac on electrically evoked Ca<sup>2+</sup> transients in rat cardiomyocytes.** Mean and SEM systolic and diastolic Ca<sup>2+</sup> levels in control conditions and in the presence of 10μM 8-CPT (a) and 50μM 8-CPT (c). Mean and SEM Ca<sup>2+</sup> transient amplitude data for 10μM 8-CPT (b) and 50μM 8-CPT (d).

***Caffeine evoked Ca<sup>2+</sup> transients and the effect of Epac activator 8-CPT in rat cardiomyocytes***

Fig 8.31 illustrates the changes in SR Ca<sup>2+</sup> load in the presence of the Epac activator, studied by perfusion of cells with caffeine. There appeared to be a trend for decrease in caffeine evoked Ca<sup>2+</sup> transients with the Epac activator. With 10µM 8-CPT there was a 12.7% decrease in the transients (n= 2 / 2). However this showed no statistical significance from control. There was a 15.7% decrease in the transients with 50µM 8-CPT (n= 2 / 2), but again this showed no statistical difference.

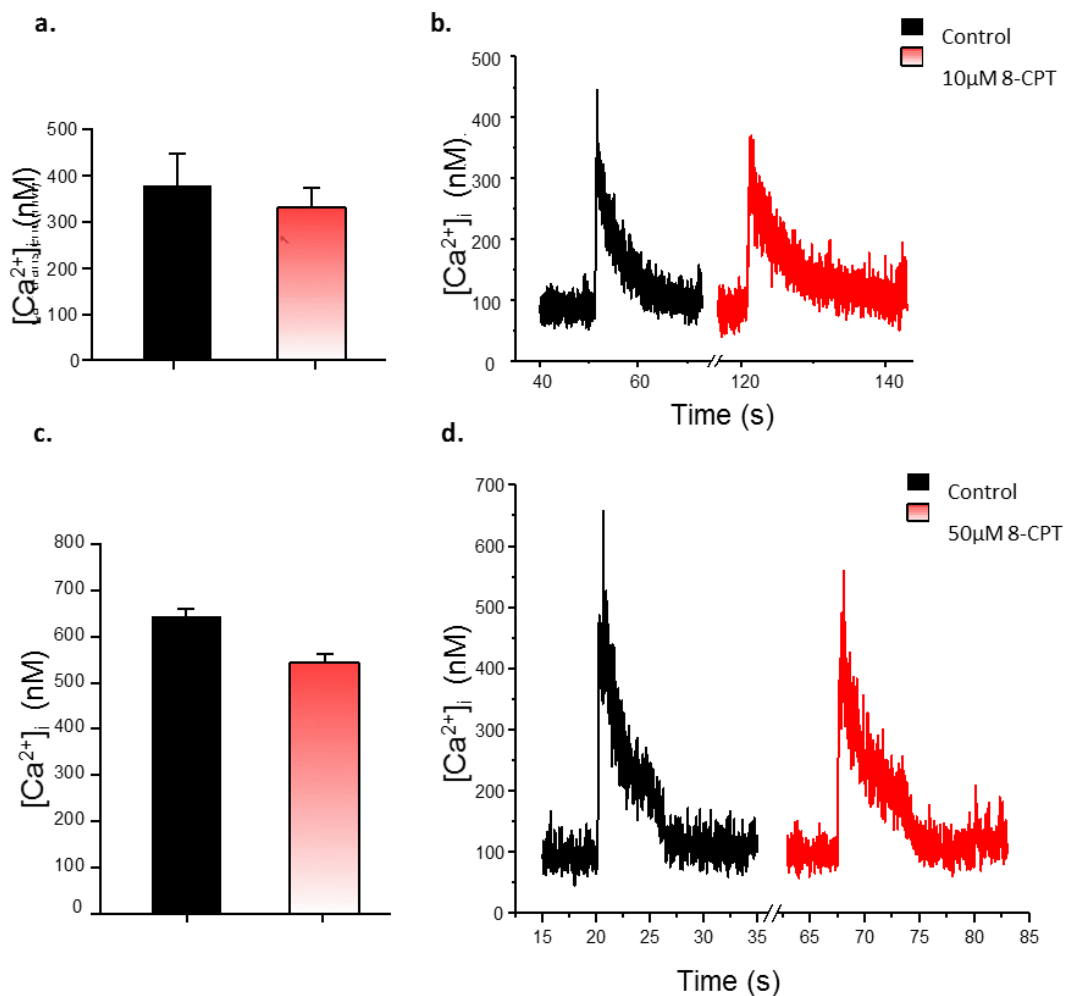
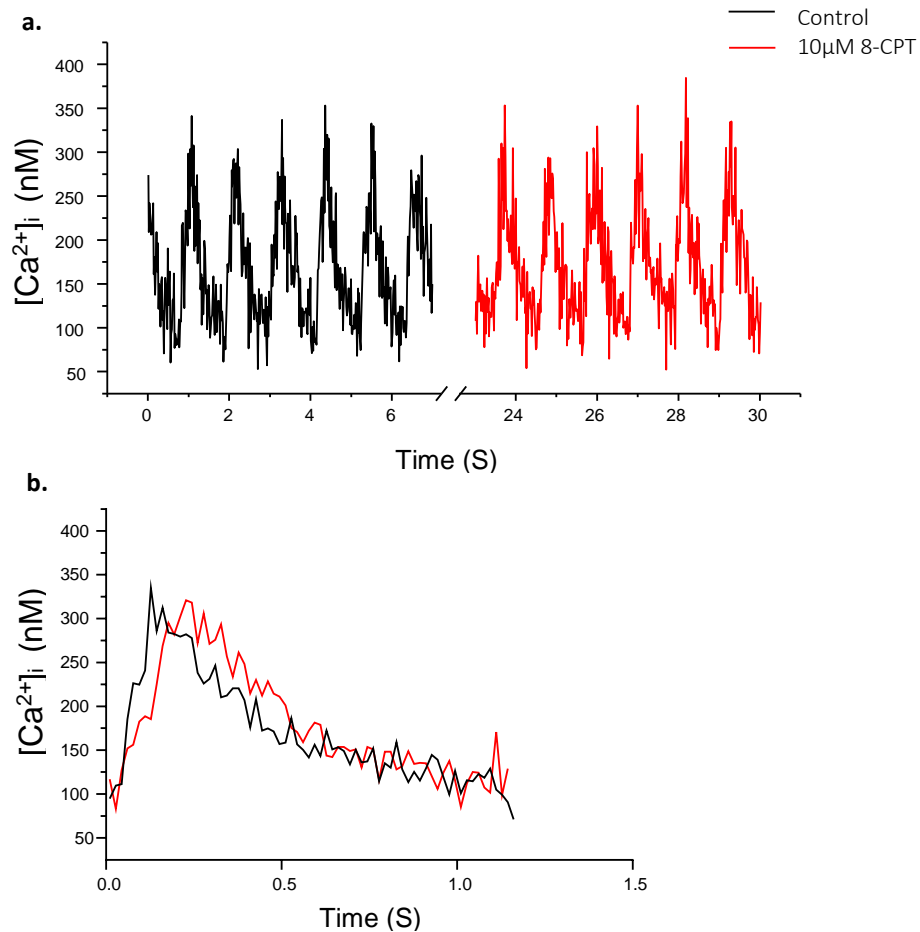


**Figure 8.31. The effect of Epac on caffeine evoked  $\text{Ca}^{2+}$  transients in rat cardiomyocytes.** Mean and SEM data displaying peak values of the caffeine evoked  $\text{Ca}^{2+}$  transients in control conditions and (a) with  $10\mu\text{M}$  8-CPT and (c)  $50\mu\text{M}$  8-CPT ( $n=2$ ). P values from statistical tests are also displayed ( $p<0.05$ ). Traces of caffeine evoked  $\text{Ca}^{2+}$  transients in control and (b) with  $10\mu\text{M}$  8-CPT and (d)  $50\mu\text{M}$  8-CPT.

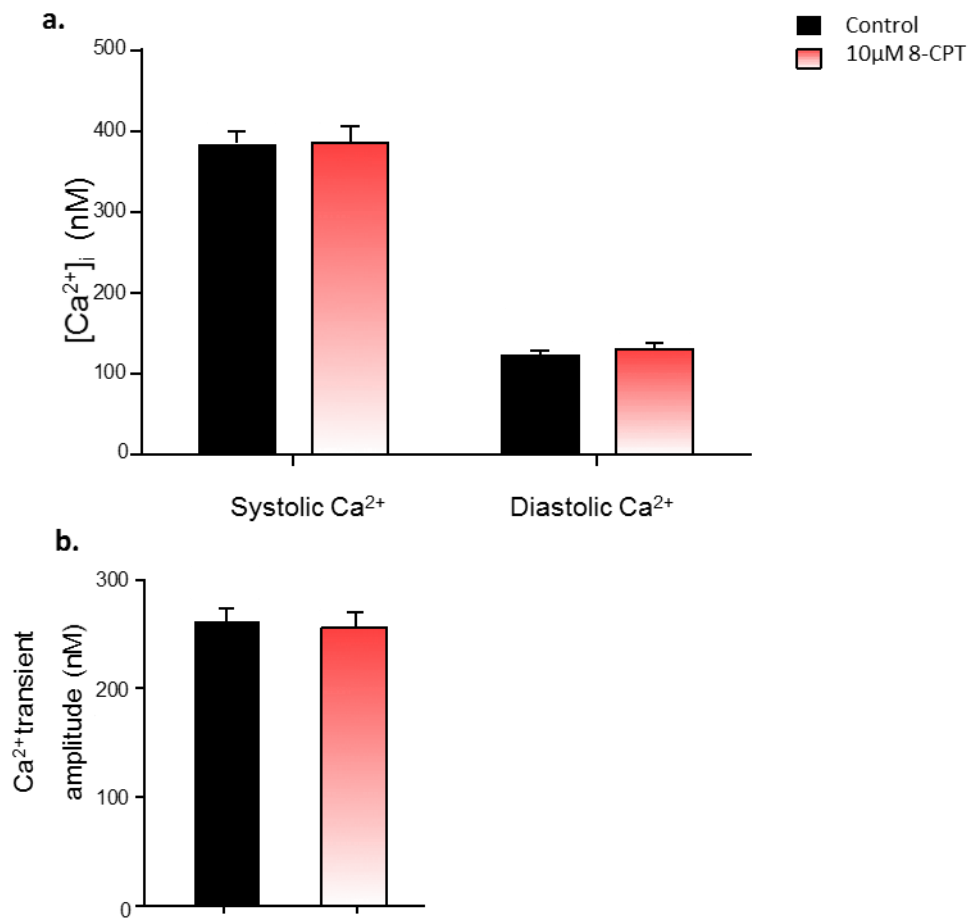
***The effect of Epac activator 8-CPT on electrically evoked  $\text{Ca}^{2+}$  transients in guinea pig cardiomyocytes***

Fig 8.32a shows the electrically evoked  $\text{Ca}^{2+}$  transients during control conditions and during perfusion of  $10\mu\text{M}$  8-CPT ( $n= 2 / 17$ ). Figure 8.32b shows 5 averaged  $\text{Ca}^{2+}$  transients for both conditions. There was no statistically significant difference in systolic  $\text{Ca}^{2+}$  between control and  $10\mu\text{M}$  8-CPT as shown in fig 8.33a. Diastolic  $\text{Ca}^{2+}$  appeared to show a trend for increase with  $10\mu\text{M}$  8-CPT, however mean data showed only an  $8.24\text{nM}$  increase (6.8% increase) between

control and 10 $\mu$ M 8-CPT with no significant difference. There was also no significant difference in Ca<sup>2+</sup> transient amplitude displayed in fig 8.33b.



**Figure 8.32. Electrically evoked Ca<sup>2+</sup> transient traces and the effect of Epac in guinea pig cardiomyocytes.** (a) Trace showing electrically evoked Ca<sup>2+</sup> transients in both control and 10 $\mu$ M 8-CPT. (b) Averaged single Ca<sup>2+</sup> transient generated from averaging 5 Ca<sup>2+</sup> transients in control and with 10 $\mu$ M 8-CPT.



**Figure 8.33. The effect of Epac on electrically evoked  $Ca^{2+}$  transients in guinea pig cardiomyocytes.** (a) Mean and SEM systolic and diastolic  $Ca^{2+}$  levels in control conditions and in the presence of 10µM 8-CPT. (b) Mean and SEM  $Ca^{2+}$  transient amplitude data. n=2 / 17.

### ***Caffeine evoked $Ca^{2+}$ transients and the effect of Epac activator 8-CPT in guinea pig cardiomyocytes***

The measure of SR  $Ca^{2+}$  load obtained by perfusion cells with caffeine is shown in fig 8.34 (n= 2 / 2). There appears to be a decrease in SR  $Ca^{2+}$  load with 10µM 8-CPT (9.98% decrease). However this is also shown to have no statistical significance.

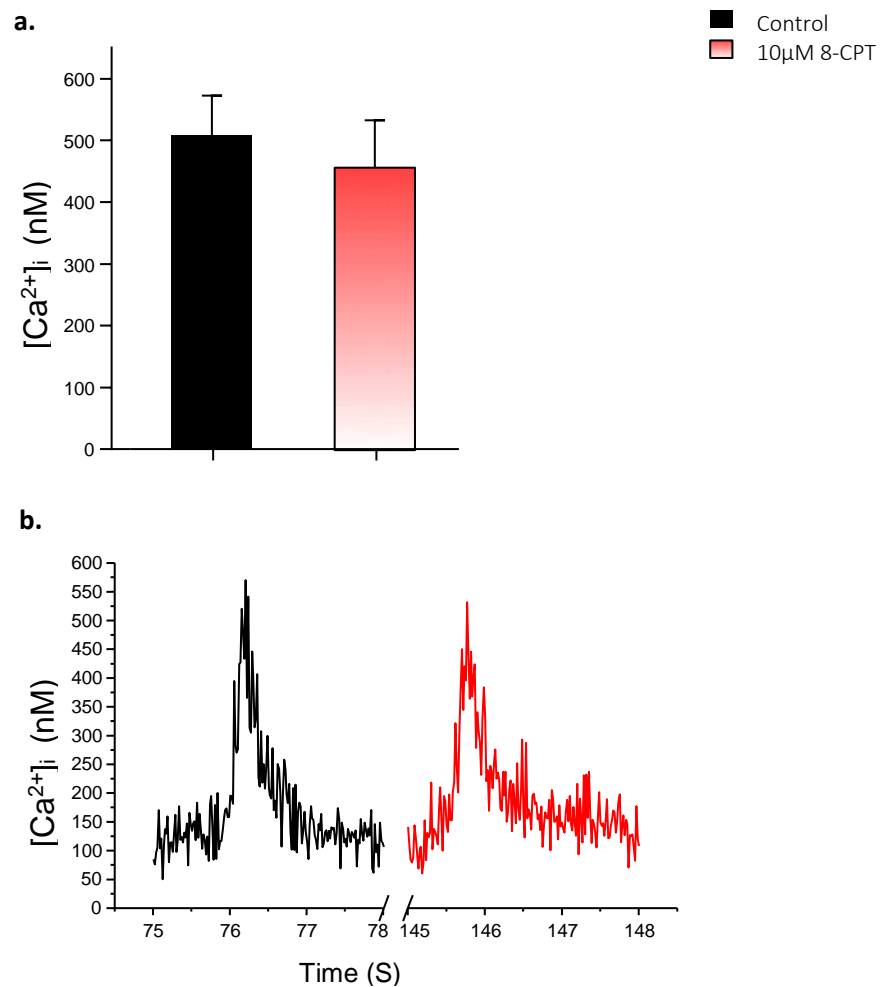


**Figure 8.34. The effect of Epac on caffeine evoked  $Ca^{2+}$  transients in guinea pig cardiomyocytes.** (a) Mean and SEM data displaying peak values of the caffeine evoked  $Ca^{2+}$  transients in control conditions and with 10  $\mu$ M 8-CPT ( $n=2 / 2$ ). (b) Traces of caffeine evoked  $Ca^{2+}$  transients in control and with 10  $\mu$ M 8-CPT.

## 8.6 Discussion

Although the results showed negative data, they were very consistent which gives greater confidence in this result. An initial concentration of 1 $\mu$ M 8-CPT was used because the mouse whole heart paper by Hothi et al (2008) also used this concentration. After observing no significant response with this concentration, a 10 $\mu$ M concentration of Epac was used, as used by Pereira et al (2007), Pereira et al (2009), Oestreich et al (2007), Oestreich et al (2009), Brette et al (2013) and Ruiz-Hurtado et al (2013) in rat and mice cardiomyocytes. This was further increased to 50 $\mu$ M during the Ca<sup>2+</sup> imaging technique. None of the previous studies have used concentrations above 50 $\mu$ M unless using concentrations >100 $\mu$ M which are not specific for Epac.

### 8.6.1 The effect of Epac activator 8-CPT on whole heart guinea pig physiology

#### *MAPD duration*

The MAPD was measured at two time points; 50% repolarization of the MAP and 90% repolarization of the MAP. This is during phase 3 of the cardiac action potential and so can provide information about the IK<sub>r</sub>, IK<sub>s</sub> and IK<sub>1</sub> channels involved in repolarization (Grunnet, 2010).

Results showed no significant changes in MAPD with either of the 8-CPT concentrations, at any of the cycle lengths. This was in accord with previous cardiomyocyte studies which have also shown a similar effect (Pereira et al., 2007; Oestreich et al., 2009; Hothi et al., 2008). In contrast, Brette et al (2013) observed lengthening of the APD with 10 $\mu$ M 8-CPT-AM that was attributed to inhibition of the steady state K<sup>+</sup> current. This was still observed in the presence of PKA inhibitors indicating that it was Epac that was causing this result. They were however unable to reproduce this result with 8-CPT and suggested that this was because 8-CPT has a poor permeability. Others have argued that the higher permeability of 8-CPT-AM is in fact disrupting Epac's compartmentalization of

signalling and thus these results are not physiologically applicable (Ruiz-Hurtado et al., 2012).

Action potential lengthening with 8-CPT was also demonstrated by Aflaki et al (2014) at APD<sub>50</sub> and APD<sub>90</sub>. This was as a response to 6 week administration of 6µM 8-CPT to guinea pigs and perhaps is more representative of chronic effects of Epac as it was attributed to decreased expression of IK<sub>s</sub>. In addition, it was found to be Epac1 that was causing the APD lengthening whereas Ca<sup>2+</sup> handling papers have demonstrated that Epac2 was responsible for the abnormal Ca<sup>2+</sup> handling and arrhythmia in the heart and Epac1 cannot replace its function (Pereira et al., 2013). This could imply that Epac's acute effects are Epac2 dependent and the chronic effects are Epac1 dependent and hence why no changes in MAPD were observed with short periods of perfusion used in this study. As Epac1 is expressed in higher concentrations in the heart (Metrich et al., 2008; Schmidt et al., 2007), this could explain why this effect is more prominent. Further supporting this, whole heart Epac experiments in mouse hearts with similar periods of perfusion did not display any changes in MAPD (Hothi et al., 2008).

### ***Electrical restitution***

In order to generate the most suitable protocol for electrical restitution in the guinea pig, several papers were examined (Fossa et al., 2007, Kazusa et al., 2014, Osadchii, 2012a, Osadchii, 2012b, Osadchii, 2014c, Osadchii, 2014b, Osadchii, 2014a, Osadchii et al., 2009, Osadchii et al., 2010, Osadchii et al., 2011, Soltysinska et al., 2011, Stark et al., 1996, Wang et al., 2015). Electrical restitution is a measure of the MAPD and its preceding diastolic interval. The relationship between these parameters acts as an indicator of arrhythmia inducibility. The S2 results show that MAPD decreased monotonically as DI decreased, which was as expected (Weiss et al., 2006).

If Epac has an arrhythmogenic effect as suggested, one would expect an increase in the RT<sub>max</sub>. RT<sub>max</sub> values of >1 increases probability of wavebreaks and the amplitude of alternans, therefore increasing arrhythmia susceptibility. There appeared to be an increase in RT<sub>max</sub> with 1µM 8-CPT at both apical and

basal sites however this showed no significant difference and this trend was not reproduced with 10 $\mu$ M 8-CPT possibly suggesting a dose dependent effect. No changes in ERP were observed as also shown by Hothi et al (2008).

Epac has however been shown to induce triggered activity in mouse hearts during electrical restitution protocols (Hothi et al., 2008), but this could not be reproduced in the guinea pig.

### ***Dynamic pacing***

The dynamic pacing protocol for guinea pigs was established by assessing protocols from various guinea pig papers (Osadchii, 2012a, Osadchii, 2012b, Osadchii et al., 2009, Osadchii et al., 2010, Osadchii et al., 2011, Soltysinska et al., 2011). As expected, MAPD decreased as CL decreased and as DI decreased. It was also expected that alternans would be observed. Alternans are beat to beat alterations in APD and Ca<sup>2+</sup> transients. They usually alternate in a repeating pattern e.g. long-short-long-short (Weiss et al., 2006). Alternans tend to occur in conditions where arrhythmia is common and therefore they can be used as a predictor of arrhythmogenesis. By plotting the last 3 MAPs of each cycle length in the protocol, observation of alternans was expected as the cycle length shortened. However, no alternans were observed in control or in the presence of the Epac activator. MAPs were consistent in amplitude and duration until immediate degeneration into VF at short cycle lengths.

A similar dynamic pacing protocol was also used by Hothi et al (2008) and this showed slightly larger alternans magnitude in the presence of 8-CPT but likewise this did not reach statistical significance.

### **8.6.2 The effect of positive control isoproterenol on whole heart guinea pig physiology**

Isoproterenol (ISO) is  $\beta$ -AR agonist and is known to increase inotropy and chronotropy of the heart. ISO causes increases in diastolic Ca<sup>2+</sup> and intracellular Ca<sup>2+</sup> overload. It has also been suggested that ISO can enhance Epac1 expression (Aflaki et al., 2014). Perfusion of ISO caused a large increase in

intrinsic heart rate and this made it difficult to pace the heart at fixed CLs. The heart could not be paced well above CLs of 200 ms, which made it difficult to apply protocols as they required longer CLs than this. As perfusion continued there was also an obvious change in MAPs. MAPD was lengthened which was expected as this effect with ISO and APD has been seen in other studies using guinea pig cardiomyocytes (Tweedie et al., 1997, Belardinelli and Isenberg, 1983, Aflaki et al., 2014), and after long periods of perfusion the MAP shape changed morphology. An increase in MAPD with ISO has also been observed in rabbit whole heart experiments (Qin et al., 2013).

As the electrical restitution protocol is a measure of arrhythmogenesis, a significant response with ISO was expected. ERP was found to be at a longer S1-S2 interval than with control, the RT curve was much steeper and the  $RT_{maxSlope}$  almost doubles in the presence of ISO. This demonstrates increased predisposition to arrhythmogenesis. Qin et al (2013) also observed increased ERP in the presence of ISO and an increase in  $RT_{maxSlope}$ . They also observed an increased incidence of ventricular arrhythmia with ISO.

Alternans were observed during the dynamic pacing protocol with ISO, also seen in the study by Qin et al (2013). As cycle lengths became shorter MAPs became more triangular, less consistent in shape and occurred at irregular intervals. Alternans were observed more frequently at shorter cycle lengths. This is observed by the scattering of the curve at the shorter CLs and DIs.

The positive control data strengthens the confidence in the data gathered with the Epac activator as it demonstrates the drugs are perfusing correctly into the heart and the parameters of the protocols are suitable enough to show difference. If Epac were to have an arrhythmogenic effect as suggested, then results should have shown similar effect as ISO. Aflaki et al (2014) found that Epac mimicked the effects of 100nM ISO, but again this was with chronic Epac administration.

### 8.6.3 Epac's effect on Ca<sup>2+</sup> handling in rat and guinea pig cardiomyocytes

Rat cardiomyocytes were initially used for the Ca<sup>2+</sup> imaging as they were more readily available and data from these cells allowed comparison to the other Ca<sup>2+</sup> handling studies that used 8-CPT (Pereira et al., 2007; Dominguez-Rodriguez et al., 2013). However, there were no statistically significant changes in Ca<sup>2+</sup> transients which was an unexpected result as the previous rat cardiomyocyte study by Pereira et al (2007) showed decreased Ca<sup>2+</sup> transient amplitude and increased probability of Ca<sup>2+</sup> sparks with 10 $\mu$ M 8-CPT. This was found using confocal microscopy with different fluorescent Ca<sup>2+</sup> dyes (Fluo-3AM and Rhod 2AM). Mouse cardiomyocyte studies showed increased amplitude of electrically evoked Ca<sup>2+</sup> transients (Oestreich et al., 2007). Other studies have also shown Epac's effects on Ca<sup>2+</sup> handling e.g. Purves et al (2009) displayed elevated intracellular Ca<sup>2+</sup> in ventricular smooth muscle cells, Kang et al (2001) showed Epac mediated CICR in pancreatic cells, Ster et al (2007) demonstrate Epac induced activation of Ca<sup>2+</sup> sensitive K<sup>+</sup> channels due to mobilization of intracellular Ca<sup>2+</sup> stores in cerebellar granule cells, Schmidt et al (2001) found Epac caused Ca<sup>2+</sup> mobilization in HEK-293 cells and neuroblastoma cells and Hothi et al (2008) showing spontaneous Ca<sup>2+</sup> transients in murine cardiomyocytes.

There has only been one other Epac study that used guinea pig cardiomyocytes, which showed I<sub>Ks</sub> downregulation with 6 $\mu$ M 8-CPT. However, as mentioned previously, the guinea pigs were administered with the Epac activator over a 6 week period before experiments took place so this study demonstrates the more chronic effects of Epac in gene transcription whereas the focus of this project was Epac's acute effects on arrhythmia induction. Calcium imaging in guinea pig cardiomyocytes with 5 minute perfusion of 8-CPT (longer perfusion was attempted, 5-15 mins, however there were still no changes) showed no changes in Ca<sup>2+</sup> transients. Diastolic Ca<sup>2+</sup> showed a trend for increase, also seen by Pereira et al (2007), but this did not reach levels of significance.

Although there did appear to be a decrease in SR Ca<sup>2+</sup> load with the Epac activator in both species, this was not large enough to be significant. Pereira et

al (2007), saw a significant decrease in SR load from 650nM to 425nM (n=10) in rat cardiomyocytes with the same concentration of 8-CPT (10 $\mu$ M). The differences could be due to the small n numbers used so far (n of 2 rat hearts, n of 2 guinea pig hearts) or also due to the difference in techniques. Pereira et al (2007) used confocal microscopy to measure SR Ca<sup>2+</sup> load and used a different ratiometric fluorescent dye; Indo-1 AM. It has been suggested that Epac causes SR Ca<sup>2+</sup> leak due to phosphorylation of RyR by CaMKII (Oestreich et al., 2009; Pereira et al., 2007; Kawasaki et al., 1998). This was also evidenced in whole heart models, where use of CaMKII inhibitors blocked Epac's arrhythmogenic effect (Hothi et al., 2008). If this were the case, we would expect SR Ca<sup>2+</sup> to be significantly decreased with 8-CPT. Another explanation is that although Epac may cause SR Ca<sup>2+</sup> leak, it does not occur in a large enough magnitude in the whole heart for it to be physiologically relevant.

#### **8.6.4 Limitations**

Although MAPs are a good representation of transmembrane action potentials, there are limitations associated with them. For example, the quality of the MAP is determined by the angle and location of the electrode on the epicardium. The placement of the electrode can affect the amount of signal interference and the shape of the MAPs. The pressure exerted by the electrode can also affect the amplitude of the MAP and if the pressure is too great then this can cause ischemia in the cells directly beneath it. There is also a tendency for MAPs to deteriorate over time in which case occasionally the MAP position had to be moved to a new site. Another limitation was that, depending on the intrinsic HR, some hearts were difficult to pace at CLs above 200ms. This made it difficult to apply the protocols which have initial CLs of 250ms and so in some case the parameters had to be modified.

However, MAPs and whole heart techniques allow for consideration of factors such as heterogeneities due to non-uniform ion channel distributions and electrical coupling, without interference from haemodynamic reflexes and humoral factors, demonstrating the importance of this method and the data it generates.

## 8.7 Conclusions

Contradictory to the hypothesis, Epac had no effect on  $\text{Ca}^{2+}$  handling and did not induce ventricular arrhythmogenesis in the guinea pig heart. The consistency of the data across a total of 11 hearts with the Epac activator relays confidence in the observed results. The lack of effect could be due to species differences because there is a higher activity of SERCA in rat ventricles than in guinea pig ventricles and there are different patterns of ion channel expression (Bers, 2002). There is also reason to believe Epac is expressed in guinea pig heart (Aflaki et al., 2014).

Under physiological conditions both Epac and PKA are coactivated. In comparison to solely Epac activation, global activation of both Epac and PKA results in increases  $\text{Ca}^{2+}$  transients, SR  $\text{Ca}^{2+}$  leak and SR  $\text{Ca}^{2+}$  load (Pereira et al., 2013). Decreased  $\text{Ca}^{2+}$  transients and SR  $\text{Ca}^{2+}$  load is seen when Epac alone is activated due to a greater SR  $\text{Ca}^{2+}$  leak (Pereira et al., 2007) so it is debatable whether this is relevant physiologically. It could also be that Epac just reduces the ability of PKA to increase SR  $\text{Ca}^{2+}$  load via  $\text{Ca}^{2+}$  current and PLB. It has also been suggested that the effects that PKA induces can overpower the effects induced by Epac (Pereira et al., 2013).

As there is evidence to suggest that Epac has no function under baseline conditions (Pereira et al., 2013), it has been proposed that Epac signalling pathways may have more relevance during pathophysiological conditions (Purves et al., 2009), hence its increased expression in HF (Ulucan et al., 2007; Metrich et al., 2008). This would explain the observed negative result. The presence of Epac under cardiovascular disease states may be worth exploring.

Increased expression of Epac in HF and the effects of increased Epac on arrhythmias could expose Epac as a potential therapeutic target (Ruiz-Hurtado et al., 2013). Aflaki et al (2014) suggested targeting of Epac-mediated electric remodelling may have a preventative effect on lethal arrhythmias.

## References

- AFLAKI, M., QI, X. Y., XIAO, L., ORDOG, B., TADEVOSYAN, A., LUO, X., MAGUY, A., SHI, Y., TARDIF, J. C. & NATTEL, S. 2014. Exchange protein directly activated by cAMP mediates slow delayed-rectifier current remodeling by sustained beta-adrenergic activation in guinea pig hearts. *Circulation research*, 114, 993-1003.
- AI, X., CURRAN, J. W., SHANNON, T. R., BERS, D. M. & POGWIZD, S. M. 2005. Ca<sup>2+</sup>/calmodulin-dependent protein kinase modulates cardiac ryanodine receptor phosphorylation and sarcoplasmic reticulum Ca<sup>2+</sup> leak in heart failure. *Circulation research*, 97, 1314-1322.
- AJIJOLA, O. A., HOWARD-QUIJANO, K., SCOVOTTI, J., VASEGHI, M., LEE, C., MAHAJAN, A. & SHIVKUMAR, K. 2015. Augmentation of cardiac sympathetic tone by percutaneous low-level stellate ganglion stimulation in humans: a feasibility study. *Physiol Rep*, 3.
- AJIJOLA, O. A., VASEGHI, M., MAHAJAN, A. & SHIVKUMAR, K. 2012. Bilateral cardiac sympathetic denervation: why, who and when? *Expert Rev Cardiovasc Ther*, 10, 947-9.
- AJIJOLA, O. A., VASEGHI, M., ZHOU, W., YAMAKAWA, K., BENHARASH, P., HADAYA, J., LUX, R. L., MAHAJAN, A. & SHIVKUMAR, K. 2013. Functional differences between junctional and extrajunctional adrenergic receptor activation in mammalian ventricle. *Am J Physiol Heart Circ Physiol*, 304, H579-88.
- ALLINGHAM, J. S., SMITH, R. & RAYMENT, I. 2005. The structural basis of blebbistatin inhibition and specificity for myosin II. *Nat Struct Mol Biol*, 12, 378-9.
- AMAR, D., ZHANG, H., MIODOWNIK, S. & KADISH, A. H. 2003. Competing autonomic mechanisms precede the onset of postoperative atrial fibrillation. *Journal of the American College of Cardiology*, 42, 1262-1268.
- AMBERG, G. C., BONEV, A. D., ROSSOW, C. F., NELSON, M. T. & SANTANA, L. F. 2003. Modulation of the molecular composition of large conductance, Ca<sup>2+</sup>-activated K<sup>+</sup> channels in vascular smooth muscle during hypertension. *The Journal of clinical investigation*, 112, 717-724.
- ANTZELEVITCH, C. 2001. Transmural dispersion of repolarization and the T wave. *Cardiovasc Res*, 50, 426-31.
- ANTZELEVITCH, C. 2005. Role of transmural dispersion of repolarization in the genesis of drug-induced torsades de pointes. *Heart Rhythm*, 2, S9-15.

- ANTZELEVITCH, C. 2007. Heterogeneity and cardiac arrhythmias: an overview. *Heart Rhythm*, 4, 964-72.
- ANTZELEVITCH, C. & BELARDINELLI, L. 2006. The role of sodium channel current in modulating transmural dispersion of repolarization and arrhythmogenesis. *J Cardiovasc Electrophysiol*, 17 Suppl 1, S79-S85.
- ANTZELEVITCH, C. & BURASHNIKOV, A. 2011. Overview of Basic Mechanisms of Cardiac Arrhythmia. *Card Electrophysiol Clin*, 3, 23-45.
- ANZOLA, J. & RUSHMER, R. F. 1956. Cardiac responses to sympathetic stimulation. *Circulation research*, 4, 302-307.
- ARDELL, J. L., RANDALL, W. C., CANNON, W. J., SCHMACHT, D. C. & TASDEMIROGLU, E. 1988. Differential sympathetic regulation of automatic, conductile, and contractile tissue in dog heart. *The American Journal of Physiology*, 255, H1050-9.
- ARMOUR, J. A. 2008. Potential clinical relevance of the 'little brain' on the mammalian heart. *Experimental physiology*, 93, 165-176.
- ARMOUR, J. A., HAGEMAN, G. R. & RANDALL, W. C. 1972. Arrhythmias induced by local cardiac nerve stimulation. *Am J Physiol*, 223, 1068-75.
- ARMOUR, J. A. & RANDALL, W. C. 1975. Functional anatomy of canine cardiac nerves. *Acta Anatomica*, 91, 510-528.
- ARORA, R. 2012. Recent insights into the role of the autonomic nervous system in the creation of substrate for atrial fibrillation: implications for therapies targeting the atrial autonomic nervous system. *Circ Arrhythm Electrophysiol*, 5, 850-9.
- ARORA, R., DAS, M. K., ZIPES, D. P. & WU, J. 2003. Optical mapping of cardiac arrhythmias. *Indian Pacing Electrophysiol J*, 3, 187-96.
- ATTIN, M. & CLUSIN, W. T. 2009. Basic concepts of optical mapping techniques in cardiac electrophysiology. *Biol Res Nurs*, 11, 195-207.
- AUSTONI, P., ROSATI, R., GREGORINI, L., BLANCHI, E., BORLOLANI, E. & SCHWARTZ, P. J. 1979. Stellectomy and exercise in man. *American Journal of Cardiology*, 43, 399.
- BAKER, L. C., WOLK, R., CHOI, B. R., WATKINS, S., PLAN, P., SHAH, A. & SALAMA, G. 2004. Effects of mechanical uncouplers, diacetyl monoxime, and cytochalasin-D on the electrophysiology of perfused mouse hearts. *Am J Physiol Heart Circ Physiol*, 287, H1771-9.
- BANVILLE, I. & GRAY, R. A. 2002. Effect of action potential duration and conduction velocity restitution and their spatial dispersion on alternans and the stability of arrhythmias. *J Cardiovasc Electrophysiol*, 13, 1141-9.

- BARTEL, S., KARCZEWSKI, P. & KRAUSE, E. G. 1993. Protein phosphorylation and cardiac function: cholinergic-adrenergic interaction. *Cardiovasc Res*, 27, 1948-53.
- BAYES DE LUNA, A., COUMEL, P. & LECLERCQ, J. F. 1989. Ambulatory sudden cardiac death: mechanisms of production of fatal arrhythmia on the basis of data from 157 cases. *Am Heart J*, 117, 151-9.
- BELARDINELLI, L. & ISENBERG, G. 1983. Actions of adenosine and isoproterenol on isolated mammalian ventricular myocytes. *Circulation research*, 53, 287-297.
- BELL, R. M., MOCANU, M. M. & YELLON, D. M. 2011. Retrograde heart perfusion: the Langendorff technique of isolated heart perfusion. *J Mol Cell Cardiol*, 50, 940-50.
- BEN-DAVID, J. & ZIPES, D. P. 1988. Differential response to right and left ansae subclaviae stimulation of early afterdepolarizations and ventricular tachycardia induced by cesium in dogs. *Circulation*, 78, 1241-50.
- BENITAH, J. P., ALVAREZ, J. L. & GOMEZ, A. M. 2010. L-type Ca<sup>2+</sup> current in ventricular cardiomyocytes. *Journal of Molecular and Cellular Cardiology*, 48, 26-36.
- BERNSTEIN, S. A. & MORLEY, G. E. 2006. Gap junctions and propagation of the cardiac action potential. *Adv Cardiol*, 42, 71-85.
- BERS, D. M. 2002. Cardiac excitation-contraction coupling. *Nature*, 415, 198-205.
- BERS, D. M. 2007a. Going to cAMP just got more complicated. *J Physiol*, 583, 415-6.
- BERS, D. M. 2008. Calcium cycling and signaling in cardiac myocytes. *Annu Rev Physiol*, 70, 23-49.
- BERS, D. M., EISNER, D. A. & VALDIVIA, H. H. 2003. Sarcoplasmic reticulum Ca<sup>2+</sup> and heart failure: roles of diastolic leak and Ca<sup>2+</sup> transport. *Circ Res*, 93, 487-90.
- BEUCKELMANN, D. J., NABAUER, M. & ERDMANN, E. 1993. Alterations of K<sup>+</sup> currents in isolated human ventricular myocytes from patients with terminal heart failure. *Circ Res*, 73, 379-85.
- BLANCHARD, E. M., SMITH, G. L., ALLEN, D. G. & ALPERT, N. R. 1990. The effects of 2,3-butanedione monoxime on initial heat, tension, and aequorin light output of ferret papillary muscles. *Pflugers Arch*, 416, 219-21.
- BOND, L. M., TUMBARELLO, D. A., KENDRICK-JONES, J. & BUSS, F. 2013. Small-molecule inhibitors of myosin proteins. *Future Med Chem*, 5, 41-52.
- BOOGERS, M. J., BORLEFFS, C. J. W., HENNEMAN, M. M., VAN BOMMEL, R. J., VAN RAMSHORST, J., BOERSMA, E., DIBBETS-SCHNEIDER, P., STOKKEL, M. P., VAN DER WALL, E. E., SCHALIJ, M. J. & BAX, J. J. 2010. Cardiac Sympathetic Denervation Assessed With 123-Iodine Metaiodobenzylguanidine

- Imaging Predicts Ventricular Arrhythmias in Implantable Cardioverter-Defibrillator Patients. *Journal of the American College of Cardiology*, 55, 2769-2777.
- BOURKE, T., VASEGHI, M., MICHOWITZ, Y., SANKHLA, V., SHAH, M., SWAPNA, N., BOYLE, N. G., MAHAJAN, A., NARASIMHAN, C., LOKHANDWALA, Y. & SHIVKUMAR, K. 2010. Neuraxial modulation for refractory ventricular arrhythmias: value of thoracic epidural anesthesia and surgical left cardiac sympathetic denervation. *Circulation*, 121, 2255-2262.
- BRACK, K. E., NARANG, R., WINTER, J. & NG, G. A. 2013. The mechanical uncoupler blebbistatin is associated with significant electrophysiological effects in the isolated rabbit heart. *Exp Physiol*, 98, 1009-27.
- BRAHMAJOTHI, M. V., MORALES, M. J., RASMUSSEN, R. L., CAMPBELL, D. L. & STRAUSS, H. C. 1997a. Heterogeneity in K<sup>+</sup> channel transcript expression detected in isolated ferret cardiac myocytes. *Pacing Clin Electrophysiol*, 20, 388-96.
- BRAHMAJOTHI, M. V., MORALES, M. J., REIMER, K. A. & STRAUSS, H. C. 1997b. Regional localization of ERG, the channel protein responsible for the rapid component of the delayed rectifier, K<sup>+</sup> current in the ferret heart. *Circ Res*, 81, 128-35.
- BRETTE, F., BLANDIN, E., SIMARD, C., GUINAMARD, R. & SALLE, L. 2013. Epac activator critically regulates action potential duration by decreasing potassium current in rat adult ventricle. *Journal of Molecular and Cellular Cardiology*, 57, 96-105.
- BRINK, P. A., CROTTI, L., CORFIELD, V., GOOSEN, A., DURRHEIM, G., HEDLEY, P., HERADIEN, M., GELDENHUYS, G., VANOLI, E., BACCHINI, S., SPAZZOLINI, C., LUNDQUIST, A. L., RODEN, D. M., GEORGE, A. L., JR. & SCHWARTZ, P. J. 2005. Phenotypic variability and unusual clinical severity of congenital long-QT syndrome in a founder population. *Circulation*, 112, 2602-10.
- BROUHA, L., CANNON, W. B. & DILL, D. B. 1936. The heart rate of the sympathectomized dog in rest and exercise. *J Physiol*, 87, 345-59.
- BUCKLEY, U., YAMAKAWA, K., TAKAMIYA, T., ANDREW ARMOUR, J., SHIVKUMAR, K. & ARDELL, J. L. 2016. Targeted stellate decentralization: Implications for sympathetic control of ventricular electrophysiology. *Heart rhythm : the official journal of the Heart Rhythm Society*, 13, 282-288.
- CAO, J.-M., CHEN, L. S., KENKNIGHT, B. H., OHARA, T., LEE, M.-H., TSAI, J., LAI, W. W., KARAGUEUZIAN, H. S., WOLF, P. L., FISHBEIN, M. C. & CHEN, P.-S.

- 2000a. Nerve Sprouting and Sudden Cardiac Death. *Circulation Research*, 86, 816-821.
- CAO, J.-M., FISHBEIN, M. C., HAN, J. B., LAI, W. W., LAI, A. C., WU, T.-J., CZER, L., WOLF, P. L., DENTON, T. A., SHINTAKU, I. P., CHEN, P.-S. & CHEN, L. S. 2000b. Relationship Between Regional Cardiac Hyperinnervation and Ventricular Arrhythmia. *Circulation*, 101, 1960-1969.
- CAZORLA, O., LUCAS, A., POIRIER, F., LACAMPAGNE, A. & LEZOUALC'H, F. 2009. The cAMP binding protein Epac regulates cardiac myofilament function. *Proceedings of the National Academy of Sciences of the United States of America*, 106, 14144-14149.
- CHEN, L., SAMPSON, K. J. & KASS, R. S. 2016. Cardiac Delayed Rectifier Potassium Channels in Health and Disease. *Card Electrophysiol Clin*, 8, 307-22.
- CHENG, J., KAMIYA, K., LIU, W., TSUJI, Y., TOYAMA, J. & KODAMA, I. 1999. Heterogeneous distribution of the two components of delayed rectifier K<sup>+</sup> current: a potential mechanism of the proarrhythmic effects of methanesulfonanilideclass III agents. *Cardiovasc Res*, 43, 135-47.
- CHENG, Y., LI, L., NIKOLSKI, V., WALLICK, D. W. & EFIMOV, I. R. 2004. Shock-induced arrhythmogenesis is enhanced by 2,3-butanedione monoxime compared with cytochalasin D. *Am J Physiol Heart Circ Physiol*, 286, H310-8.
- CHOW, L. T., CHOW, S. S., ANDERSON, R. H. & GOSLING, J. A. 1995. The innervation of the human myocardium at birth. *Journal of anatomy*, 187 ( Pt 1), 107-114.
- CHRISTENSEN, A. E., SELHEIM, F., DE ROOIJ, J., DREMIER, S., SCHWEDE, F., DAO, K. K., MARTINEZ, A., MAENHAUT, C., BOS, J. L., GENIESER, H. G. & DOSKELAND, S. O. 2003. cAMP analog mapping of Epac1 and cAMP kinase. Discriminating analogs demonstrate that Epac and cAMP kinase act synergistically to promote PC-12 cell neurite extension. *The Journal of biological chemistry*, 278, 35394-35402.
- CHUNG, J. M., CHUNG, K. & WURSTER, R. D. 1975. Sympathetic preganglionic neurons of the cat spinal cord: horseradish peroxidase study. *Brain Res*, 91, 126-31.
- CHUNG, K., CHUNG, J. M., LAVELLE, F. W. & WURSTER, R. D. 1979. Sympathetic neurons in the cat spinal cord projecting to the stellate ganglion. *J Comp Neurol*, 185, 23-9.
- CINCA, J., EVANGELISTA, A., MONTOYO, J., BARUTELL, C., FIGUERAS, J., VALLE, V., RIUS, J. & SOLER-SOLER, J. 1985. Electrophysiologic effects of unilateral right and left stellate ganglion block on the human heart. *Am Heart J*, 109, 46-54.

- CLUSIN, W. T. 2003. Calcium and cardiac arrhythmias: DADs, EADs, and alternans. *Crit Rev Clin Lab Sci*, 40, 337-75.
- COHEN, L. B., KEYNES, R. D. & HILLE, B. 1968. Light scattering and birefringence changes during nerve activity. *Nature*, 218, 438-41.
- COHEN, L. B. & SALZBERG, B. M. 1978. Optical measurement of membrane potential. *Rev Physiol Biochem Pharmacol*, 83, 35-88.
- COLEMAN, M. A., BOS, J. M., JOHNSON, J. N., OWEN, H. J., DESCHAMPS, C., MOIR, C. & ACKERMAN, M. J. 2012. Videoscopic left cardiac sympathetic denervation for patients with recurrent ventricular fibrillation/malignant ventricular arrhythmia syndromes besides congenital long-QT syndrome. *Circulation. Arrhythmia and electrophysiology*, 5, 782-788.
- COOPER, T. 1965. Physiologic and pharmacologic effects of cardiac denervation. *Fed Proc*, 24, 1428-31.
- COOPER, T. 1967. The functional significance of the cardiac nerves. *Annals of Internal Medicine*, 66, 440-442.
- COOTE, J. H. 1988. The organisation of cardiovascular neurons in the spinal cord. *Reviews of physiology, biochemistry and pharmacology*, 110, 147-285.
- COOTE, J. H. 2001. Multiple oscillators in autonomic control. *The Journal of physiology*, 533, 313.
- COOTE, J. H. & CHAUHAN, R. A. 2016. The sympathetic innervation of the heart: Important new insights. *Auton Neurosci*, 199, 17-23.
- CORONEL, R., WILMS-SCHOPMAN, F. J., OPTHOF, T. & JANSE, M. J. 2009. Dispersion of repolarization and arrhythmogenesis. *Heart Rhythm*, 6, 537-43.
- CORR, P. B. & CRAFFORD, W. A., JR. 1981. Enhanced alpha-adrenergic responsiveness in ischemic myocardium: role of alpha-adrenergic blockade. *Am Heart J*, 102, 605-12.
- CORR, P. B., SHAYMAN, J. A., KRAMER, J. B. & KIPNIS, R. J. 1981. Increased alpha-adrenergic receptors in ischemic cat myocardium. A potential mediator of electrophysiological derangements. *J Clin Invest*, 67, 1232-6.
- CRICK, S. J., ANDERSON, R. H., HO, S. Y. & SHEPPARD, M. N. 1999a. Localisation and quantitation of autonomic innervation in the porcine heart II: endocardium, myocardium and epicardium. *Journal of anatomy*, 195 ( Pt 3), 359-373.
- CRICK, S. J., SHEPPARD, M. N., HO, S. Y. & ANDERSON, R. H. 1999b. Localisation and quantitation of autonomic innervation in the porcine heart I: conduction system. *Journal of anatomy*, 195 ( Pt 3), 341-357.

- CURRAN, J., BROWN, K. H., SANTIAGO, D. J., POGWIZD, S., BERS, D. M. & SHANNON, T. R. 2010. Spontaneous Ca waves in ventricular myocytes from failing hearts depend on Ca(2+)-calmodulin-dependent protein kinase II. *J Mol Cell Cardiol*, 49, 25-32.
- DAE, M. W. & BOTVINICK, E. H. 1990. Imaging of the heart using metaiodobenzylguanidine. *Journal of thoracic imaging*, 5, 31-36.
- DAE, M. W., O'CONNELL, J. W., BOTVINICK, E. H., AHEARN, T., YEE, E., HUBERTY, J. P., MORI, H., CHIN, M. C., HATTNER, R. S. & HERRE, J. M. 1989. Scintigraphic assessment of regional cardiac adrenergic innervation. *Circulation*, 79, 634-644.
- DAO, K. K., TEIGEN, K., KOPPERUD, R., HODNELAND, E., SCHWEDE, F., CHRISTENSEN, A. E., MARTINEZ, A. & DOSKELAND, S. O. 2006. Epac1 and cAMP-dependent protein kinase holoenzyme have similar cAMP affinity, but their cAMP domains have distinct structural features and cyclic nucleotide recognition. *The Journal of biological chemistry*, 281, 21500-21511.
- DE ROOIJ, J., ZWARTKRUIS, F. J., VERHEIJEN, M. H., COOL, R. H., NIJMAN, S. M., WITTINGHOFER, A. & BOS, J. L. 1998. Epac is a Rap1 guanine-nucleotide-exchange factor directly activated by cyclic AMP. *Nature*, 396, 474-477.
- DELGADO, J. M. 1960. Circulatory effects of cortical stimulation. *Physiological reviews. Supplement*, 4, 146-178.
- DEUCHARS, S. A. 2007. Multi-tasking in the spinal cord--do 'sympathetic' interneurons work harder than we give them credit for? *The Journal of physiology*, 580, 723-729.
- DEUCHARS, S. A., MILLIGAN, C. J., STORNETTA, R. L. & DEUCHARS, J. 2005. GABAergic neurons in the central region of the spinal cord: a novel substrate for sympathetic inhibition. *The Journal of neuroscience : the official journal of the Society for Neuroscience*, 25, 1063-1070.
- DITTRICH, M., JUREVICIUS, J., GEORGET, M., ROCHAIS, F., FLEISCHMANN, B., HESCHELER, J. & FISCHMEISTER, R. 2001. Local response of L-type Ca(2+) current to nitric oxide in frog ventricular myocytes. *J Physiol*, 534, 109-21.
- DODGE-KAFKA, K. L., SOUGHAYER, J., PARE, G. C., CARLISLE MICHEL, J. J., LANGE BERG, L. K., KAPILOFF, M. S. & SCOTT, J. D. 2005. The protein kinase A anchoring protein mAKAP coordinates two integrated cAMP effector pathways. *Nature*, 437, 574-578.

- DOMINGUEZ-RODRIGUEZ, A., ALVAREZ, J. L., RUIZ-HURTADO, G., LEZOUALC'H, F., BENITAH, J.-P. & GOMEZ, A. M. 2013. Epac Effects on Cardiac Ionic Currents. *Biophysical Journal*, vol. 104 (2), p. 282a.
- DONALD, D. E. 1974. Myocardial performance after excision of the extrinsic cardiac nerves in the dog. *Circ Res*, 34, 417-24.
- DOU, Y., ARLOCK, P. & ARNER, A. 2007. Blebbistatin specifically inhibits actin-myosin interaction in mouse cardiac muscle. *Am J Physiol Cell Physiol*, 293, C1148-53.
- DUN, N. J. & MO, N. 1989. Inhibitory postsynaptic potentials in neonatal rat sympathetic preganglionic neurones in vitro. *The Journal of physiology*, 410, 267-281.
- DYBKOVA, N., WAGNER, S., BACKS, J., HUND, T. J., MOHLER, P. J., SOWA, T., NIKOLAEV, V. O. & MAIER, L. S. 2014. Tubulin polymerization disrupts cardiac beta-adrenergic regulation of late I<sub>Na</sub>. *Cardiovascular research*, 103, 168-177.
- EFIMOV, I. R., NIKOLSKI, V. P. & SALAMA, G. 2004. Optical imaging of the heart. *Circ Res*, 95, 21-33.
- EISNER, D. A. & SIPIDO, K. R. 2004. Sodium calcium exchange in the heart: necessity or luxury? *Circ Res*, 95, 549-51.
- FALLAVOLLITA, J. A., HEAVEY, B. M., LUISI, A. J., MICHALEK, S. M., BALDWA, S., MASHTARE, T. L., HUTSON, A. D., DEKEMP, R. A., HAKA, M. S., SAJJAD, M., CIMATO, T. R., CURTIS, A. B., CAIN, M. E. & CANTY, J. M. 2014. Regional Myocardial Sympathetic Denervation Predicts the Risk of Sudden Cardiac Arrest in Ischemic Cardiomyopathy. *Journal of the American College of Cardiology*, 63, 141-149.
- FARMAN, G. P., TACHAMPA, K., MATEJA, R., CAZORLA, O., LACAMPAGNE, A. & DE TOMBE, P. P. 2008. Blebbistatin: use as inhibitor of muscle contraction. *Pflugers Arch*, 455, 995-1005.
- FAST, V. G. 2005. Recording Action Potentials Using Voltage-Sensitive Dyes. In: DHEIN, S., MOHR, F. W. & DELMAR, M. (eds.) *Practical Methods in Cardiovascular Research*. Berlin, Heidelberg: Springer Berlin Heidelberg.
- FEDOROV, V. V., LOZINSKY, I. T., SOSUNOV, E. A., ANYUKHOVSKY, E. P., ROSEN, M. R., BALKE, C. W. & EFIMOV, I. R. 2007. Application of blebbistatin as an excitation-contraction uncoupler for electrophysiologic study of rat and rabbit hearts. *Heart Rhythm*, 4, 619-26.
- FLEMING, J. W., STRAWBRIDGE, R. A. & WATANABE, A. M. 1987. Muscarinic receptor regulation of cardiac adenylate cyclase activity. *J Mol Cell Cardiol*, 19, 47-61.

- FLEMING, W. W. 1962. Supersensitivity of the cat heart to catecholamine-induced arrhythmias following reserpine pretreatment. *Proc Soc Exp Biol Med*, 111, 484-6.
- FOREMAN, R. D., LINDEROTH, B., ARDELL, J. L., BARRON, K. W., CHANDLER, M. J., HULL, S. S., JR., TERHORST, G. J., DEJONGSTE, M. J. & ARMOUR, J. A. 2000. Modulation of intrinsic cardiac neurons by spinal cord stimulation: implications for its therapeutic use in angina pectoris. *Cardiovascular research*, 47, 367-375.
- FOSSA, A. A., GORCZYCA, W., WISIALOWSKI, T., YASGAR, A., WANG, E., CRIMIN, K., VOLBERG, W. & ZHOU, J. 2007. Electrical alternans and hemodynamics in the anesthetized guinea pig can discriminate the cardiac safety of antidepressants. *Journal of pharmacological and toxicological methods*, 55, 78-85.
- FOZZARD, H. A. 1992. Afterdepolarizations and triggered activity. *Basic Res Cardiol*, 87 Suppl 2, 105-13.
- FRANZ, M. R. 1999. Current status of monophasic action potential recording: theories, measurements and interpretations. *Cardiovasc Res*, 41, 25-40.
- FRANZ, M. R. 2003. The electrical restitution curve revisited: steep or flat slope--which is better? *J Cardiovasc Electrophysiol*, 14, S140-7.
- FUKUDA, K., KANAZAWA, H., AIZAWA, Y., ARDELL, J. L. & SHIVKUMAR, K. 2015. Cardiac innervation and sudden cardiac death. *Circulation research*, 116, 2005-2019.
- FUKUHARA, S., SAKURAI, A., SANO, H., YAMAGISHI, A., SOMEKAWA, S., TAKAKURA, N., SAITO, Y., KANGAWA, K. & MOCHIZUKI, N. 2005. Cyclic AMP potentiates vascular endothelial cadherin-mediated cell-cell contact to enhance endothelial barrier function through an Epac-Rap1 signaling pathway. *Molecular and cellular biology*, 25, 136-146.
- FURNIVAL, C. M., LINDEN, R. J. & SNOW, H. M. 1973. Chronotropic and inotropic effects on the dog heart of stimulating the efferent cardiac sympathetic nerves. *The Journal of physiology*, 230, 137-153.
- FURUKAWA, T., KIMURA, S., FURUKAWA, N., BASSETT, A. L. & MYERBURG, R. J. 1992. Potassium rectifier currents differ in myocytes of endocardial and epicardial origin. *Circ Res*, 70, 91-103.
- FURUKAWA, Y., WALLICK, D. W., CARLSON, M. D. & MARTIN, P. J. 1990. Cardiac electrical responses to vagal stimulation of fibers to discrete cardiac regions. *Am J Physiol*, 258, H1112-8.

- GARCIA-CALVO, R., CHORRO, F. J., SENDRA, M., ALBEROLA, A., SANCHIS, J., NAVARRO, J., VALENTIN, V., LOPEZ-MERINO, V. & SUCH, L. 1992. The effects of selective stellate ganglion manipulation on ventricular refractoriness and excitability. *Pacing Clin Electrophysiol*, 15, 1492-503.
- GARDNER, R. T. & HABECKER, B. A. 2013. Infarct-Derived Chondroitin Sulfate Proteoglycans Prevent Sympathetic Reinnervation after Cardiac Ischemia-Reperfusion Injury. *The Journal of Neuroscience*, 33, 7175-7183.
- GARDNER, R. T., WANG, L., LANG, B. T., CREGG, J. M., DUNBAR, C. L., WOODWARD, W. R., SILVER, J., RIPPLINGER, C. M. & HABECKER, B. A. 2015. Targeting protein tyrosine phosphatase  $\sigma$  after myocardial infarction restores cardiac sympathetic innervation and prevents arrhythmias. 6, 6235.
- GARFINKEL, A., KIM, Y. H., VOROSHILOVSKY, O., QU, Z., KIL, J. R., LEE, M. H., KARAGUEUZIAN, H. S., WEISS, J. N. & CHEN, P. S. 2000. Preventing ventricular fibrillation by flattening cardiac restitution. *Proc Natl Acad Sci U S A*, 97, 6061-6.
- GAZTANAGA, L., MARCHLINSKI, F. E. & BETENSKY, B. P. 2012. Mechanisms of cardiac arrhythmias. *Rev Esp Cardiol (Engl Ed)*, 65, 174-85.
- GEIS, W. P., KAYE, M. P. & RANDALL, W. C. 1973. Major autonomic pathways to the atria and S-A and A-V nodes of the canine heart. *Am J Physiol*, 224, 202-8.
- GETTES, L. S. & REUTER, H. 1974. Slow recovery from inactivation of inward currents in mammalian myocardial fibres. *The Journal of Physiology*, 240, 703-724.
- GILBEY, M.P. 1997. Fundamental Aspects of the Control of Sympathetic Preganglionic Neuronal Discharge, Central Nervous Control of Autonomic Function, *The Netherlands: Harwood Academic Publishers*; 1997. pp. 1–28.
- GIROUARD, S. D., LAURITA, K. R. & ROSENBAUM, D. S. 1996. Unique properties of cardiac action potentials recorded with voltage-sensitive dyes. *J Cardiovasc Electrophysiol*, 7, 1024-38.
- GLOERICH, M. & BOS, J. L. 2010. Epac: defining a new mechanism for cAMP action. *Annual Review of Pharmacology and Toxicology*, 50, 355-375.
- GOODALL, M. & KIRSHNER, N. 1956. Effect of cervico-thoracic ganglionectomy on the adrenaline and noradrenaline content in the mammalian heart. *J Clin Invest*, 35, 649-56.
- GORDON, L., WHARTON, J., GAER, J. A., INGLIS, G. C., TAYLOR, K. M. & POLAK, J. M. 1993. Quantitative immunohistochemical assessment of bovine myocardial innervation before and after cryosurgical cardiac denervation. *Cardiovascular research*, 27, 318-326.

- GRIMALDI, R., DE LUCA, A., KORNET, L., CASTAGNO, D. & GAITA, F. 2012. Can spinal cord stimulation reduce ventricular arrhythmias? *Heart Rhythm*, 9, 1884-7.
- GRUNNET, M. 2010. Repolarization of the cardiac action potential. Does an increase in repolarization capacity constitute a new anti-arrhythmic principle? *Acta physiologica (Oxford, England)*, 198 Suppl 676, 1-48.
- GUO, T., ZHANG, T., MESTRIL, R. & BERS, D. M. 2006. Ca<sup>2+</sup>/Calmodulin-dependent protein kinase II phosphorylation of ryanodine receptor does affect calcium sparks in mouse ventricular myocytes. *Circulation research*, 99, 398-406.
- HADLEY, R. W. & HUME, J. R. 1987. An intrinsic potential-dependent inactivation mechanism associated with calcium channels in guinea-pig myocytes. *J Physiol*, 389, 205-22.
- HADLEY, R. W. & HUME, J. R. 1988. Calcium channel antagonist properties of Bay K 8644 in single guinea pig ventricular cells. *Circ Res*, 62, 97-104.
- HAGEMAN, G. R., GOLDBERG, J. M., ARMOUR, J. A. & RANDALL, W. C. 1973. Cardiac dysrhythmias induced by autonomic nerve stimulation. *Am J Cardiol*, 32, 823-30.
- HAN, J. & MOE, G. K. 1964. Nonuniform recovery of excitability in ventricular muscle. *Circ Res*, 14, 44-60.
- HASAN, W., JAMA, A., DONOHUE, T., WERNLI, G., ONYSZCHUK, G., AL-HAFEZ, B., BILGEN, M. & SMITH, P. G. 2006. Sympathetic hyperinnervation and inflammatory cell NGF synthesis following myocardial infarction in rats. *Brain Research*, 1124, 142-154.
- HASENFUSS, G. 1998. Animal models of human cardiovascular disease, heart failure and hypertrophy. *Cardiovasc Res*, 39, 60-76.
- HAUSWIRTH, O., NOBLE, D. & TSIEN, R. W. 1972. The dependence of plateau currents in cardiac Purkinje fibres on the interval between action potentials. *The Journal of Physiology*, 222, 27-49.
- HAUTVAST, R. W., DEJONGSTE, M. J., STAAL, M. J., VAN GILST, W. H. & LIE, K. I. 1998. Spinal cord stimulation in chronic intractable angina pectoris: a randomized, controlled efficacy study. *Am Heart J*, 136, 1114-20.
- HAWS, C. W. & BURGESS, M. J. 1978. Effects of bilateral and unilateral stellate stimulation on canine ventricular refractory periods at sites overlapping innervation. *Circulation research*, 42, 195-198.

- HAWS, C. W. & LUX, R. L. 1990. Correlation between in vivo transmembrane action potential durations and activation-recovery intervals from electrograms. Effects of interventions that alter repolarization time. *Circulation*, 81, 281-8.
- HAYASHI, H., MIYAUCHI, Y., CHOU, C. C., KARAGUEUZIAN, H. S., CHEN, P. S. & LIN, S. F. 2003. Effects of cytochalasin D on electrical restitution and the dynamics of ventricular fibrillation in isolated rabbit heart. *J Cardiovasc Electrophysiol*, 14, 1077-84.
- HELMS, M. N., CHEN, X. J., RAMOSEVAC, S., EATON, D. C. & JAIN, L. 2006. Dopamine regulation of amiloride-sensitive sodium channels in lung cells. *American journal of physiology. Lung cellular and molecular physiology*, 290, L710-L722.
- HERING, D., LAMBERT, E. A., MARUSIC, P., WALTON, A. S., KRUM, H., LAMBERT, G. W., ESLER, M. D. & SCHLAICH, M. P. 2013. Substantial reduction in single sympathetic nerve firing after renal denervation in patients with resistant hypertension. *Hypertension*, 61, 457-64.
- HERRMANN, C., WRAY, J., TRAVERS, F. & BARMAN, T. 1992. Effect of 2,3-butanedione monoxime on myosin and myofibrillar ATPases. An example of an uncompetitive inhibitor. *Biochemistry*, 31, 12227-32.
- HERTTING, G. & SCHIEFTHALER, T. 1964. The Effect of Stellate Ganglion Excision on the Catecholamine Content and the Uptake of H3-Norepinephrine in the Heart of the Cat. *Int J Neuropharmacol*, 3, 65-9.
- HIKOSAKA, H. 1966. The effects of stellate ganglionectomy on the distribution, uptake and storage of noradrenaline in the dog heart. *Jpn J Pharmacol*, 16, 157-64.
- HIRST, R. A., HARRISON, C., HIROTA, K. & LAMBERT, D. G. 2006. Measurement of [Ca<sup>2+</sup>]<sub>i</sub> in whole cell suspensions using fura-2. *Methods in molecular biology (Clifton, N.J.)*, 312, 37-45.
- HJALMARSON, A. 1997. Effects of beta blockade on sudden cardiac death during acute myocardial infarction and the postinfarction period. *Am J Cardiol*, 80, 35J-39J.
- HODES, R. 1939. Exercise in the sympathectomized cat. *Am J Physiol* 126: 171-179.
- HOFFMAN, B. F., CRANFIELD, P. F., LEPESCHKIN, E., SURAWICZ, B. & HERRLICH, H. C. 1959. Comparison of cardiac monophasic action potentials recorded by intracellular and suction electrodes. *Am J Physiol*, 196, 1297-301.
- HOLZ, G. G., KANG, G., HARBECK, M., ROE, M. W. & CHEPURNY, O. G. 2006. Cell physiology of cAMP sensor Epac. *The Journal of physiology*, 577, 5-15.
- HONEGGER, K. J., CAPUANO, P., WINTER, C., BACIC, D., STANGE, G., WAGNER, C. A., BIBER, J., MURER, H. & HERNANDO, N. 2006. Regulation of sodium-

- proton exchanger isoform 3 (NHE3) by PKA and exchange protein directly activated by cAMP (EPAC). *Proceedings of the National Academy of Sciences of the United States of America*, 103, 803-808.
- HOPKINS, D. A. & ARMOUR, J. A. 1984. Localization of sympathetic postganglionic and parasympathetic preganglionic neurons which innervate different regions of the dog heart. *The Journal of comparative neurology*, 229, 186-198.
- HOTHI, S. S., GURUNG, I. S., HEATHCOTE, J. C., ZHANG, Y., BOOTH, S. W., SKEPPER, J. N., GRACE, A. A. & HUANG, C. L. 2008. Epac activation, altered calcium homeostasis and ventricular arrhythmogenesis in the murine heart. *Pflugers Archiv : European journal of physiology*, 457, 253-270.
- HUGENHOLTZ, P. G. 1962. Electrocardiographic abnormalities in cerebral disorders. Report of six cases and review of the literature. *American Heart Journal*, 63, 451-461.
- IDEKER, R. E., SMITH, W. M., BLANCHARD, S. M., REISER, S. L., SIMPSON, E. V., WOLF, P. D. & DANIELEY, N. D. 1989. The assumptions of isochronal cardiac mapping. *Pacing Clin Electrophysiol*, 12, 456-78.
- ITO, H. & ONO, K. 1995. A rapidly activating delayed rectifier K<sup>+</sup> channel in rabbit sinoatrial node cells. *Am J Physiol*, 269, H443-52.
- JACOBSON, A. F., SENIOR, R., CERQUEIRA, M. D., WONG, N. D., THOMAS, G. S., LOPEZ, V. A., AGOSTINI, D., WEILAND, F., CHANDNA, H. & NARULA, J. 2010. Myocardial Iodine-123 Meta-Iodobenzylguanidine Imaging and Cardiac Events in Heart Failure. *Journal of the American College of Cardiology*, 55, 2212-2221.
- JALIFE, J., MORLEY, G. E., TALLINI, N. Y. & VAIDYA, D. 1998. A fungal metabolite that eliminates motion artifacts. *J Cardiovasc Electrophysiol*, 9, 1358-62.
- JÄNIG, W. 2006. *The integrative action of the autonomic nervous system: Neurobiology of homeostasis*. Cambridge University Press, Cambridge.
- JANIG, W. 1986. Spinal cord integration of visceral sensory systems and sympathetic nervous system reflexes. *Prog Brain Res*. 67, 255-276.
- JANSE, M. J. 2004. Electrophysiological changes in heart failure and their relationship to arrhythmogenesis. *Cardiovasc Res*, 61, 208-17.
- JANSE, M. J., SCHWARTZ, P. J., WILMS-SCHOPMAN, F., PETERS, R. J. & DURRER, D. 1985. Effects of unilateral stellate ganglion stimulation and ablation on electrophysiologic changes induced by acute myocardial ischemia in dogs. *Circulation*, 72, 585-95.

- JANVIER, N. C., MCMORN, S. O., HARRISON, S. M., TAGGART, P. & BOYETT, M. R. 1997. The Role of Na<sup>+</sup>-Ca<sup>2+</sup> Exchange Current in Electrical Restitution in Ferret Ventricular Cells. *The Journal of Physiology*, 504, 301-314.
- JONNESCO, T. 1921. Traitement chirurgical de l'angine de poitrine par la résection du sympathique cervico-thoracique. *Presse Med*, 20, 221-230.
- JOST, N., PAPP, J. G. & VARRO, A. 2007. Slow delayed rectifier potassium current (IKs) and the repolarization reserve. *Ann Noninvasive Electrocardiol*, 12, 64-78.
- JOU, C. J., SPITZER, K. W. & TRISTANI-FIROUZI, M. 2010. Blebbistatin effectively uncouples the excitation-contraction process in zebrafish embryonic heart. *Cell Physiol Biochem*, 25, 419-24.
- KAMOSINSKA, B., NOWICKI, D., SZULCZYK, A. & SZULCZYK, P. 1991. Spinal segmental sympathetic outflow to cervical sympathetic trunk, vertebral nerve, inferior cardiac nerve and sympathetic fibres in the thoracic vagus. *Journal of the Autonomic Nervous System*, 32, 199-204.
- KANG, G., CHEPURNY, O. G. & HOLZ, G. G. 2001. cAMP-regulated guanine nucleotide exchange factor II (Epac2) mediates Ca<sup>2+</sup>-induced Ca<sup>2+</sup> release in INS-1 pancreatic beta-cells. *The Journal of physiology*, 536, 375-385.
- KANG, G., CHEPURNY, O. G., MALESTER, B., RINDLER, M. J., REHMANN, H., BOS, J. L., SCHWEDE, F., COETZEE, W. A. & HOLZ, G. G. 2006. cAMP sensor Epac as a determinant of ATP-sensitive potassium channel activity in human pancreatic beta cells and rat INS-1 cells. *The Journal of physiology*, 573, 595-609.
- KANG, G., CHEPURNY, O. G., RINDLER, M. J., COLLIS, L., CHEPURNY, Z., LI, W. H., HARBECK, M., ROE, M. W. & HOLZ, G. G. 2005. A cAMP and Ca<sup>2+</sup> coincidence detector in support of Ca<sup>2+</sup>-induced Ca<sup>2+</sup> release in mouse pancreatic beta cells. *The Journal of physiology*, 566, 173-188.
- KANG, G., JOSEPH, J. W., CHEPURNY, O. G., MONACO, M., WHEELER, M. B., BOS, J. L., SCHWEDE, F., GENIESER, H. G. & HOLZ, G. G. 2003. Epac-selective cAMP analog 8-pCPT-2'-O-Me-cAMP as a stimulus for Ca<sup>2+</sup>-induced Ca<sup>2+</sup> release and exocytosis in pancreatic beta-cells. *The Journal of biological chemistry*, 278, 8279-8285.
- KARMA, A. 1993. Spiral breakup in model equations of action potential propagation in cardiac tissue. *Physical Review Letters*, 71, 1103-1106.
- KARMA, A. 1994. Electrical alternans and spiral wave breakup in cardiac tissue. *Chaos*, 4, 461-472.

- KAWASAKI, H., SPRINGETT, G. M., MOCHIZUKI, N., TOKI, S., NAKAYA, M., MATSUDA, M., HOUSMAN, D. E. & GRAYBIEL, A. M. 1998. A family of cAMP-binding proteins that directly activate Rap1. *Science (New York, N.Y.)*, 282, 2275-2279.
- KAZUSA, K., NAKAMURA, Y., WATANABE, Y., ANDO, K. & SUGIYAMA, A. 2014. Effects of pH on nifekalant-induced electrophysiological change assessed in the Langendorff heart model of guinea pigs. *Journal of pharmacological sciences*, 124, 153-159.
- KEAST, J. R., LUCKENSMEYER, G. B. & SCHEMANN, M. 1995. All pelvic neurons in male rats contain immunoreactivity for the synthetic enzymes of either noradrenaline or acetylcholine. *Neurosci Lett*, 196, 209-12.
- KETTLEWELL, S., WALKER, N. L., COBBE, S. M., BURTON, F. L. & SMITH, G. L. 2004. The electrophysiological and mechanical effects of 2,3-butane-dione monoxime and cytochalasin-D in the Langendorff perfused rabbit heart. *Exp Physiol*, 89, 163-72.
- KIMURA, K., KANAZAWA, H., IEDA, M., KAWAGUCHI-MANABE, H., MIYAKE, Y., YAGI, T., ARAI, T., SANO, M. & FUKUDA, K. 2010. Norepinephrine-induced nerve growth factor depletion causes cardiac sympathetic denervation in severe heart failure. *Autonomic Neuroscience*, 156, 27-35.
- KIRPEKAR, S. M., CERVONI, P. & FURCHGOTT, R. F. 1962. Catecholamine content of the cat nictitating membrane following procedures sensitizing it to norepinephrine. *J Pharmacol Exp Ther*, 135, 180-90.
- KNISLEY, S. B. 1995. Transmembrane voltage changes during unipolar stimulation of rabbit ventricle. *Circ Res*, 77, 1229-39.
- KOCSIS, B. & GYIMESI-PELCZER, K. 1998. Spinal segments communicating resting sympathetic activity to postganglionic nerves of the stellate ganglion. *The American Journal of Physiology*, 275, R400-9.
- KOLEGA, J. 2004. Phototoxicity and photoinactivation of blebbistatin in UV and visible light. *Biochem Biophys Res Commun*, 320, 1020-5.
- KOSTREVA, D. R., ZUPERKU, E. J., CUSICK, J. F. & KAMPINE, J. P. 1977. Ventral root mapping of cardiac nerves in the canine using evoked potentials. *The American Journal of Physiology*, 232, H590-5.
- KOVACS, M., TOTH, J., HETENYI, C., MALNASI-CSIZMADIA, A. & SELLERS, J. R. 2004. Mechanism of blebbistatin inhibition of myosin II. *J Biol Chem*, 279, 35557-63.

- KRALIOS, F. A., MARTIN, L., BURGESS, M. J. & MILLAR, K. 1975. Local ventricular repolarization changes due to sympathetic nerve-branch stimulation. *Am J Physiol*, 228, 1621-6.
- KUMAR, R., WILDERS, R., JOYNER, R. W., JONGSMA, H. J., VERHEIJCK, E. E., GOLOD, D. A., VAN GINNEKEN, A. C. G. & GOOLSBY, W. N. 1996. Experimental Model for an Ectopic Focus Coupled to Ventricular Cells. *Circulation*, 94, 833-841.
- KUO, C. S., MUNAKATA, K., REDDY, C. P. & SURAWICZ, B. 1983. Characteristics and Possible Mechanism of Ventricular Arrhythmia Dependent on the Dispersion of Action-Potential Durations. *Circulation*, 67, 1356-1367.
- LA ROVERE, M. T., BIGGER, J. T., JR., MARCUS, F. I., MORTARA, A. & SCHWARTZ, P. J. 1998. Baroreflex sensitivity and heart-rate variability in prediction of total cardiac mortality after myocardial infarction. ATRAMI (Autonomic Tone and Reflexes After Myocardial Infarction) Investigators. *Lancet (London, England)*, 351, 478-484.
- LAHAT, H., EL DAR, M., LEVY-NISSENBAUM, E., BAHAN, T., FRIEDMAN, E., KHOURY, A., LORBER, A., KASTNER, D. L., GOLDMAN, B. & PRAS, E. 2001. Autosomal recessive catecholamine- or exercise-induced polymorphic ventricular tachycardia: clinical features and assignment of the disease gene to chromosome 1p13-21. *Circulation*, 103, 2822-7.
- LAITINEN, P. J., BROWN, K. M., PIIPPO, K., SWAN, H., DEVANEY, J. M., BRAHMBHATT, B., DONARUM, E. A., MARINO, M., TISO, N., VIITASALO, M., TOIVONEN, L., STEPHAN, D. A. & KONTULA, K. 2001. Mutations of the cardiac ryanodine receptor (RyR2) gene in familial polymorphic ventricular tachycardia. *Circulation*, 103, 485-90.
- LANGENDORFF, O. 1895. Untersuchungen am uberlebenden Säugethierherzen. *Pflügers Arch*, 61, 291–332.
- LAROCHE-JOUBERT, N., MARSY, S., MICHELET, S., IMBERT-TEBOUL, M. & DOUCET, A. 2002. Protein kinase A-independent activation of ERK and H,K-ATPase by cAMP in native kidney cells: role of Epac I. *The Journal of biological chemistry*, 277, 18598-18604.
- LARRABEE, M. G. & BRONK, D. W. 1947. Prolonged facilitation of synaptic excitation in sympathetic ganglia. *J Neurophysiol*, 10, 139-54.
- LAURITA, K. R. & SINGAL, A. 2001. Mapping action potentials and calcium transients simultaneously from the intact heart. *Am J Physiol Heart Circ Physiol*, 280, H2053-60.

- LEHMAN, W., CRAIG, R. & VIBERT, P. 1994. Ca<sup>2+</sup>-induced tropomyosin movement in Limulus thin filaments revealed by three-dimensional reconstruction. *Nature*, 368, 65-7.
- LEVI, A. J., DALTON, G. R., HANCOX, J. C., MITCHESON, J. S., ISSBERNER, J., BATES, J. A., EVANS, S. J., HOWARTH, F. C., HOBAL, I. A. & JONES, J. V. 1997. Role of intracellular sodium overload in the genesis of cardiac arrhythmias. *J Cardiovasc Electrophysiol*, 8, 700-21.
- LEWIS, D. I., SERMASI, E. & COOTE, J. H. 1993. Excitatory and indirect inhibitory actions of 5-hydroxytryptamine on sympathetic preganglionic neurones in the neonate rat spinal cord in vitro. *Brain research*, 610, 267-275.
- LI, G. R., LAU, C. P., DUCHARME, A., TARDIF, J. C. & NATTEL, S. 2002. Transmural action potential and ionic current remodeling in ventricles of failing canine hearts. *Am J Physiol Heart Circ Physiol*, 283, H1031-41.
- LI, G. R., LAU, C. P., LEUNG, T. K. & NATTEL, S. 2004a. Ionic current abnormalities associated with prolonged action potentials in cardiomyocytes from diseased human right ventricles. *Heart Rhythm*, 1, 460-8.
- LI, W., KNOWLTON, D., VAN WINKLE, D. M. & HABECKER, B. A. 2004b. Infarction alters both the distribution and noradrenergic properties of cardiac sympathetic neurons. *American Journal of Physiology - Heart and Circulatory Physiology*, 286, H2229-H2236.
- LIANG, C. S. 2007. Cardiac sympathetic nerve terminal function in congestive heart failure. *Acta Pharmacol Sin*, 28, 921-7.
- LIAO, K., YU, L., ZHOU, X., SAREN, G., WANG, S., WANG, Z., HUANG, B., YANG, K. & JIANG, H. 2015. Low-level baroreceptor stimulation suppresses atrial fibrillation by inhibiting ganglionated plexus activity. *Can J Cardiol*, 31, 767-74.
- LICHTMAN, J. W. & CONCHELLO, J. A. 2005. Fluorescence microscopy. *Nat Methods*, 2, 910-9.
- LICHTMAN, J. W., PURVES, D. & YIP, J. W. 1980. Innervation of sympathetic neurones in the guinea-pig thoracic chain. *J Physiol*, 298, 285-99.
- LINZ, D., MAHFOUD, F., SCHOTTEN, U., UKENA, C., HOHL, M., NEUBERGER, H. R., WIRTH, K. & BOHM, M. 2013a. Renal sympathetic denervation provides ventricular rate control but does not prevent atrial electrical remodeling during atrial fibrillation. *Hypertension*, 61, 225-31.
- LINZ, D., MAHFOUD, F., SCHOTTEN, U., UKENA, C., NEUBERGER, H. R., WIRTH, K. & BOHM, M. 2013b. Effects of electrical stimulation of carotid baroreflex and

- renal denervation on atrial electrophysiology. *J Cardiovasc Electrophysiol*, 24, 1028-33.
- LIU, D. W. & ANTZELEVITCH, C. 1995. Characteristics of the delayed rectifier current (IKr and IKs) in canine ventricular epicardial, midmyocardial, and endocardial myocytes. A weaker IKs contributes to the longer action potential of the M cell. *Circ Res*, 76, 351-65.
- LIU, Y.-B., WU, C.-C., LU, L.-S., SU, M.-J., LIN, C.-W., LIN, S.-F., CHEN, L. S., FISHBEIN, M. C., CHEN, P.-S. & LEE, Y.-T. 2003. Sympathetic Nerve Sprouting, Electrical Remodeling, and Increased Vulnerability to Ventricular Fibrillation in Hypercholesterolemic Rabbits. *Circulation Research*, 92, 1145-1152.
- LIU, Y., CABO, C., SALOMONSZ, R., DELMAR, M., DAVIDENKO, J. & JALIFE, J. 1993. Effects of diacetyl monoxime on the electrical properties of sheep and guinea pig ventricular muscle. *Cardiovasc Res*, 27, 1991-7.
- LOEW, L. M., COHEN, L. B., DIX, J., FLUHLER, E. N., MONTANA, V., SALAMA, G. & WU, J. Y. 1992. A naphthyl analog of the aminostyryl pyridinium class of potentiometric membrane dyes shows consistent sensitivity in a variety of tissue, cell, and model membrane preparations. *J Membr Biol*, 130, 1-10.
- LOPSHIRE, J. C., ZHOU, X., DUSA, C., UEYAMA, T., ROSENBERGER, J., COURTNEY, N., UJHELYI, M., MULLEN, T., DAS, M. & ZIPES, D. P. 2009. Spinal cord stimulation improves ventricular function and reduces ventricular arrhythmias in a canine postinfarction heart failure model. *Circulation*, 120, 286-94.
- LOWN, B., EHRLICH, L., LIPSCHULTZ, B. & BLAKE, J. 1961. Effect of digitalis in patients receiving reserpine. *Circulation*, 24, 1185-91.
- LUKAS, A. & ANTZELEVITCH, C. 1996. Phase 2 reentry as a mechanism of initiation of circus movement reentry in canine epicardium exposed to simulated ischemia. *Cardiovasc Res*, 32, 593-603.
- LUNDBERG, J. M., FRANCO-CERECEDA, A., LACROIX, J. S. & PERNOW, J. 1991. Release of vasoactive peptides from autonomic and sensory nerves. *Blood Vessels*, 28, 27-34.
- MADAMANCHI, A. 2007. Beta-adrenergic receptor signaling in cardiac function and heart failure. *Mcgill J Med*, 10, 99-104.
- MAESAKO, M., ARAKI, J., LEE, S., DOI, Y., IMAOKA, T., IRIBE, G., MOHRI, S., HIRAKAWA, M., HARADA, M. & SUGA, H. 2000. 2,3-Butanedione monoxime suppresses primarily total calcium handling in canine heart. *Jpn J Physiol*, 50, 543-51.

- MAHAJAN, A., MOORE, J., CESARIO, D. A. & SHIVKUMAR, K. 2005. Use of thoracic epidural anesthesia for management of electrical storm: a case report. *Heart Rhythm*, 2, 1359-62.
- MALLIANI, A., SCHWARTZ, P. J. & ZANCHETTI, A. 1980. Neural mechanisms in life-threatening arrhythmias. *Am Heart J*, 100, 705-15.
- MANGMOOL, S., SHUKLA, A. K. & ROCKMAN, H. A. 2010. beta-Arrestin-dependent activation of Ca(2+)/calmodulin kinase II after beta(1)-adrenergic receptor stimulation. *The Journal of cell biology*, 189, 573-587.
- MANGONI, M. E. & NARGEOT, J. 2008. Genesis and regulation of the heart automaticity. *Physiol Rev*, 88, 919-82.
- MANNHEIMER, C., ELIASSON, T., ANDERSSON, B., BERGH, C. H., AUGUSTINSSON, L. E., EMANUELSSON, H. & WAAGSTEIN, F. 1993. Effects of spinal cord stimulation in angina pectoris induced by pacing and possible mechanisms of action. *BMJ*, 307, 477-80.
- MANNING, J.W., COTTON, M.D.V. 1962. Mechanism of cardiac arrhythmias induced by diencephalic stimulation. *Am. J. Phys.* 203, 1120–1124.
- MANTRAVADI, R., GABRIS, B., LIU, T., CHOI, B. R., DE GROAT, W. C., NG, G. A. & SALAMA, G. 2007. Autonomic nerve stimulation reverses ventricular repolarization sequence in rabbit hearts. *Circ Res*, 100, e72-80.
- MARRON, K., WHARTON, J., SHEPPARD, M. N., GULBENKIAN, S., ROYSTON, D., YACOUB, M. H., ANDERSON, R. H. & POLAK, J. M. 1994. Human endocardial innervation and its relationship to the endothelium: an immunohistochemical, histochemical, and quantitative study. *Cardiovascular research*, 28, 1490-1499.
- MAYATI, A., LEVOIN, N., PARIS, H., N'DIAYE, M., COURTOIS, A., URIAC, P., LAGADIC-GOSSMANN, D., FARDEL, O. & LE FERREC, E. 2012. Induction of intracellular calcium concentration by environmental benzo(a)pyrene involves a beta2-adrenergic receptor/adenylyl cyclase/Epac-1/inositol 1,4,5-trisphosphate pathway in endothelial cells. *The Journal of biological chemistry*, 287, 4041-4052.
- MCKILLOP, D. F., FORTUNE, N. S., RANATUNGA, K. W. & GEEVES, M. A. 1994. The influence of 2,3-butanedione 2-monoxime (BDM) on the interaction between actin and myosin in solution and in skinned muscle fibres. *J Muscle Res Cell Motil*, 15, 309-18.
- MEISSNER, A., ECKARDT, L., KIRCHHOF, P., WEBER, T., ROLF, N., BREITHARDT, G., VAN AKEN, H. & HAVERKAMP, W. 2001. Effects of thoracic epidural anesthesia with and without autonomic nervous system blockade on cardiac

- monophasic action potentials and effective refractoriness in awake dogs. *Anesthesiology*, 95, 132-8; discussion 6A.
- MELGARI, D., BRACK, K. E., ZHANG, C., ZHANG, Y., EL HARCHI, A., MITCHESON, J. S., DEMPSEY, C. E., NG, G. A. & HANCOX, J. C. 2015. hERG potassium channel blockade by the HCN channel inhibitor bradycardic agent ivabradine. *Journal of the American Heart Association*, 4, 10.1161/JAHA.115.001813.
- METRICH, M., LUCAS, A., GASTINEAU, M., SAMUEL, J. L., HEYMES, C., MOREL, E. & LEZOUALC'H, F. 2008. Epac mediates beta-adrenergic receptor-induced cardiomyocyte hypertrophy. *Circulation research*, 102, 959-965.
- MOE, A. E., MARX, S., BANANI, N., LIU, M., MARQUARDT, B. & WILSON, D. M. 2005. Improvements in LED-based fluorescence analysis systems. *Sensors and Actuators B: Chemical*, 111–112, 230-241.
- MOREL, E., MARCANTONI, A., GASTINEAU, M., BIRKEDAL, R., ROCHAIS, F., GARNIER, A., LOMPRES, A. M., VANDECASTEELE, G. & LEZOUALC'H, F. 2005. cAMP-binding protein Epac induces cardiomyocyte hypertrophy. *Circulation research*, 97, 1296-1304.
- MYLES, R. C., BERNUS, O., BURTON, F. L., COBBE, S. M. & SMITH, G. L. 2010. Effect of activation sequence on transmural patterns of repolarization and action potential duration in rabbit ventricular myocardium. *American Journal of Physiology-Heart and Circulatory Physiology*, 299, H1812-H1822.
- MYLES, R. C., WANG, L., KANG, C., BERS, D. M. & RIPPLINGER, C. M. 2012. Local beta-adrenergic stimulation overcomes source-sink mismatch to generate focal arrhythmia. *Circ Res*, 110, 1454-64.
- NATHAN, D. & BEELER, G. W., JR. 1975. Electrophysiologic correlates of the inotropic effects of Isoproterenol in canine myocardium. *Journal of Molecular and Cellular Cardiology*, 7, 1-15.
- NATTEL, S. 2008. Delayed-rectifier potassium currents and the control of cardiac repolarization: Noble and Tsien 40 years after. *The Journal of Physiology*, 586, 5849-5852.
- NERBONNE, J. M. & GUO, W. 2002. Heterogeneous expression of voltage-gated potassium channels in the heart: roles in normal excitation and arrhythmias. *J Cardiovasc Electrophysiol*, 13, 406-9.
- NERBONNE, J. M. & KASS, R. S. 2005. Molecular physiology of cardiac repolarization. *Physiol Rev*, 85, 1205-53.

- NG, G. A. 2016a. Feasibility of selection of antiarrhythmic drug treatment on the basis of arrhythmogenic mechanism - Relevance of electrical restitution, wavebreak and rotors. *Pharmacol Ther.*
- NG, G. A. 2016b. Neuro-cardiac interaction in malignant ventricular arrhythmia and sudden cardiac death. *Autonomic Neuroscience : Basic & Clinical.*
- NG, G. A. 2017. Feasibility of selection of antiarrhythmic drug treatment on the basis of arrhythmogenic mechanism - Relevance of electrical restitution, wavebreak and rotors. *Pharmacol Ther*, 176, 1-12.
- NG, G. A., BRACK, K. E. & COOTE, J. H. 2001. Effects of direct sympathetic and vagus nerve stimulation on the physiology of the whole heart--a novel model of isolated Langendorff perfused rabbit heart with intact dual autonomic innervation. *Experimental physiology*, 86, 319-329.
- NG, G. A., BRACK, K. E., PATEL, V. H. & COOTE, J. H. 2007. Autonomic modulation of electrical restitution, alternans and ventricular fibrillation initiation in the isolated heart. *Cardiovascular research*, 73, 750-760.
- NG, G. A., COBBE, S. M. & SMITH, G. L. 1998. Non-uniform prolongation of intracellular Ca<sup>2+</sup> transients recorded from the epicardial surface of isolated hearts from rabbits with heart failure. *Cardiovasc Res*, 37, 489-502.
- NG, G. A., MANTRAVADI, R., WALKER, W. H., ORTIN, W. G., CHOI, B. R., DE GROAT, W. & SALAMA, G. 2009. Sympathetic nerve stimulation produces spatial heterogeneities of action potential restitution. *Heart rhythm : the official journal of the Heart Rhythm Society*, 6, 696-706.
- NICOLSON, W. B., MCCANN, G. P., BROWN, P. D., SANDILANDS, A. J., STAFFORD, P. J., SCHLINDWEIN, F. S., SAMANI, N. J. & NG, G. A. 2012. A novel surface electrocardiogram-based marker of ventricular arrhythmia risk in patients with ischemic cardiomyopathy. *J Am Heart Assoc*, 1, e001552.
- NINOMIYA, I., MALPAS, S. C., MATSUKAWA, K., SHINDO, T. & AKIYAMA, T. 1993. The amplitude of synchronized cardiac sympathetic nerve activity reflects the number of activated pre- and postganglionic fibers in anesthetized cats. *Journal of the Autonomic Nervous System*, 45, 139-147.
- NJA, A. & PURVES, D. 1977. Specific innervation of guinea-pig superior cervical ganglion cells by preganglionic fibres arising from different levels of the spinal cord. *J Physiol*, 264, 565-83.
- NOLASCO, J. B. & DAHLEN, R. W. 1968. A graphic method for the study of alternation in cardiac action potentials. *J Appl Physiol*, 25, 191-6.

- NORRIS, J. E., FOREMAN, R. D. & WURSTER, R. K. 1974. Responses of the canine heart to stimulation of the first five ventral thoracic roots. *The American Journal of Physiology*, 227, 9-12.
- NORRIS, J. E., LIPPINCOTT, D. & WURSTER, R. D. 1977. Responses of canine endocardium to stimulation of the upper thoracic roots. *The American Journal of Physiology*, 233, H655-9.
- NORRIS, J. E. & RANDALL, W. C. 1977. Responses of the canine myocardium to stimulation of thoracic cardiac nerves. *Am J Physiol*, 232, H485-94.
- NOVARA, M., BALDELLI, P., CAVALLARI, D., CARABELLI, V., GIANCIPPOLI, A. & CARBONE, E. 2004. Exposure to cAMP and beta-adrenergic stimulation recruits Ca(V)<sub>3</sub> T-type channels in rat chromaffin cells through Epac cAMP-receptor proteins. *The Journal of physiology*, 558, 433-449.
- NYKJAER, A., LEE, R., TENG, K. K., JANSEN, P., MADSEN, P., NIELSEN, M. S., JACOBSEN, C., KLIEMANNEL, M., SCHWARZ, E., WILLNOW, T. E., HEMPSTEAD, B. L. & PETERSEN, C. M. 2004. Sortilin is essential for proNGF-induced neuronal cell death. *Nature*, 427, 843-848.
- OESTREICH, E. A., MALIK, S., GOONASEKERA, S. A., BLAXALL, B. C., KELLEY, G. G., DIRKSEN, R. T. & SMRCKA, A. V. 2009. Epac and phospholipase Cepsilon regulate Ca<sup>2+</sup> release in the heart by activation of protein kinase Cepsilon and calcium-calmodulin kinase II. *The Journal of biological chemistry*, 284, 1514-1522.
- OESTREICH, E. A., WANG, H., MALIK, S., KAPROTH-JOSLIN, K. A., BLAXALL, B. C., KELLEY, G. G., DIRKSEN, R. T. & SMRCKA, A. V. 2007. Epac-mediated activation of phospholipase C(epsilon) plays a critical role in beta-adrenergic receptor-dependent enhancement of Ca<sup>2+</sup> mobilization in cardiac myocytes. *The Journal of biological chemistry*, 282, 5488-5495.
- OGRODNIK, J. & NIGGLI, E. 2010. Increased Ca(2+) leak and spatiotemporal coherence of Ca(2+) release in cardiomyocytes during beta-adrenergic stimulation. *J Physiol*, 588, 225-42.
- OLGIN, J. E., TAKAHASHI, T., WILSON, E., VERECKEI, A., STEINBERG, H. & ZIPES, D. P. 2002. Effects of thoracic spinal cord stimulation on cardiac autonomic regulation of the sinus and atrioventricular nodes. *Journal of Cardiovascular Electrophysiology*, 13, 475-481.
- OPPENHEIMER, S. M. 1994. Neurogenic cardiac effects of cerebrovascular disease. *Current opinion in neurology*, 7, 20-24.

- OPTHOF, T., MISIER, A. R., CORONEL, R., VERMEULEN, J. T., VERBERNE, H. J., FRANK, R. G., MOULIJN, A. C., VAN CAPELLE, F. J. & JANSE, M. J. 1991. Dispersion of refractoriness in canine ventricular myocardium. Effects of sympathetic stimulation. *Circ Res*, 68, 1204-15.
- OSADCHII, O. E. 2012a. Effects of ventricular pacing protocol on electrical restitution assessments in guinea-pig heart. *Experimental physiology*, 97, 807-821.
- OSADCHII, O. E. 2012b. Electrophysiological determinants of arrhythmic susceptibility upon endocardial and epicardial pacing in guinea-pig heart. *Acta physiologica (Oxford, England)*, 205, 494-506.
- OSADCHII, O. E. 2014a. Impact of hypokalemia on electromechanical window, excitation wavelength and repolarization gradients in guinea-pig and rabbit hearts. *PLoS one*, 9, e105599.
- OSADCHII, O. E. 2014b. Impaired epicardial activation-repolarization coupling contributes to the proarrhythmic effects of hypokalaemia and dofetilide in guinea pig ventricles. *Acta physiologica (Oxford, England)*, 211, 48-60.
- OSADCHII, O. E. 2014c. Reduced intrinsic heart rate is associated with reduced arrhythmic susceptibility in guinea-pig heart. *Scandinavian Cardiovascular Journal : SCJ*, 48, 357-367.
- OSADCHII, O. E., BENTZEN, B. H. & OLESEN, S. P. 2009. Chamber-specific effects of hypokalaemia on ventricular arrhythmogenicity in isolated, perfused guinea-pig heart. *Experimental physiology*, 94, 434-446.
- OSADCHII, O. E., LARSEN, A. P. & OLESEN, S. P. 2010. Predictive value of electrical restitution in hypokalemia-induced ventricular arrhythmogenicity. *American journal of physiology.Heart and circulatory physiology*, 298, H210-20.
- OSADCHII, O. E., SOLTYSINSKA, E. & OLESEN, S. P. 2011. Na<sup>+</sup> channel distribution and electrophysiological heterogeneities in guinea pig ventricular wall. *American journal of physiology.Heart and circulatory physiology*, 300, H989-1002.
- PANDIT, S. V. & JALIFE, J. 2013. Rotors and the Dynamics of Cardiac Fibrillation. *Circulation Research*, 112, 849.
- PARDINI, B. J., LUND, D. D. & SCHMID, P. G. 1989. Organization of the sympathetic postganglionic innervation of the rat heart. *Journal of the Autonomic Nervous System*, 28, 193-201.
- PARDINI, B. J. & WURSTER, R. D. 1984. Identification of the sympathetic preganglionic pathway to the cat stellate ganglion. *J Auton Nerv Syst*, 11, 13-25.
- PARKER, I. 2003. Photonics for biologists. *Methods Enzymol*, 360, 345-82.

- PEREIRA, L., CHENG, H., LAO, D. H., NA, L., VAN OORT, R. J., BROWN, J. H., WEHRENS, X. H., CHEN, J. & BERS, D. M. 2013. Epac2 mediates cardiac beta1-adrenergic-dependent sarcoplasmic reticulum Ca<sup>2+</sup> leak and arrhythmia. *Circulation*, 127, 913-922.
- PEREIRA, L., METRICH, M., FERNANDEZ-VELASCO, M., LUCAS, A., LEROY, J., PERRIER, R., MOREL, E., FISCHMEISTER, R., RICHARD, S., BENITAH, J. P., LEZOUALC'H, F. & GOMEZ, A. M. 2007. The cAMP binding protein Epac modulates Ca<sup>2+</sup> sparks by a Ca<sup>2+</sup>/calmodulin kinase signalling pathway in rat cardiac myocytes. *The Journal of physiology*, 583, 685-694.
- PEREIRA, L., RUIZ-HURTADO, G., MOREL, E., LAURENT, A. C., METRICH, M., DOMINGUEZ-RODRIGUEZ, A., LAUTON-SANTOS, S., LUCAS, A., BENITAH, J. P., BERS, D. M., LEZOUALC'H, F. & GOMEZ, A. M. 2012. Epac enhances excitation-transcription coupling in cardiac myocytes. *Journal of Molecular and Cellular Cardiology*, 52, 283-291.
- PIERCE, M. L., DEUCHARS, J. & DEUCHARS, S. A. 2010. Spontaneous rhythmogenic capabilities of sympathetic neuronal assemblies in the rat spinal cord slice. *Neuroscience*, 170, 827-838.
- PIESKE, B., MAIER, L. S. & SCHMIDT-SCHWEDA, S. 2002. Sarcoplasmic reticulum Ca<sup>2+</sup> load in human heart failure. *Basic research in cardiology*, 97 Suppl 1, 163-71.
- POGWIZD, S. M. & BERS, D. M. 2004. Cellular basis of triggered arrhythmias in heart failure. *Trends Cardiovasc Med*, 14, 61-6.
- POLLACK, G. H. 1977. Cardiac pacemaking: an obligatory role of catecholamines? *Science*, 196, 731-8.
- POPPE, H., RYBALKIN, S. D., REHMANN, H., HINDS, T. R., TANG, X. B., CHRISTENSEN, A. E., SCHWEDE, F., GENIESER, H. G., BOS, J. L., DOSKELAND, S. O., BEAVO, J. A. & BUTT, E. 2008. Cyclic nucleotide analogs as probes of signaling pathways. *Nature methods*, 5, 277-278.
- POTAPOVA, I. A., COHEN, I. S. & DORONIN, S. V. 2007. Voltage-gated ion channel Kv4.3 is associated with Rap guanine nucleotide exchange factors and regulates angiotensin receptor type 1 signaling to small G-protein Rap. *The FEBS journal*, 274, 4375-4384.
- PRACEJUS, N. H., FARMER, D. G. & MCALLEN, R. M. 2015. Segmental origins of cardiac sympathetic nerve activity in rats. *Autonomic Neuroscience : Basic & Clinical*, 187, 45-49.

- PRIOLA, D. V. 1969. Individual chamber sensitivity to norepinephrine after unilateral cardiac denervation. *Am J Physiol*, 216, 604-14.
- PRIORI, S. G., MANTICA, M. & SCHWARTZ, P. J. 1988. Delayed afterdepolarizations elicited in vivo by left stellate ganglion stimulation. *Circulation*, 78, 178-185.
- PRIORI, S. G., NAPOLITANO, C., MEMMI, M., COLOMBI, B., DRAGO, F., GASPARINI, M., DESIMONE, L., COLTORTI, F., BLOISE, R., KEEGAN, R., CRUZ FILHO, F. E., VIGNATI, G., BENATAR, A. & DELOGU, A. 2002. Clinical and molecular characterization of patients with catecholaminergic polymorphic ventricular tachycardia. *Circulation*, 106, 69-74.
- PRIORI, S. G., NAPOLITANO, C., TISO, N., MEMMI, M., VIGNATI, G., BLOISE, R., SORRENTINO, V. & DANIELI, G. A. 2001. Mutations in the cardiac ryanodine receptor gene (hRyR2) underlie catecholaminergic polymorphic ventricular tachycardia. *Circulation*, 103, 196-200.
- PURVES, G. I., KAMISHIMA, T., DAVIES, L. M., QUAYLE, J. M. & DART, C. 2009. Exchange protein activated by cAMP (Epac) mediates cAMP-dependent but protein kinase A-insensitive modulation of vascular ATP-sensitive potassium channels. *The Journal of physiology*, 587, 3639-3650.
- QIN, D., ZHANG, Z. H., CAREF, E. B., BOUTJDIR, M., JAIN, P. & EL-SHERIF, N. 1996. Cellular and ionic basis of arrhythmias in postinfarction remodeled ventricular myocardium. *Circ Res*, 79, 461-73.
- QIN, H., KAY, M. W., CHATTIPAKORN, N., REDDEN, D. T., IDEKER, R. E. & ROGERS, J. M. 2003. Effects of heart isolation, voltage-sensitive dye, and electromechanical uncoupling agents on ventricular fibrillation. *Am J Physiol Heart Circ Physiol*, 284, H1818-26.
- QIN, M., LIU, T., HU, H., WANG, T., YU, S. & HUANG, C. 2013. Effect of isoprenaline chronic stimulation on APD restitution and ventricular arrhythmogenesis. *Journal of cardiology*, 61, 162-168.
- RAAKE, P. W., ZHANG, X., VINGE, L. E., BRINKS, H., GAO, E., JALEEL, N., LI, Y., TANG, M., MOST, P., DORN, G. W., HOUSER, S. R., KATUS, H. A., CHEN, X. & KOCH, W. J. 2012. Cardiac G-Protein-Coupled Receptor Kinase 2 Ablation Induces a Novel Ca<sup>2+</sup> Handling Phenotype Resistant to Adverse Alterations and Remodeling After Myocardial Infarction. *Circulation*, 125, 2108.
- RANDALL, W.C. 1977. Sympathetic Control of the Heart. In: Randall,W.C. (Ed.), *Neural Regulation of the Heart*. Oxford University Press, New York, pp. 45–94.
- RANDALL, W. C., ARMOUR, J. A., GEIS, W. P. & LIPPINCOTT, D. B. 1972. Regional cardiac distribution of the sympathetic nerves. *Fed Proc*, 31, 1199-208.

- RANDALL, W. C. & MCNALLY, H. 1960. Augmentor action of the sympathetic cardiac nerves in man. *Journal of applied physiology*, 15, 629-631.
- RANDALL, W. C., RINKEMA, L. E. & JONES, S. B. 1984. Local epicardial chemical ablation of vagal input to sino-trial and atrioventricular regions of the canine heart. *J Auton Nerv Syst*, 11, 145-59.
- RANDALL, W. C. & ROHSE, W. G. 1956. The augmentor action of the sympathetic cardiac nerves. *Circulation research*, 4, 470-475.
- RANDALL, W. C., SZENTIVANYI, M., PACE, J. B., WECHSLER, J. S. & KAYE, M. P. 1968a. Patterns of sympathetic nerve projections onto the canine heart. *Circulation research*, 22, 315-323.
- RANDALL, W. C., WECHSLER, J. S., PACE, J. B. & SZENTIVANYI, M. 1968b. Alterations in myocardial contractility during stimulation of the cardiac nerves. *Am J Physiol*, 214, 1205-12.
- RANGARAJAN, S., ENSERINK, J. M., KUIPERIJ, H. B., DE ROOIJ, J., PRICE, L. S., SCHWEDE, F. & BOS, J. L. 2003. Cyclic AMP induces integrin-mediated cell adhesion through Epac and Rap1 upon stimulation of the beta 2-adrenergic receptor. *The Journal of cell biology*, 160, 487-493.
- RASKIN, J. S., LIU, J. J., SUN, H., NEMECEK, A., BALAJI, S. & RASLAN, A. M. 2016. Minimal access posterior approach for extrapleural thoracic sympathectomy: a cadaveric study and cases. *World neurosurgery*.
- REHMANN, H., SCHWEDE, F., DOSKELAND, S. O., WITTINGHOFER, A. & BOS, J. L. 2003. Ligand-mediated activation of the cAMP-responsive guanine nucleotide exchange factor Epac. *The Journal of biological chemistry*, 278, 38548-38556.
- REIKEN, S., WEHRENS, X. H., VEST, J. A., BARBONE, A., KLOTZ, S., MANCINI, D., BURKHOFF, D. & MARKS, A. R. 2003. Beta-blockers restore calcium release channel function and improve cardiac muscle performance in human heart failure. *Circulation*, 107, 2459-2466.
- RICCIO, M. L., KOLLER, M. L. & GILMOUR, R. F. 1999. Electrical Restitution and Spatiotemporal Organization During Ventricular Fibrillation. *Circulation Research*, 84, 955.
- RIO, C. L. D., HAMLIN, R. L. & BILLMAN, G. E. 2016. Myocardial Electrotonic Coupling Modulates Repolarization Heterogeneities in vivo: Implications for the Assessment of Pro-Arrhythmic Liabilities in vitro and in silico. *The FASEB Journal*, 30, 1274.7-1274.7.
- RIPPLINGER, C. M., NOUJAIM, S. F. & LINZ, D. 2016. The nervous heart. *Prog Biophys Mol Biol*, 120, 199-209.

- ROBERTS, O. L., KAMISHIMA, T., BARRETT-JOLLEY, R., QUAYLE, J. M. & DART, C. 2013. Exchange protein activated by cAMP (Epac) induces vascular relaxation by activating Ca<sup>2+</sup>-sensitive K<sup>+</sup> channels in rat mesenteric artery. *The Journal of physiology*, 591, 5107-5123.
- ROGERS, M. C., ABILDSKOV, J. A. & PRESTON, J. B. 1973. Cardiac effects of stimulation and block of the stellate ganglion. *Anesthesiology*, 39, 525-33.
- ROHDE, G. K., DAWANT, B. M. & LIN, S. F. 2005. Correction of motion artifact in cardiac optical mapping using image registration. *IEEE Trans Biomed Eng*, 52, 338-41.
- ROSE, J., ARMOUNDAS, A. A., TIAN, Y., DISILVESTRE, D., BURYSEK, M., HALPERIN, V., O'ROURKE, B., KASS, D. A., MARBAN, E. & TOMASELLI, G. F. 2005. Molecular correlates of altered expression of potassium currents in failing rabbit myocardium. *Am J Physiol Heart Circ Physiol*, 288, H2077-87.
- ROSENBAUM, D. 2001. In: Rosenbaum DS JJ (Ed.) *Optical Mapping of Cardiac Excitation and Arrhythmias*. Armonk, NY: Futura, 2-7.
- ROZANSKI, G. J., XU, Z., WHITNEY, R. T., MURAKAMI, H. & ZUCKER, I. H. 1997. Electrophysiology of rabbit ventricular myocytes following sustained rapid ventricular pacing. *J Mol Cell Cardiol*, 29, 721-32.
- RUBART, M. & ZIPES, D. P. 2005. Mechanisms of sudden cardiac death. *J Clin Invest*, 115, 2305-15.
- RUBIN, E. & PURVES, D. 1980. Segmental organization of sympathetic preganglionic neurons in the mammalian spinal cord. *J Comp Neurol*, 192, 163-74.
- RUECKSCHLOSS, U. & ISENBERG, G. 2001. Cytochalasin D reduces Ca<sup>2+</sup> currents via cofilin-activated depolymerization of F-actin in guinea-pig cardiomyocytes. *J Physiol*, 537, 363-70.
- RUIZ-HURTADO, G., DOMINGUEZ-RODRIGUEZ, A., PEREIRA, L., FERNANDEZ-VELASCO, M., CASSAN, C., LEZOUALC'H, F., BENITAH, J. P. & GOMEZ, A. M. 2012. Sustained Epac activation induces calmodulin dependent positive inotropic effect in adult cardiomyocytes. *Journal of Molecular and Cellular Cardiology*, 53, 617-625.
- RUIZ-HURTADO, G., MOREL, E., DOMINGUEZ-RODRIGUEZ, A., LLACH, A., LEZOUALC'H, F., BENITAH, J. P. & GOMEZ, A. M. 2013. Epac in cardiac calcium signaling. *J Mol Cell Cardiol*, 58, 162-71.
- SAG, C. M., WADSACK, D. P., KHABBAZZADEH, S., ABESSER, M., GREFE, C., NEUMANN, K., OPIELA, M. K., BACKS, J., OLSON, E. N., BROWN, J. H., NEEF, S., MAIER, S. K. & MAIER, L. S. 2009. Calcium/calmodulin-dependent protein

- kinase II contributes to cardiac arrhythmogenesis in heart failure. *Circulation.Heart failure*, 2, 664-675.
- SALAMA, G., LOMBARDI, R. & ELSON, J. 1987. Maps of optical action potentials and NADH fluorescence in intact working hearts. *Am J Physiol*, 252, H384-94.
- SALAMA, G. & MORAD, M. 1976. Merocyanine 540 as an optical probe of transmembrane electrical activity in the heart. *Science*, 191, 485-7.
- SAMAAN, A. 1935. Muscular work in dogs submitted to different conditions of cardiac and splanchnic innervations. *J Physiol*, 83, 313-31.
- SASAKI, S., DAITOKU, K., IWASA, A. & MOTOMURA, S. 2000. NO is involved in MCh-induced accentuated antagonism via type II PDE in the canine blood-perfused SA node. *Am J Physiol Heart Circ Physiol*, 279, H2509-18.
- SCHMIDT, M., DEKKER, F. J. & MAARSINGH, H. 2013. Exchange protein directly activated by cAMP (epac): a multidomain cAMP mediator in the regulation of diverse biological functions. *Pharmacological reviews*, 65, 670-709.
- SCHMIDT, M., EVELLIN, S., WEERNINK, P. A., VON DORP, F., REHMANN, H., LOMASNEY, J. W. & JAKOBS, K. H. 2001. A new phospholipase-C-calcium signalling pathway mediated by cyclic AMP and a Rap GTPase. *Nature cell biology*, 3, 1020-1024.
- SCHMIDT, M., SAND, C., JAKOBS, K. H., MICHEL, M. C. & WEERNINK, P. A. 2007. Epac and the cardiovascular system. *Current opinion in pharmacology*, 7, 193-200.
- SCHRICKER, A. A., LALANI, G. G., KRUMMEN, D. E. & NARAYAN, S. M. 2014. Rotors as Drivers of Atrial Fibrillation and Targets for Ablation. *Current Cardiology Reports*, 16, 509.
- SCHWARTZ, P. J. 1984. The rationale and the role of left stellectomy for the prevention of malignant arrhythmias. *Ann N Y Acad Sci*, 427, 199-221.
- SCHWARTZ, P. J. 2010. Efficacy of left cardiac sympathetic denervation has an unforeseen side effect: medicolegal complications. *Heart rhythm : the official journal of the Heart Rhythm Society*, 7, 1330-1332.
- SCHWARTZ, P. J. 2014. Cardiac sympathetic denervation to prevent life-threatening arrhythmias. *Nat Rev Cardiol*, 11, 346-53.
- SCHWARTZ, P. J. & MALLIANI, A. 1975. Electrical alternation of the T-wave: clinical and experimental evidence of its relationship with the sympathetic nervous system and with the long Q-T syndrome. *Am Heart J*, 89, 45-50.
- SCHWARTZ, P. J., PRIORI, S. G., CERRONE, M., SPAZZOLINI, C., ODERO, A., NAPOLITANO, C., BLOISE, R., DE FERRARI, G. M., KLERSY, C., MOSS, A. J.,

- ZAREBA, W., ROBINSON, J. L., HALL, W. J., BRINK, P. A., TOIVONEN, L., EPSTEIN, A. E., LI, C. & HU, D. 2004. Left cardiac sympathetic denervation in the management of high-risk patients affected by the long-QT syndrome. *Circulation*, 109, 1826-1833.
- SCHWARTZ, P. J., SNEBOLD, N. G. & BROWN, A. M. 1976a. Effects of unilateral cardiac sympathetic denervation on the ventricular fibrillation threshold. *The American Journal of Cardiology*, 37, 1034-1040.
- SCHWARTZ, P. J. & STONE, H. L. 1979. Effects of unilateral stellectomy upon cardiac performance during exercise in dogs. *Circ Res*, 44, 637-45.
- SCHWARTZ, P. J. & STONE, H. L. 1982a. Left stellectomy and denervation supersensitivity in conscious dogs. *Am J Cardiol*, 49, 1185-90.
- SCHWARTZ, P. J. & STONE, H. L. 1982b. The role of the autonomic nervous system in sudden coronary death. *Ann N Y Acad Sci*, 382, 162-80.
- SCHWARTZ, P. J., STONE, H. L. & BROWN, A. M. 1976b. Effects of unilateral stellate ganglion blockade on the arrhythmias associated with coronary occlusion. *Am Heart J*, 92, 589-99.
- SCHWARTZ, P. J., VERRIER, R. L. & LOWN, B. 1977. Effect of stellectomy and vagotomy on ventricular refractoriness in dogs. *Circ Res*, 40, 536-40.
- SEINO, S. & SHIBASAKI, T. 2005. PKA-dependent and PKA-independent pathways for cAMP-regulated exocytosis. *Physiological Reviews*, 85, 1303-1342.
- SELLIN, L. C. & MCARDLE, J. J. 1994. Multiple effects of 2,3-butanedione monoxime. *Pharmacol Toxicol*, 74, 305-13.
- SERONE, A. P. & ANGUS, J. A. 1999. Neuropeptide Y is a prejunctional inhibitor of vagal but not sympathetic inotropic responses in guinea-pig isolated left atria. *Br J Pharmacol*, 127, 383-90.
- SHANNON, T. R., POGWIZD, S. M. & BERS, D. M. 2003. Elevated sarcoplasmic reticulum Ca<sup>2+</sup> leak in intact ventricular myocytes from rabbits in heart failure. *Circ Res*, 93, 592-4.
- SHEN, M. J. & ZIPES, D. P. 2014. Role of the autonomic nervous system in modulating cardiac arrhythmias. *Circulation research*, 114, 1004-1021.
- SHERIDAN, D. J., PENKOSKE, P. A., SOBEL, B. E. & CORR, P. B. 1980. Alpha adrenergic contributions to dysrhythmia during myocardial ischemia and reperfusion in cats. *J Clin Invest*, 65, 161-71.
- SHIBASAKI, T., TAKAHASHI, H., MIKI, T., SUNAGA, Y., MATSUMURA, K., YAMANAKA, M., ZHANG, C., TAMAMOTO, A., SATOH, T., MIYAZAKI, J. & SEINO, S. 2007. Essential role of Epac2/Rap1 signaling in regulation of insulin

- granule dynamics by cAMP. *Proceedings of the National Academy of Sciences of the United States of America*, 104, 19333-19338.
- SMANI, T., CALDERON-SANCHEZ, E., GOMEZ-HURTADO, N., FERNANDEZ-VELASCO, M., CACHOFEIRO, V., LAHERA, V., ORDONEZ, A. & DELGADO, C. 2010. Mechanisms underlying the activation of L-type calcium channels by urocortin in rat ventricular myocytes. *Cardiovascular research*, 87, 459-466.
- SMITH, F. M. 1999. Extrinsic inputs to intrinsic neurons in the porcine heart in vitro. *The American Journal of Physiology*, 276, R455-67.
- SMITH, F. M., VERMEULEN, M. & CARDINAL, R. 2016. Long-term spinal cord stimulation modifies canine intrinsic cardiac neuronal properties and ganglionic transmission during high-frequency repetitive activation. *Physiological Reports*, 4.
- SMRCKA, A. V., OESTREICH, E. A., BLAXALL, B. C. & DIRKSEN, R. T. 2007. EPAC regulation of cardiac EC coupling. *The Journal of physiology*, 584, 1029-1031.
- SNYDERS, D. J. 1999. Structure and function of cardiac potassium channels. *Cardiovasc Res*, 42, 377-90.
- SOLTYSINSKA, E., OLESEN, S. P. & OSADCHII, O. E. 2011. Myocardial structural, contractile and electrophysiological changes in the guinea-pig heart failure model induced by chronic sympathetic activation. *Experimental physiology*, 96, 647-663.
- SOMEKAWA, S., FUKUHARA, S., NAKAOKA, Y., FUJITA, H., SAITO, Y. & MOCHIZUKI, N. 2005. Enhanced functional gap junction neofunction by protein kinase A-dependent and Epac-dependent signals downstream of cAMP in cardiac myocytes. *Circulation research*, 97, 655-662.
- SOUTHERLAND, E. M., MILHORN, D. M., FOREMAN, R. D., LINDEROTH, B., DEJONGSTE, M. J., ARMOUR, J. A., SUBRAMANIAN, V., SINGH, M., SINGH, K. & ARDELL, J. L. 2007. Preemptive, but not reactive, spinal cord stimulation mitigates transient ischemia-induced myocardial infarction via cardiac adrenergic neurons. *Am J Physiol Heart Circ Physiol*, 292, H311-7.
- SPACH, M. S. & BARR, R. C. 1975. Ventricular intramural and epicardial potential distributions during ventricular activation and repolarization in the intact dog. *Circ Res*, 37, 243-57.
- SPANSWICK, D., PICKERING, A. E., GIBSON, I. C. & LOGAN, S. D. 1994. Inhibition of sympathetic preganglionic neurons by spinal glycinergic interneurons. *Neuroscience*, 62, 205-216.

- SPEAR, J. F., MICHELSON, E. L. & MOORE, E. N. 1983. Reduced space constant in slowly conducting regions of chronically infarcted canine myocardium. *Circ Res*, 53, 176-85.
- SPURGEON, H. A., PRIOLA, D. V., MONTOYA, P., WEISS, G. K. & ALTER, W. A., 3RD 1974. Catecholamines associated with conductile and contractile myocardium of normal and denervated dog hearts. *J Pharmacol Exp Ther*, 190, 466-71.
- SRIVASTAVA, S.C., ROBSON, A.O. 1964. Electrocardiographic abnormalities associated with subarachnoid haemorrhage. *Lancet*, 2, 431-433.
- STARAS, K., CHANG, H. S. & GILBEY, M. P. 2001. Resetting of sympathetic rhythm by somatic afferents causes post-reflex coordination of sympathetic activity in rat. *The Journal of physiology*, 533, 537-545.
- STARK, G., SCHWARZL, I., STARK, U., DECRINIS, M. & TRITTHART, H. A. 1996. Rate-dependent effects of ajmaline and propafenone on atrioventricular conduction. *European journal of pharmacology*, 310, 29-35.
- STER, J., DE BOCK, F., GUERINEAU, N. C., JANOSSY, A., BARRERE-LEMAIRE, S., BOS, J. L., BOCKAERT, J. & FAGNI, L. 2007. Exchange protein activated by cAMP (Epac) mediates cAMP activation of p38 MAPK and modulation of Ca<sup>2+</sup>-dependent K<sup>+</sup> channels in cerebellar neurons. *Proceedings of the National Academy of Sciences of the United States of America*, 104, 2519-2524.
- STRACK, A. M., SAWYER, W. B., HUGHES, J. H., PLATT, K. B. & LOEWY, A. D. 1989. A general pattern of CNS innervation of the sympathetic outflow demonstrated by transneuronal pseudorabies viral infections. *Brain research*, 491, 156-162.
- STRAIGHT, A. F., CHEUNG, A., LIMOUZE, J., CHEN, I., WESTWOOD, N. J., SELLERS, J. R. & MITCHISON, T. J. 2003. Dissecting temporal and spatial control of cytokinesis with a myosin II inhibitor. *Science*, 299, 1743-7.
- SULAKHE, P. V. & VO, X. T. 1995. Regulation of phospholamban and troponin-I phosphorylation in the intact rat cardiomyocytes by adrenergic and cholinergic stimuli: roles of cyclic nucleotides, calcium, protein kinases and phosphatases and depolarization. *Mol Cell Biochem*, 149-150, 103-26.
- SUNDARAM, K., MURUGAIAN, J., KRIEGER, A. & SAPRU, H. 1989a. Microinjections of cholinergic agonists into the intermediolateral cell column of the spinal cord at T1-T3 increase heart rate and contractility. *Brain Res*, 503, 22-31.
- SUNDARAM, K., MURUGAIAN, J. & SAPRU, H. 1989b. Cardiac responses to the microinjections of excitatory amino acids into the intermediolateral cell column of the rat spinal cord. *Brain Res*, 482, 12-22.

- SURAWICZ, B. 1997. Ventricular fibrillation and dispersion of repolarization. *J Cardiovasc Electrophysiol*, 8, 1009-12.
- SUSZKIW, J. B. 2012. Chapter 32 - Synaptic Transmission A2 - Sperelakis, Nicholas. *Cell Physiology Source Book (Fourth Edition)*. San Diego: Academic Press.
- SZABO, G., SZENTANDRASSY, N., BIRO, T., TOTH, B. I., CZIFRA, G., MAGYAR, J., BANYASZ, T., VARRO, A., KOVACS, L. & NANASI, P. P. 2005. Asymmetrical distribution of ion channels in canine and human left-ventricular wall: epicardium versus midmyocardium. *Pflugers Arch*, 450, 307-16.
- SZENTADRASSY, N., BANYASZ, T., BIRO, T., SZABO, G., TOTH, B. I., MAGYAR, J., LAZAR, J., VARRO, A., KOVACS, L. & NANASI, P. P. 2005. Apico-basal inhomogeneity in distribution of ion channels in canine and human ventricular myocardium. *Cardiovasc Res*, 65, 851-60.
- SZENTIVANYI, M., PACE, J. B., WECHSLER, J. S. & RANDALL, W. C. 1967. Localized myocardial responses to stimulation of cardiac sympathetic nerves. *Circulation research*, 21, 691-702.
- SZULCZYK, A. & SZULCZYK, P. 1987. Spinal segmental preganglionic outflow to cervical sympathetic trunk and postganglionic cardiac sympathetic nerves. *Brain research*, 421, 127-134.
- TAGGART, P., CRITCHLEY, H., VAN DUIJVENDODEN, S. & LAMBIASE, P. D. 2016. Significance of neuro-cardiac control mechanisms governed by higher regions of the brain. *Auton Neurosci*, 199, 54-65.
- TAGGART, P., SUTTON, P., CHALABI, Z., BOYETT, M. R., SIMON, R., ELLIOTT, D. & GILL, J. S. 2003. Effect of adrenergic stimulation on action potential duration restitution in humans. *Circulation*, 107, 285-9.
- TAGGART, P., SUTTON, P., LAB, M., DEAN, J. & HARRISON, F. 1990. Interplay between adrenaline and interbeat interval on ventricular repolarisation in intact heart in vivo. *Cardiovasc Res*, 24, 884-95.
- TAMARGO, J., CABALLERO, R., GOMEZ, R., VALENZUELA, C. & DELPON, E. 2004. Pharmacology of cardiac potassium channels. *Cardiovasc Res*, 62, 9-33.
- TAN, A. Y., ZHOU, S., JUNG, B. C., OGAWA, M., CHEN, L. S., FISHBEIN, M. C. & CHEN, P. S. 2008. Ectopic atrial arrhythmias arising from canine thoracic veins during in vivo stellate ganglia stimulation. *American journal of physiology. Heart and circulatory physiology*, 295, H691-8.
- TATARCHENKO, L. A., IVANOV, A. & SKOK, V. I. 1990. Organization of the tonically active pathways through the superior cervical ganglion of the rabbit. *J Auton Nerv Syst*, 30 Suppl, S163-8.

- TER HORST, G. J., HAUTVAST, R. W., DE JONGSTE, M. J. & KORF, J. 1996. Neuroanatomy of cardiac activity-regulating circuitry: a transneuronal retrograde viral labelling study in the rat. *Eur J Neurosci*, 8, 2029-41.
- TER HORST, G. J., VAN DEN BRINK, A., HOMMINGA, S. A., HAUTVAST, R. W., RAKHORST, G., METTENLEITER, T. C., DE JONGSTE, M. J., LIE, K. I. & KORF, J. 1993. Transneuronal viral labelling of rat heart left ventricle controlling pathways. *Neuroreport*, 4, 1307-10.
- THOMAS, D., KARLE, C. A. & KIEHN, J. 2006. The cardiac hERG/IKr potassium channel as pharmacological target: structure, function, regulation, and clinical applications. *Curr Pharm Des*, 12, 2271-83.
- TOMITA, T., TAKEI, M., SAIKAWA, Y., HANAOKA, T., UCHIKAWA, S., TSUTSUI, H., ARUGA, M., MIYASHITA, T., YAZAKI, Y., IMAMURA, H., KINOSHITA, O., OWA, M. & KUBO, K. 2003. Role of autonomic tone in the initiation and termination of paroxysmal atrial fibrillation in patients without structural heart disease. *Journal of cardiovascular electrophysiology*, 14, 559-564.
- TRENDELENBURG, U. & WEINER, N. 1962. Sensitivity of the nictitating membrane after various procedures and agents. *J Pharmacol Exp Ther*, 136, 152-61.
- TSE, H.-F., TURNER, S., SANDERS, P., OKUYAMA, Y., FUJII, K., CHEUNG, C.-W., RUSSO, M., GREEN, M. D. S., YIU, K.-H., CHEN, P., SHUTO, C., LAU, E. O. Y. & SIU, C.-W. 2015. Thoracic Spinal Cord Stimulation for Heart Failure as a Restorative Treatment (SCS HEART study): First-in-man experience. *Heart Rhythm*, 12, 588-595.
- TWEEDIE, D., O'GARA, P., HARDING, S. E. & MACLEOD, K. T. 1997. The effect of alterations to action potential duration on beta-adrenoceptor-mediated aftercontractions in human and guinea-pig ventricular myocytes. *Journal of Molecular and Cellular Cardiology*, 29, 1457-1467.
- UEDA, H., SUGIMOTO, T., MURAO, S., GOTO, H., KATO, K., KATAYAMA, S. & ITO, K. 1962. Changes in cardiac rate and rhythm produced by electrical stimulation of the brain stem of dogs. *Japanese heart journal*, 3, 455-475.
- UEDA, H., YANAI, Y., MURAO, S., HARUMI, K., MASHIMA, S., KUROIWA, A., SUGIMOTO, T. & SHIMOMURA, D. 1964. Electrocardiographic and Vectorcardiographic Changes Produced by Electrical Stimulation of the Cardiac Nerves. *Jpn Heart J*, 5, 359-72.
- UENO, H., SHIBASAKI, T., IWANAGA, T., TAKAHASHI, K., YOKOYAMA, Y., LIU, L. M., YOKOI, N., OZAKI, N., MATSUKURA, S., YANO, H. & SEINO, S. 2001.

- Characterization of the gene EPAC2: structure, chromosomal localization, tissue expression, and identification of the liver-specific isoform. *Genomics*, 78, 91-98.
- UIJTDEHAAGE, S. H. & THAYER, J. F. 2000. Accentuated antagonism in the control of human heart rate. *Clin Auton Res*, 10, 107-10.
- ULUCAN, C., WANG, X., BALJINNYAM, E., BAI, Y., OKUMURA, S., SATO, M., MINAMISAWA, S., HIROTANI, S. & ISHIKAWA, Y. 2007. Developmental changes in gene expression of Epac and its upregulation in myocardial hypertrophy. *American journal of physiology.Heart and circulatory physiology*, 293, H1662-72.
- UNDROVINAS, A. I., SHANDER, G. S. & MAKIELSKI, J. C. 1995. Cytoskeleton modulates gating of voltage-dependent sodium channel in heart. *Am J Physiol*, 269, H203-14.
- VAN STEE, E. W. 1978. Autonomic innervation of the heart. *Environmental health perspectives*, 26, 151-158.
- VARRO, A., LATHROP, D. A., HESTER, S. B., NANASI, P. P. & PAPP, J. G. 1993. Ionic currents and action potentials in rabbit, rat, and guinea pig ventricular myocytes. *Basic Res Cardiol*, 88, 93-102.
- VASEGHI, M., GIMA, J., KANAAN, C., AJIJOLA, O. A., MARMUREANU, A., MAHAJAN, A. & SHIVKUMAR, K. 2014. Cardiac sympathetic denervation in patients with refractory ventricular arrhythmias or electrical storm: intermediate and long-term follow-up. *Heart rhythm : the official journal of the Heart Rhythm Society*, 11, 360-366.
- VASEGHI, M., LUX, R. L., MAHAJAN, A. & SHIVKUMAR, K. 2012a. Sympathetic stimulation increases dispersion of repolarization in humans with myocardial infarction. *Am J Physiol Heart Circ Physiol*, 302, H1838-46.
- VASEGHI, M., YAMAKAWA, K., SINHA, A., SO, E. L., ZHOU, W., AJIJOLA, O. A., LUX, R. L., LAKS, M., SHIVKUMAR, K. & MAHAJAN, A. 2013. Modulation of regional dispersion of repolarization and T-peak to T-end interval by the right and left stellate ganglia. *Am J Physiol Heart Circ Physiol*, 305, H1020-30.
- VASEGHI, M., ZHOU, W., SHI, J., AJIJOLA, O. A., HADAYA, J., SHIVKUMAR, K. & MAHAJAN, A. 2012b. Sympathetic innervation of the anterior left ventricular wall by the right and left stellate ganglia. *Heart Rhythm*, 9, 1303-9.
- VASSALLE, M., LEVINE, M. J. & STUCKEY, J. H. 1968. On the sympathetic control of ventricular automaticity. The effects of stellate ganglion stimulation. *Circulation research*, 23, 249-258.

- VATNER, D. E., LAVALLEE, M., AMANO, J., FINIZOLA, A., HOMCY, C. J. & VATNER, S. F. 1985. Mechanisms of supersensitivity to sympathomimetic amines in the chronically denervated heart of the conscious dog. *Circulation Research*, 57, 55.
- VERRIER, R. L., THOMPSON, P. L. & LOWN, B. 1974. Ventricular vulnerability during sympathetic stimulation: role of heart rate and blood pressure. *Cardiovascular research*, 8, 602-610.
- VISWANATHAN, P. C. & RUDY, Y. 2000. Cellular arrhythmogenic effects of congenital and acquired long-QT syndrome in the heterogeneous myocardium. *Circulation*, 101, 1192-8.
- VOLDERS, P. G., STENGL, M., VAN OPSTAL, J. M., GERLACH, U., SPATJENS, R. L., BEEKMAN, J. D., SIPIDO, K. R. & VOS, M. A. 2003. Probing the contribution of IKs to canine ventricular repolarization: key role for beta-adrenergic receptor stimulation. *Circulation*, 107, 2753-60.
- WAINGER, B. J., DEGENNARO, M., SANTORO, B., SIEGELBAUM, S. A. & TIBBS, G. R. 2001. Molecular mechanism of cAMP modulation of HCN pacemaker channels. *Nature*, 411, 805-10.
- WALTON, R. D., BENSON, A. P., HARDY, M. E., WHITE, E. & BERNUS, O. 2013. Electrophysiological and structural determinants of electrotonic modulation of repolarization by the activation sequence. *Front Physiol*, 4, 281.
- WANG, S., ZHOU, X., HUANG, B., WANG, Z., ZHOU, L., CHEN, M., YU, L. & JIANG, H. 2016. Spinal cord stimulation suppresses atrial fibrillation by inhibiting autonomic remodeling. *Heart Rhythm*, 13, 274-81.
- WANG, Y., YUAN, J., QIAN, Z., ZHANG, X., CHEN, Y., HOU, X. & ZOU, J. 2015. Beta2 Adrenergic Receptor Activation Governs Cardiac Repolarization and Arrhythmogenesis in a Guinea Pig Model of Heart Failure. *Scientific reports*, 5, 7681.
- WEHRENS, X. H., LEHNART, S. E. & MARKS, A. R. 2005. Intracellular calcium release and cardiac disease. *Annu Rev Physiol*, 67, 69-98.
- WEISS, J. N., KARMA, A., SHIFERAW, Y., CHEN, P. S., GARFINKEL, A. & QU, Z. 2006. From pulsus to pulseless: the saga of cardiac alternans. *Circ Res*, 98, 1244-53.
- WESTFALL, D. P. & FLEMING, W. W. 1968. The sensitivity of the guinea-pig pacemaker to norepinephrine and calcium after pretreatment with reserpine. *J Pharmacol Exp Ther*, 164, 259-69.
- WHARTON, J., POLAK, J. M., GORDON, L., BANNER, N. R., SPRINGALL, D. R., ROSE, M., KHAGANI, A., WALLWORK, J. & YACOUB, M. H. 1990.

- Immunohistochemical demonstration of human cardiac innervation before and after transplantation. *Circulation research*, 66, 900-912.
- WILDE, A. A., BHUIYAN, Z. A., CROTTI, L., FACCHINI, M., DE FERRARI, G. M., PAUL, T., FERRANDI, C., KOOLBERGEN, D. R., ODERO, A. & SCHWARTZ, P. J. 2008. Left cardiac sympathetic denervation for catecholaminergic polymorphic ventricular tachycardia. *The New England journal of medicine*, 358, 2024-2029.
- WINTER, J., TANKO, A. S., BRACK, K. E., COOTE, J. H. & NG, G. A. 2012. Differential cardiac responses to unilateral sympathetic nerve stimulation in the isolated innervated rabbit heart. *Autonomic Neuroscience : Basic & Clinical*, 166, 4-14.
- WOLK, R., COBBE, S. M., HICKS, M. N. & KANE, K. A. 1999. Functional, structural, and dynamic basis of electrical heterogeneity in healthy and diseased cardiac muscle: implications for arrhythmogenesis and anti-arrhythmic drug therapy. *Pharmacol Ther*, 84, 207-31.
- WU, G., DESIMONE, C. V., SUDDENDORF, S. H., ASIRVATHAM, R. S., ASIRVATHAM, S. J., HUANG, C., CHEN, P. S. & CHA, Y. M. 2016. Effects of stepwise denervation of the stellate ganglion: Novel insights from an acute canine study. *Heart rhythm : the official journal of the Heart Rhythm Society*, 13, 1395-1401.
- WU, J., BIERMANN, M., RUBART, M. & ZIPES, D. P. 1998. Cytochalasin D as excitation-contraction uncoupler for optically mapping action potentials in wedges of ventricular myocardium. *J Cardiovasc Electrophysiol*, 9, 1336-47.
- XIE, Y., SATO, D., GARFINKEL, A., QU, Z. & WEISS, J. N. 2010. So Little Source, So Much Sink: Requirements for Afterdepolarizations to Propagate in Tissue. *Biophysical Journal*, 99, 1408-1415.
- YAMAGUCHI, N., XU, L., PASEK, D. A., EVANS, K. E. & MEISSNER, G. 2003. Molecular basis of calmodulin binding to cardiac muscle Ca(2+) release channel (ryanodine receptor). *The Journal of biological chemistry*, 278, 23480-23486.
- YAN, G. X., WU, Y., LIU, T., WANG, J., MARINCHAK, R. A. & KOWEY, P. R. 2001. Phase 2 early afterdepolarization as a trigger of polymorphic ventricular tachycardia in acquired long-QT syndrome : direct evidence from intracellular recordings in the intact left ventricular wall. *Circulation*, 103, 2851-6.
- YANOWITZ, F., PRESTON, J. B. & ABILDSKOV, J. A. 1966. Functional distribution of right and left stellate innervation to the ventricles. Production of neurogenic electrocardiographic changes by unilateral alteration of sympathetic tone. *Circulation research*, 18, 416-428.

- YIP, K. P. 2006. Epac-mediated Ca(2+) mobilization and exocytosis in inner medullary collecting duct. *American journal of physiology.Renal physiology*, 291, F882-90.
- YUSTE, R., KONNERTH, A. 2005. Imaging in neuroscience and development: A laboratory manual. *Cold Spring Harbor Laboratory Press*; New York.
- ZAZA, A., MALFATTO, G. & SCHWARTZ, P. J. 1991. Sympathetic modulation of the relation between ventricular repolarization and cycle length. *Circulation research*, 68, 1191-1203.
- ZHANG, L. M., WANG, Z. & NATTEL, S. 2002. Effects of sustained beta-adrenergic stimulation on ionic currents of cultured adult guinea pig cardiomyocytes. *American journal of physiology.Heart and circulatory physiology*, 282, H880-9.
- ZIPES, D. P. & WELLENS, H. J. 1998. Sudden cardiac death. *Circulation*, 98, 2334-2351.
- ZYGMUNT, A. C., EDDLESTONE, G. T., THOMAS, G. P., NESTERENKO, V. V. & ANTZELEVITCH, C. 2001. Larger late sodium conductance in M cells contributes to electrical heterogeneity in canine ventricle. *Am J Physiol Heart Circ Physiol*, 281, H689-97.
- ZYGMUNT, A. C., GOODROW, R. J. & ANTZELEVITCH, C. 2000. I(NaCa) contributes to electrical heterogeneity within the canine ventricle. *Am J Physiol Heart Circ Physiol*, 278, H1671-8.